AUSTRALIAN NATIONAL ANTARCTIC RESEARCH EXPEDITIONS

A N A R E

R E S E A R C H

N O T E S

48

Australian upper atmospheric and space physics research in Antarctica, 1987

Edited by G.B. Burns and M. Craven

ANTARCTIC DIVISION
DEPARTMENT OF SCIENCE

ANARE RESEARCH NOTES (ISSN 0729-6533)

This series allows rapid publication in a wide range of disciplines. Copies of this and other ANARE Research Notes are available from the Antarctic Division. Any person who has participated in Australian National Antarctic Research Expeditions is invited to publish through this series. Before submitting manuscripts authors should obtain a style guide from:

The Publications Office
Antarctic Division
Channel Highway
Kingston
Tasmania 7150
Australia.

Published April 1987
ISBN: 0 642 11319 X

CONTENTS

PREFACE

The impetus for this collection of short papers was the workshops on solar terrestrial and space physics at the Australian Institute of Physics Seventh National Congress held at the University of Adelaide between 25 and 29 August 1986.

Four papers are from the geomagnetic variations, pulsations and ULF workshop convened by Dr F. Menk, nine are from the high latitude ionosphere and upper atmosphere physics workshop convened by Dr F. Jacka, five are from the middle atmosphere program workshop convened by Dr W.G. Elford, one on auroral radar at Davis is from Dr N.N. Voloshinov and eight are invited papers on future Antarctic research programs from various authors eminent in their particular fields of research; a total of 27 papers in all.

The majority of papers are preliminary. They are published in this short form so that the physics community may be kept informed of current and future directions of Australian Antarctic upper atmospheric and space physics research. It is expected that most papers will appear in a fuller form in appropriate journals in the near future.

The editors would like to thank the convenors, and contributors to the publication for producing written papers. The Director, Antarctic Division, Department of Science gave permission to publish, and Antarctic Division staff prepared manuscripts and some diagrams.

Gary Burns, Mike Craven
Upper Atmosphere Physics Section
Antarctic Division

1. Pc3 MAGNETIC PULSATIONS AT DAVIS

R.J. Morris (1) and K.D. Cole (2)

(1) Antarctic Division
Department of Science
Kingston, Tas., Australia, 7150.

(2) Physics Department
La Trobe University
Bundoora, Vic., Australia, 3083.

ABSTRACT

A brief morphological study of Pc3 (10-45 s) ULF magnetic pulsations observed at the polar cusp latitude station, Davis, Antarctica ($\phi \sim 74.5°$) is presented. A significant observation of these deeply amplitude-modulated near monochromatic Pc3 magnetic pulsations are their exceptionally large amplitudes, i.e. $\leq$ 32 nT; which may provide a ground diagnostic for the location of the last closed magnetic field lines, adjacent to the dayside polar cusp. Observational analyses include, both diurnal and seasonal amplitude and occurrence distributions, power spectral analyses, dynamic sonagrams and polarization studies.

1.1 INTRODUCTION

The scientific literature abounds with extensive experimental and theoretical reports on Pc3 (10-45 s) geomagnetic pulsations. However the fundamental question as to whether their origin is internal or external to the magnetosphere, remains unanswered. Substantial experimental evidence suggests that these exogenic pulsations are driven and controlled by the solar wind parameters Vsw, Θ_{xB} and IMF, i.e., solar wind speed, IMF cone angle and the interplanetary magnetic field, respectively (Yumoto, in press).

Moreover, two external source mechanisms connected with the high latitude polar cusp magnetopause region, have been proposed to interpret the observational and dynamical morphology of Pc3 emissions. Firstly, the surface wave model involving the Kelvin-Helmholtz instability at the high latitude magnetopause (Miura 1984, Yumoto et al. 1985) and secondly, the

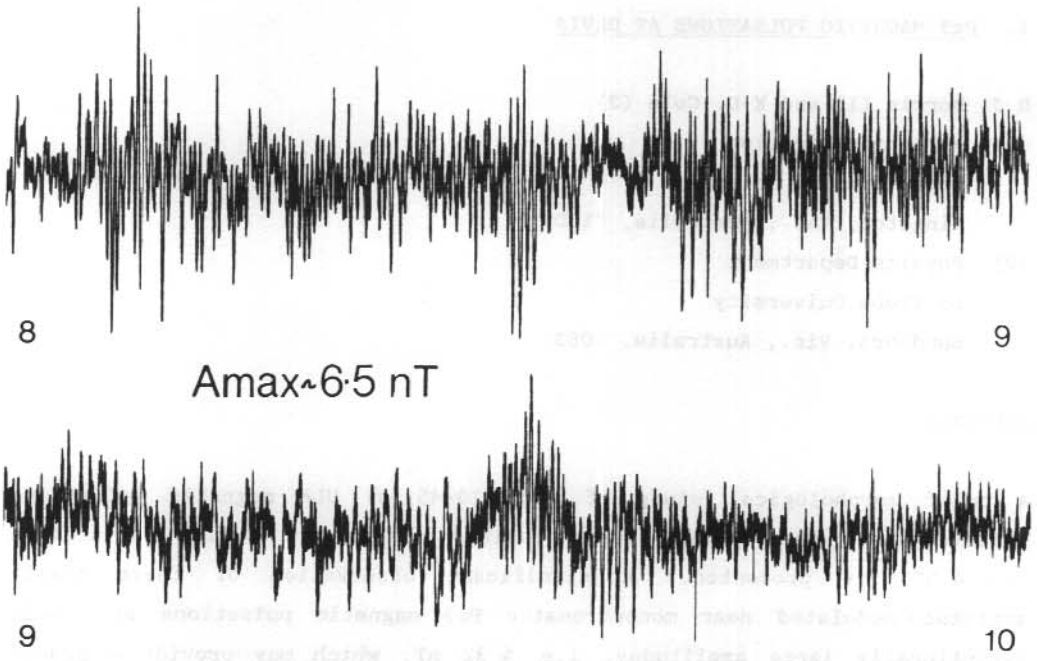

Figure 1. Amplitude-time record for Davis Pc3 event of 27 November 1981.

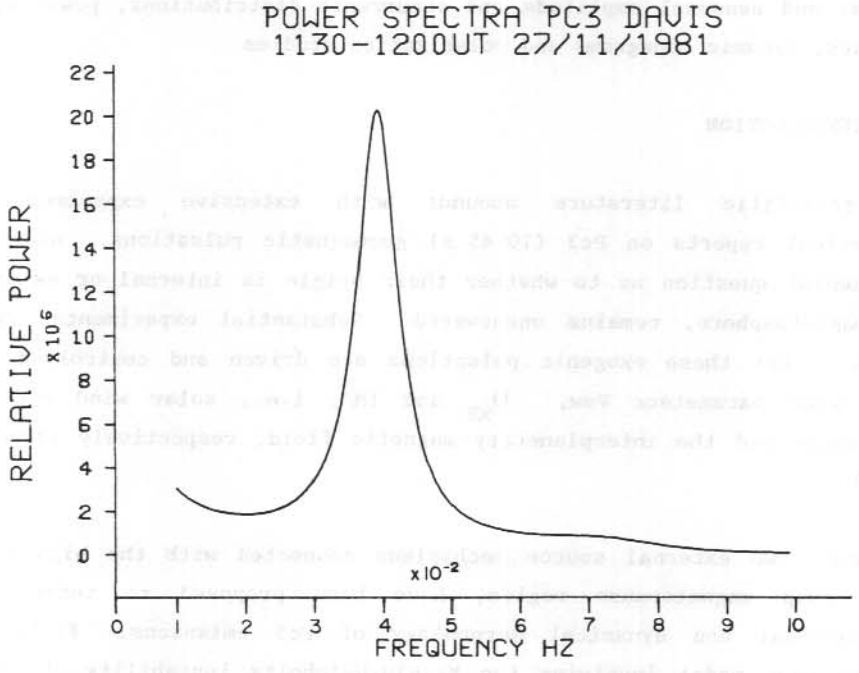

Figure 2. Power spectrum for Davis Pc3 event observed on 27 November 1981.

penetration by upstream ULF waves of the collisionless bow shock region, across the cusp region magnetopause (Russell et al. 1983, Russell and Hoppe 1983, Yumoto et al. 1984).

The observations of Pc3 pulsations extend from upstream of the Earth's bow shock to regions within the magnetosphere and on the ground (Arthur and McPherron 1977, Greenstadt and Olson 1976, Greenstadt and Olson 1979, Takahashi et al. 1981, Russell and Hoppe 1983, Wolfe et al. 1985, Lin et al. in press). Surprisingly, considering the current theoretical implication of the cusp region magnetopause for Pc3 pulsation generation and control, only negligible ground based data, at both the polar cusp and polar cap latitudes, have been cited (Bol'shakova and Troitskaya 1984, Engebretson et al. in press).

This paper presents some new preliminary morphological results on Pc3 geomagnetic pulsations observed at Davis station, Antarctica (gg 68.6°E, 78.0°E; gm 76.8°S, 119.0°E, Λ = 74.5°S), between February 1981 and March 1982. Davis, to a first order approximation is a polar cap station between 14 UT and 6 UT (i.e. night-side) and would lie under the dayside auroral oval (i.e. polar cusp) between 6 UT and 14 UT for magnetic activity with Kp = 3 (Morris and Cole 1985).

Data were acquired utilising a two component horizontal induction magnetometer, aligned along the magnetic north and east directions.

1.2 DESCRIPTION

Preliminary analysis of Davis 1981 magnetic pulsation data, revealed the prolific occurrence of Pc3 (10-45 s) relative to other regimes. Figure 1 illustrates an amplitude-time record of near monochromatic quasi-sinusoidal Pc3 oscillations, for the interval 8-10 UT on the 27 November 1981. Power spectral analyses of this event showed that oscillation periods, ranged between T (min) ~ 15-23 s and T (max) ~ 25-43 s, whilst the mean power peaks in the range, T (peak) ~ 20-29 s, during the interval 6-13 UT. A representative power spectrum for this Pc3 event (1130-1200 UT) is given by Figure 2, where T (peak) = 25 s (0.04 Hz).

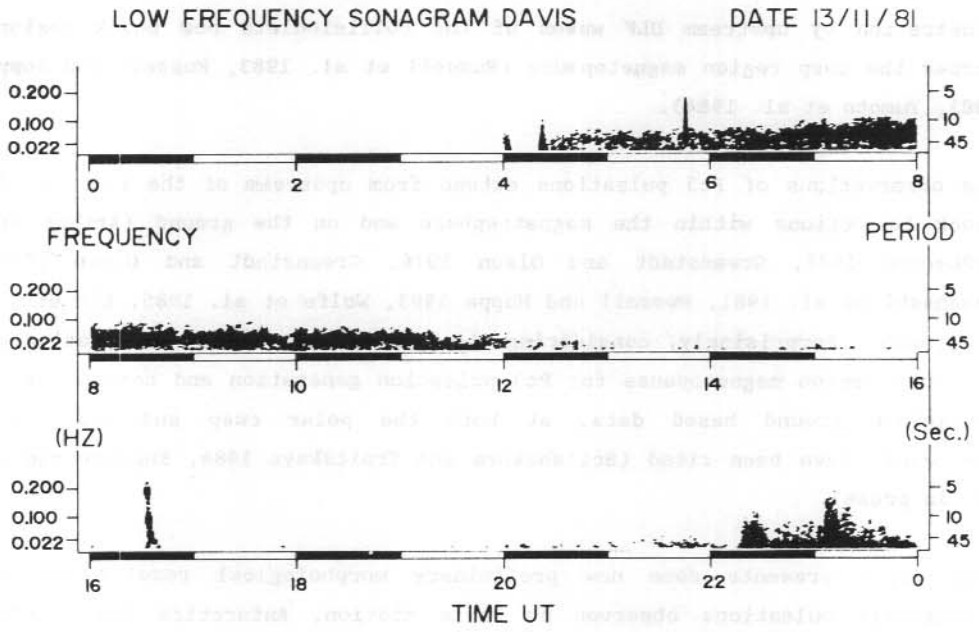

Figure 3. A film sonagram for Davis Pc3 event of 13 November 1981.

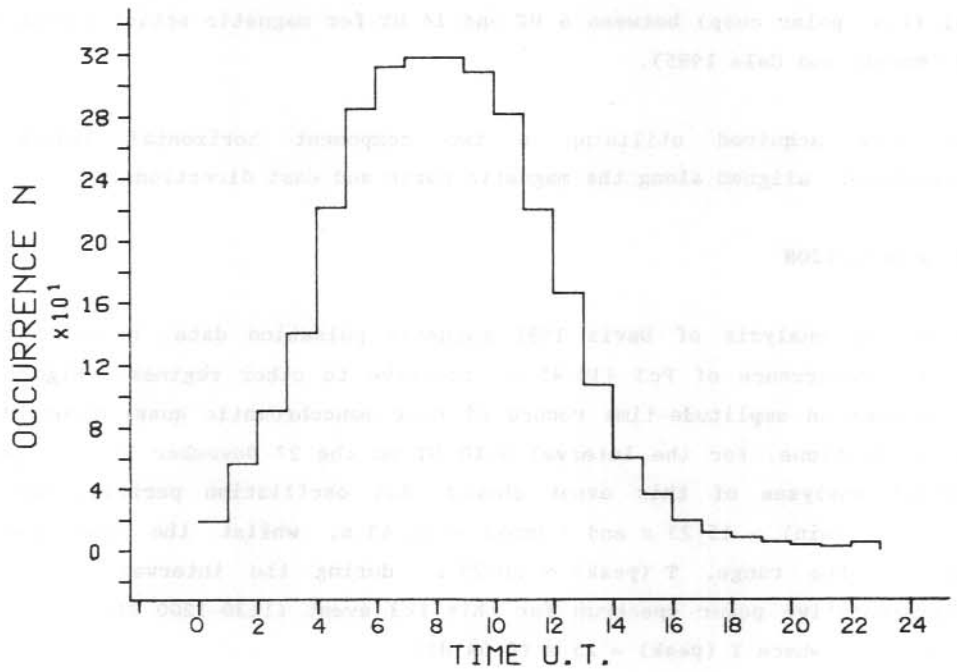

Figure 4. No. vs UT for Davis 1981 Pc3 events.

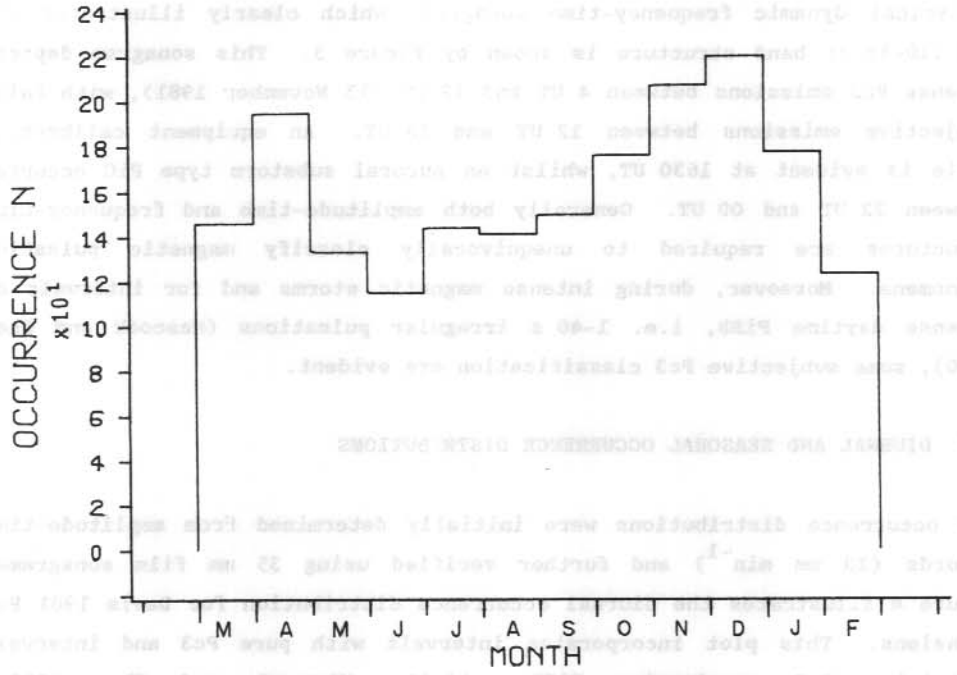

Figure 5. No. vs Month for Davis 1981 Pc3 events.

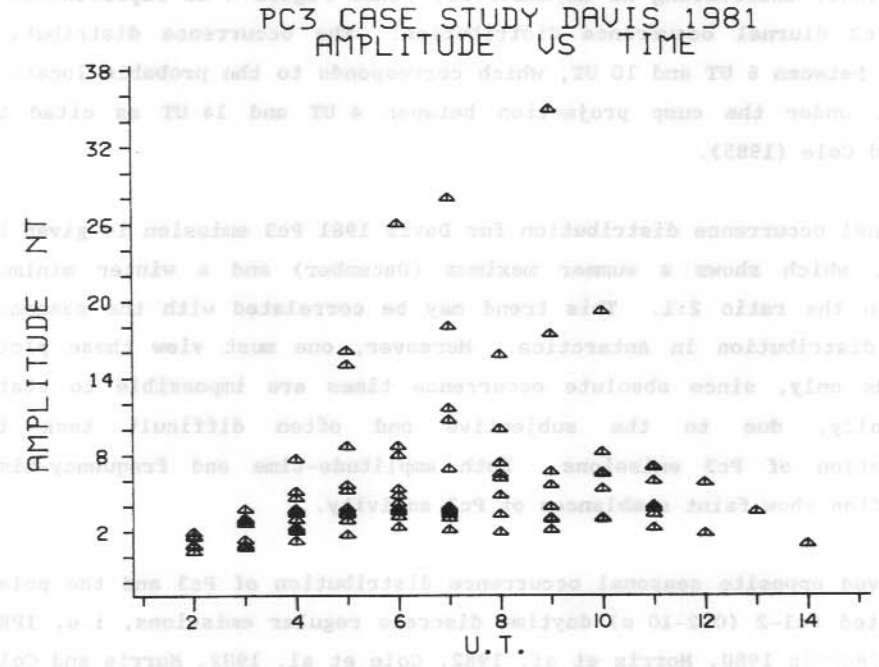

Figure 6. Amplitude vs UT for case study Pc3 events.

A typical dynamic frequency-time sonagram, which clearly illustrates the Pc3 (10-45 s) band structure is shown by Figure 3. This sonagram depicts intense Pc3 emissions between 4 UT and 12 UT (13 November 1981), with faint subjective emissions between 12 UT and 13 UT. An equipment calibration cycle is evident at 1630 UT, whilst an auroral substorm type PiC occurred between 22 UT and 00 UT. Generally both amplitude-time and frequency-time structures are required to unequivocally classify magnetic pulsation phenomena. Moreover, during intense magnetic storms and for intervals of intense daytime PiBB, i.e. 1-40 s irregular pulsations (Heacock and Chao 1980), some subjective Pc3 classification are evident.

1.3 DIURNAL AND SEASONAL OCCURRENCE DISTRIBUTIONS

The occurrence distributions were initially determined from amplitude-time records (20 mm min^{-1}) and further verified using 35 mm film sonagrams. Figure 4 illustrates the diurnal occurrence distribution for Davis 1981 Pc3 emissions. This plot incorporates intervals with pure Pc3 and intervals containing Pc3 overlapping PiBB activity (Heacock and Chao 1980). Individual plots of both Pc3 categories depicted near identical occurrence distributions, introducing no asymmetries, hence Figure 4 is representative of the Pc3 diurnal occurrence distribution. The occurrence distribution maximizes between 6 UT and 10 UT, which corresponds to the probable location of Davis, under the cusp projection between 4 UT and 14 UT as cited by Morris and Cole (1985).

The seasonal occurrence distribution for Davis 1981 Pc3 emission is given by Figure 5, which shows a summer maximum (December) and a winter minimum (June), in the ratio 2:1. This trend may be correlated with the seasonal daylight distribution in Antarctica. Moreover, one must view these plots for trends only, since absolute occurrence times are impossible to state unequivocally, due to the subjective and often difficult task in classification of Pc3 emissions. Both amplitude-time and frequency-time domains often show faint semblances of Pc3 activity.

The observed opposite seasonal occurrence distribution of Pc3 and the polar cusp related Pc1-2 (0.2-10 s) daytime discrete regular emissions, i.e. IPRP and IPCP (Morris 1980, Morris et al. 1982, Cole et al. 1982, Morris and Cole 1985), and serpentine emission (SE) (Morris and Cole in press, Gul'elmi and

Dovbnya 1974), may imply that the source region for these intense high latitude Pc3 magnetic pulsations are connected to the last closed magnetic field lines, adjacent to the dayside polar cusp.

1.4 AMPLITUDES

Davis Pc3 emissions have exceptionally large amplitudes, with A $\leq$ 32 nT, which by far exceeds amplitudes 'in situ', both upstream of the bow shock and within the magnetosphere, as well as at both lower and higher latitudes. A case study of eleven days with Pc3 events, illustrating the diurnal amplitude maximum around and several hours before local magnetic noon (i.e. ~0945 UT), is given in Figure 6, a plot of amplitude VS UT. Figure 7 illustrates that Pc3 amplitudes increase monotonically with increasing Kp, however even for Kp $\leq$ 3, Pc3 amplitudes $\leq$ 32 nT are observed.

In order to determine the seasonal amplitude distribution of Pc3 emissions, three days of Pc3 occurrence per month, for Kp $\leq$ 3 during the hours before and around local magnetic noon (i.e. 5 $\leq$ UT $\leq$ 10), had their amplitude-time records scaled and averaged. Figure 8, a plot of amplitude VS month, shows the strong seasonal Pc3 intensity variation, with a summer to winter amplitude ratio of 3:1. This plot further indicates that event occurrence statistics alone cannot comprehensively represent the physical nature of Pc3 emissions. Hence, the maximal amplitudes of Pc3 magnetic pulsations at Davis are indicative of the close proximity to their source region, presumably the polar cusp or the adjacent region of last closed magnetic field lines.

1.5 POLARIZATION

The polarization characteristics of twenty days of Davis 1981 Pc3 emissions were investigated for their sense of rotation, in order to determine the wave propagation mode. Figure 9 illustrates the polarization ellipses as recorded on an X-Y plotter, for Pc3 emissions occurring between 5 UT and 10 UT on 13 November 1981. The convention for the sense of rotation for the Southern Hemisphere, when looking along the direction of the magnetic field is as follows: clockwise rotation corresponds to left-hand polarized waves

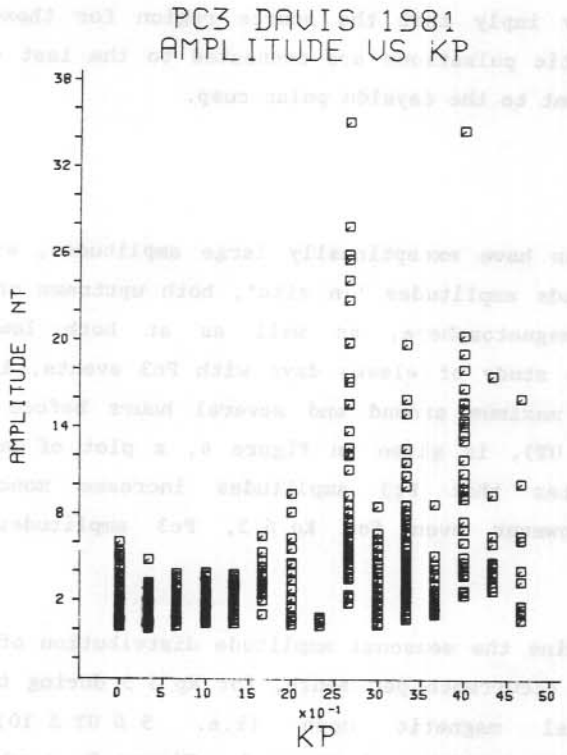

Figure 7. Amplitude vs Kp for case study Pc3 events.

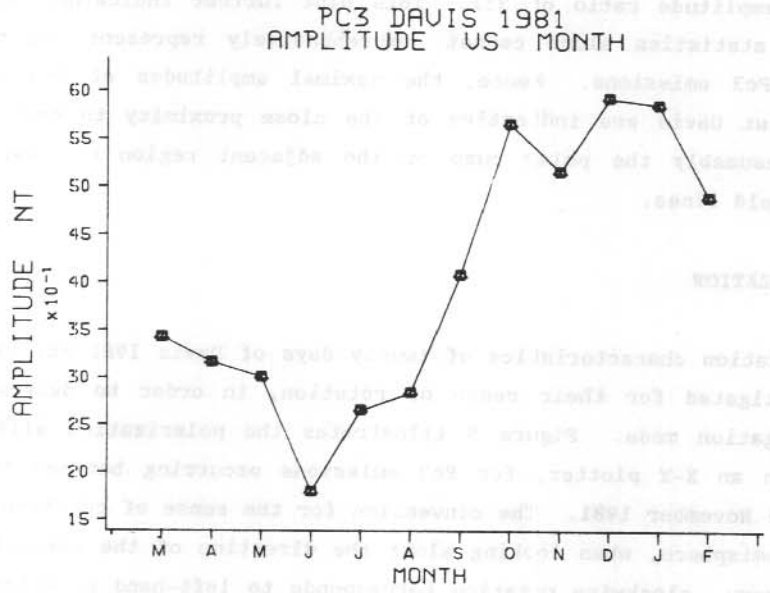

Figure 8. Amplitude vs Month for representative 1981 Pc3 events.

(L) and counter clockwise rotation corresponds to right-hand polarized waves (R) (Fraser and Summers 1972).

Figure 9 depicts the change in sense of rotation for Pc3 magnetic pulsations, characteristic of Davis records, in which between 0501 UT and 0653 UT, it is L, between 0717 UT and 0725 UT, L and R, and between 0730 UT and 1002 UT, R. Similarly, the results of twenty days of Pc3 emissions were investigated and the results are presented by Figure 10, a plot of polarization mode against time (UT). Here the dark, hatched and light regions correspond respectively, to L polarization, transitional polarization i.e. L↔R, and R polarization senses. The most obvious trend being the diurnal transition, from L polarization to R polarization, generally exhibiting a transitional interval of ten minutes, between 0650 UT and 0810 UT. Some nine days had distinctive transitional intervals, ranging from five to sixty minutes, where both rotation senses were clearly evident.

On two occasions the Pc3 emission rotation sense reverted to the initial direction, i.e. L → R → L after some two hours.

Furthermore, the seasonal analysis of representative Pc3 event polarization demonstrates the consistent trend in the polarization transition from L-waves to R-waves around local geographic noon (~ 0648 UT). This observation may imply that the source region or propagation path for Pc3 emissions are independent of season.

1.6 DISCUSSION AND CONCLUSION

The penetration of upstream ULF magnetic pulsations across the magnetopause was earlier suggested by Troitskaya et al. (1971). Recent observations by Hoppe and Russell (1983) lead to the Yumoto et al. (1985) model of upstream ULF waves transversely penetrating the equatorial region magnetopause and ultimately contributing to the low latitude Pc3 magnetic pulsations. Yumoto et al. (1985) attributed the occurrence of high latitude Pc3 pulsations to the Kelvin-Helmholtz instability.

However, Engebretson et al. (in press) presented a conflicting point of view, in which cusp region Pc3 result from the penetration of upstream ULF waves across the high latitude magnetopause, with subsequent amplification

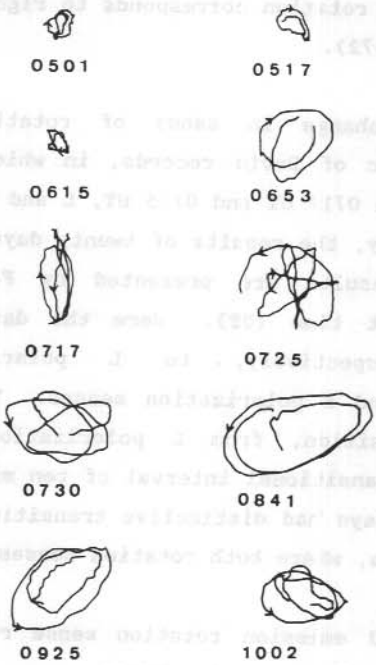

Figure 9. Polarization ellipses for the Davis Pc3 event of 13 November 1981.

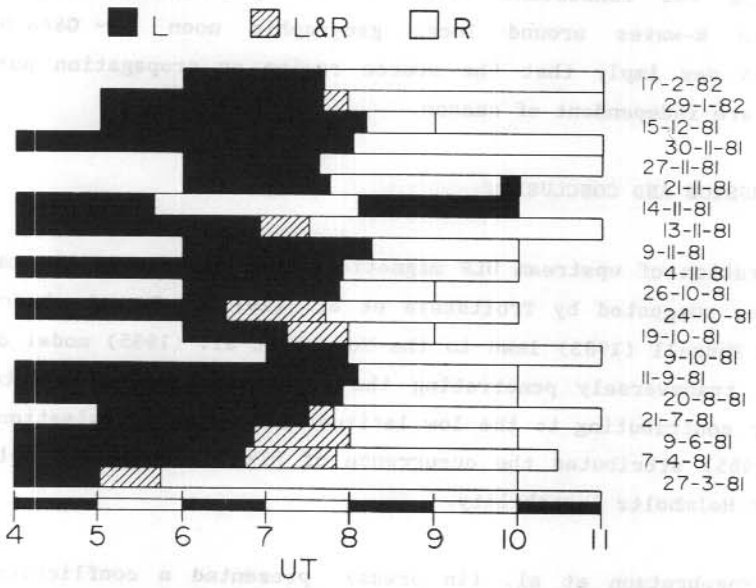

Figure 10. A composite plot of polarization mode against UT for representative Pc3 events observed throughout 1981.

by other mechanisms, including the Kelvin-Helmholtz instability. These authors also proposed that high latitude Pc3 pulsations could propagate through the ionospheric F duct (Lanzerotti et al. 1981), and contribute to the origin of low latitude Pc3 magnetic pulsations.

This obvious variance in theoretical interpretation can only be resolved by the investigation of additional high latitude Pc3 emissions. Since both hypotheses invoke mechanisms associated with the cusp region magnetopause, then ground observations at the cusp and at adjacent latitudes must be sought.

Perhaps an alternative source mechanism is required to explain the intense cusp latitude Pc3 magnetic pulsation amplitudes, their interesting polarization characteristics, their diurnal and seasonal morphological properties and their association with magnetic activity, i.e. Kp, as presented in this paper.

A tentative hypothesis for impulsive wave generation is that it is associated with abrupt transitions of the last 'closed' magnetic field line, adjacent to the polar cusp, to an 'open' condition. During the transition damped longitudinal Alfvén surface waves may be generated, whose eigenmodes are manifest in Pc3 magnetic pulsations. Consecutive amplitude-modulated bursts may correspond to repeated field line transitions, which are driven and controlled by the solar wind parameters Vsw, Θ_{xB} and IMF (Bz). Moreover, the amplitude of the waves produced would be a function of parameters of the plasma, which permeates the moving magnetic field lines.

The observed polarization characteristics may be related to the direction of magnetic field aligned currents (FAC) flowing towards/away from the ionosphere. Thus the dominant L-polarization transition to R-polarization could result from the reverse in direction of FAC around local geographic noon.

Finally, the authors emphasize the significance of ground observations of magnetic pulsations at the cusp region and at adjacent latitudes as a diagnostic tool for monitoring the coupling of solar wind energy into the magnetosphere.

1.7 REFERENCES

Arthur, C.W. and McPherron, R.L. (1977). Interplanetary magnetic field conditions associated with synchronous orbit observations of Pc3 magnetic pulsations. Journal of Geophysical Research 82:5138-5142.

Bol'shakova, O.V. and Troitskaya, V.A. (1984). The relation of the high-latitude maximum of Pc3 intensity to the dayside cusp. Geomagnetism and Aeronomy 24:633-635.

Cole, K.D., Morris, R.J., Matveeva, E.T., Troitskaya, V.A. and Pokhotelov, O.A. (1982). The relationship of the boundary layer of the magnetosphere to IPRP events. Planetary and Space Science 30:129-136.

Engebretson, M.J., Meng, C.I., Arnoldy, R.L. and Cahill, L.J. (in press). Pc3 pulsations observed near the south polar cusp. Journal of Geophysical Research.

Fraser, B.J. and Summers, W.R. (1972). Polarizations of Pc1 micropulsations through ionospheric ducts. Nature Physical Science 235:170-171.

Greenstadt, E.W. and Olson, J.V. (1976). Pc3, 4 activity and interplanetary field orientation. Journal of Geophysical Research 81:5911-5920.

Greenstadt, E.W. and Olson, J.V. (1979). Geomagnetic pulsations signals and hourly distributions of IMF orientation. Journal of Geophysical Research 84:1493-1498.

Gul'elmi, A.V. and Dovbnya, B.V. (1974). Hydromagnetic emission of the interplanetary plasma. Astrophysics and Space Science 31:21-29.

Heacock, R.R. and Chao, J.K. (1980). Type Pi magnetic field pulsations at very high latitudes and their relation to plasma convection in the magnetosphere. Journal of Geophysical Research 85:1203-1213.

Hoppe, M.M. and Russell, C.T. (1983). Plasma rest frame frequencies and polarizations of the low-frequency upstream waves: ISEE 1 and 2 observations. Journal of Geophysical Research 88:2021-2028.

Lanzerotti, L.J., Medford, L.V., MacLennan, C.G., Hasegawa, T., Acuna, M.H. and Dolce, S.R. (1981). Polarization characteristics of hydromagnetic waves at low geomagnetic latitudes. Journal of Geophysical Research 86:5500-5506.

Lin, N.G., Cahill, L.J, Jr., Engebretson, M.J., Sugiura, M. and Arnoldy, R.L. (in press). Dayside pulsation events near the plasmapause. Planetary and Space Science.

Miura, A. (1984). Anomalous transport by magnetohydrodynamic Kelvin-Helmholtz instabilities in the solar wind-magnetosphere interaction. Journal of Geophysical Research 89:801-818.

Morris, R.J. (1980). Intervals of pulsations with rising periods: IPRP MSc Thesis, La Trobe University.

Morris, R.J., Cole, K.D., Matveeva, E.T. and Troitskaya, V.A. (1982). Hydromagnetic "whistles" at the dayside cusps: IPRP events. Planetary and Space Science 30:113-127.

Morris, R.J. and Cole, K.D. (1985). Pc1-2 discrete regular daytime pulsation bursts at high latitudes. Planetary and Space Science 33:53-67.

Morris, R.J. and Cole, K.D. (in press). 'Serpentine emission' at the high latitude Antarctic station, Davis. Planetary and Space Science.

Russell, C.T. and Hoppe, M.M. (1983). Upstream waves and particles. Space Science Reviews 34:155-172.

Russell, C.T., Luhmann, J.G., Odera, T.J. and Stuart, W.F. (1983). The rate of occurrence of dayside Pc3,4 pulsations: the L-value dependence of the IMF cone angle effect. Geophysical Research Letters 10:663-666.

Takahashi, K., McPherron, R.L., Greenstadt, E.W. and Neeley, C.A. (1981). Factors controlling the occurrence of Pc3 magnetic pulsations at synchronous orbit. Journal of Geophysical Research 86:5472-5484.

Troitskaya, V.A., Plyasova-Bakunina, T.A. and Gul'elmi, A.V. (1971). Relationship between Pc2-4 pulsations and the interplanetary magnetic field. Dokl. Akad. Nauk. SSR 197:1312-1314.

Wolfe, A., Meloni, A., Lanzerotti, L.J., MacLennan, C.G., Bamber, J. and Venkatesan, D. (1985). Dependence of hydromagnetic energy spectra near L=2 and L=3 on upstream solar wind parameters. Journal of Geophysical Research 90:5117-5131.

Yumoto, K., Saito, T., Tsurutani, B.T., Smith, E.J. and Akasofu, S.-I. (1984). Relationship between the IMF magnitude and Pc3 magnetic pulsations in the magnetosphere. Journal of Geophysical Research 89:9731-9740.

Yumoto, K., Saito, T., Akasofu, S.-I., Tsurutani, B.T. and Smith, E.J. (1985). Propagation mechanism of daytime Pc3-4 pulsations observed at synchronous orbit and multiple ground-based stations. Journal of Geophysical Research 90:6439-6450.

Yumoto, K. (in press). Generation and propagation mechanism of low-latitude magnetic pulsations - a review. Journal of Geophysical Research.

2. PULSATING AURORA AND MAGNETIC Pi(c) PULSATIONS

M. Craven and G.B. Burns
Antarctic Division
Department of Science
Kingston, Tas., Australia, 7150.

ABSTRACT

Strong peak-to-peak correlations, with average time delays less than a second, between auroral optical N_2^+1NG(0,1) band intensity variations and magnetic Pi(c) pulsations, as observed at Macquarie Island (geographic co-ordinates 54.5°S, 158.7°E, invariant latitude 64.5°S), provide convincing evidence of a local ionospheric production mechanism for the magnetic pulsations.

Theoretical modelling of an auroral pulsation patch, as per Oguti and Hayashi (1984), is used to explain the general properties of the magnetic pulsations. The polarization of the Pi(c) pulsations is shown to be controlled principally by a delay between the Hall and Pedersen current fluctuations as measured at the ground, and the direction of the background E-region electric field.

2.1 INTRODUCTION

Pulsating aurora is a phenomenon with peak intensities generally around visual threshold limits of 1-2 kR (always less than 10 kR) at 427.8 nm. They are commonly observed post auroral breakup in the morning sector of the auroral oval.

Individual patches range from 10-100 km across with a quasi-periodic brightness fluctuation period in the range 2-20 s. Intricate shapes persist throughout several pulsations despite drift velocities of the order 0.1-1.0 kms^{-1}. Neighbouring patches may pulsate independently of each other in phase and period.

Magnetic pulsations accompany these phenomena at all times, and detailed correspondence is common.

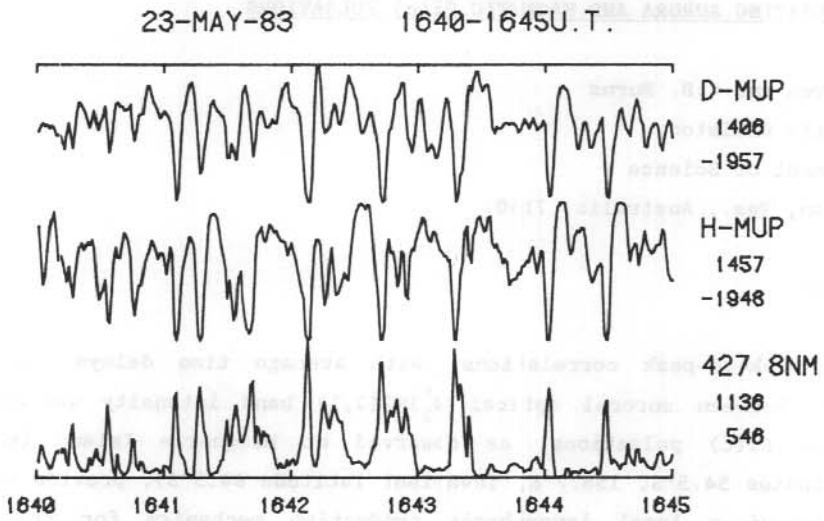

Figure 1. 5-minute, 5 Hz observational data file with maximum and minimum amplitudes indicated to the right of each file.

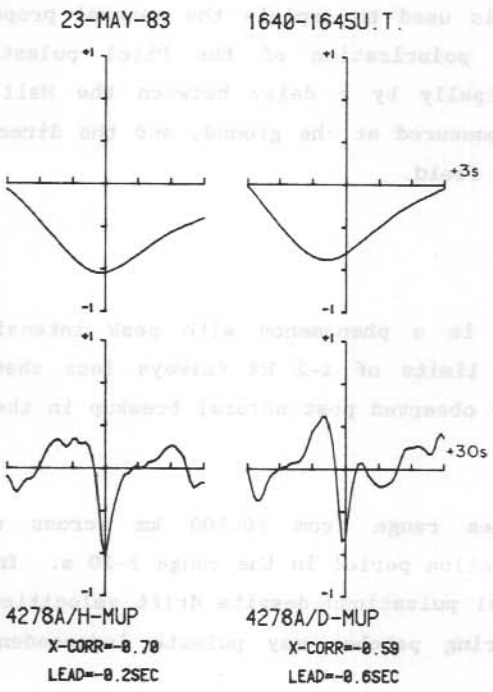

Figure 2. Correlation functions for the magnetic components with the 427.8 nm optical file. Lower figures cover the range ±30 s, upper figures are expanded versions over ±3 s.

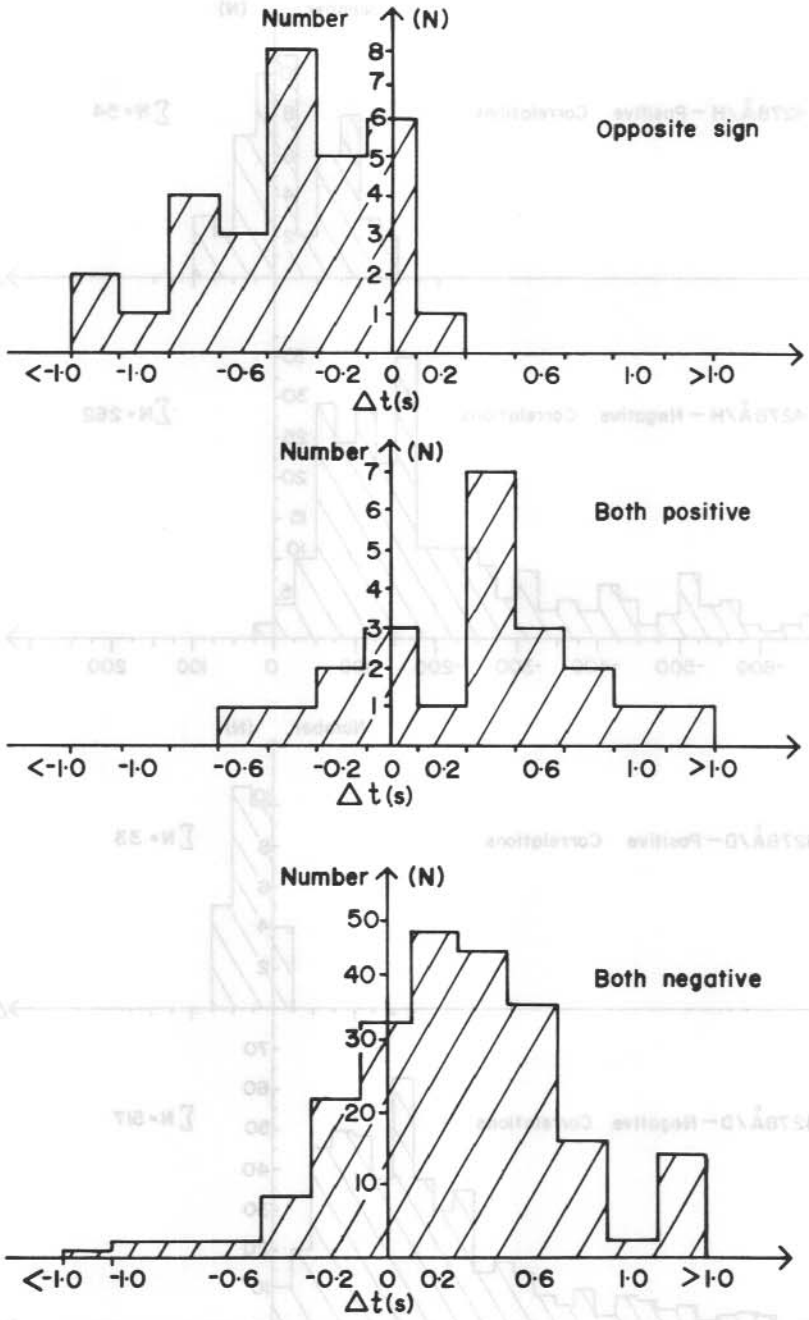

Figure 3. Histograms of the lead/lag relationship between the two magnetic pulsation components. The H component pulsations generally lead the D component pulsations when both return the same correlation sign.

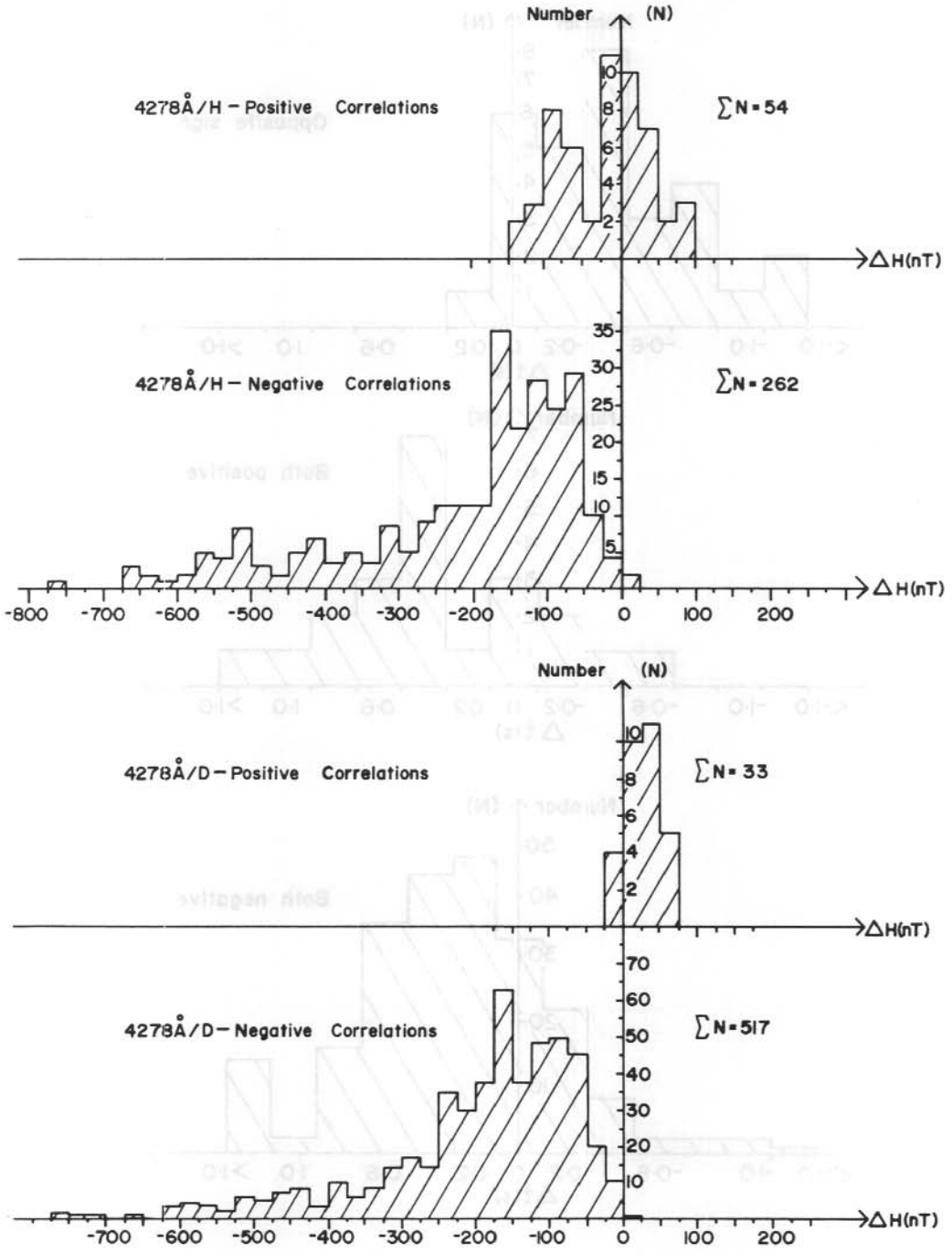

Figure 4. Changes in the main field H-component reflects strongly the correlation sign for both magnetic pulsation components.

(General references: Cresswell and Davis 1966, Heacock 1967, Royrvik and Davis 1977, Johnstone 1978)

2.2 OBSERVATIONS

The Macquarie Island instrumentation employs a 30° half-angle zenith oriented photometer to detect the auroral pulsations, and two horizontal plane, mutually orthogonal induction coils oriented in the H (northwards) and D (eastwards) directions to monitor the magnetic fluctuations. Figure 1 shows the 5-minute, 5 Hz data collection format for a highly correlated event. Commonly a negative correlation between the magnetic components and the optical pulsations, as displayed in Figure 2, is observed.

Positive correlations for either or both magnetic components with the optical pulsations tend to occur in early evening or late morning, at times when rotations of the ionospheric electric field can be expected.

The optical fluctuations lead the H-component pulsations by 0.2 s on average, and the D-component by 0.6 s for the situation where both magnetic components are negatively correlated with the optical variations. In a statistically averaged sense a similar situation exists when both correlations return positive values. However, the D-component tends to lead the H-component when only one of the correlations is positive. Histograms of 1983 Macquarie Island data presented in Figure 3 depict this reversal.

The sign of the correlation for both components is well reflected by the change in the large-scale H magnetic field component (Figure 4) indicating that E-region currents are responsible for the magnetic pulsations. No correlation exists for the D-component magnetic pulsations and the broadscale D-component of the main field (Figure 5) which is known to be effected by other than E-region currents (Brekke et al. 1974).

2.3 THEORETICAL MODELLING

2.3.1 Physical processes

Consider the ambient auroral ionosphere where an equatorward electric field and upward magnetic field produce equatorward Pedersen, and westward Hall

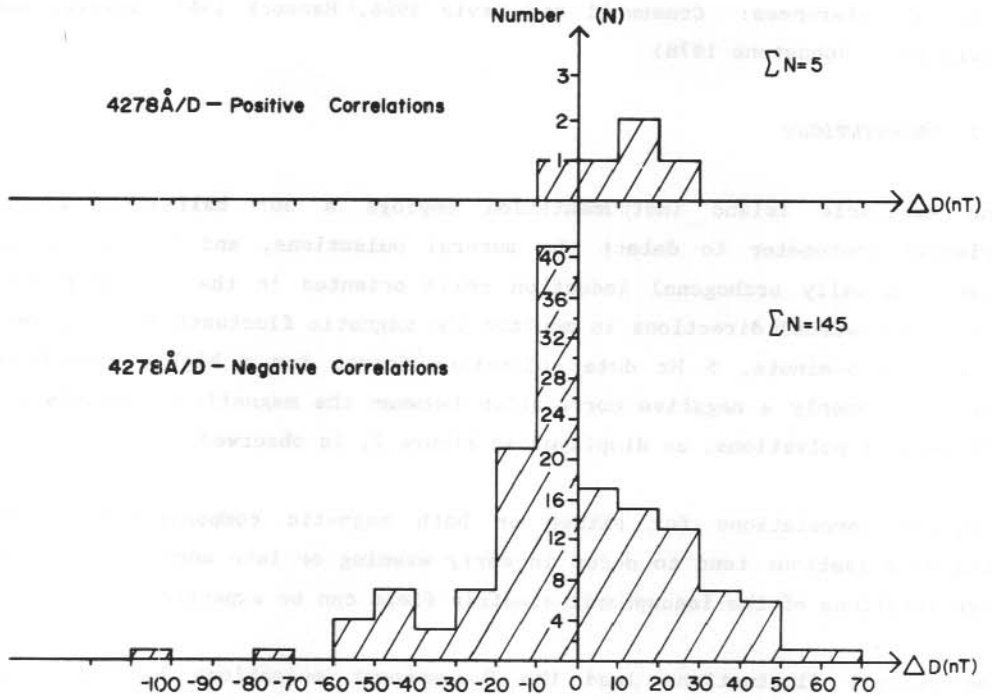

Figure 5. The D-component pulsations do not follow the trend of the main field D-component.

currents. Suppose a patch of enhanced conductivity is suddenly produced by the ionizing action of a burst of electrons.

Since pulsation maxima exhibit a spectral hardening rather than a simple increase of the ambient flux (Bryant et al. 1975, McEwen et al. 1981), then the increased current flow within the patch will be rotated anti-clockwise from the background current direction as indicated in Figure 6.

Enhanced flow within the patch causes a charge buildup around the boundary producing a polarization electric field pointing roughly ESE. A polarization Pedersen current flows in this direction, and a Hall contribution flows to the NNE. The total perturbation current within the patch will be the sum of these and the Hall and Pedersen enhancement currents due to the conductivity increase.

One further complication is that the ionospheric current can also discharge along the field lines around the boundary. This results in a reduction of the effective polarization currents, and a full analysis takes all of these factors into account.

2.3.2 Mathematical analysis

This development follows Oguti and Hayashi (1984) but a different factor governing the field-line contribution will be noted. A solution is required to the Laplace equation:

$$\nabla^2 U = 0 \qquad (1)$$

Expressing the potential in polar co-ordinates with the electric field directed along the $\phi=0$ direction:

$$U(r,\phi) = \sum_{n=o}^{n=\infty} [A_n r^n + B_n r^{-n}] \cos(n\phi + \alpha_n) \qquad (2)$$

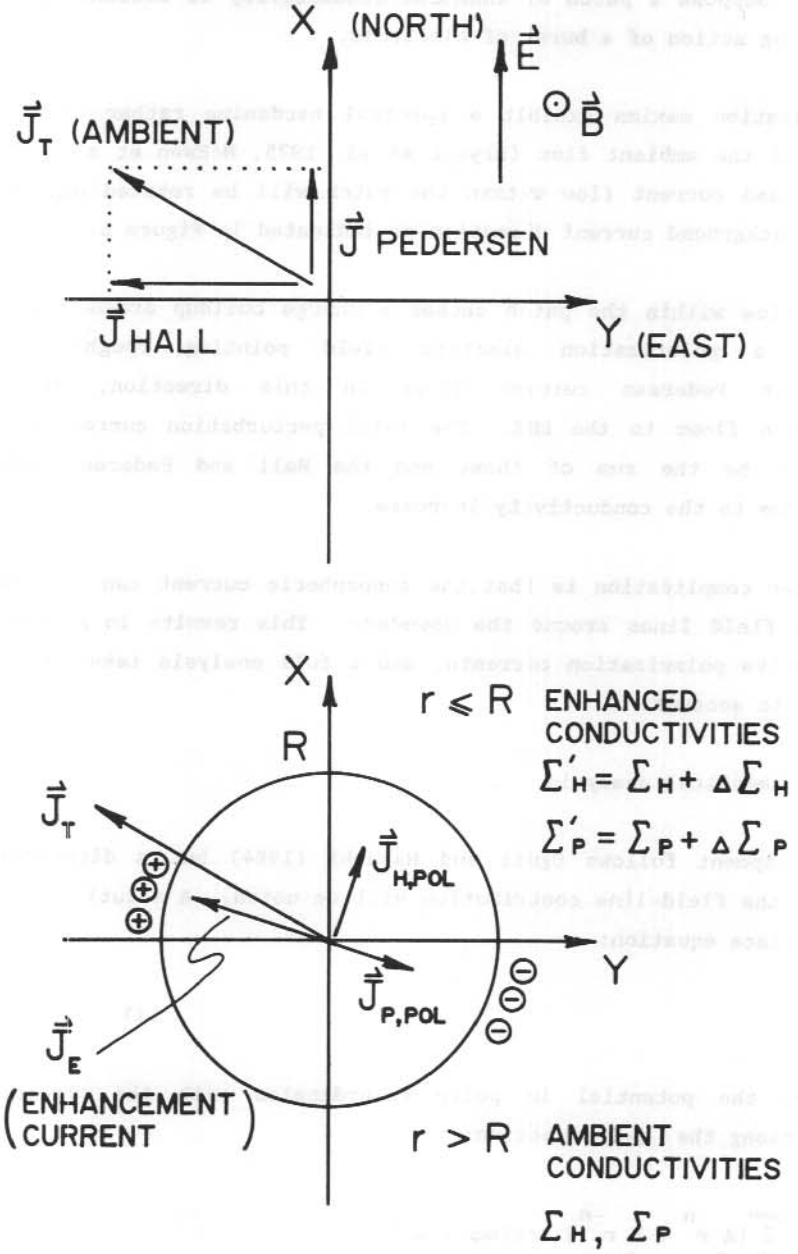

Figure 6. Co-ordinate system showing orientation of currents and fields used in the mathematical analysis of an enhanced conductivity region in the ionosphere.

considerations of:

1. $r \to 0$, U must remain finite,
2. $r \to \infty$, U must remain finite and
3. U must be continuous for all r

lead to:

$$U(r,\phi) = D(R^2/r)\cos(\phi + \alpha) \quad \text{for } r > R$$
$$U'(r,\phi) = Dr\cos(\phi + \alpha) \quad \text{for } r \leq R \qquad (3)$$

where R is the radius of the patch of increased ionisation (see Figure 6).

So for the electric field components:

$$E_r = E\cos\phi - \frac{\partial U}{\partial r}$$

$$E_\phi = -E\sin\phi - \frac{1}{r}\frac{\partial U}{\partial \phi} \qquad (4)$$

Co-efficients D and α are determined from the boundary condition for the divergence of the ionospheric (horizontal) current:

$$\mathrm{div}_\perp J_\perp = -M\,\mathrm{div}_\perp E_\perp \qquad (5)$$

where M is a factor expressing the contribution of field line discharge around the boundary.

Complete expressions yield:

$$D = \frac{\{[2\Delta\Sigma_H(\Sigma_P + M)]^2 + [\Delta\Sigma_P^2 + \Delta\Sigma_H^2 + 2\Delta\Sigma_P(\Sigma_P + M)]^2\}^{1/2}}{\Delta\Sigma_H^2 + \Delta\Sigma_P^2 + 4(\Sigma_P + M)(\Sigma_P + \Delta\Sigma_P + M)} \cdot E \qquad (6)$$

and

$$\tan\alpha = \frac{2\Delta\Sigma_H(\Sigma_P + M)}{\Delta\Sigma_P^2 + \Delta\Sigma_H^2 + 2\Delta\Sigma_P(\Sigma_P + M)} \qquad (7)$$

where Σ_P, Σ_H are the height-integrated Pedersen and Hall conductivities, and $\Delta\Sigma_P$, $\Delta\Sigma_H$ their respective enhancements. For the currents:

$$J_r = \Sigma_P E_r + \Sigma_H E_\phi, \qquad J_\phi = \Sigma_P E_\phi - \Sigma_H E_r \tag{8a}$$

and in (x,y) coordinates, with the E-region electric field in the positive x-direction:

$$J_x = J_r \cos\phi - J_\phi \sin\phi , \quad J_y = J_r \sin\phi + J_\phi \cos\phi \tag{8b}$$

so the modification currents can be written:

$$J_x' = \Delta\Sigma_P E - D (\Sigma_P' \cos\alpha - \Sigma_H' \sin\alpha)$$

$$J_y' = -\Delta\Sigma_H E + D (\Sigma_P' \sin\alpha + \Sigma_H' \cos\alpha) , \quad r \leq R \tag{9}$$

and:

$$J_x = D \frac{R^2}{r^2} [\Sigma_P \cos(2\phi + \alpha) + \Sigma_H \sin(2\phi + \alpha)]$$

$$J_y = D \frac{R^2}{r^2} [\Sigma_P \sin(2\phi + \alpha) - \Sigma_H \cos(2\phi + \alpha)] , \quad r > R \tag{10}$$

where:

$$\Sigma_P' = \Sigma_P + \Delta\Sigma_P , \quad \Sigma_H' = \Sigma_H + \Delta\Sigma_H$$

We can specify M by relating it to the percentage, P, of the ionospheric current which is discharged along the field lines:

$$P = \frac{\text{Total field aligned discharge current}}{\text{Total field aligned + ionospheric discharge current}} \times 100 \tag{11}$$

Evaluating appropriate integrals produces:

$$M = \frac{[\Sigma_H^2 + \Sigma_P^2]^{1/2}}{2} \cdot \frac{P}{100 - P} \tag{12}$$

This differs from the expression derived by Oguti and Hayashi (1984). They quote:

$$M = \frac{[\Sigma_P + \Sigma_P']}{2} \cdot \frac{P}{100 - P} \tag{13}$$

2.4 DISCUSSION

The modification current system will vary as the electron concentration in the patch increases (increasing the Hall and Pedersen conductivities) following the ionization pulse, and decays as the electrons are removed. This varying current will result in a magnetic perturbation recorded on the ground.

Induction coils essentially measure the derivative of the magnetic field variation. The optical pulses are better correlated with the derivative of the magnetic field than the magnetic field itself, as argued by Oguti and Hayashi (1984) from the ionospheric rate equation:

$$\frac{dN_e}{dt} = Q - \alpha N_e^2 \qquad (14)$$

They show that the auroral luminosity of a patch is proportional to the ionization rate Q. Since the period of the pulsations is generally smaller than the ionization relaxation time (α is the effective recombination co-efficient), then the luminosity is proportional to the time derivative of electron density, N_e, which is in turn proportional to the magnetic field effect.

Due to the nature of the induction coils they respond to the initial rapid ionization pulse only, when Q is large. They do not detect the more gradual decay, and so the optical pulses do in fact correlate with the derivative of the magnetic field. Burns and Cole (1985) show, with a crude model, that velocity dispersal of electrons in a field-aligned current can also yield this relationship.

The authors postulate that there is a delay between the magnetic fluctuations recorded on the ground resulting from the Hall and Pedersen variations, and that this delay results from the altitude difference of the respective Hall (105 km) and Pedersen (120 km) current systems. This, along with the E-region electric field, essentially controls the polarization of the magnetic pulsation recorded at the ground site.

There are a number of mechanisms which may contribute to this delay:

1. Velocity dispersal of the electrons from a geomagnetic equatorial source causing excitation at lower altitudes first (Bryant et al. 1975).
2. Propagation time of a ULF wave through the ionosphere being dependent upon the length of the propagation path through an ionized medium (Campbell 1970, Francis and Karplus 1960).
3. The rate at which the electron concentration increases following an ionization pulse depends on the free electron concentration itself (Jones and Rees 1973). During pulsating aurora the electron concentration at Hall current altitudes may exceed that at the Pedersen altitude.

The major influence controlling magnetic perturbations on the ground will be the modification currents J_x' and J_y' within the enhanced conductivity region itself, since, as equation (10) shows, external modification currents diminish as $1/r^2$ from the centre of the patch. Conductivity enhancements of 20%, 50% and 100% (with no spectral hardening) were used by Oguti and Hayashi (1984), however the authors choose to consider conductivity enhancements of 5% in the Pedersen and 10% in the Hall, as measured for an actual pulsating aurora by MacDougall et al. (1981).

The ratio Σ_P/Σ_H is of the order 0.25–0.50 for diffuse aurora (Arnoldy et al. 1982), and rarely less than 0.25 even for disturbed night-time conditions (Brekke et al. 1974), though it may approach 1.0 as measured for an event during the Canadian Pulsating Aurora Campaign (MacDougall et al. 1981). For the range 25% < P < 75%, J_x' and J_y' vary only slowly for a Σ_P/Σ_H ratio between 0.25–1.0 at any given percentage, P, of field-aligned discharge current (see Figure 7).

Oguti and Hayashi (1984) adopt a figure of 55% for P which translates to approximately 52% for our formulation of the factor M (c.f. equations (12) and (13)) with a Σ_P/Σ_H ratio of 0.5. For a field-aligned discharge rate around 50%, Figure 7 shows that $|J_x'|$ is slightly greater than $|J_y'|$. Under normal conditions of an equatorward E-region electric field, this results in a D-component magnetic pulsation slightly larger than that of the H-component. This is in accord with the general observation that D-dot is better correlated with the optical variations than H-dot (Engebretson et al. 1983, Burns and Cole 1985). This observation in turn places an upper limit on P of roughly 60% (for thereafter $|J_y'|>|J_x'|$).

Since J_x' is positive equatorward, the initial current increase produces a westward disturbance in the D-component magnetic ground variation, yielding a negative correlation with the optical pulsations (since D is defined positive eastward). Similarly, a negative J_y' indicates a westward perturbation current, and hence a southward magnetic effect, resulting in a negative H-component/optical correlation as well, as is generally observed.

The currents J_x' and J_y' both depend on Hall and Pedersen conductivity terms (equation (9)), and Table 1 indicates the individual breakdown for a variety of Σ_P/Σ_H ratios. The figures show that J_x' and J_y' are both dominated by Hall conductivity effects.

	J_x'			J_y'	
Σ_P/Σ_H	Hall	Pedersen	Total	Hall	Pedersen
Total					
0.2	.076	.008	.084	-.087	.015	-.072
0.3	.065	.011	.076	-.086	.019	-.067
0.4	.057	.015	.072	-.085	.022	-.063
0.5	.050	.018	.068	-.085	.024	-.061
0.6	.045	.021	.066	-.084	.026	-.058

Table 1. Breakdown of the Hall and Pedersen contributions which go to make up the total modification currents in the enhanced region (for a P = 50% and 5% Pedersen and 10% Hall conductivity enhancements). Current figures need to be multiplied by the factor $E\Sigma_H$ to give true current values.

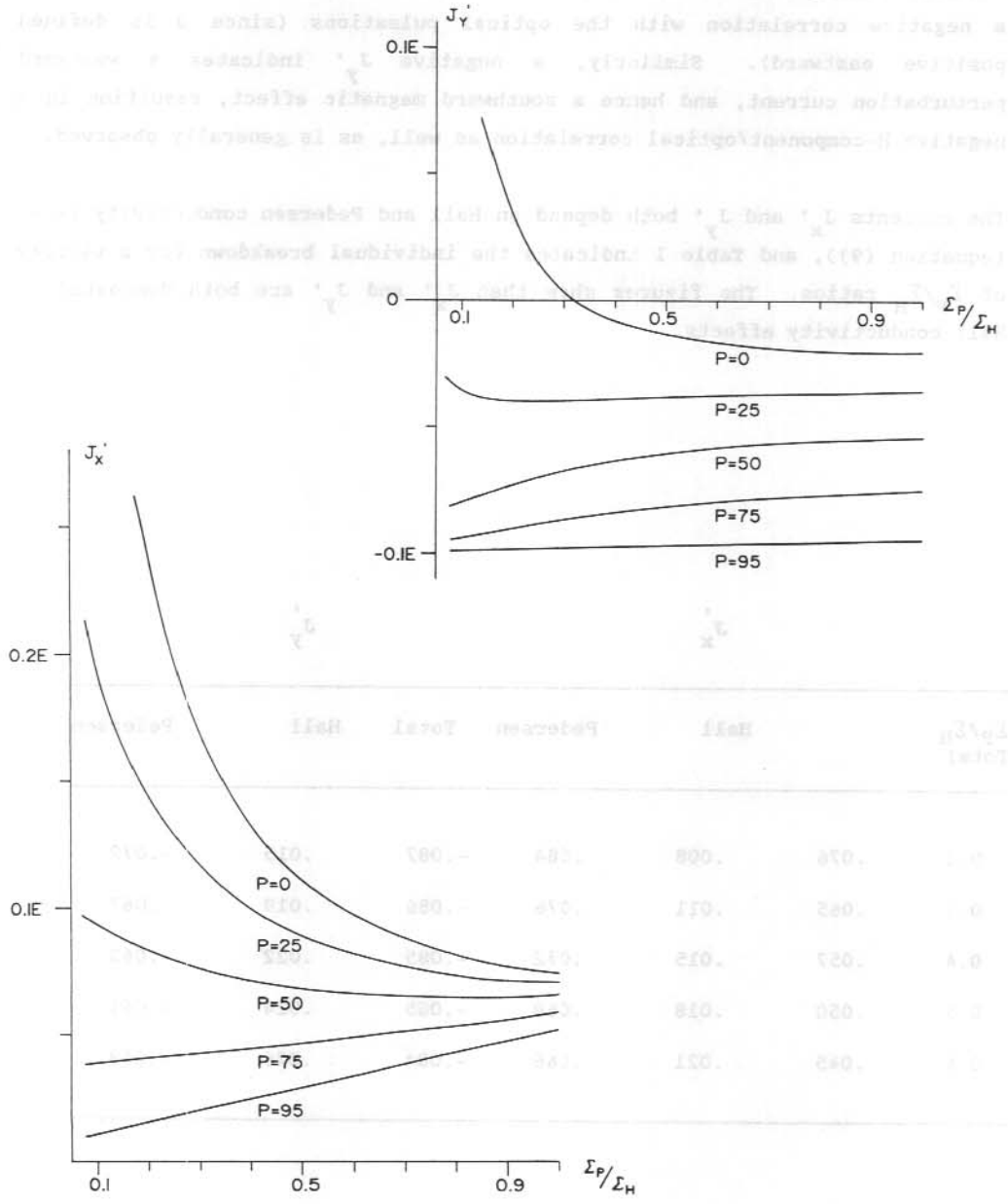

Figure 7. Computer generated plots of the equatorward (J_x') and easterly (J_y') modification currents inside the region of enhanced conductivity.

Measurements indicate that $\Delta\Sigma_H$, $\Delta\Sigma_P$ are small (MacDougall et al. 1981), for which the co-efficients, D and cosα turn out to be small. Equation (9) then shows that J_x' arises from the sum of Hall and Pedersen contributions, whilst J_y' is the result of a difference of terms. Our assumption is that Hall effects peak prior to the Pedersen. Summing these contributions, as in J_x', will produce a maximum somewhere between the time of the Hall and Pedersen peaks, whilst the difference of these terms, as in J_y', will tend to advance the overall peak slightly ahead of the Hall fluctuation maximum. This predicts that the H-component pulsations (from J_y'), should lead the D-component (from J_x'), as is typically observed (see Figure 3(c)).

For the conditions $\Sigma_P/\Sigma_H \geq 0.25$ and 25%< P <75% Figure 7 shows that $J_x'>0$, and $J_y'<0$, so that both magnetic components will always yield negative correlations with the optical pulsations under typical ionospheric conditions. As noted, positive correlations do occur. These are most likely attributed to rotations of the E-region electric field itself. Our data indicate that the occurrence of positive correlations is restricted to early evening and late morning hours, at times when rotations of the E-region electric field are likely (Rostoker and Hron 1975).

Consider what transpires as the E-region electric field rotates clockwise from its normal equatorward orientation. With an eastward electric field, there will be an eastward current, being the sum of Hall and Pedersen effects, producing a positive H-dot correlation. The difference current now flows north producing a negative D-dot correlation, and the authors predict that it must now lead the H-component fluctuation. Continuing this argument, an E-region electric field directed south results in southward (positive D-dot) and eastward (positive H-dot) currents, with the H-component magnetic fluctuation leading the D-component again. Finally a westward electric field generates westward (negative H-dot) and southward (positive D-dot) currents with the D-component leading. These predictions are strongly borne out by the lead/lag data shown in Figure 3.

2.5 CONCLUSION

The theoretical model reproduces all the salient features of the observational data set for reasonable values of the relevant ionospheric

parameters. Further consideration of the field-aligned contribution would be desirable however.

A final step required is to calculate the magnitude of the expected ground magnetic disturbances and compare these with the observations.

2.6 REFERENCES

Arnoldy, R.L., Dragoon, K., Cahill, L.J., Mende, S.B. and Rosenberg, T.J. (1982). Detailed correlations of magnetic field and riometer observations at L=4.2 with pulsating aurora. Journal of Geophysical Research 87:10449-10456.

Brekke, A., Doupnik, J.R. and Banks, P.M. (1974). Incoherent scatter measurement of E-region conductivities and currents in the auroral zone. Journal of Geophysical Research 79:3773-3790.

Bryant, D.A., Smith, M.F. and Courtier, G.M. (1975). Distant modulation of electron intensity during the expansion phase of an auroral substorm. Planetary Space Science 23:867-878.

Burns, G.B. and Cole, K.D. (1985). Ionospheric sources of Pi(c) pulsations. Journal of Atmospheric and Terrestrial Physics 47: 587-599.

Campbell, W.H. (1970). Rapid auroral luminosity fluctuations and geomagnetic field pulsations. Journal of Geophysical Research 75: 6182-6208.

Cresswell, G.R. and Davis, T.N. (1966). Observations on pulsating auroras. Journal of Geophysical Research 71:3155-3163.

Engebretson, M.J., Cahill, L.J., Arnoldy, R.L., Mende, S.B. and Rosenberg, T.J. (1983). Correlated irregular magnetic pulsations and optical emissions observed at Siple Station, Antarctica. Journal of Geophysical Research 88:4841-4852.

Francis, W.E. and Karplus, R. (1960). Hydromagnetic waves in the ionosphere. Journal of Geophysical Research 65:3593-3600.

Heacock, R.R. (1967). Two subtypes of type Pi micropulsations. Journal of Geophysical Research 72:3905-3917.

Johnstone, A.D. (1978) Pulsating aurora. Nature 274:119-126.

Jones, R.A. and Rees, M.H. (1973). Time dependent studies of the aurora, I, Ion density and composition. Planetary Space Science 21:537-557.

MacDougall, J.W., Koehler, J.A., Hofstee, J. and McEwen, D.J. (1981) Ionosonde observations of pulsating auroras. Canadian Journal of Physics 59:1049-1055.

McEwen, D.J., Yee, E., Whalen, B.A. and Yau, A.W. (1981). Electron energy measurements in pulsating aurora. Canadian Journal of Physics 59: 1106-1115.

Oguti, T. (1976). Recurrent auroral patterns. Journal of Geophysical Research 81:1782-1786.

Oguti, T. and Hayashi, K. (1984). Multiple correlation between auroral and magnetic pulsations 2. Determination of electric currents and electric fields around a pulsating auroral patch. Journal of Geophysical Research 89:7467-7481.

Rostoker, G and Hron, M. (1975). The eastward electrojet in the dawn sector. Planetary Space Science 23:1377-1389.

Royrvik, O. and Davis, T.N. (1977). Pulsating aurora: local and global morphology. Journal of Geophysical Research 82:4720-4740.

3. CONJUGATE EFFECTS FROM GROUND EXCITATION OF ULF WAVES IN THE IONOSPHERE

D.J. Webster (1), B.J. Fraser (1), M.T. Rietveld (2) and F.W. Menk (1)

(1) University of Newcastle
Newcastle, N.S.W., Australia, 2308.

(2) Max-Planck-Institut fur Aeronomie
Postfach 20
D-3411 Katlenburg-Lindau, Federal Republic of Germany.

ABSTRACT

An attempt to observe possible conjugate reception of Pcl waves produced by modulated ionospheric heating experiments is reported. A number of successful experiments were conducted in 1984 by the Max-Planck-Institut using the Tromso HF radio transmitters to modulate ionospheric conductivities in the frequency range 0.25 to 8.0 Hz. ULF waves at the modulating frequencies were detected 17 km from the transmitter site. The Newcastle pulsations group operates a ULF induction coil magnetometer at Mawson, the closest station to the conjugate point of Tromso. Recordings taken at Mawson during the heating experiments have been spectrally analysed using digital pure state detection techniques to search for conjugate effects. The results obtained and their interpretation are presented.

3.1 INTRODUCTION

A series of ionospheric heating experiments were conducted in February/March 1984 using the HF transmitter facilities at Tromso (Rietveld, 1985). A heating frequency of 4.04 MHz and 270 MW effective radiated power, illuminating an area of ionosphere approximately 30 km in diameter, was modulated at ULF frequencies ranging from 0.25 to 8.0 Hz. In most cases the modulation was turned on for pulse durations of 3.5 minutes with 2.5 minute intervals between.

An induction coil magnetometer, situated 17 km from the heating facility, was used to monitor any Pcl waves excited by the modulation of ionospheric currents. Figure 1 shows the spectrogram of signals detected on one occasion, corresponding to the modulation times and frequencies. In the

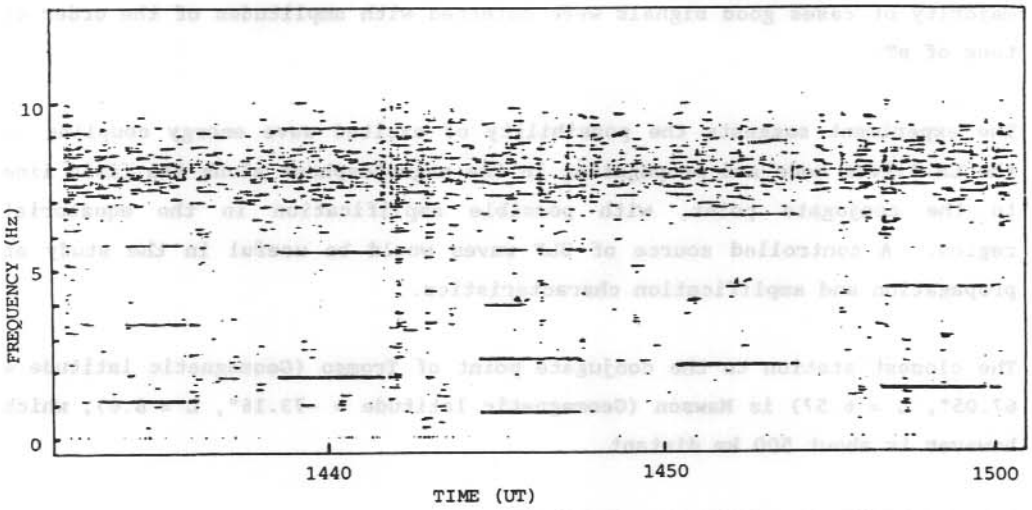

Figure 1. Spectrogram of the EW component of signals detected 17 km from the heating facility (Rietveld 1985). Odd harmonics are due to the square wave modulation.

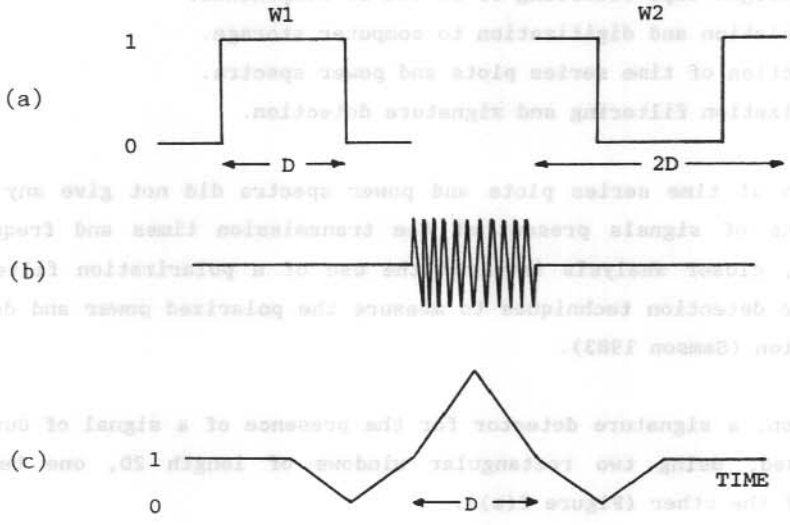

Figure 2. Signature detector for signal of duration D.

(a) Window W1 and its inverse W2

(b) Ideal signal

(c) Approximate response of a sliding detector $R = X_{W1}/X_{W2}$

majority of cases good signals were detected with amplitudes of the order of tens of pT.

The experiment suggests the possibility of excited wave energy coupling to the LH Alfven mode and propagating in the magnetosphere along the field line to the conjugate point, with possible amplification in the equatorial region. A controlled source of ULF waves would be useful in the study of propagation and amplification characteristics.

The closest station to the conjugate point of Tromso (Geomagnetic latitude = 67.05°, L = 6.57) is Mawson (Geomagnetic latitude = -73.16°, L = 8.6), which however is about 500 km distant.

3.2 EXPERIMENTAL DETAILS AND ANALYSIS

The processing stages performed in the conjugate experiment are outlined as follows.

1. Induction coil magnetometer operated at Mawson during the Tromso heating experiment.
2. FM analogue tape recording of NS and EW components.
3. Demodulation and digitization to computer storage.
4. Inspection of time series plots and power spectra.
5. Polarization filtering and signature detection.

Inspection of time series plots and power spectra did not give any obvious indications of signals present at the transmission times and frequencies. Therefore, closer analysis involved the use of a polarization filter using pure state detection techniques to measure the polarized power and degree of polarization (Samson 1983).

In addition, a signature detector for the presence of a signal of duration D was devised, using two rectangular windows of length 2D, one being the inverse of the other (Figure 2(a)).

The two windows W1 and W2, were applied to measurements of:

1. total power,
2. polarized power and
3. degree of polarization,

over the same total time interval 2D. Average values of each measurement were then calculated for each window. The ratio R of measurements of W1 and W2 was used as a signal detector.

Consider an ideal signal of duration D (Figure 2(b)). Then, as the detector is moved over the signal, its output varies approximately as shown (Figure 2(c)).

Measurements of total power, polarized power, degree of polarization and R for each of these, were made at successive intervals of 0.5 minutes, and then displayed in a table format as functions of time and frequency (Figure 3). This enabled a measurement to be viewed in the context of its surroundings and also allowed for an unknown propagation time delay. For the frequencies involved, this was estimated to be between 0.5 and 2.5 minutes.

Results obtained on simulated noise yielded values of degree of polarization averaging about 0.25 and mostly in the range 0.10 to 0.40. R(degree of polarization) averaged about 1.0 and was seldom above 1.5. Therefore the following criteria were adopted in evaluating the measurements.

1. Degree of polarization > 0.4.
2. R(degree of polarization), R(Polarized power) show a positive signature.
3. Satisfy a subjective evaluation of the spectrogram to exclude cases where the signal is obviously part of some other structure.

3.3 RESULTS

In all, forty-three different intervals were analysed, with frequencies ranging from 0.25 to 4.0 Hz, and times between 1200 and 2400 UT (+ 07 for LT) on 29 February to 2 March 1984. None of the intervals clearly satisfied the above criteria.

Figure 3 illustrates a typical case. While a signal at 1.85 Hz shows a positive R(polarized power) signature, the delay of 3 minutes is probably too great. R(degree of polarization) also shows a mildly positive signature, but is part of a region extending to 2.3 Hz. The degree of

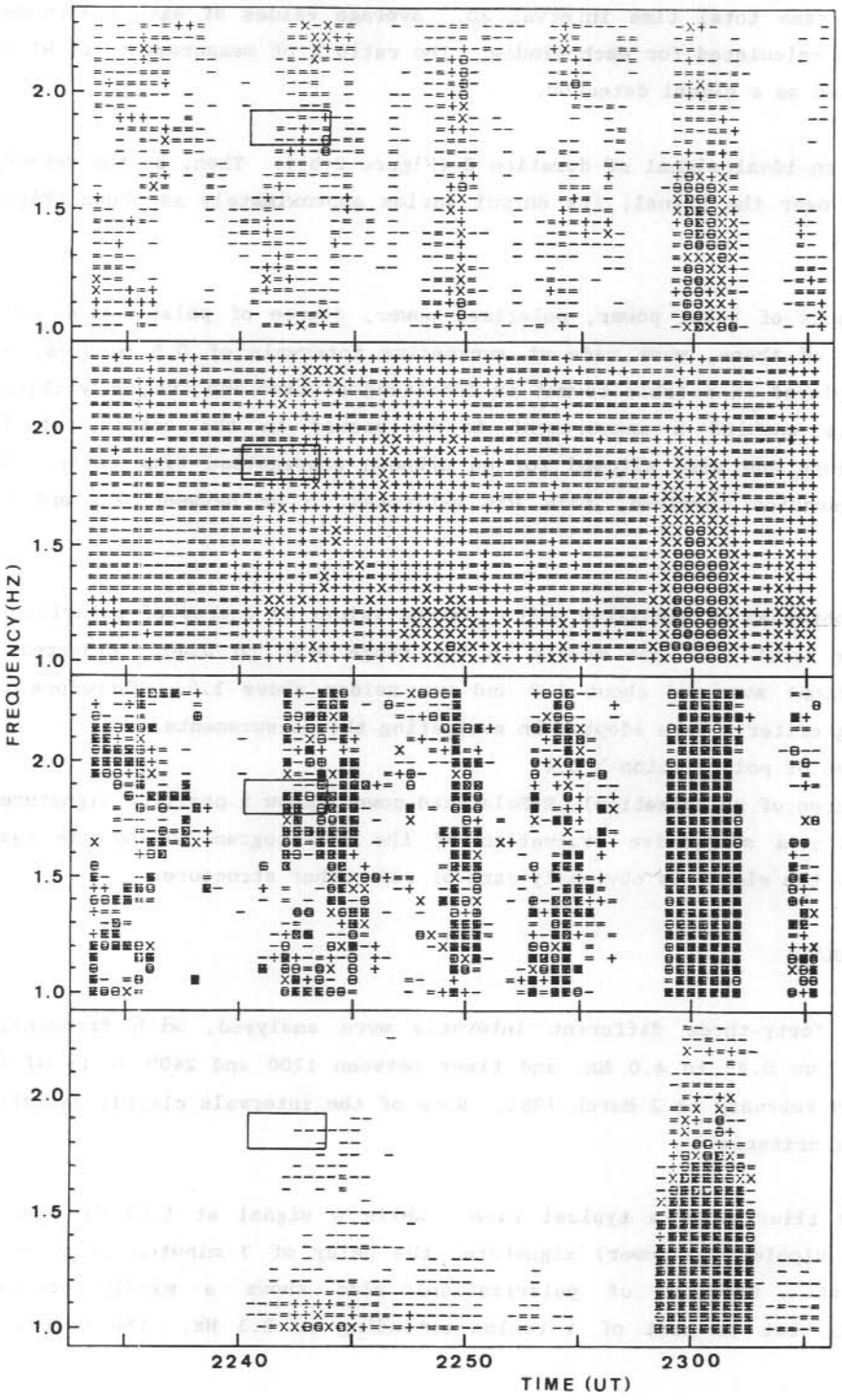
(d)
KEY
100
120 –
140 =
160 +
180 X
200 ⊖
220 ⊜
240 ⊕
260 ⊠
280 ■
(c)
10
20 –
30 =
40 +
50 X
60 ⊖
70 ⊜
80 ⊕
90 ⊠
100 ■
(b)
100
120 –
140 =
160 +
180 X
200 ⊖
220 ⊜
240 ⊕
260 ⊠
280 ■
(a)
30
60 –
90 =
120 +
150 X
180 ⊖
210 ⊜
240 ⊕
270 ⊠
300 ■
FREQUENCY (HZ)
2.0
1.5
1.0
2240
2250
2300
TIME (UT)

polarization is also too low and the polarized power table indicates that it may be part of a wide band signal associated with the strong activity at 0.25 Hz.

3.4 DISCUSSION

The negative result is probably to be expected in view of the following consideration.

1. There are a number of factors affecting the chance of reception. Mawson is a significant distance from the conjugate point, requiring ionospheric F2 ducting with consequent attenuation. In addition, there is attenuation at each ionosphere and during magnetospheric propagation. Amplification would probably be required.
2. The probability of reception is also reduced by the small sample size and limited number of days of transmission. The occurrence of natural Pcl emissions is itself small, indicating that conditions suitable for amplification in the magnetosphere are rare.
3. Although waves at all frequencies were excited equally at Tromso when conditions were favourable, propagation of the higher frequencies may not be likely when the frequency distribution of natural Pcl events at this latitude is considered. Two thirds of the intervals analysed involved frequencies above 1 Hz.

Figure 3. Example: Mawson results for the interval 2233 - 2306 UT 2 March 1984. At Tromso, modulation was at 1.85 Hz during the interval 2238:30 - 2242 UT. Measurements are shown at the centre time of the detector window (3.5 minutes). The small boxes enclose measurements representing propagation time delays of from 0 to 3 minutes. Panels represent (from the bottom):

(a) Polarized power (using window W1). Arbitrary linear scale clipped at a level of 300.

(b) R(polarized power) x 100. A value of 100 represents equal measurements by the two windows, hence no positive signature.

(c) Degree of polarization x 100 (using window W1).

(d) R(degree of polarization) x 100.

4. A good proportion of the transmission intervals occurred at times of auroral activity at Mawson. The ionosphere under these conditions would probably not support F2 duct propagation. There were also times of radio frequency interference. A pre-noon time interval may be more suitable.
5. The local K index at Mawson during the intervals analysed was mostly between 4 and 7, following a quiet period, once again providing unfavourable conditions.

In conclusion, a rigorous examination of data was made with no definite evidence of conjugate reception of ULF waves excited by modulated ionospheric heating.

3.5 REFERENCES

Rietveld, M.T. (1985). Ground and in situ excitation of waves in the ionospheric plasma. Journal of Atmospheric and Terrestrial Physics 47: 1283-1296.

Samson, J.C. (1983). Pure states, polarized waves, and principal components in the spectra of multiple, geophysical time-series. Geophysical Journal of the Royal Astronomical Society 72:647-664.

4. GROUND-SATELLITE STUDIES OF Pc1 PULSATION PROPAGATION

W.J. Kemp (1), B.J. Fraser and D.J. Webster
Physics Department
University of Newcastle
Newcastle, N.S.W., Australia, 2308.
(1) Now at Physics Department
University of New England
Armidale, N.S.W., Australia, 2350.

ABSTRACT

The magnetospheric generation and propagation characteristics of ion cyclotron waves associated with Pc1 emission observed on 16 December 1977 between 1540-1615 UT in a frequency band 0.5-0.8 Hz by a network of four middle and low latitude ground stations are determined using ground source location techniques and ISEE-1 plasma data. The source region at L = 4.7 ± 0.7 is determined at ionospheric heights using signal arrival times at the four ground stations assuming an elliptical wavefront geometry for propagation in the F2 region ionospheric duct. This is just inside the steep plasmapause seen by ISEE-1 at L = 4.9 ± 0.1. The ion cyclotron wave packet interhemispheric bounce period measured from the ground spectra increases with time from 140 to 155 s during the event but is in agreement with dispersion calculations undertaken using ISEE-1 electron density and cool to cold ion composition data in a H^+ plasma with 8-10% He^+ and ≤ 1% O^+ ions. The Pc1 emission band seen on the ground (0.5-0.8 Hz) corresponds to the propagation region between the equatorial O^+ and He^+ characteristic frequencies. With these results it is possible to completely describe the wave generation mechanism and the magnetosphere-ionosphere propagation characteristics for this event.

4.1 INTRODUCTION

It is well known that Pc1 (0.2-5 Hz) geomagnetic pulsations observed on the ground are generated by an ion cyclotron resonance interaction in the magnetosphere between hydromagnetic waves and energetic protons (Mauk and McPherron 1980, Roux et al. 1982). The waves propagate as left-hand (LH) polarised ion cyclotron wave packets along field-aligned paths in the

magnetosphere to the ionosphere where some of the energy is coupled to the right-hand (RH) mode and propagates by way of the F2 region ionospheric duct from the secondary source at the foot of the field line to higher and lower latitudes (Manchester 1968). The remaining energy is reflected back into the magnetosphere and gives rise to a wave packet bouncing between hemispheres.

An important aspect of the theory of structured Pc1 pulsations is the precise location of the region of generation and amplification and the associated L value of the field line along which they propagate. Theoretical studies of ion cyclotron instability processes (Kennel and Petschek 1966, Criswell 1969) suggest that the waves are generated in the equatorial L = 4-8 region of the magnetosphere during the recovery phase of magnetic storms, when the plasmapause expands into the spatial region of the ring current. This suggests a source region in the vicinity of the plasmapause (Cornwall et al. 1970, Kawamura et al. 1982). This conclusion is supported by the absence of structured Pc1 emissions at synchronous orbit (L = 6.6) (Perraut 1982) which is generally at a higher altitude than the plasmapause except during the late afternoon and evening in the dusk bulge region. On the other hand, unstructured emissions characteristic of high latitudes on the ground are seen predominantly at synchronous orbit (Perraut et al. 1984).

Recently a method to study the wavefront geometry and locate the ionospheric source region with an accuracy of ± 3-4° in latitude and longitude has been discussed in detail by Kemp (1983) and briefly by Fraser et al. (1984). This method determines an elliptical wavefront shape using the full correlation analysis technique employed in ionospheric drift analysis measurements. The source location of the event and group velocities are determined from the time delays in the arrival time of the wavefront at four stations. The number of stations required may be reduced if reliable polarization data are available to contribute to the source location (Webster and Fraser 1985).

The most conclusive way to estimate the reliability and accuracy of ground-based source location techniques is to relate the results to direct observations of the primary source waves in the magnetosphere using spacecraft data. A brief study of a Pc1 emission seen in association with

the electron density profile from a radial outbound ISEE-1 pass identified a source region just inside a steep plasmapause (Kemp 1983, Fraser et al. 1984). A more extensive study of this Pc1 emission, including ISEE-1 wave and ion composition data, are reported in this paper.

The following sections describe the analysis of the Pc1 ion cyclotron wave event recorded on the ground by a network of recording stations in south east Australia in conjunction with corresponding observations of plasma and wave data from an outbound low latitude ISEE -1 pass through the plasmapause region of the magnetosphere. This provides a unique opportunity to relate ground spectral observations with wave propagation mechanisms in the magnetosphere.

4.2 SOURCE LOCATION

Pc1 emission wave energy is propagated from a reasonably localized high latitude ionospheric secondary source region at the foot of the field line to middle and low latitude stations in the ionospheric duct. It is assumed that the signal wavefront expands outwards with time from this source region in a series of concentric ellipses. The ellipse parameters are calculated from the full correlation analysis technique used in ionospheric drift analysis measurements (Briggs 1984). The basic problem involves the determination of a large scale amplitude distribution observed at a limited number of spaced stations. Here the amplitude distribution is the spatial shape of the localized wavefront. By equating the distance between the source and the wavefront ellipse to the group velocity, the group velocity and the source region position can be determined from measured propagation time delays between four stations (Kemp 1983).

Observations of the wave polarization vector in the plane of the earth may also be used to locate the source of ducted emissions. If homogeneous plane waves propagate in the duct the major axis of a linearly polarized ellipse will indicate the group ray direction of arrival (Summers 1974). Horizontal propagation paths in the duct are traced taking into account refraction from f_oF2 gradients. This technique has been used by Webster and Fraser (1985) to locate the high latitude source regions for a number of Pc1 emission events.

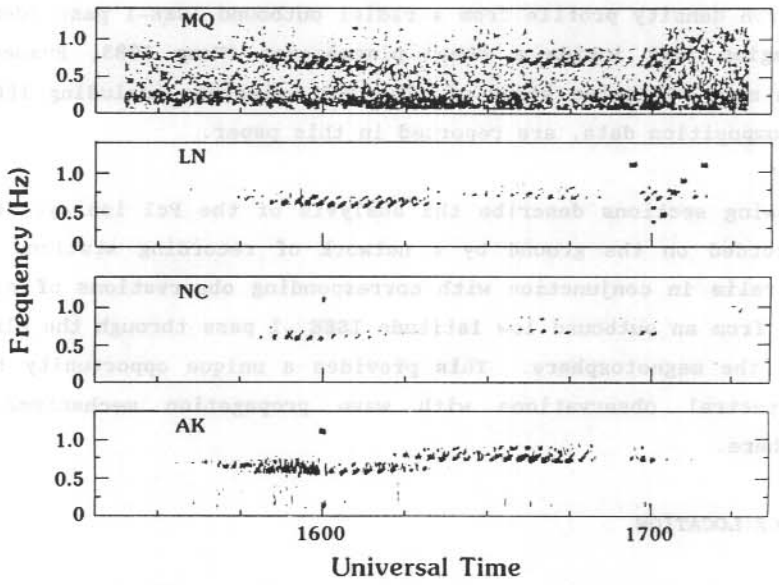

Figure 1. A Pc1 emission event recorded at four stations in Australasia between 1540-1710 UT on 16 December 1977. The stations are Macquarie Island (MQ, L = 4.3), Launceston (LN, L = 2.7), Newcastle (NC, L = 1.8) and Auckland (AK, L = 1.9).

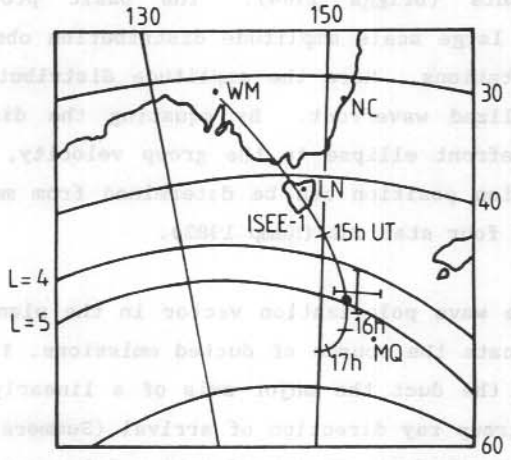

Figure 2. The magnetic field line footprint for the outbound ISEE-1 orbit and the corresponding Pc1 emission source location on 16 December 1977 between 1540-1620 UT. The solid circle on the ISEE orbit indicates the location of the plasmapause determined from the electron density profile.

The dynamic spectra observed at four stations for the Pc1 emission event to be studied are shown in Figure 1. Details of the station locations are given in Fraser (1976) and Webster and Fraser (1985). Two discrete frequency bands are seen from 1540-1620 UT covering a frequency band 0.5-0.8 Hz and from 1612-1700 UT with a bandwidth 0.7-0.9 Hz. For the present study the first event over the time interval 1500-1615 UT was analysed in detail. The full correlation analysis technique yielded a wavefront ellipse geometry with ellipticity of 0.46 ± 0.06 and a major axis directed 18 ± 16° south of east. Using both the time delay and the polarization methods provided an ionospheric source located at L = 4.7 ± 0.7 with an azimuthal spread of ± 4°. This location is plotted as crossed error bars in Figure 2.

4.3 ISEE 1 OBSERVATIONS

At the time of the Pc1 emission event illustrated in Figure 1 the ISEE-1/2 spacecraft pair were outbound in the same local time sector at a latitude of 25°N. The footprint of the magnetic field line passing through the ISEE-1 orbit is plotted in Figure 2. The orbit intersects the error bars of the ground located source region and data from the UCLA fluxgate magnetometer experiment (Russell, 1978) were analysed for wave activity between 1500-1700 UT. Waves at 0.68 Hz with an amplitude of about 1 nT were seen around 1500 UT. At these radial distances (L = 5.5) the earth's field is changing quite rapidly, making it difficult to completely despin the magnetometer data. Furthermore, the spin frequency at 0.7 Hz is almost identical with the wave frequency and prevented a detailed analysis of the wave properties.

The plasma environment over the 1500-1700 UT interval of this outbound ISEE-1 is summarized in Figure 3. The top plot shows the electron density data deducted from the University of Iowa plasma wave experiment (Anderson, private communication) and indicating a sharp plasmapause changing density from 150 to 4 cm^{-3} over a range of 0.2 Re at L = 4.9. The time here is about 03 LT and steep plasmapause gradients are typical during the early morning night-time hours. The location of the Pc1 emission source determined using ground-based measurements is indicated by the dashed vertical line with error bars at L = 4.7 ± 0.7. From the error range it can be seen that the source may be inside, on, or outside the plasmapause. However, wave packet bounce period results presented in the next section verify that the source must be in the high density region, inside the

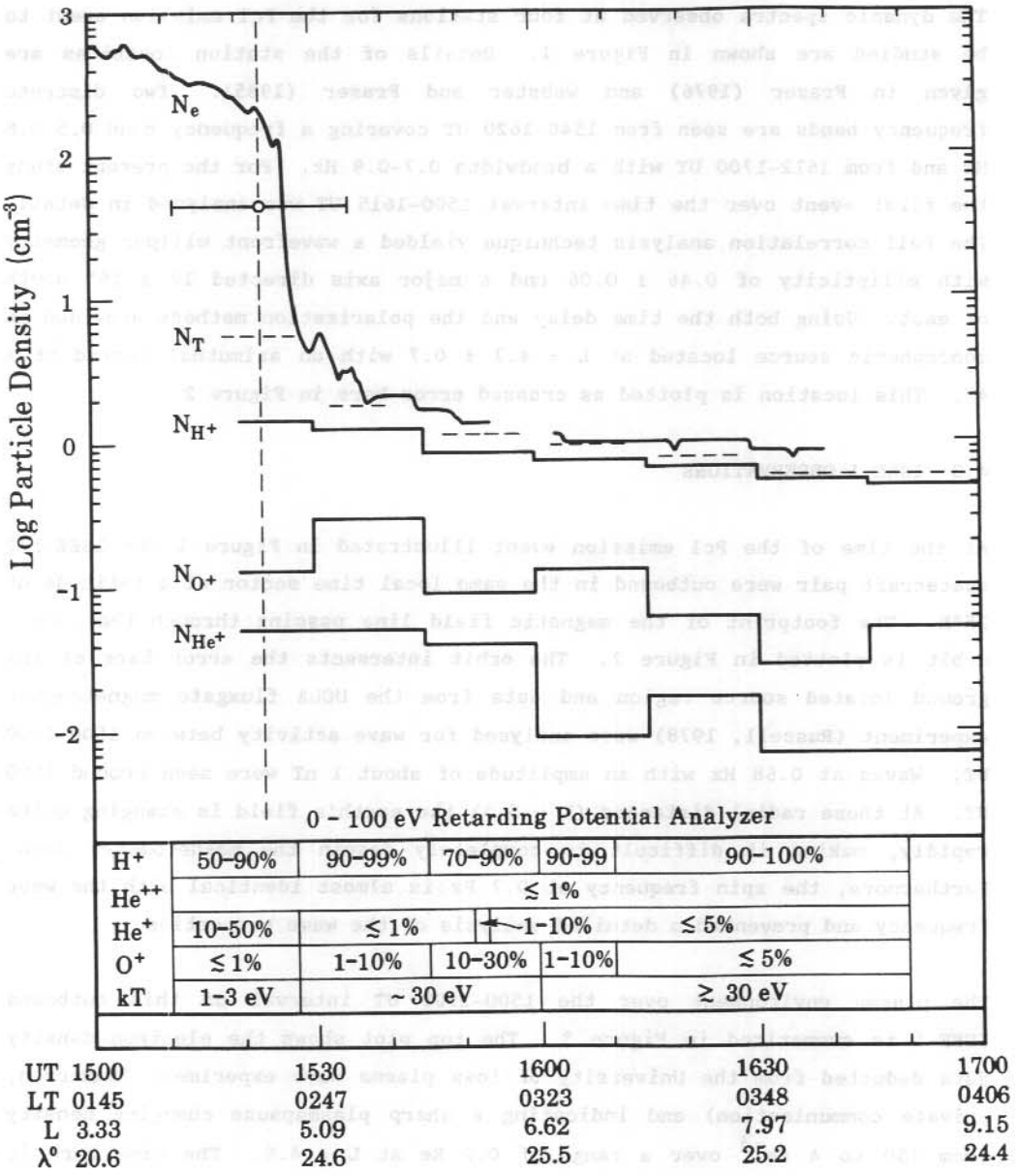

Figure 3. The plasma environment observed by ISEE-1 in association with the Pc1 ion cyclotron wave emission. The vertical dashed line with error bars at L = 4.7 ± 0.7 indicates the radial location of the Pc1 source.

plasmapause. The three lower plots, labelled N_{H^+}, N_{O^+}, and N_{He^+} indicate the densities of the 0.1-16 keV/e warm plasma constituents observed by the Lochkheed retarding potential analyser (RPA) and averaged over 20 minute intervals (Lennartsson, private communication). The density N_T (dashed bars) represents the total ion density in the energy range 0.01-16 keV/e. In the plasma trough (L > 5.0) this closely matches the sum of the 0.1-16 keV/e constituents plotted indicating that there is very little <100 eV cool plasma in the trough which is a warm region. However, inside the plasmapause at L = 4.9 (~1520 UT) N_T is well in excess of the sum of the warm constituents (0.1-16 kev/e) and is over an order of magnitude lower than N_e. This indicates the presence of a cooler (10-100 eV) plasma and the predominance of a cool-cold (<10 eV) plasma in the plasmasphere. The tabulations at the bottom of Figure 3 show rough estimates of the 0-100 eV/e thermal ions from the RPA experiment. The various ions are indicated on the left and estimates assume a flowing Maxwellian for each ion species. Precise values of number densities cannot be evaluated because of large and rapid fluctuations in both densities and flow velocities. In the plasmasphere around L = 4.9 the plasma is predominantly H^+ (50-90%) and He^+ (10-50%) with very little O^+ (< 1%). The warm and cool plasma observations will be used in Sections 4.4 and 4.5 to model the ion cyclotron wave propagation and wave instability mechanisms for the Pc1 emission event.

4.4 WAVE PROPAGATION

For ion cyclotron wave propagation the magnetosphere is considered a zero temperature neutral plasma containing electrons, protons, and He^+ and O^+ heavy ions. If the 0-100 eV ion relative concentrations in Figure 3 are considered representative of the cold plasma, which may not be unreasonable within the plasmasphere, then it is possible to calculate reasonably accurately the group travel time bounce period for the ion cyclotron wave packet propagation. This may then be compared with measured bounce periods which relate to the fine structure element spacing seen in the emissions in Figure 1.

The calculations are based on the method developed by Fraser (1972). The group refractive index of the ion cyclotron wave takes the form

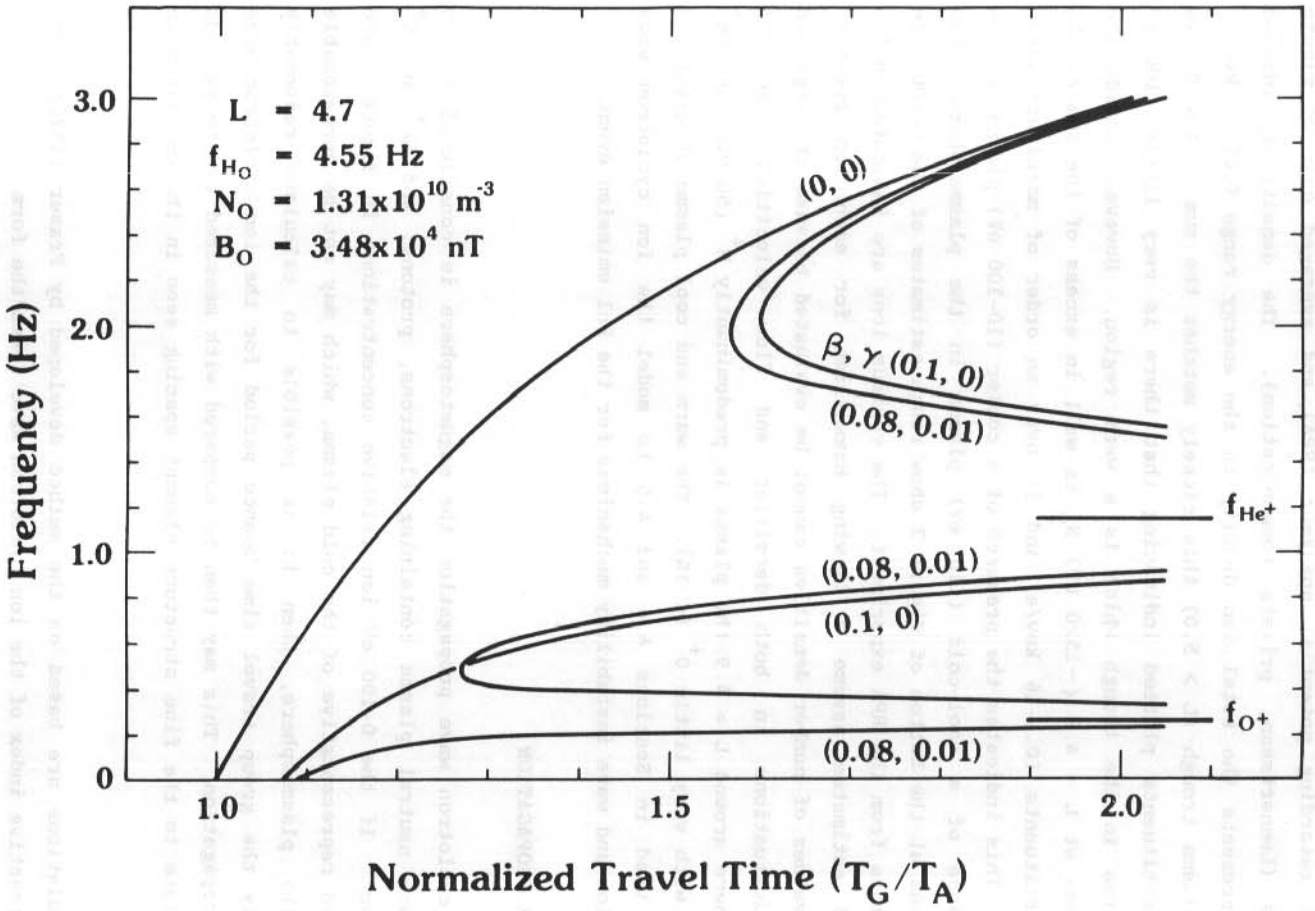

Figure 4. Dispersion curves for LH mode ion cyclotron wave propagation along the L = 4.7 field line in multiple ion plasma. The relative fractional concentrations of He^+ and O^+ (β,) are given in parentheses.

$$\mu'(\lambda,\beta,\gamma) = \mu_A \left| \frac{1-\lambda/2}{(1-\lambda)^2} - \frac{\beta(8\lambda-4)}{(4\lambda-1)^2} - \frac{\gamma(128\lambda-16)}{(16\lambda-1)^2} \right| \cdot \left| \frac{1}{(1-\gamma)} - \frac{4\beta}{(4\lambda-1)} - \frac{16\gamma}{(16\lambda-1)} \right|^{-1/2} \quad (1)$$

where λ is the wave frequency normalized to the proton cyclotron frequency, β the fractional He^+ ion concentration, γ the fractional O^+ ion concentration and μ_A the refractive index at zero frequency in the absence of He^+ and O^+ ions ($\beta=\gamma=0$).

The double hop transit time of an ion cyclotron wave packet bouncing between hemispheres is given by

$$T_G(\lambda,\alpha,\beta,\gamma) = 2/c \int_{path} \mu'(\lambda,\beta,\gamma)ds \quad (2)$$

where α is the fractional concentration of the protons and $\alpha+\beta+\gamma = 1$.

In order to undertake this integration a dipole field model is assumed with $B = B_o L^{-3}$ in the equatorial plane with B_o chosen to provide a main field magnitude agreeing with that measured by ISEE-1 at 24°N latitude and mapped back to the equator. A plasma density distribution model $N = N_o L^{-3}$ is used with N_o chosen to provide N which matches the measured electron concentration (N_e) at L = 4.7. It is assumed that the ion and electron densities at the equator are the same as those measured by ISEE -1 off the equator. The major contribution to T_G occurs close to the equator and to avoid the singularities associated with the F_{He^+} and the O^+ cyclotron frequency f_{O^+} (λ = 0.25 and 0.063) it is assumed that the He^+ and O^+ ions are confined to within latitudes ± 10° of the equator. Plots of the normalized travel time T_G/T_A, where T_A is the Alfven (zero frequency) travel time, are shown in Figure 4. The He^+ and O^+ heavy ion concentrations used to plot Figure 4 were 8% He^+ with 1% O^+ (0.08, 0.01) and 10% He^+ with no O^+ (0.1, 0). The dispersion curve for a pure H^+ plasma (0, 0) is also plotted. The He^+ concentrations chosen represent the lower end of the measure 10-50% contribution indicated by the cool ions in Figure 3. It will be shown later that this He^+ concentration provides the best agreement with experimental results. There are two non-propagation stop-bands indicated in

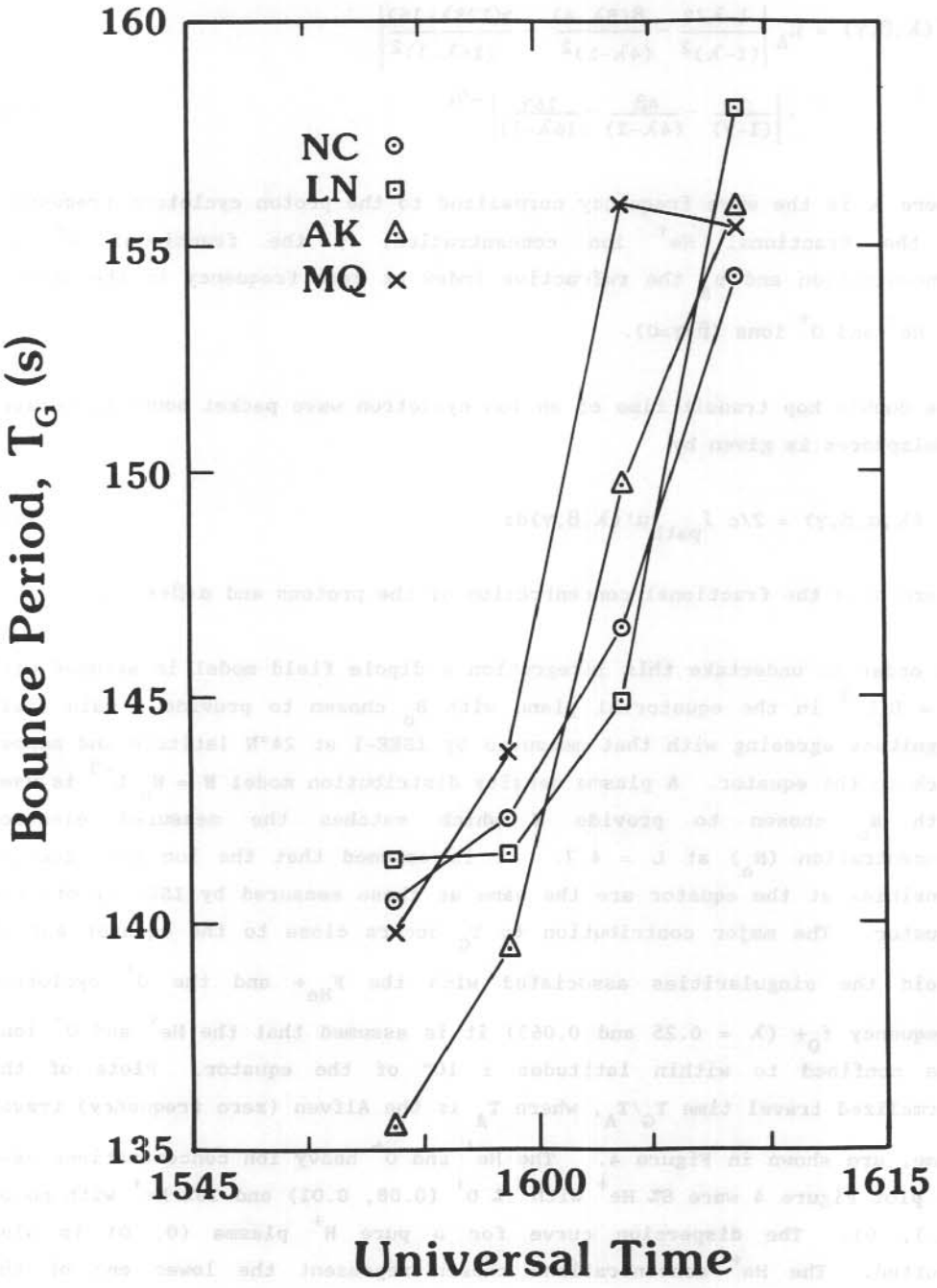

Figure 5. Experimentally determined ion cyclotron wave packet group bounce period. Data relate to the fine structure element spacing in the 0.57-069 Hz bandwidth slice through the dynamic spectra shown in Figure 1.

Figure 4, one between f_{O^+} and the O^+ cutoff frequency, and the other between f_{He^+} and the He^+ cutoff frequency (Young et al. 1981, Fraser and McPherron 1982). Since parallel propagation is assumed there is no crossover of wave modes.

It is now of interest to compare the dispersion results in Figure 4, which indicate allowed propagation bands and expected normalized travel times, with experimental data determined from the wave properties shown in Figure 1. The computed T_G travel times should relate to the fine structure element spacing seen in the wave spectra which is a measure of the wave packet double hop bounce period. The measured bounce periods for the four stations over the 1553-1609 UT interval were determined using envelope detection and spectral analysis techniques described by Samson (1983) and are plotted in Figure 5 over this time interval and in a bandwidth 0.57-0.69 Hz. The bounce period shows a systematic increase with time at all stations from 140 s to 155 s. Increases in T_G with time may indicate that the wave source is slowly drifting to higher L shells (Fraser 1968) or is associated with a changing plasma density with time. However, a change in plasma density over such a short time may not be expected since the plasmapause region is stable in this early morning local time sector (Higel and Lei 1984). The segments of the dispersion curves from Figure 4 over the 0.4-0.8 Hz frequency band between f_{O^+} and f_{He^+} are plotted in Figure 6.

Superimposed on this figure is a box showing the range of experimentally measured bounce periods ΔT_G = 155-140 s over a bandwidth Δf = 0.69-0.57 Hz. It should be remembered that the overall emission bandwidth was 0.5-0.8 Hz over the considered time interval. The wave packet bounce periods calculated from dispersion theory with concentrations of He^+ of 8 and 10% and O^+ of 0 and 1% agree well with the measured bounce periods. With a fixed O^+ concentration of 1% the minimum and maximum limits placed on the He^+ concentration by the box are 6% and 12%.

4.5 DISCUSSION AND CONCLUSIONS

It has been shown that the source of a structured Pc1 ion cyclotron emission event is in the high density plasmasphere at L = 4.7 ± 0.7, just inside a steep plasmapause at L = 4.9 ± 0.1. An associated ISEE-1 outbound pass

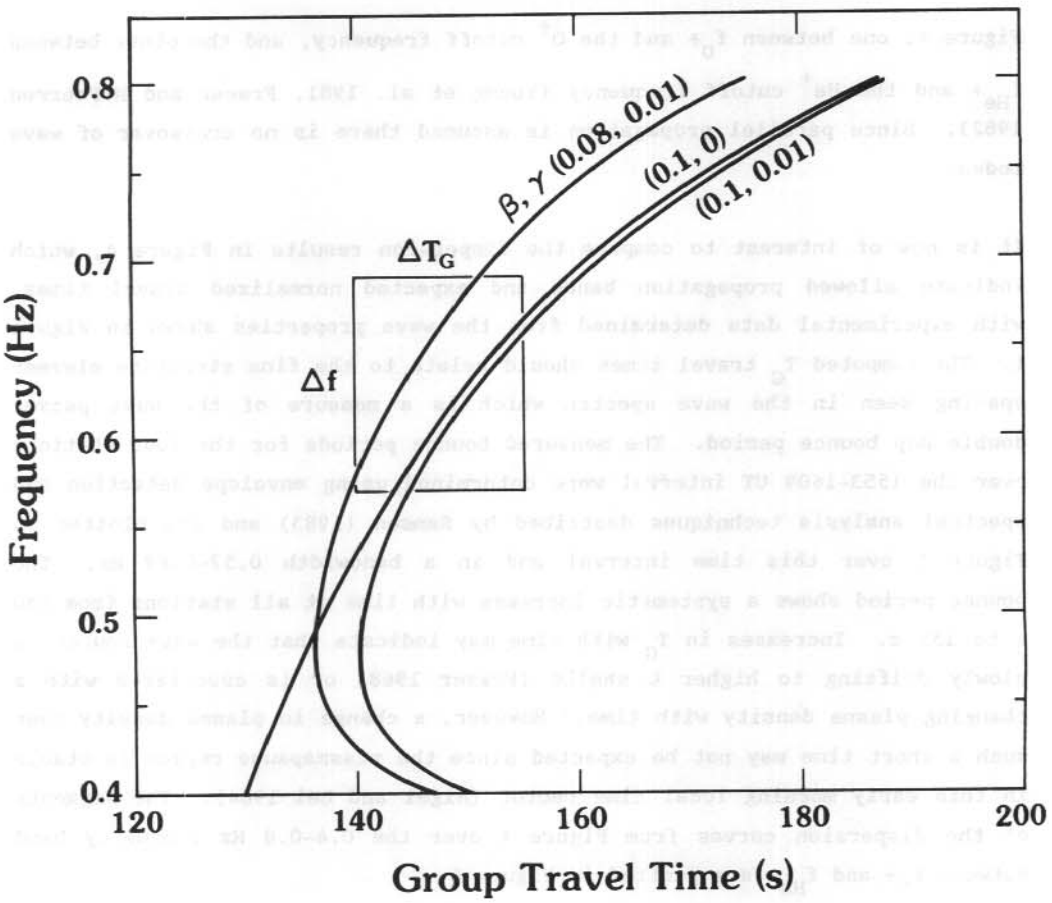

Figure 6. A section of the dispersion curves in Figure 4 for the frequency range 0.4-0.8 Hz. Also shown is the Δf, ΔT_G box defined by the experimental results with Δf = 0.69-0.57 Hz and ΔT_G = 155-140 s.

identified signal amplitudes of 1 nT at the same frequency but the spacecraft magnetometer data could not be analysed because of spin contamination. However, ISEE-1 plasma data providing the electron, and warm (0.1-16 keV/e) and cool (< 100 eV/e) H^+, He^+ and O^+ ion radial profiles were available. These data were used to determine the dispersive propagation characteristics of an ion cyclotron wave packet bouncing between hemispheres along the L = 4.7 field line in a multicomponent plasma. The bounce periods were found to agree with those measured experimentally from the Pc1 emission fine structure element spacing (Figure 1) provided the He^+ and O^+ concentrations were about 10% and 1% respectively.

The concentration of 10% is at the low end of the 10-50% range suggested from the 0-100 eV/e cool He^+ RPA results in Figure 3. There are a number of arguments that can be suggested to support a lower He^+ concentration than that indicated by the RPA experiment. Firstly, the ISEE-1 0-100 eV/e measurements may not truly represent the cold plasma density. There may be a cold population which is not seen because of the shielding provided by spacecraft charging (Olsen 1982). Charging is a particular problem where the spacecraft is ramming the plasmapause and the high density plasmasphere. Secondly, in the presence of waves the densities estimated from particle detector measurements may be inaccurate by up to one order of magnitude (B.J. Mauk 1985, private communication). Therefore, a lower He^+ fractional concentration of 10% may not be unreasonable.

As the ion cyclotron wave packet propagates down the field line from the equator into an increasing ambient field there will be a location where the wave frequency, which is between the equatorial f_{O^+} and f_{He^+}, will match the local f_{O^+} and be reflected (Dowden 1966). However, if the wave normal angle is non-zero then the LH ion cyclotron wave will undergo a polarization reversal where the wave frequency matches the oxygen crossover frequency. The wave then becomes RH polarized and is not affected by the oxygen cyclotron resonance (Young et al. 1981). In this situation a field aligned duct would be required to guide the RH mode wave energy down to the ionosphere and the ground. Directly under the source RH polarization may be expected. In the present ground data MQ is situated nearest the source (Figure 2) and LH elliptical polarization was observed throughout the wave event. The more distant lower latitude stations showed linear or mixed

linear and RH polarization which is more typical for ionospherically ducted signals. Therefore, it cannot be concluded that the wave undergoes a polarization reversal in the magnetosphere at the O^+ cross over frequency. Alternatively, some of the LH ion cyclotron wave packet energy may tunnel through the cyclotron resonance region (Dowden 1966, Perraut et al. 1984). This is most likely to occur when O^+ concentrations are only a few percent, a situation which is satisfied here with $\approx$ 1% of O^+ ions.

Consideration of the error associated with the source region determination of L = 4.7 ± 0.7 does not eliminate the possibility that the source may be in the low density trough region immediately outside the plasmapause. However, calculation of ion cyclotron wave packet group travel times using the ISEE-1 plasma data for this region gives T_G = 18-20 s which is not a realistic time considering the experimental bounce periods measured were 140-155 s.

In summary, this study provides a consistent description of ion cyclotron wave packets generated by the proton cyclotron instability propagating along a field-aligned path in the plasmasphere just inside the plasmapause and transmitting energy into the F2 region ionospheric duct. The duct then distributes the wave energy over a wide area to ground stations. This integrated result has been made possible by the verification of the ground source location technique by ISEE-1 magnetometer observations and the agreement of ground measured wave packet bounce periods with those calculated using ISEE-1 plasma data.

ACKNOWLEDGMENTS

Thanks are due to C.T. Russell for providing the ISEE-1 magnetometer data, W. Lennartsson and R.R. Anderson for ISEE-1 plasma data and R.L. McPherron and J.C. Samson for helpful discussions. This work was supported by the Australian Research Grants Scheme. Part of the work was undertaken while B.J. Fraser was on study leave at UCLA and R.L. McPherron is thanked for support during this time.

4.6 REFERENCES

Briggs, B.H. (1984). The analysis of spaced sensor records by correlation techniques. MAP Handbook 13:166-186.

Cornwall, J.M., Coroniti, F.V. and Thorne, R.M. (1970). Turbulent loss of ring current protons. Journal of Geophysical Research 75:4699-4709.

Criswell, D.R. (1969). Pc1 micropulsation activity and magnetospheric amplification of 0.2 to 5.0 Hz hydromagnetic waves. Journal of Geophysical Research 74:205-224.

Dowden, R.L. (1966). Micropulsation "nose whistlers". A helium explanation. Planetary and Space Science 14:1273-1280.

Fraser, B.J. (1968). Temporal variations in Pc1 geomagnetic micropulsations. Planetary and Space Science 16:111-124.

Fraser, B.J. (1972). Propagation of Pc1 micropulsations in a proton-helium magnetosphere. Planetary and Space Science 20:1883-1893.

Fraser, B.J. (1976). Pc1 geomagnetic pulsation source regions and ionospheric waveguide propagation. Journal of Atmospheric and Terrestrial Physics 38:1141-1148.

Fraser, B.J., Kemp, W.J. and Webster, D.J. (1984). Pc1 source regions and their relationship to the plasmapause. Proceedings of the Conference on the Achievements of the IMS ESA SP-217:609-613.

Fraser, B.J. and McPherron, R.L. (1982). Pc1-2 magnetic pulsation spectra and heavy ion effects at synchronous orbit: ATS 6 results. Journal of Geophysical Research 87:4560-4566.

Higel, B. and Lei, W. (1984). Electron density and plasmapause characteristics at 6.6 R_E: A statistical study of the GEOS 2 relaxation sounder data. Journal of Geophysical Research 89:1583-1601.

Kawamura, M., Kuwashima, M. and Toya, T. (1982). Comparative study of magnetic Pc1 pulsations observed at low and high latitudes: source region and generation mechanism of periodic hydromagnetic emissions. Proceedings of the Fourth Symposium on Coordinated Observations of the Ionosphere and Magnetosphere in the Polar Regions. Memoirs of National Institute of Polar Research (Japan) Special Issue 22:3-16.

Kemp, W.J. (1983). Multistation observations of Pc1 geomagnetic pulsations at middle and low latitudes. PhD Thesis, University of Newcastle.

Kennel, C.F. and Petschek, J. (1966). Limit on stably trapped particle fluxes. Journal of Geophysical Research 71:1-28.

Manchester, R.N. (1968). Correlation of Pc1 micropulsations at spaced stations. Journal of Geophysical Research 73:3549-3556.

Mauk, B.H. and McPherron, R.L. (1980). An experimental test of the electromagnetic ion cyclotron instability within the earth's magnetosphere. Physics of Fluids 23:2111-2127.

Olsen, R.C. (1982). The hidden ion population of the magnetosphere. Journal of Geophysical Research 87:3481-3488.

Perraut, S. (1982). Wave particle interactions in the ULF range: GEOS-1 and -2 results. Planetary and Space Science 30:1219-1227.

Perraut, S., Gendrin, R., Roux, A. and de Villedary, C. (1984). Ion cyclotron waves: Direct comparison between ground-based measurements and observations in the source region. Journal of Geophysical Research 89:195-202.

Roux, A., Perraut, S., Rauch, J.L., de Villedary, C., Kremser. G., Korth, A. and Young, D.T. (1982). Wave particle interactions near Ω_{He^+} observed on board GEOS-1 and -2. 2, Generation of ion cyclotron waves and heating of He^+ ions. Journal of Geophysical Research 87: 8174-8190.

Russell, C.T. (1978). The ISEE 1 and 2 fluxgate magnetometers. IEEE Transactions on Geoscience Electronics 16:239-242.

Samson, J.C. (1983). Pure states, polarized waves and principal components in the spectra of multiple geophysical time series. Geophysical Journal of the Royal Astronomical Society 72:647-664.

Summers, W.R. (1974). Production mechanisms for the observed behaviour of the low latitude Pc1 polarization ellipse. Planetary and Space Science 22:801-810.

Webster, D.J. and Fraser, B.J. (1985). Source regions of low latitude Pc1 pulsations and their relationship to the plasmapause. Planetary and Space Science 33:777-793.

Young, D.T., Perraut, S., Roux, A., de Villedary, C., Gendrin, R., Korth, A., Kremser, G. and Jones, D. (1981). Wave particle interactions near Ω_{He^+} observed on board GEOS-1 and -2, 1, Propagation of ion cyclotron waves in He^+ rich plasma. Journal of Geophysical Research 86:6755-6772.

5. MORPHOLOGY OF THE MIDDAY RADIO AURORA IN THE SOUTHERN HEMISPHERE

N.N. Voloshinov
Polar Geophysical Institute
Murmansk, 183002, U.S.S.R.

ABSTRACT

A joint Australian/USSR auroral radar experiment was conducted at Mawson and Davis, Antarctica, over the austral 1979-80 and 1982-83 seasons respectively. The experimental technique is described and a statistical analysis of results presented. It is found that:

1. the southern hemisphere midday cusp is always above 74° corrected geomagnetic latitude;
2. the probability of observation of radio auroras with the southernmost Davis radar is maximum under the projection of the midday cusp and depends on solar illumination conditions; and
3. the probability of radio aurora occurrence in this cusp region displays a weak dependence on magnetic activity.

5.1 INTRODUCTION

The high latitude geomagnetic cusp or cleft is the region where solar wind plasma gains direct entry to the magnetosphere independent of other geomagnetic processes. The midday cusp region is thus of great interest to geophysicists, since the solar-terrestrial interaction can be observed directly under its projection onto the earth's surface. The exact location of the cusp has been investigated with all-sky cameras (e.g. Bond and Thomas 1971, Davis and DeWitt 1963, Vorobjev et al. 1975) and using spacecraft observations (Kamide et al. 1976, Gault et al. 1981, Murphree et al. 1981, Meng and Lundin 1986), and by indirect methods such as tracing discrete cusp-associated geomagnetic pulsations (Troitskaya and Bolshakova 1977). Generally the cusp seems to be located between 75° and 79° geomagnetic latitude near the noon meridian. Since optical observations near the midday part of the auroral oval are hindered by sunlight, meteorological conditions and geographic factors (Cogger et al. 1977), and discrete geomagnetic pulsation phenomena may often be masked by the generally high level of background activity at high latitudes (Fraser-Smith 1982). VHF radar

methods of detecting the small scale ionospheric electron density irregularities associated with auroral activity are an attractive alternative method of studying cusp morphology. These irregularities are field-aligned structures and the radar signal must propagate perpendicular to the magnetic field line in the region of interest for the scattered signal to return to the radar site.

VHF radar observations are constrained to restricted regions of the auroral ionosphere by the aspect sensitivity of the radar installation (Ogawa et al. 1980). In the Northern Hemisphere available aspect angles do not permit extensive observation of the midday cusp region. However a limited zone exists in Antarctica where the aspect angle requirement is satisfied at very high latitudes and thus where radar observations of the midday cusp can be obtained without aspect angle restrictions (Cole et al. 1979). Two Australian stations are located within this region: Mawson (geographic coordinates 67°36'S, 62°52'E) and Davis (geographic coordinates 68°35'S, 77°58'E).

An Australian National Antarctic Research Expedition (ANARE) auroral radar was installed and operated at Mawson in 1973 (Zmood 1976) on a frequency of 42.1 MHz. Two major peaks in echo distribution were observed, near 06-07 MLT and near 23-24 MLT. A third minor peak near 15-16 MLT connected with auroral surges (Akasofu 1968) was also found.

Auroral radar observations were subsequently conducted within the framework of a joint USSR/Australian radio aurora experiment. An auroral radar supplied by the Geophysical Institute, Murmansk, was installed and operated by the author at Mawson over 1979-81 and at Davis in 1982-83. This paper describes the experimental techniques used at Mawson and Davis and presents results of a statistical analysis of echo occurrence obtained during the above intervals.

5.2 THE EXPERIMENT

Figures 1 and 2 show aspect angle profiles in terms of corrected geomagnetic co-ordinates for an auroral radar located at Mawson and Davis respectively and assuming a reflection height of 110 km. This is a reasonable altitude

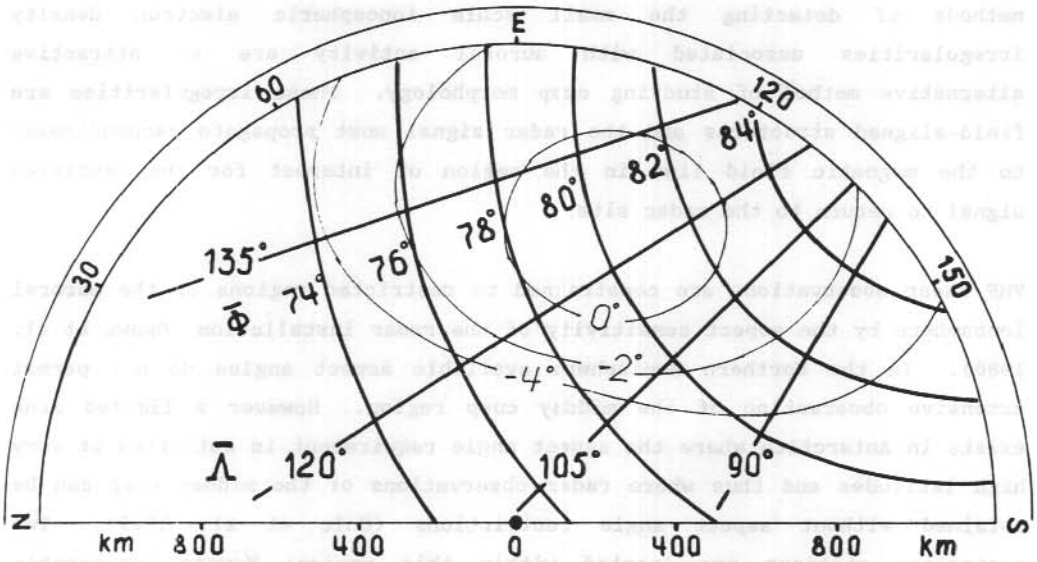

Figure 1. Area observed by the Mawson auroral radar, located at point 'O'. Isolines show aspect angles and corrected geomagnetic coordinates are used. The radio horizon at Mawson due to the Antarctic ice plateau is indicated by the thick dashed line.

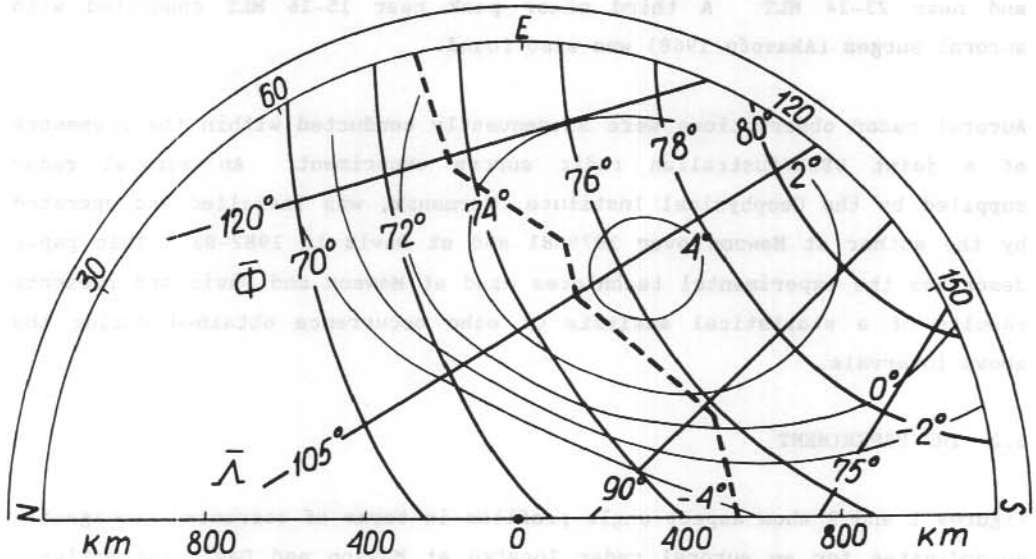

Figure 2. Area observed by the Davis auroral radar, as for Figure 1. Good aspect angle conditions occur over the latitude range 74° - 84°

near which meter-scale electron density irregularities generated by the E-region auroral electrojet may be expected (Ogawa et al. 1980).

Relevant parameters of the radars are summarised in Table 1.

Received echoes were processed by a special analogue computer and averaged over about one second. They were then displayed on a CRT screen in the form of equal amplitude isolines. A photograph of a typical radio auroral return received at Davis is given in Figure 3. The concentric rings indicate range from the radar in 100 km units, the innermost corresponding to a 300 km radius. The '0' mark on the azimuth disc indicates geographic north. The first echo contour corresponds to received signal at the receiver threshold (0.25 μV), and subsequent isointensity contours are separated by 3 dB. Universal time is shown.

The radar performed one sweep every minute. For the purpose of this investigation photographs of returns were checked for echoes at all distances and azimuths at twenty minute intervals. Radio aurora occurrence frequency distributions were thus derived in terms of the range to, and the azmith of, the reflecting region. Referring to the co-ordinate projections given in Figures 1 and 2 it was then possible to determine the dependence of radio aurora occurrence on corrected geomagnetic latitude and local geomagnetic time.

Table 1. Mawson and Davis auroral radar parameters.

Frequency:	88 ~ 92 MHz
Peak pulse power:	60 kW
Pulse width:	8μ sec
Pulse repetition rate:	50 Hz
Receiver noise temperature:	5 kT_D
Pre-detection bandwidth:	125 kHz
Total sensitivity:	0.25 μV
Antenna gain:	18dB (per half)
Antenna beam width:	21° (per half)
Antenna rotation rate:	1 rpm

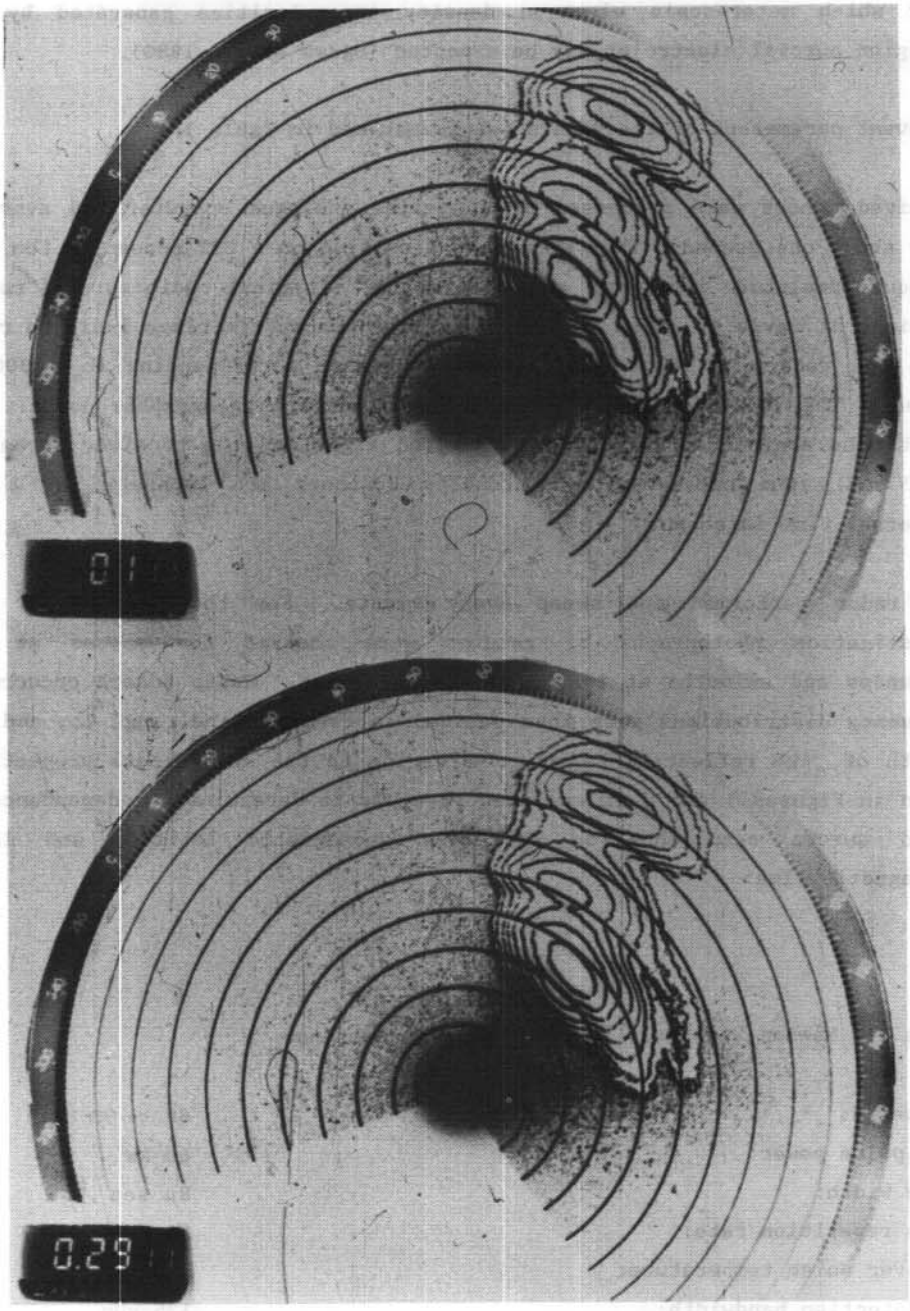

Figure 3. Typical photographs of the auroral radar display. Signal is represented by equal intensity isolines. Circular lines indicate range from the radar to the reflection region, in 100 km units, starting at 300 km from Davis. The 'O' on the azimuth disc indicates the south geographic pole.

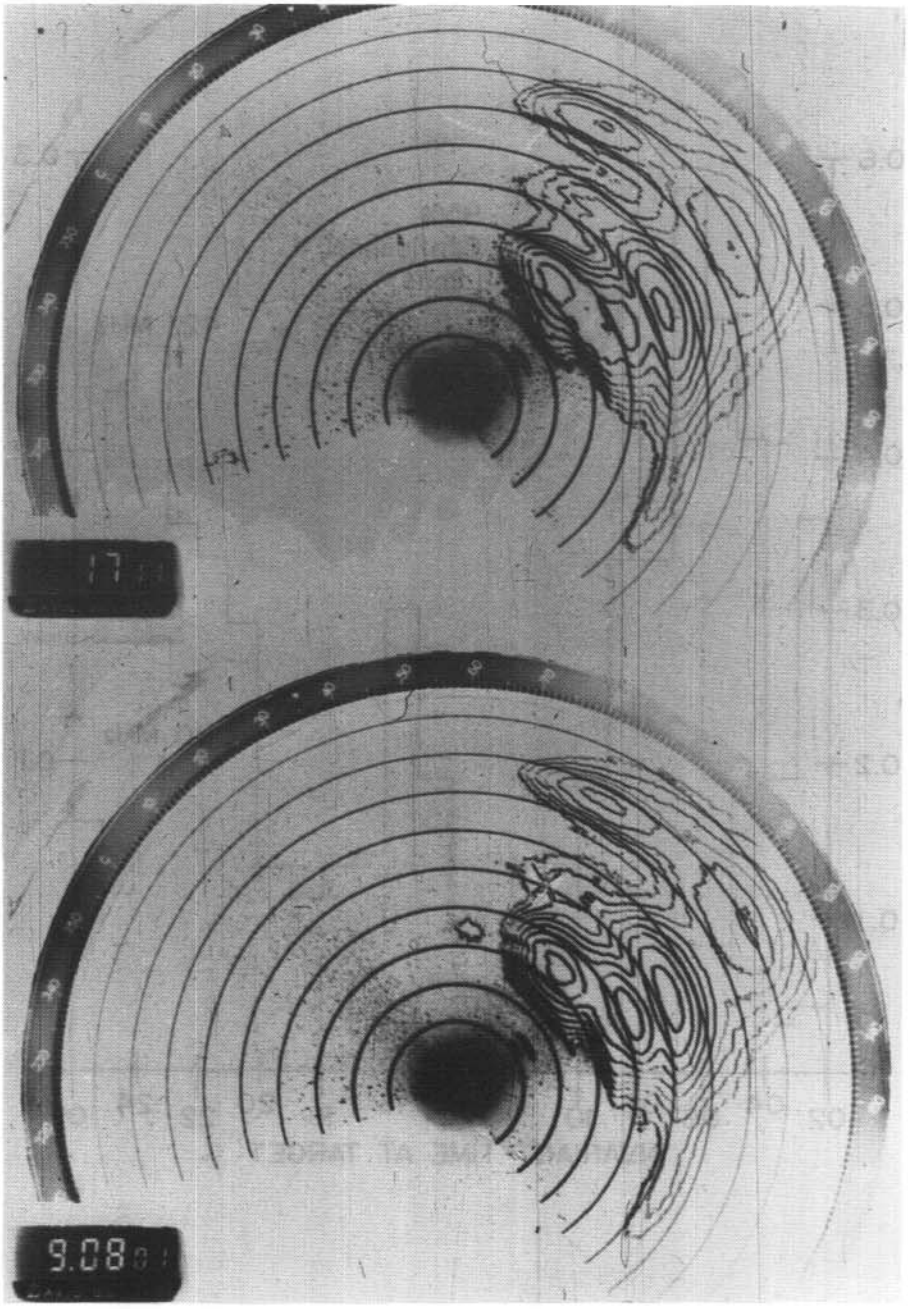
17
9.08

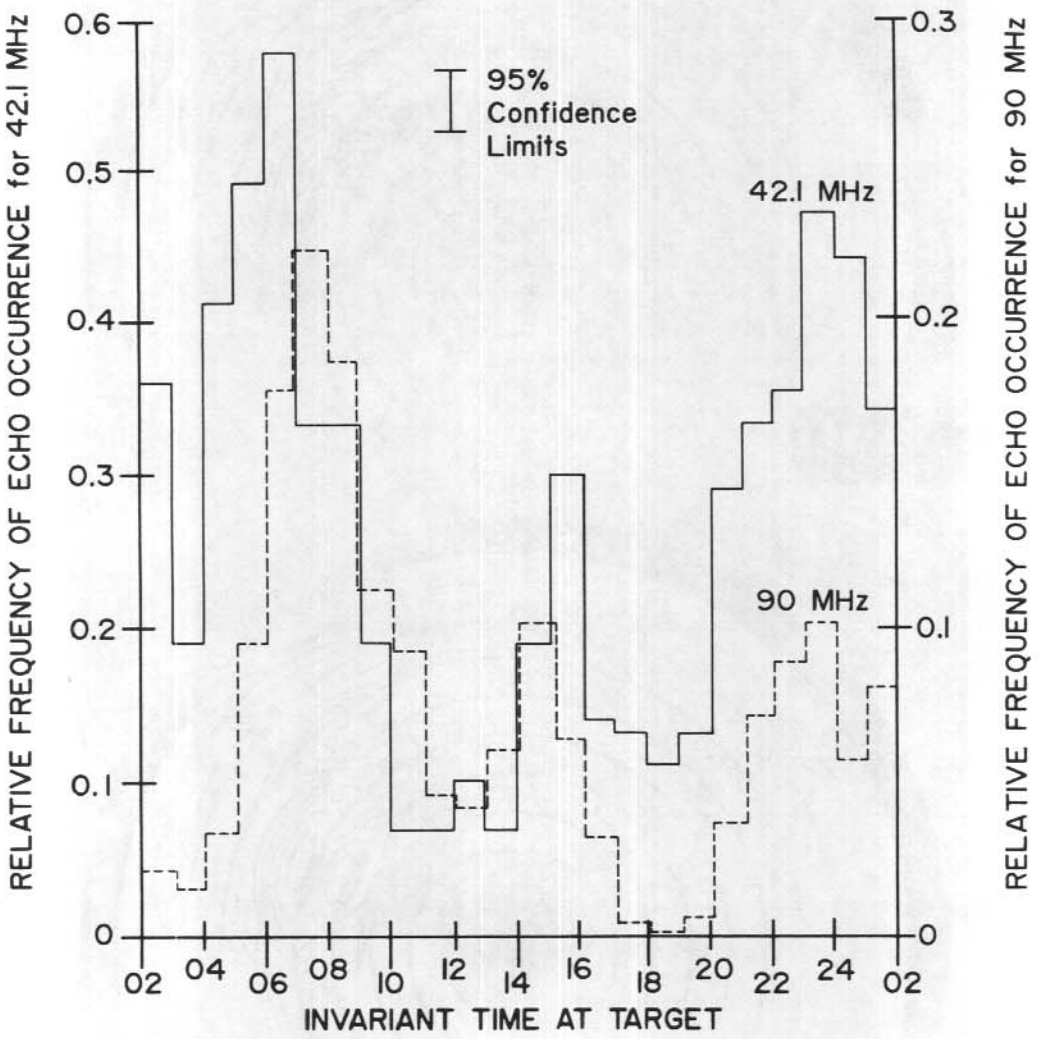

Figure 4. Histogram showing variation in the relative frequency of auroral echo occurrence with time. The solid line shows data from 1973 at 45 MHz (Zmood 1976); dashed line data from 1979 - 1981 at 90 MHz

5.3 RESULTS AND DISCUSSION

5.3.1 Diurnal variation

A histogram showing the average occurrence frequency of radar echoes observed at Mawson over the period May 1979 - April 1981 is shown by the dashed line in Figure 4. Superimposed on this is the occurrence frequency determined at Mawson in 1973 with the ANARE auroral radar operating at 42 MHz (solid line, Zmood 1976). General features of the distributions are similar and may be broadly interpreted in terms of motion of the auroral oval into the region probed by the radar. The different operating frequencies of the radars may account for the slight variations in the exact location and amplitude of the peaks in the distribution. Both histograms lack the midday peak expected from the detection of cusp-associated irregularities.

The heavy dashed line in Figure 1 indicates the auroral radar radiohorizon created by the proximity of the Antarctic ice plateau at Mawson. Consequently the Mawson auroral radar was limited to reflections obtained from up to 74° corrected geomagnetic latitude. Since the 90 MHz echo histogram was obtained from data averaged over all levels of geomagnetic activity we may conclude that the appearance of the cusp at latitudes less than 74° is an event of very low probability.

For the purpose of a morphological study of cusp zone radio auroras, the radar was relocated at Davis early in 1982, where aspect angle conditions permit continuous observation over the range of corrected geomagnetic latitude from 74° to 84°. The occurrence of radar returns at the Davis radar within this range is thus determined solely by geomagnetic processes associated with the appearance of radio auroras.

Figure 5 shows the monthly diurnal variation in radio aurora observation at Davis. The increased probability of radio aurora detection in summer months is most likely connected with the enchanced solar illumination and hence higher conductivity of the polar atmosphere in these months.

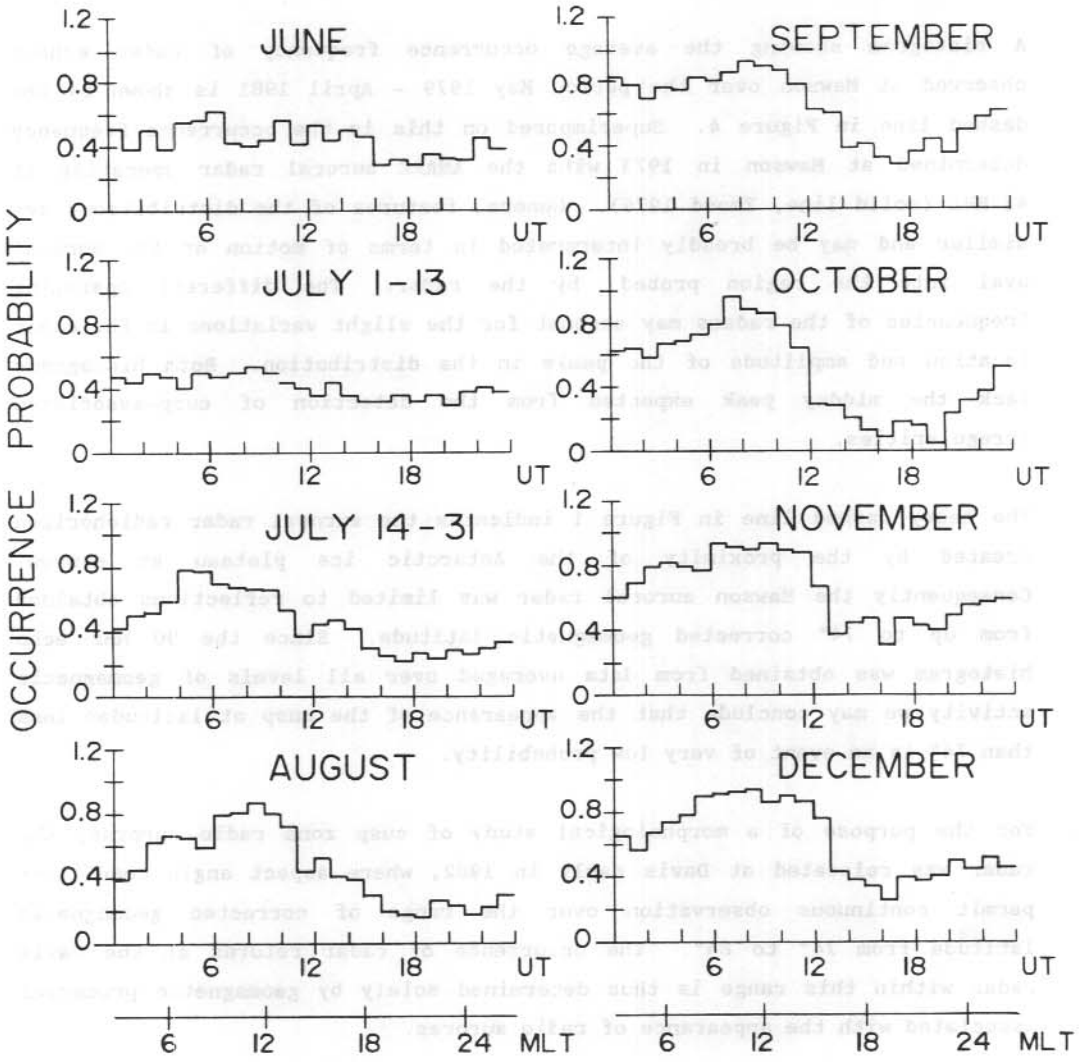

Figure 5. Diurnal variation of the relative frequency of echo detection for different months at Davis over 1982.

5.3.2 Seasonal variation

The enhanced conductivity which exists under the projection of the cusp creates favourable conditions for the connection of field-aligned currents and hence for the appearance of electric fields with levels above the threshold for developing small scale electron density irregularities. Reference to Figure 5 shows that before 15 July winter conditions of solar illumination were present at Davis and a relatively low probability of detecting radio auroras was found. The histograms after 15 July are typical of summer conditions, when the probability of detecting radio auroras at Davis increased to near unity in the noon sector. Thus it is possible to observe radio auroras in the midday cusp region at any level of geomagnetic activity during summer.

The asymmetry in the data around 15 July may be accounted for by the strong increase of conductivity in the polar ionosphere associated with a high energy (>5 MeV) solar proton flux. Strong polar cap absorption (PCA) of greater than 20 dB intensity developed during the period 9–20 July, with another smaller PCA event (maximum 5 dB absorption) occurring from 22–26 July (Benkova et al. 1983).

5.3.3 Dependence on geomagnetic activity

In order to investigate the variation of the location of the cusp with geomagnetic activity all the available Davis auroral radar data were divided into three groups, corresponding to conditions of very quiet geomagnetic activity (daily sum of 3-hourly Kp indices, $K_{sum} < 13$); moderate activity ($13 \leq K_{sum} \leq 30$); and disturbed periods ($K_{sum} > 30$). The respective planetary pictures for these three levels of geomagnetic activity over winter and summer seasons are shown in Figure 6. Two features are present in the data. Firstly, the latitudinal location of the cusp does not appear to vary greatly between winter and summer. Similarly, no pronounced seasonal variation in the local time of maximum radio aurora occurrence, i.e. temporal location of the cusp, is present.

Secondly, the probability of recording radio auroras in the midday cusp region does not depend strongly on magnetic activity. The effect of enhanced magnetic activity is to cause an enlargement of the spatial and

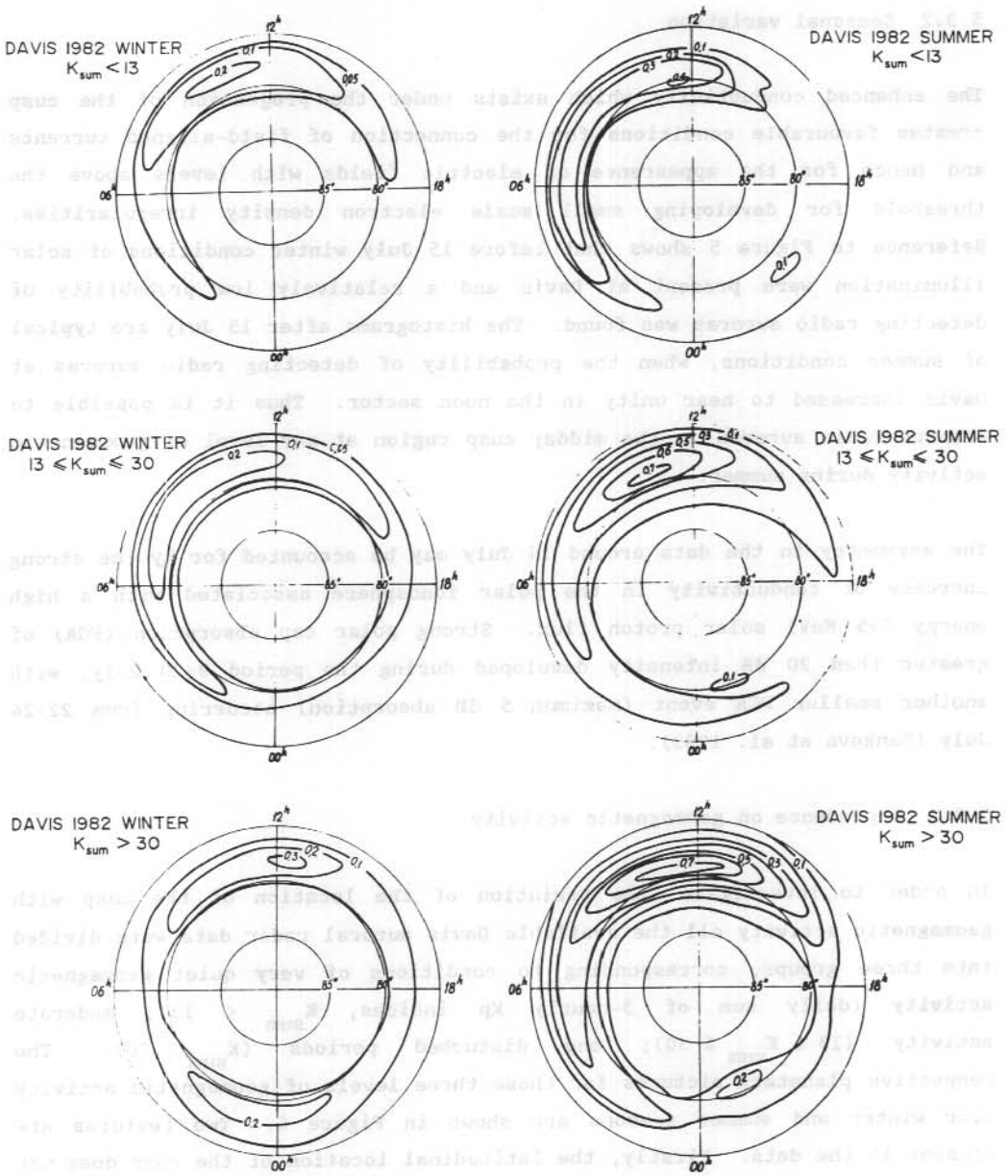

Figure 6. Polar plots showing the probability of observing radio auroras at Davis as a function of local time during winter and summer months, for

(a) $K_{sum} < 13$, quiet magnetic conditions;

(b) $13 \leq K_{sum} \leq 30$, moderately disturbed; and

(c) $K_{sum} > 30$, active conditions.

temporal region over which radio auroras may expect to be detected, without markedly altering the exact location or time of the peak. Further, Figure 7 shows the variation in the probability of detecting a radio aurora as a function of planetary magnetic activity, for the night and dayside auroral ovals during summer. The probability of registering a radio aurora in the nightside auroral oval depends directly on magnetic activity. This is expected since the nightside phenomena will be substorm associated. However the probability of observing a radio aurora in the midday cusp during summer is high under all but the quietest of magnetic conditions.

5.4 SUMMARY

1. An auroral radar located at Mawson did not detect any reflections from the midday cusp region in more than one year of operation near solar maximum phase. This means that the dayside cusp in the Southern Hemisphere does not move to less than 74° corrected geomagnetic latitude under any conditions of magnetic disturbance.

2. The probability of radio aurora occurrence with the radar at Davis was maximum in the region of the midday cusp, depending on solar illumination conditions (up to 100% in summer).
3. The probability of observing radio auroras within the cusp varies only weakly with magnetic activity.

ACKNOWLEDGMENTS

The author is grateful to the Mawson 1979 and Davis 1982 Officers-in-Charge, Mr Rex Burchill and Mr Konrad Beinssen, respectively, and personnel at the stations for their assistance in installing and operating radars. The author would also like to thank Mr Peter Magill and Dr Fred Menk for their technical and scientific advice. Sincere thanks to Dr O.A. Troshichev of the Arctic and Antarctic Research Institute at Leningrad for discussions on this paper.

5.5 REFERENCES

Akasofu, S.-I (1968). Polar and magnetospheric substorms. D Reidel, Dordrecht.

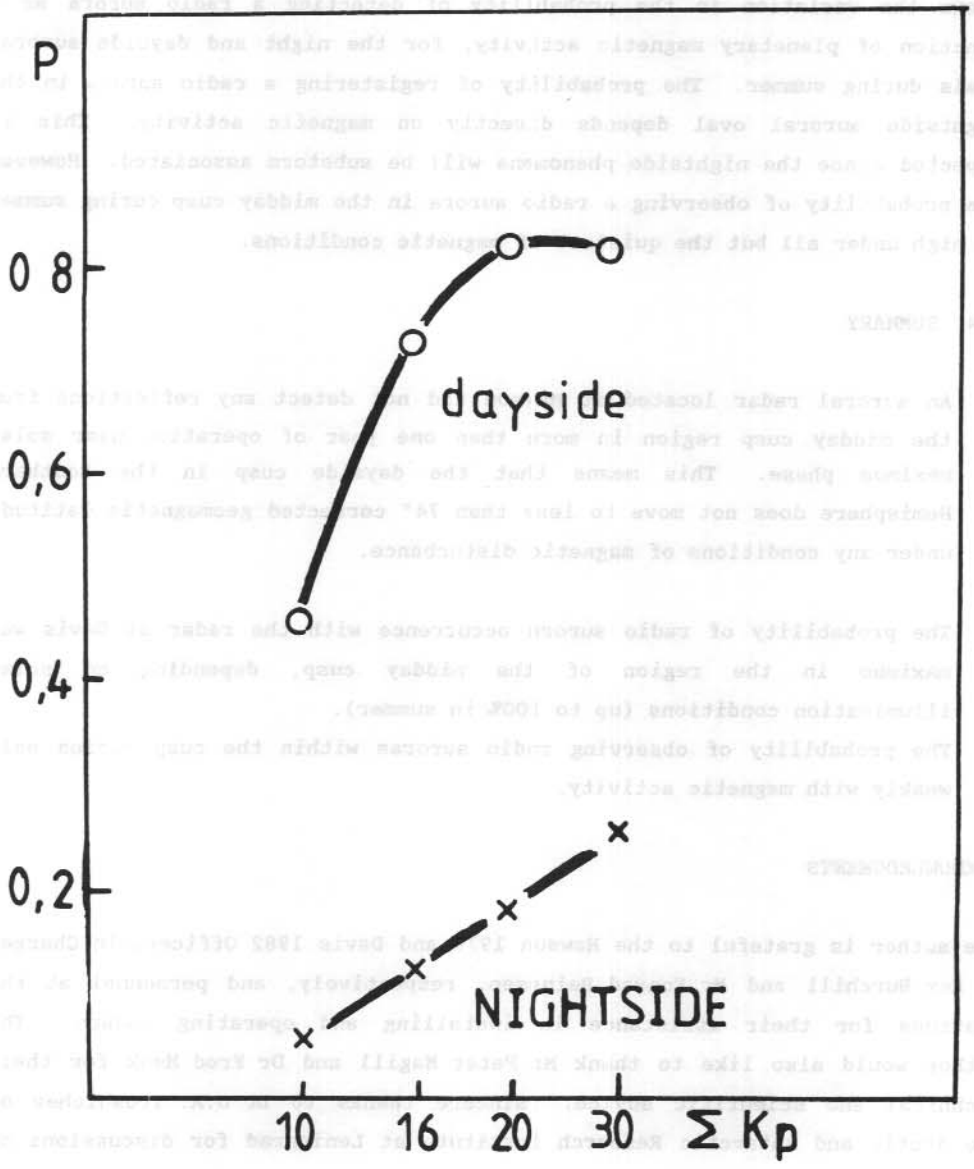

Figure 7. Dependence of the probability of detecting radio auroras at Davis in 1982 on magnetic activity for the nightside and dayside parts of the auroral oval.

Benkova, N.P., Vasil'ev, K.N., Ishkov, V.N., Kariner, N.S., Kozlov, E.F., Samorakin, N.M., Kolesnikova, L.A., Lavrova, E.V., Nepomnyashaya, E.V., Novikov, A.M., Pereyaslova, N.K. and Fomicher, V.V. (1983). Helio - and geophysical phenomena in July 1982. Geomagnetism and Aeronomy 23 (5):579-582.

Bond, F.R. and Thomas, I.L. (1971). The southern auroral oval. Australian Journal of Physics 24:97-102.

Cogger, L.L., Murphree, J.S., Ismail, S. and Anger, C.D. (1977). Characteristics of dayside 5577 and 3914 aurora. Geophysical Research Letters 4(10):413-416.

Cole, K.D., Bond, F.R., Raspopov, O.M., Sverdlov, Y.L. and Voloshinov, N.N. (1979). Radar exploration of the ionosphere in the dayside cusp. Antarctic Division Technical Memorandum Number 90. Department of Science, Melbourne.

Davis, T.N. and DeWitt, R.N. (1963). Twenty-four hour observations of aurora at the southern auroral oval. Journal of Geophysical Research 68(23):6237-6241.

Fraser-Smith, A.C. (1982). ULF/lower ELF electromagnetic field measurements in the polar caps. Reviews of Geophysics and Space Physics 20(3): 497-512.

Gault, W.A., Koehler, R.A., Link, R. and Shepperd, G.G. (1981). Observations of the optical spectrum of the dayside magnetospheric cleft aurora. Planetary and Space Science 29:321-334.

Kamide, Y., Burch, J.L., Winningham, J.D. and Akasofu, S.-I. (1976). Dependence of the latitude of the cleft on the interplanetary magnetic field and substorm activity. Journal of Geophysical Research 81(4): 698-704.

Meng, C.-I. and Lundin, R. (1986). Auroral morphology of the midday oval. Journal of Geophysical Research 91(A2):1572-1584.

Murphree, J.S., Cogger, L.L. and Anger, C.D. (1981). Characteristics of the instantaneous auroral oval in the 1200-1800 MLT sector. Journal of Geophysical Research 86(A9):7657-7668.

Ogawa, T., Balsley, B.B., Ecklund, W.L., Carter, D.A. and Johnston, P.E. (1980). Aspect angle dependence of irregularity phase velocities in the auroral electrojet. Geophysical Research Letters 7 (12): 1081-1084.

Troitskaya, V.A. and Bolshakova, O.V. (1977). Diurnal latitude variation of the location of the dayside cusp. Planetary and Space Science 25: 1167-1169.

Vorobjev, V.G., Gustafsson, G., Starkov, G.V., Feldstein, Y.I. and Shevnina, N.F. (1975). Dynamics of day and night aurora during substorms. Planetary and Space Science 23:269-278.

Zmood, I.J. (1976) VHF radar observations of the dayside auroral oval. Antarctic Division Technical Memorandum Number 87. Department of Science, Melbourne.

6. WINDS AND TEMPERATURES IN THE SODIUM LAYER AT 90 KM

P. Greet and F. Jacka
Mawson Institute for Antarctic Research
University of Adelaide
Adelaide, S.A., Australia, 5000.

ABSTRACT

Twilight measurements on the atmospheric atomic sodium spectral line emissions have been made using the Mawson Institute's Fabry-Perot spectrometer at Mt. Torrens, near Adelaide, using an instrument bandwidth of ~1 pm. The sodium is confined to a thin layer at about 90 km height and it resonantly scatters sunlight in the D1 and D2 lines. When the Earth's shadow covers the layer the emission intensities rapidly drop to nighttime values which are too low to permit useful measurements of temperature and wind.

The analysis of the line profiles is complicated by the hyperfine structure of the emissions. Two hyperfine groups approximately 2 pm apart can be clearly resolved in both the D1 and D2 profiles. If the instrument profile is deconvolved from the recorded profile the source profile is obtained: from this the wind and temperature can be estimated. Details of the analysis are discussed and preliminary results presented. By using a dual scanning Fabry-Perot spectrometer it is proposed to extend this work through the daylight hours both at Mt. Torrens and at Mawson, Antarctica.

6.1 INTRODUCTION

The sodium D1 λ589.592 nm and D2 λ588.995 nm emission lines are among the brightest features in the dayglow spectrum. As a prelude to studies of the dynamics of the upper atmosphere based on daytime observations of these lines some measurements have been made during twilight using the Mawson Institute's Fabry-Perot spectrometer (FPS) at Mt. Torrens in the Adelaide hills.

The D line emissions result from excitation of neutral sodium atoms. They have previously been studied extensively with photometers and, more

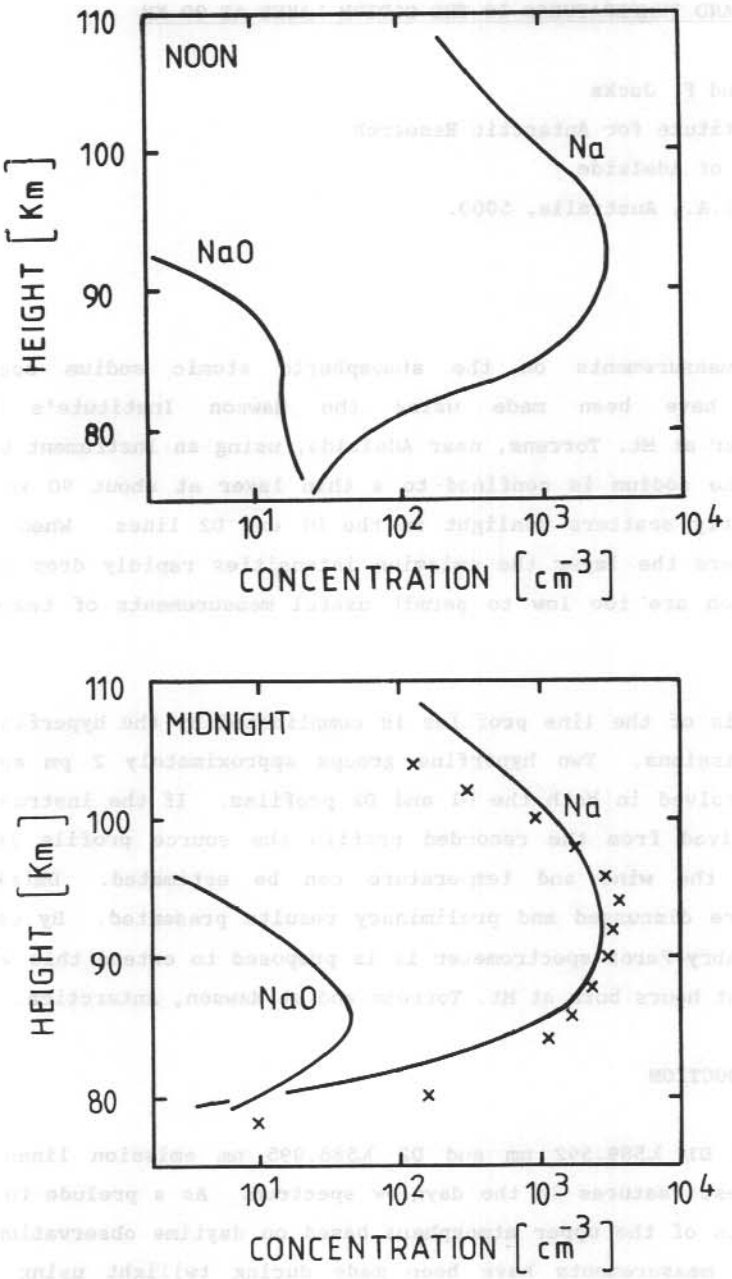

Figure 1. Sodium constituents for noon and midnight from model calculations. The crosses represent an average of lidar profiles. (From Kirchoff 1983). The peak of the layer is fairly stable. Changes in the bottom-side and top-side scale heights occur over twilight.

recently, lidars. Lidar studies have shown the emission layer to be about 10 km thick centered at about 88-90 km in altitude. Sodium atom densities of about 5×10^{9} m^{-3} are typical at the peak of the layer. Chemical models of the layer have been developed to explain its existence and some of the changes which have been observed (Kirchoff and Clemesha 1983, Jegou et al. 1985). Figure 1 illustrates a typical layer as derived from one such model. The shape varies slightly from day to night but peak densities and the general character are reasonably stable. The models are good in their ability to describe the layer both structurally and dynamically.

The sodium D lines in the airglow spectrum are excited weakly photochemically and strongly by resonant scattering of sunlight - typical intensities are about 30 R and 10 kR respectively (Kirchoff 1983, Hunten and Wallace 1967).

6.2 DATA

For daytime observing a dual FPS will be used incorporating a high resolution etalon, a low resolution etalon, and a 0.3 nm filter. Figure 2 illustrates the passbands of these three components. The present twilight observations were made using only the high resolution etalon and the 0.3 nm filter. This is satisfactory provided no other emissions fall within the passband of the filters used. The low resolution etalon is required for rejection of the scattered solar spectrum within the filter passband.

In the evening, the background of Rayleigh scattering slowly decreases as the sun sets enabling the sodium emissions to be distinguished. Figure 3 shows a series of zenith profiles from one evening. Each profile is the sum of about fifty scans in a five minute interval. The Fraunhofer absorption line can be seen in the first few profiles. This feature needs to be removed from the recorded profile before analysis can be done. Approximately four or five profiles can be obtained in one evening in which no contamination is present. From these profiles winds and temperatures could be derived as for nightglow FPS observations (Wilksch 1975).

As the sun sets on the layer, the sodium emission rapidly decreases in intensity and the profiles broaden as the photochemical reaction, which is exothermic, becomes the dominant source of photons. The last profile in Figure 3 is of mainly photochemical origin and was acquired over a longer

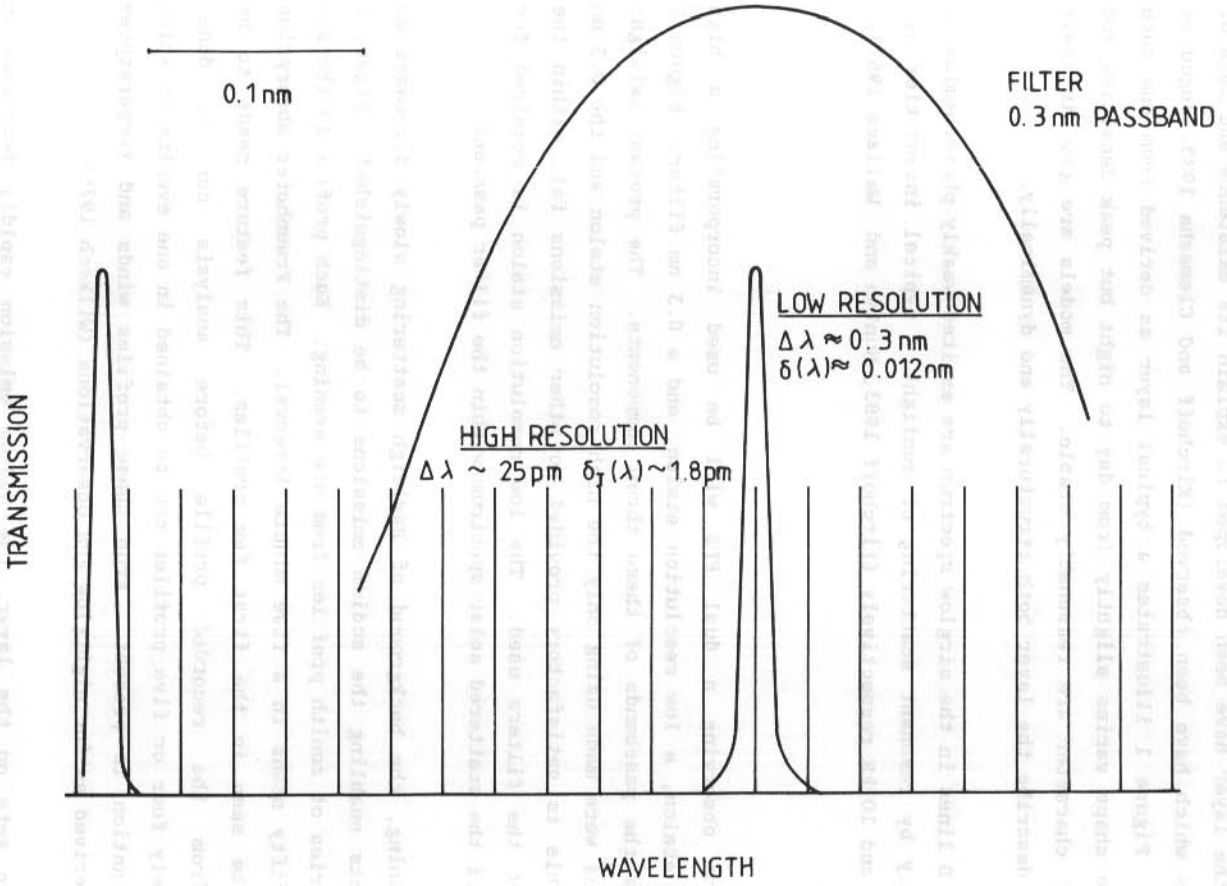

Figure 2. Passbands of the three components in the dual Fabry-Perot etalon system used for dayglow measurements. The twilight measurements have been made with the high resolution etalon and filter only.

period - about ten minutes. The nighttime intensity of the photochemical emission is very low; this, coupled with scattering of light from sodium street lamps, makes nighttime observations useless at Mt. Torrens.

Data were obtained on approximately thirty twilights from January to May 1986; about twenty of these were at dusk and about ten at dawn. Although some D2 observations were made, only D1 zenith observations will be presented here.

6.3 ANALYSIS

To estimate winds and temperatures the instrument profile must first be deconvolved from the recorded profile to give the sodium emission line profile. Figure 4 shows a schematic representation of the analysis procedure. The instrument function is derived from a record of a Hg-198, λ546 nm, profile. The source function at 546 nm (assumed to be a gaussian shape emitted by Hg atoms at 300 K) and the Airy function are deconvolved and the Airy function computed for the sodium wavelength is used to determine the instrument profile at that wavelength. To calculate the Airy functions the reflective finesse at the Hg and sodium wavelengths must be known - see Jacka (1984). The source function for the sodium emission, if assumed to be at 200 K, is approximately eleven channels wide in the data acquisition system while the instrument function is approximately sixteen channels wide. As a consequence the estimated source profile is reasonably sensitive to changes in the variables involved in deriving the instrument function. A change in temperature of the Hg lamp of 50 K results in a change in estimated temperature of 5 K in the sodium emission. Reflective finesse values need to be known rather accurately.

The source profile for the sodium emission is not a simple gaussian shape. The D1 line has 2 x 2 and the D2 line 2 x 3 hyperfine components. In the D1 line the two groups of hyperfine components are separated about 2.1 pm and each group is about 0.2 pm wide (very small compared to the doppler width). If the instrument profile is deconvolved from the recorded profile the hyperfine components appear as two gaussian shapes. The positions of the peaks of the two gaussians contain the wind information and the width of each gaussian the temperature but these parameters are more difficult to extract than for a simple gaussian shape.

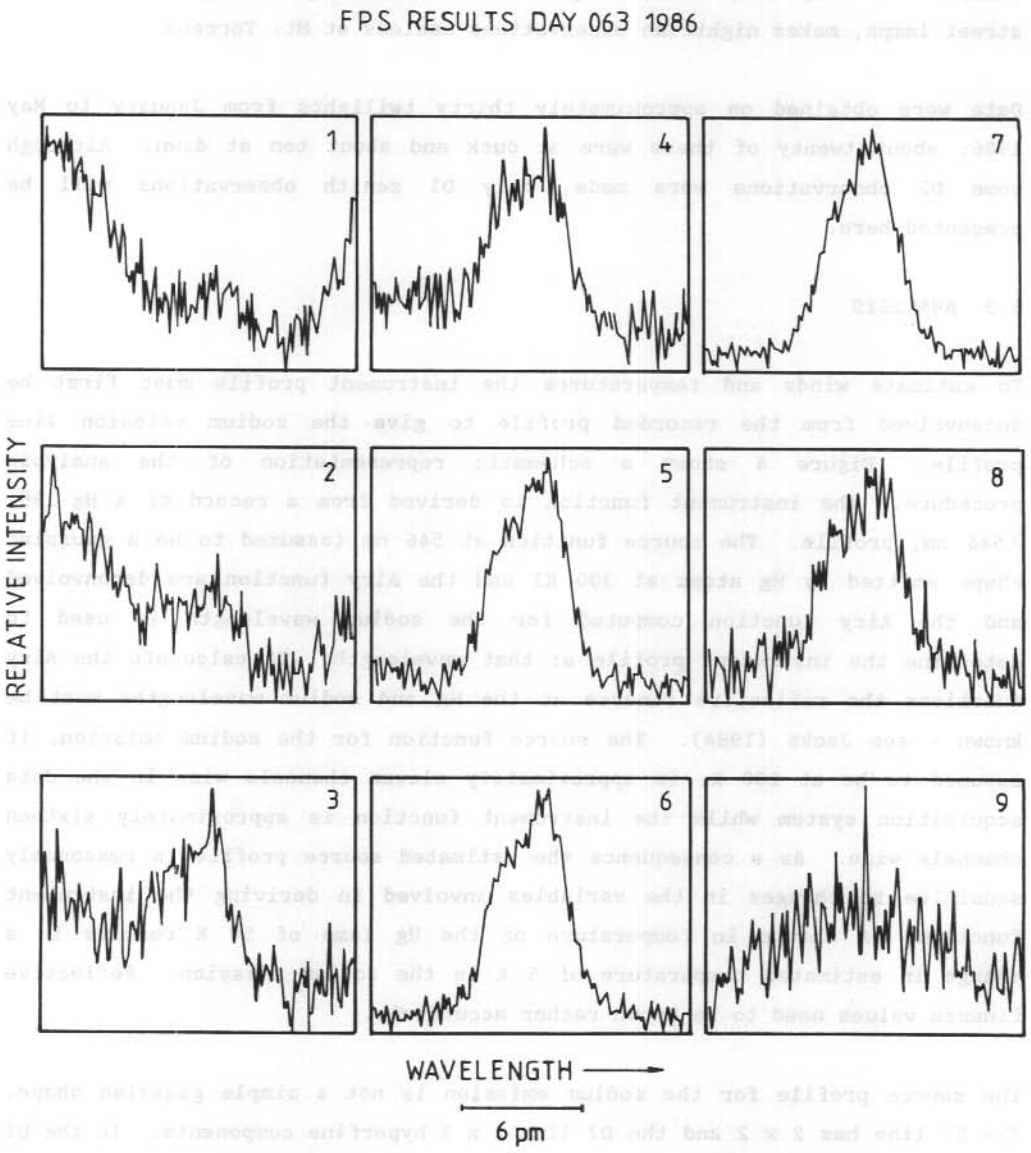

Figure 3. Sodium D1 line profiles from dusk on DOY 063. In profiles 1-4 the features of the solar spectrum can be seen. Profiles 5-8 should be suitable for analysis and profile 9 shows photochemical broadening which occurs after sunset on the sodium layer.

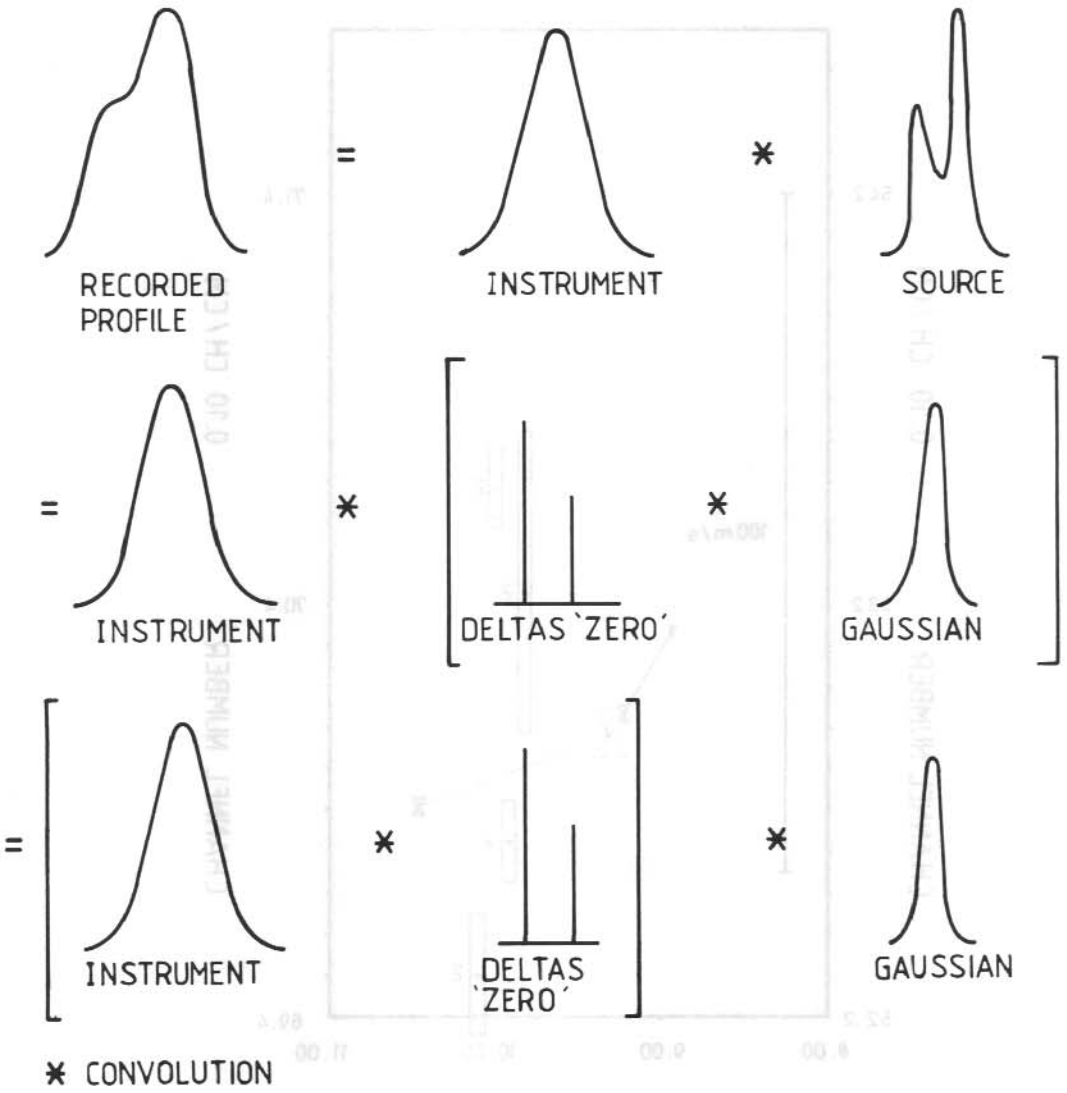

Figure 4. The recorded profile is the convolution of the instrument and source profiles. To obtain winds and temperatures from the source profiles the hyperfine structure must be incorporated in the analysis.

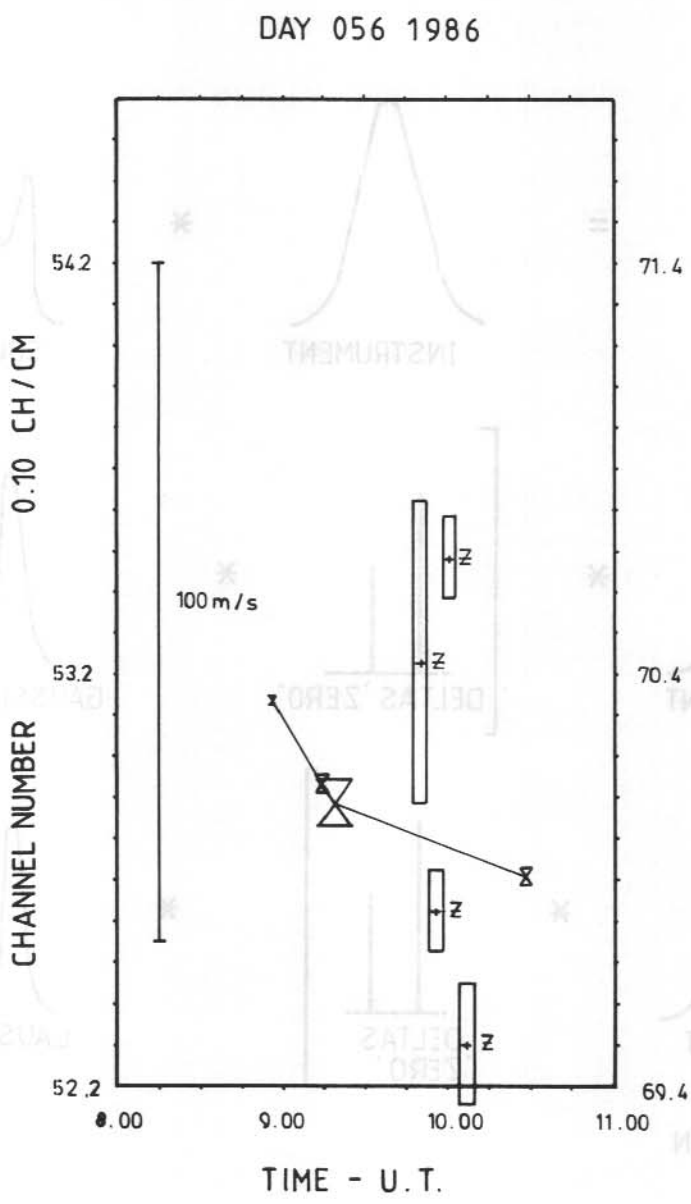

Figure 5. The results of the five parameter fit for peak position for dusk on DOY 056. The boxes indicate sodium D1 line profile peak positions and the bow-ties from calibration profiles using a Hg 198 lamp.

Two different approaches to the data reduction have been examined. In the first the emission profile at zero degrees Kelvin is represented by two delta functions the spacing and relative intensities of which are taken from Chamberlain (1961). The convolution of this zero K profile and the instrument profile (the system profile) is then deconvolved with the recorded profile. This yields a gaussian curve the location and width of which estimate the wind and temperature of the emitting region. The fitting is done in the fourier transform domain and only the noise-free points are used.

In the second method five parameters were fitted, two peak positions, two intensities, and one temperature. The residuals from this second method showed least structure and, tentatively, this method is favoured. The average separation estimated between the two fitted gaussians was slightly larger than that assumed in the first method (2.2 ± 0.2 pm as compared with 2.1 pm) and the average ratio of the two intensities was the same (0.60 ± 0.05). These values are averages from three series of twilight measurements. Further investigation of the most appropriate fitting routine is being made.

6.4 RESULTS

All results presented in this section are from the second method above, i.e. the five parameter fit of two gaussians to the source profile. Figure 5 shows the results of this analysis of peak position (wavelength) for day of year (DOY) 056. The bow-ties are measurements of etalon drift using the Hg calibration lamp. The boxes give peak positions as obtained from the sodium profiles; the width of the box indicates the profile acquisition time. Variation in peak position is found in all data sets so far analysed. No absolute velocities can be determined as a sodium lamp which does not show self reversal in the line profile was not available for calibration. Assuming a zero reference wavelength these peak positions can be interpreted as vertical velocities.

Figure 6 shows velocities obtained from three twilights, from days 054 and 056. The velocities, up to ± 25 ms^{-1}, obtained are considerably larger than those obtained using radio methods at Buckland Park, about 50 km away - typically 1 - 2 ms^{-1} in the height range 60-98 km, with 2 km height

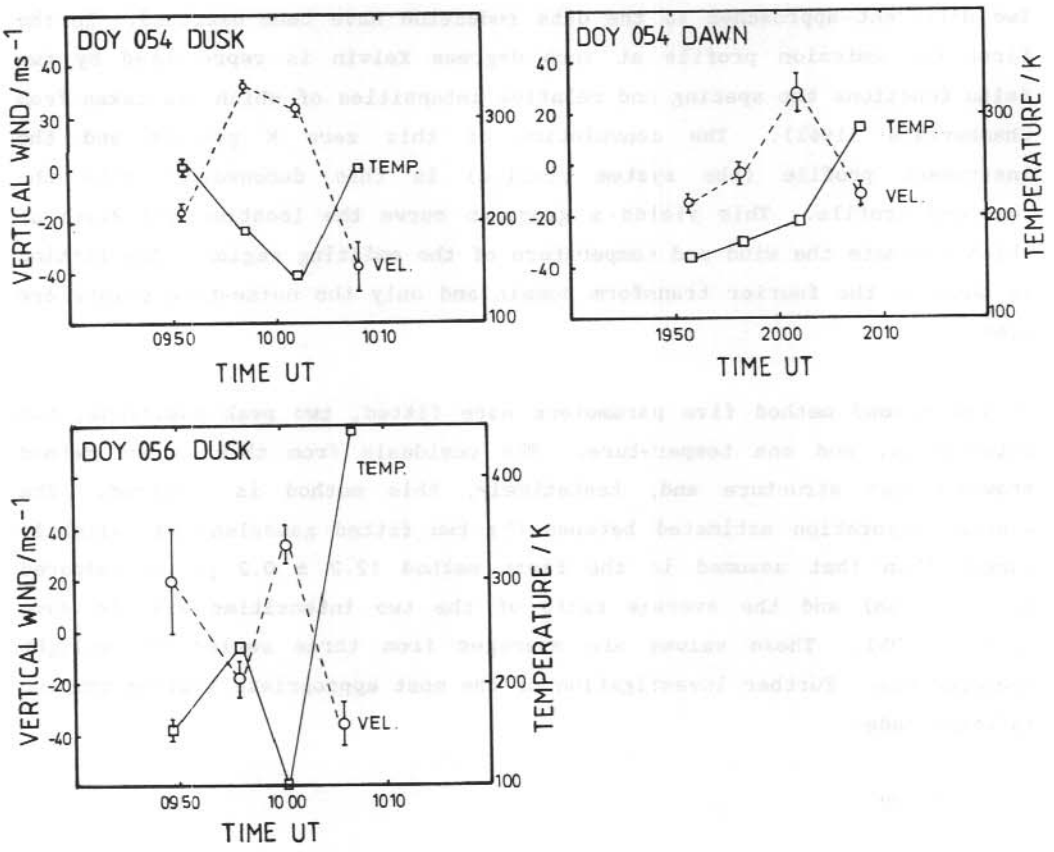

Figure 6. Vertical velocities and temperatures obtained from three twilight periods, both dusk and dawn for DOY 054 and dusk on DOY 056. The circles are velocity measurements and the squares temperature measurements.

resolution and about five minute time resolution (Murphy 1984). Larger velocities (15 - 20 ms^{-1}) have been measured at 100-200 km altitudes using the auroral 558 nm oxygen emission at high latitudes (Peteherych et al. 1985) and rocket techniques at both mid and high latitudes (Rieger 1974). Such velocities have been ascribed to gravity wave perturbations.

It is possible that the velocities measured are due to waves produced by rapid changes occurring in the sunlight/shadow boundary of the twilight atmosphere. (Granier and Megie (1982), using lidar measurements, have observed large changes in the top-side and bottom-side scale heights of the sodium layer during twilight).

Also there is a slight possibility that the shift in peak position of the profiles is due to changes in the background solar spectrum not accounted for in this preliminary analysis.

The sodium layer is near the mesopause, the coldest region of the atmosphere and the Southern Hemisphere summer mesopause is the coldest region of earth's atmosphere. The 1972 CIRA model atmosphere depicts temperatures of about 160 K at Mt. Torrens (mid-latitudes). (Mawson, at higher latitudes, has mesopause summer temperatures of about 140 K.) Lidar studies of sodium hyperfine structure at northern mid-latitudes have obtained temperatures of about 205 K, in agreement with the CIRA model (Fricke and von Zahn 1985).

Figure 6 shows temperatures obtained from the profiles of DOY 054 and 056. The final one in the dusk profiles is broadened because of the exothermicity of the reaction producing the emission. In the dawn data the final profile may be broadened because of incomplete subtraction of the background. Even if this variation is ignored changes are obvious in the temperatures obtained. In some cases the changes in temperature correlate with changes in velocity. Whether these temperature changes are real or not will be seen when the analysis has progressed further.

6.5 CONCLUSIONS

Although considerable work still remains to be done on the analysis of the twilight results presented here the observations are very promising. The time resolution is very good and should also be good in daytime observations.

The second (low resolution) interferometer at Mt. Torrens is again in operation and in future studies longer time sequences of data will be available. Using the dual interferometer at Mawson, Antarctica, over the 1986/87 summer, long sequences of sodium daytime results will be obtained. It will be possible, weather permitting, to obtain continuous twenty-four hour observations of the sodium dayglow emissions. Observations made with the dual etalon systems will remove some of the possible variations unaccounted for in the results presented here. They will also allow measurements to be made when the sodium layer is not suffering the rapid changes which occur at twilight.

ACKNOWLEDGMENT

This work is supported by the Australian Research Grants Scheme.

6.6 REFERENCES

Chamberlain, J.W. (1961). Physics of the Aurora and Airglow. Academic Press, London.

Fricke, K.H. and von Zahn, U. (1985). Mesopause temperatures derived from probing the hyperfine structure of the D2 resonance line of sodium by lidar. Journal of Atmospheric and Terrestrial Physics 47:499-512.

Granier, C. and Megie, G. (1982). Daytime lidar measurements of the mesospheric sodium layer. Planetary and Space Science 30:169-177.

Hunten, D.M. and Wallace, L. (1967). Rocket measurements of the sodium dayglow. Journal of Geophysical Research 72:69-79.

Jacka, F. (1984). Application of Fabry-Perot spectrometers for measurement of upper atmosphere temperature and winds. In: Vincent, R.A. (Ed.). Middle Atmosphere Program Handbook for MAP 13:19-40.

Jegou, J.P., Granier, C., Channin, M.L. and Megie, G. (1985). General theory of the alkali metals present in the earth's upper atmosphere. II Seasonal and meridional variations. Annales Geophysicae 3:299-312.

Kirchoff, V.W.J.H. (1983). Atmospheric sodium chemistry and diurnal variations: An up-date. Geophysical Research Letters 10:721-724.

Kirchoff, V.W.J.H. and Clemesha, B.R. (1983). The atmospheric neutral sodium layer: 2 Diurnal variations. Journal of Geophysical Research 88:442-450.

Murphy, D. (1984). Vertical motions in the mesosphere. M.Sc Thesis, University of Adelaide.

Peteherych, S., Shepherd, G.G. and Walker, J.K. (1985). Observations of vertical E-region neutral winds in two intense auroral arcs. Planetary and Space Science 33:869-873.

Rieger, E. (1974). Neutral air motions from barium releases experiments - 1 Vertical winds. Journal of Atmospheric and Terrestrial Physics 36: 1377-1385.

Wilksch, P.A. (1975). Measurement of thermospheric temperatures and winds using a Fabry-Perot spectrometer. PhD Thesis, University of Adelaide.

7. WINDS IN THE MIDDLE ATMOSPHERE AT MAWSON, ANTARCTICA: I. MEAN CIRCULATION AND LARGE SCALE MOTIONS

A. Phillips (1) and R.A. Vincent (2)

(1) Mawson Institute for Antarctic Research

(2) Department of Physics
University of Adelaide
Adelaide, S.A., Australia, 5000.

ABSTRACT

Winds in the height range 70-110 km have been recorded continuously since July 1984, using the 'partial reflection drifts method' at Mawson station (67°S, 63°E). This large data-set enables study of the mean circulation and the results can be compared with those from similar high-latitude stations operating in the Northern Hemisphere. Initial results show that there is a high degree of similarity between Mawson and Poker Flat, Alaska, in the zonal components but not as much in the meridional components. Comparisons with recent wind models are also made.

7.1 INTRODUCTION

During the summer of 1981-82, the Mawson Institute, in conjunction with the Physics Department of the University of Adelaide, operated a Partial Reflection Drift radar (PRD) at Mawson, Antarctica (see McLeod and Vincent 1985). In 1984, a similar system, utilising an on-line computer began operation and has been recording data continuously up to the present. The PRD technique has been used for many years at Adelaide and a number of stations throughout the world, but to the authors' knowledge, there are only two stations in the Antarctic, the other one being at New Zealand's Scott Base.

Briefly the PRD technique involves transmitting a powerful radio pulse (2 MHz) in a vertical beam upwards where weak echoes are partially reflected from ionisation in the region of 60 - 100 km. The pattern of ionisation drifts with the wind, and the reflections from it produce a moving distribution of field strength over the ground. The height resolution of the PRD is approximately 4 km. The experiment takes about two minutes to

acquire data for each wind measurement and the time between consecutive readings (for a given height) is at best five minutes. Typically two to three measurements per hour are obtained in the 80–100 km region. Below 70 km, there is usually insufficient ionisation to produce reflections and at 110 km or so, the high refractive index of the E-region totally reflects the signal.

At Mawson an on-line minicomputer stores and then analyses the received signal and derives real-time wind information in the region of 70–110 km. Figure 1 shows the total number of data points acquired as a function of height at different seasons of the year. Note that the data acquisition maximises around 85–90 km although there is some seasonal variation. During the winter and equinoxes much more data are obtained from lower heights, especially below 80 km.

7.2 ZONAL WINDS

Figure 2 shows a summary of the mean winds for 1985; each arrow represents a complete month's data averaged for each 4 km height interval. The most obvious feature of the graph is the geostrophic wind derived by the hemispheric differences in heat input – eastwards in winter and westwards in summer. During March and October the winds reverse direction. The March reversal is slow and generally, the winds blow towards the south for the whole month. However, the onset of the westward wind in October occurs very suddenly (within three to six days) in about the third week of October. This E-W jet maximises at 80–85 km and diminishes gradually with height. Above 100 km, the winds do not show an obvious annual variation.

Figure 3 illustrates the zonal component of winds observed at both Mawson and Poker Flat, Alaska (Tetenbaum and Avery 1986) which is at a similar latitude to Mawson. The light regions represent eastward winds and the shaded regions westward winds. At Mawson during October there is a sudden onset, at all heights, of a westward (-ve) motion, which reaches a maximum value of around 40 ms^{-1} in December, at 80–90 km. Eastward winds commence at 100–110 km during December and gradually descend. By April, all winds in the region 75–100 km are eastward. The gradual change to eastward wind stands in marked contrast to the onset of the summer westward wind.

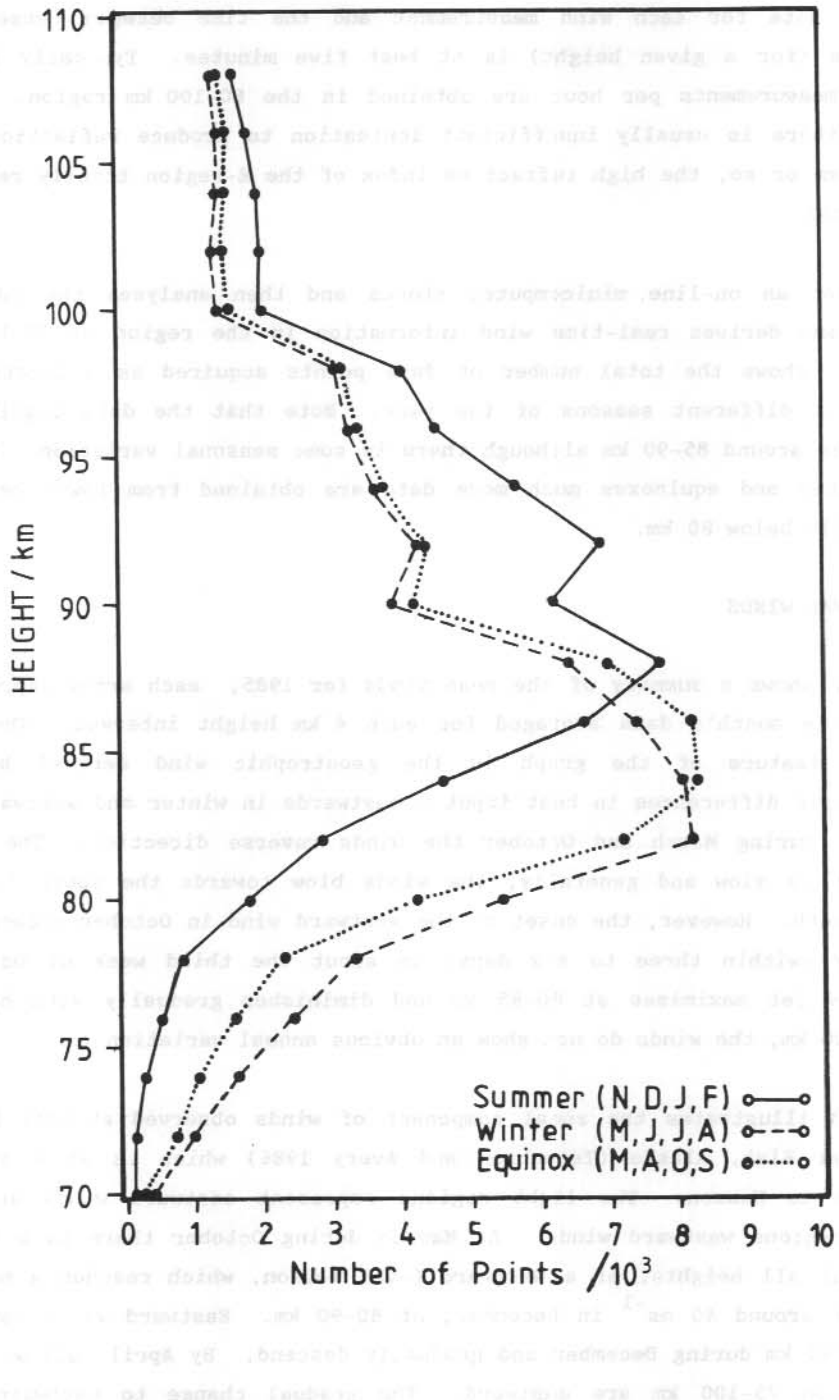

Figure 1. Height distribution of data acquired during 1985. The total number of data points is shown for each season.

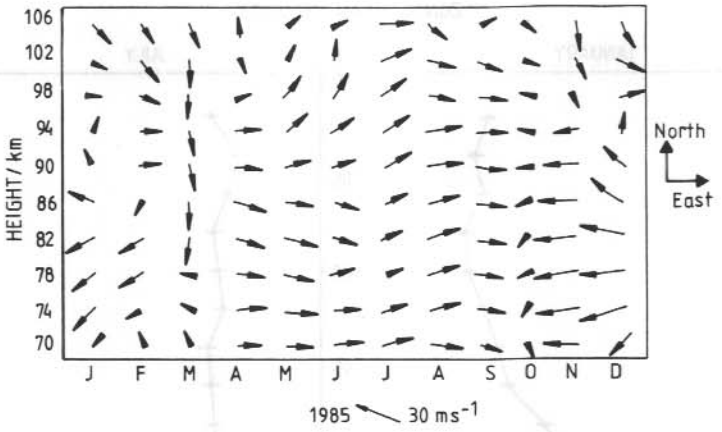

Figure 2. Summary of mean winds 70–108 km for 1985. Each vector represents the average of one months wind data averaged over 4 km and centred on the height indicated.

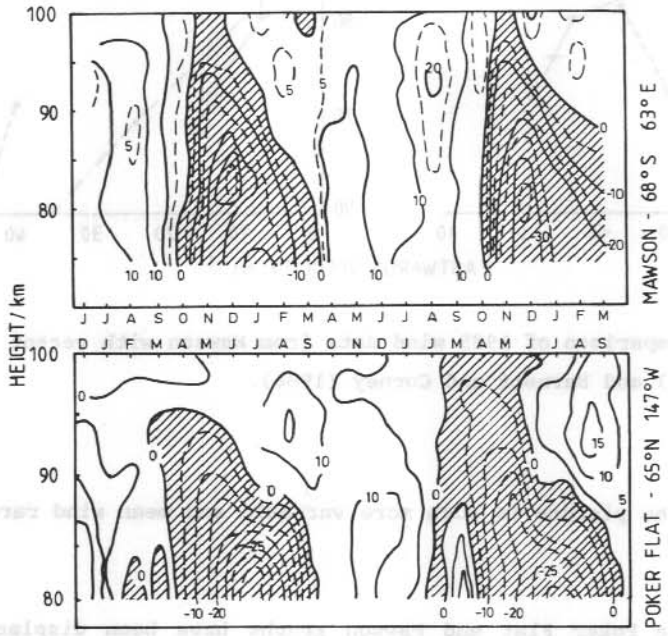

Figure 3. A comparison of the zonal mean wind between Mawson (68°S, 63°E) and Poker Flat (65°N, 147°W) (Tetenbaum and Avery 1986). Shaded regions indicate westward wind with contours drawn at 5 ms^{-1} intervals; unshaded regions indicate eastward wind. Timescales are displaced by six months to compare seasons.

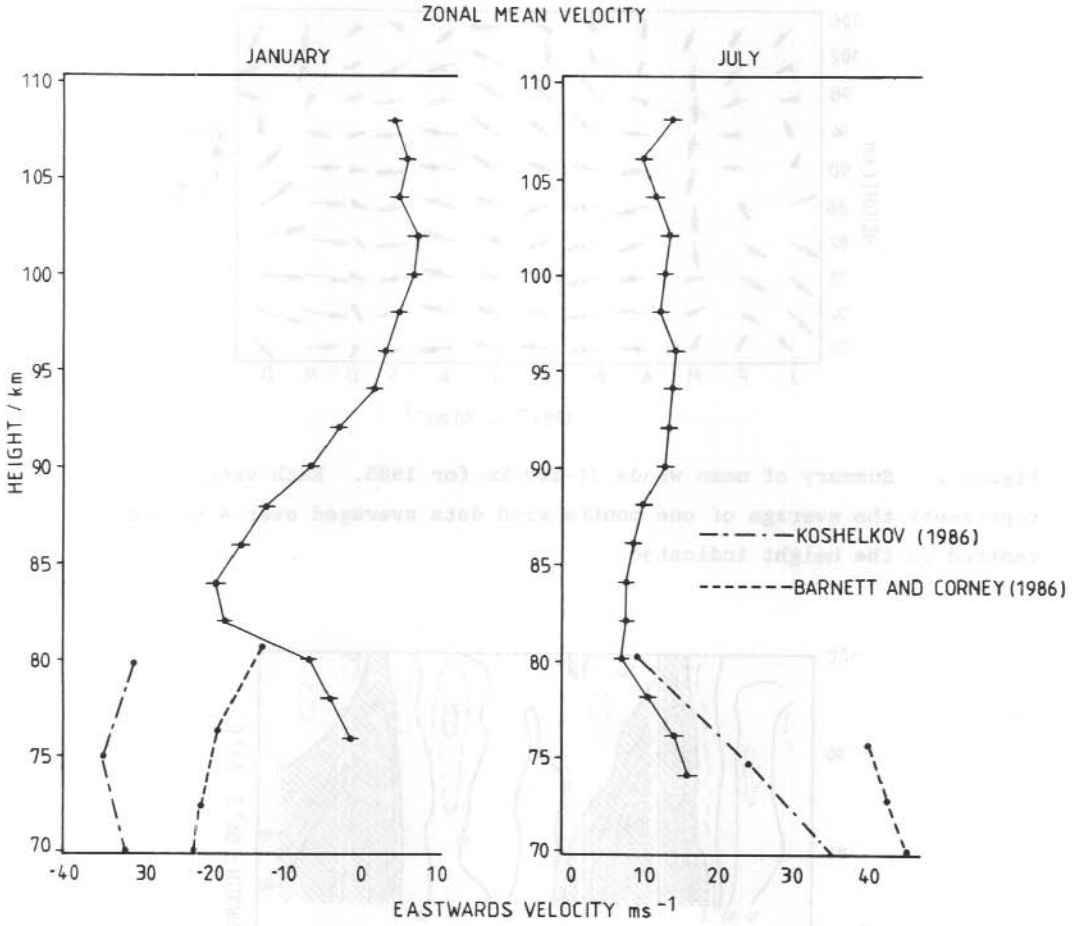

Figure 4. A comparison of 1985 wind data from Mawson with recent models by Koshelkov (1986) and Barnett and Corney (1986).

Above 100 km, the picture is much more variable and mean wind rarely exceeds 10 ms^{-1}.

In Figure 3 the Poker Flat and Mawson graphs have been displaced in time relative to each other by six months. There is a broad similarity; both sites showing westward winds in summer and eastward winds in winter. The maxima occur at roughly the same height and time of season, with an amplitude of 30-40 ms^{-1} eastwards for the summer wind, and 15-20 ms^{-1} westwards for the winter wind.

The change in wind direction at the spring equinox does not appear so suddenly at Poker Flat, compared with Mawson. Although only 1983-84 Poker Flat data are shown here, earlier data suggest this is a regular feature for the Northern Hemisphere. Also the northern spring equinox reversal occurs up to one month earlier.

Some recent models do not compare very well with the data in the 70-80 km region. Barnett and Corney (1985) incorporate satellite data in their model, and Koshelkov (1986) has incorporated Mawson data in his. Figure 4 compares the model predictions for the zonal wind for January and July 1985. Clearly some adjustment to these models is required as both tend to overestimate the velocities.

7.3 MERIDIONAL WINDS

The meridional components of the winds are shown in Figure 5 without time displacement. As compared with the zonal winds these are much weaker and

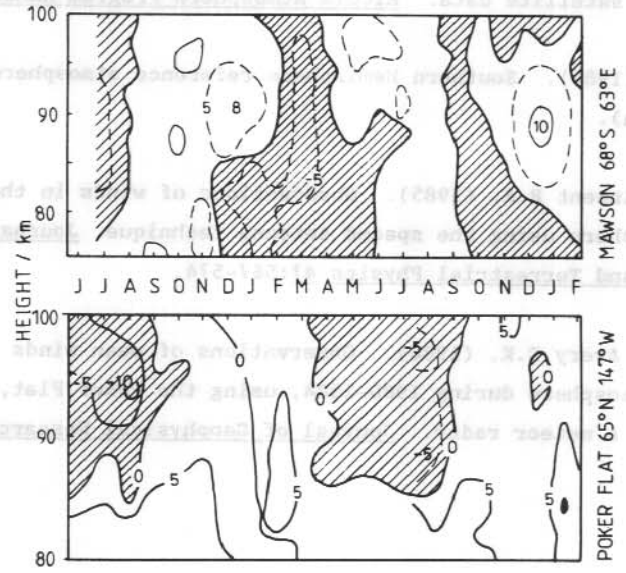

Figure 5. A comparison of the meridional mean wind between Mawson (68°S, 63°E) and Poker Flat (65°N, 147°W) (Tetenbaum and Avery 1986). Shaded regions indicate southward wind with contours drawn at 5 ms^{-1} intervals; unshaded regions indicate northward wind.

show less inter-annual and inter-hemisphere similarity. These variations are tentatively attributed to variations with season and between hemispheres in the rate of momentum transfer from planetary waves and gravity waves. Maximum flow occurs in local summer (equatorward) at ~10 ms^{-1} maximising near 90 km. Winter is more variable possibly due to the influence of quasistationary and travelling, planetary waves which can penetrate the mesosphere.

ACKNOWLEDGMENTS

The observations discussed here were carried out at the Australian National Antarctic Research Expedition's station at Mawson, Antarctica. The authors thank the Director, Antarctic Division, Department of Science for logistic support. This work was supported by the Australian Research Grants Scheme.

7.4 REFERENCES

Barnett J.J. and Corney, M. (1985). Middle atmosphere reference model derived from satellite data. Middle Atmosphere Program Handbook 16:47.

Koshelkov Yu.P. (1986). Southern Hemisphere reference atmosphere. (Private communication).

MacLeod R. and Vincent R.A. (1985). Observations of winds in the Antarctic summer mesosphere using the spaced antenna technique. Journal of Atmospheric and Terrestrial Physics 47:567-574.

Tetenbaum D. and Avery S.K. (1986). Observations of mean winds and tides in the upper mesosphere during 1980-1984, using the Poker Flat, Alaska, MST Radar as a meteor radar. Journal of Geophysical Research (in press).

8. WINDS IN THE MIDDLE ATMOSPHERE AT MAWSON, ANTARCTICA: II. TIDES

A. Phillips (1) and R.A. Vincent (2)
(1) Mawson Institute for Antarctic Research
(2) Department of Physics
University of Adelaide
Adelaide, S.A., Australia, 5000.

ABSTRACT

Winds in the region 70-110 km have been recorded continuously using the 'partial reflection drifts method' at Mawson station (67°S, 63°E) since July 1984. The large, continuous data set allows the study of atmospheric tides.

Atmospheric tides at high latitudes are of particular interest because diurnal propagating modes are inhibited, allowing study of non-propagating modes in isolation.

Results from Mawson are compared with those from the Poker Flat MST radar at similar latitude in Alaska.

8.1 INTRODUCTION

The term 'atmospheric tide' is used in this paper to mean any fluctuation in an atmospheric variable (such as temperature, pressure or windspeed) which shows periodicity of one day, or subharmonics of a day. On the earth's surface atmospheric tidal oscillations are very small. For instance, the tidal pressure variation measured at the equator is about 0.5% of the background pressure. However, in the middle atmosphere, tidal effects are much larger and with amplitudes as high as 10-50 ms^{-1}, which is comparable with the magnitude of the background wind.

Figure 1 shows an example of tidal winds in the middle atmosphere. These data, taken at Mawson during March 1985 have been filtered to leave only oscillations whose period is ten to fourteen hours. The dominant tidal

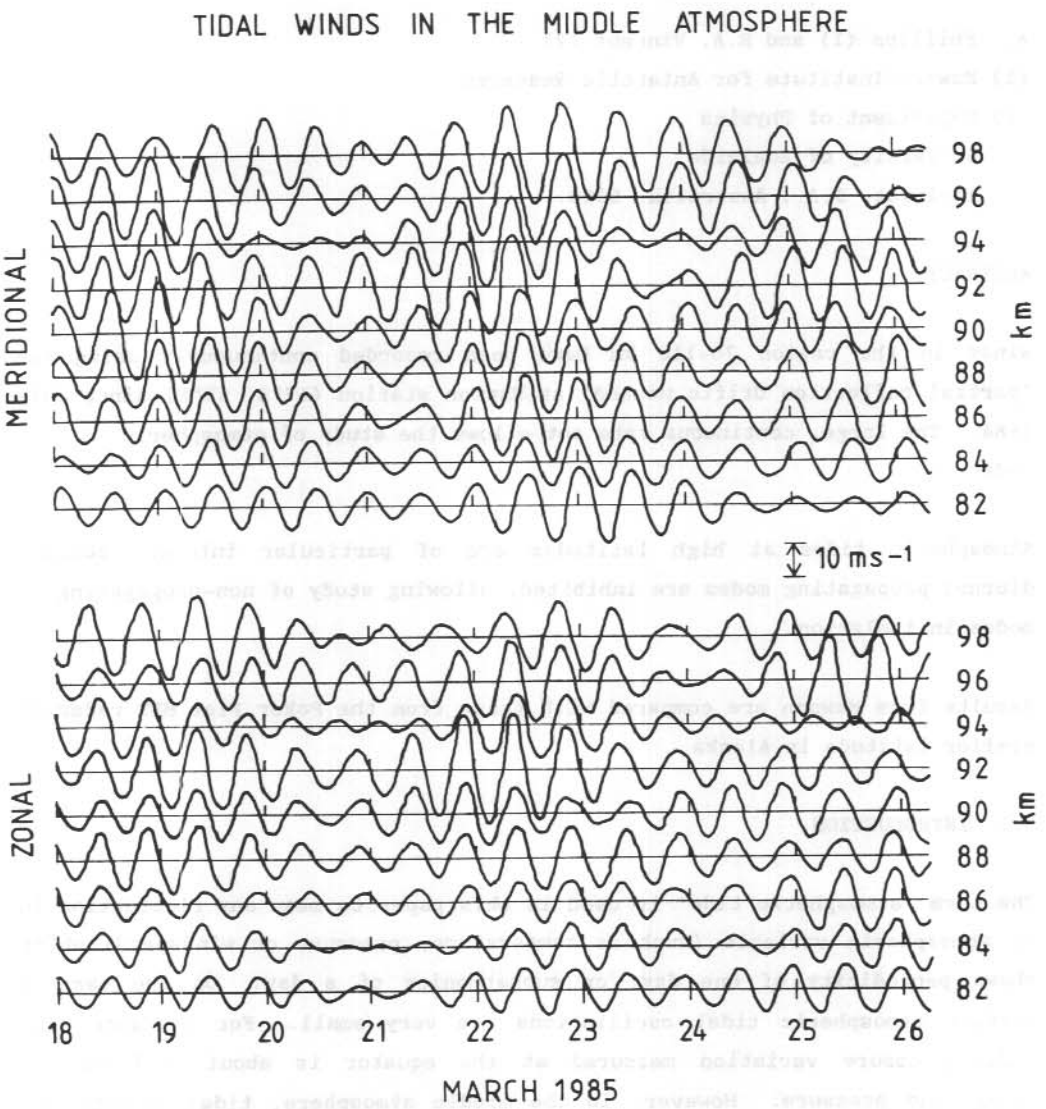

Figure 1. An example of tidal winds observed in the Antarctic mesosphere. The data have been filtered leaving only the ten to fourteen hour oscillations. At high latitude, the twelve hour tide is strong and dominant in this diagram.

oscillation shown here is the twelve hour, or semidiurnal tide, and this diagram also highlights several of the features of tidal propagation in general.

It is noted that the amplitude and phase of the tide is quite variable from day to day. The mechanism for this sudden enhancement of the tide is not understood, and may be due to variations in propagation of tidal waves from the troposphere and stratosphere.

The meridional component shows an oscillation at all heights with a steady phase shift with height such that the oscillation occurs at earlier times with increasing altitude. Tidal theory attributes this phase slope to a wave that is propagating phase downwards and energy upwards.

The zonal wind also shows a similar phase progression though the phase is shifted by 1/4 of a cycle ahead of that of the meridional wind indicating an elliptically polarised wave. These are the typical characteristics of a propagating tidal wind in the middle atmosphere.

It is possible to predict the approximate amplitudes of the various tidal modes of oscillation by looking at the Hough functions and their related velocity expansion functions. A Hough function derives from the eigenvalue solutions to the Laplace tidal equation. Figure 2 shows normalised Hough functions (Forbes 1982a,b) of several diurnal and semidiurnal modes as a function of latitude; Adelaide and Mawson are marked. To obtain actual tidal amplitudes, the normalised curves must be multiplied by tabulated factors. However, the Laplace tidal equation assumes, amongst other things, a zero background wind. Therefore these curves do not give a precise prediction of tidal amplitudes, but they do give a general idea of what modes are likely to be present at a given latitude.

Observe that modes either have reflective symmetry about the equator (symmetric modes) or, they do not (anti-symmetric modes). This is indicated by the oddness or evenness of the mode number (the S subscript). The superscript indicates the number of oscillations per day. A negative mode number indicates an evanescent or non- (vertically) propagating tide.

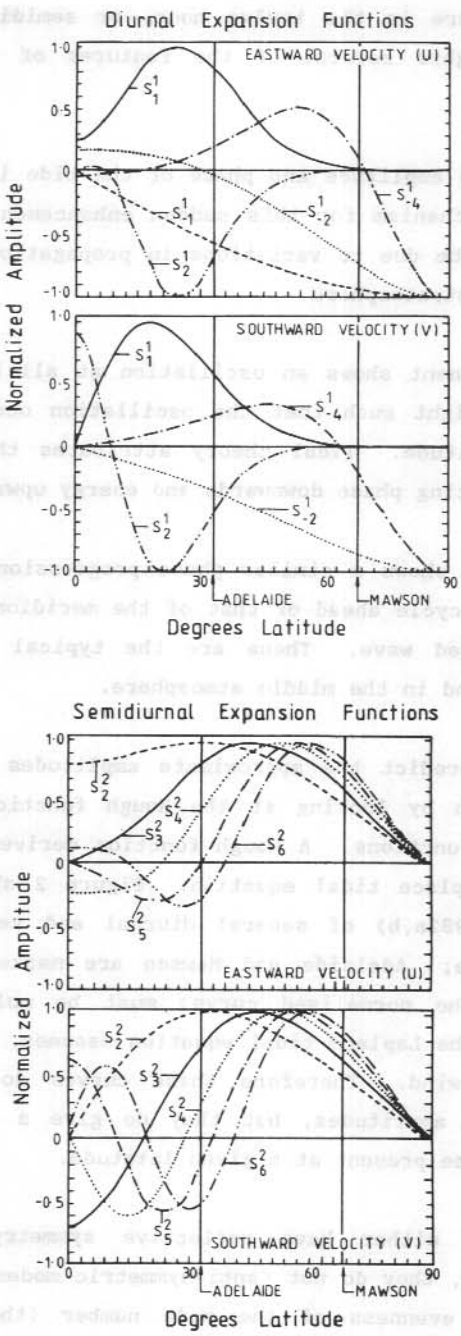

Figure 2. Hough velocity expansion functions (from Forbes 1982a,b) with lines indicating the latitude of Mawson, Antarctica, and Adelaide, South Australia.

The only diurnal functions with significant amplitude at the latitude of Mawson are the evanescent modes. Since middle latitudes yield a mixture of propagating and evanescent waves, high latitude observations should allow the study of evanescent diurnal modes in isolation. However, recent tidal theory (Vial 1986, Forbes and Hagan 1986) suggests that the effect of dissipation on the propagating S_1^1 mode is to broaden the response so it extends to higher latitudes.

For the semidiurnal Hough functions, only propagating modes are shown and they are much more persistant to high latitude. From consideration of these diagrams and their normalisation factors, the semidiurnal tide is expected to be dominant at the latitude of Mawson.

8.2 THE DIURNAL TIDE

In Figure 3 the amplitude and phases of the diurnal tide (derived from 1985 Mawson data) are shown averaged over a complete year, as well as seasonally. Generally, the amplitude increases with height and the meridional amplitude is much larger than the zonal. Diurnal amplitudes are typically 5-10 ms^{-1}.

The diurnal phase profiles are consistent with predictions; that is, the meridional phase profiles are almost vertical, indicating that the tide is evanescent. The zonal phase profiles are nearly vertical except for a sharp change in phase around 85-95 km. The explanation for this is uncertain, but it is sometimes suggested to be due to interference between modes (Elford 1974).

8.3 THE SEMIDIURNAL TIDE

If a comparison is made with the semidiurnal winds in Figure 4, it is clear that the semidiurnal amplitude is large, which is expected at high latitude. The semidiurnal amplitudes are typically 10-20 ms^{-1}, with a broad maxima around 85-95 km. As with the diurnal tide, the meridional component of the semidiurnal tide is generally much stronger than the zonal component, especially around the equinoxes.

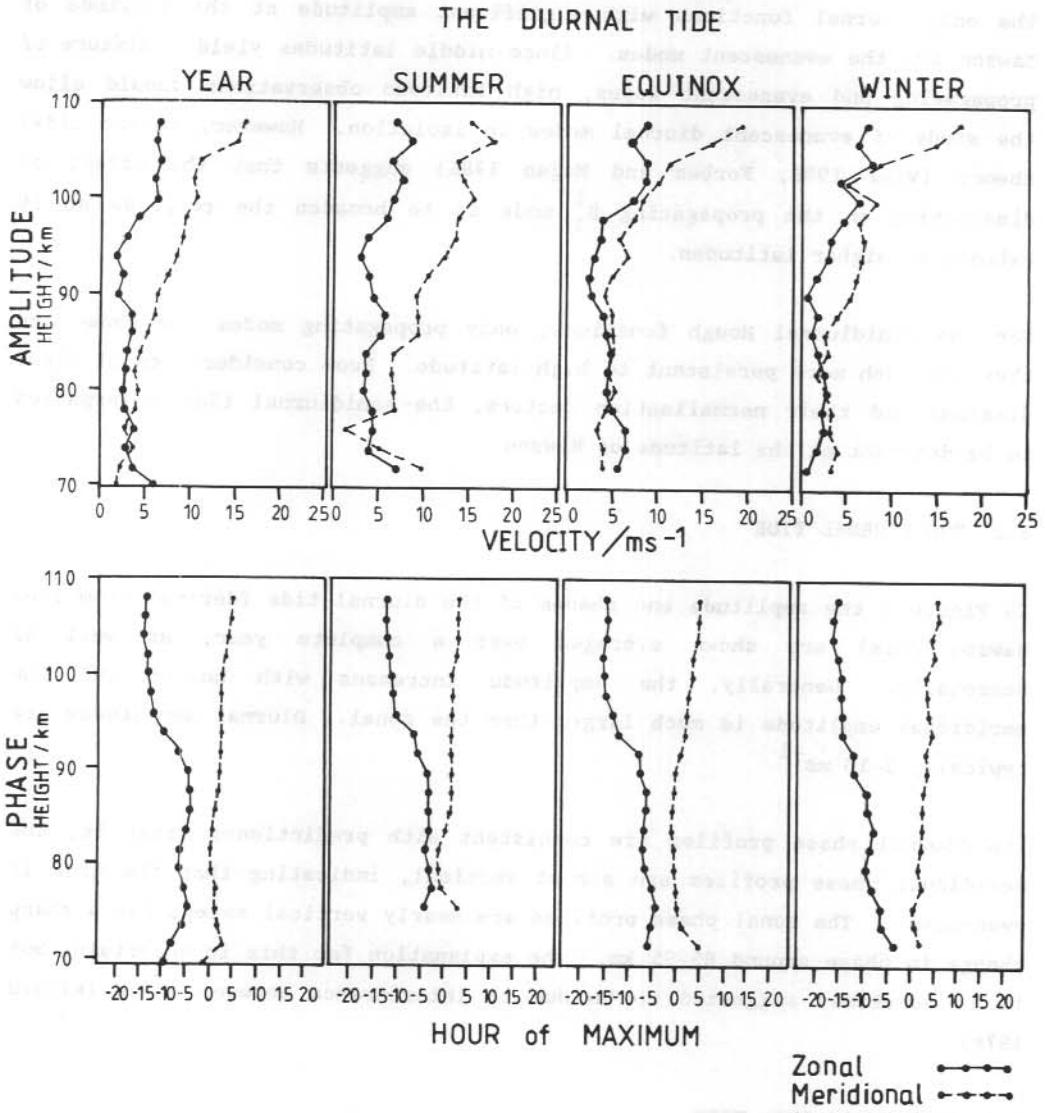

Figure 3. Amplitude and phase profiles of the diurnal tide averaged seasonally and over a complete year (1985). The phase hour is in local solar mean time.

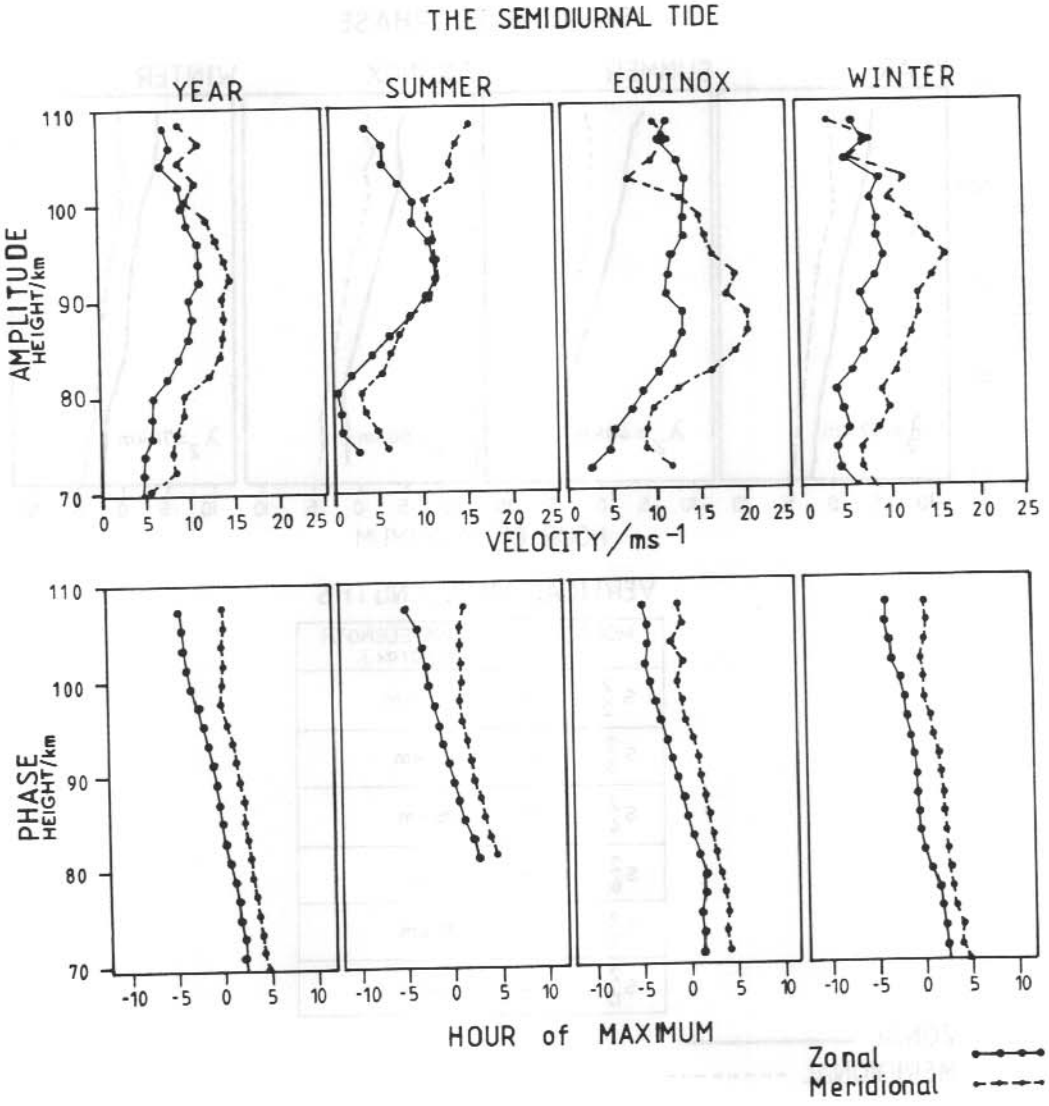

Figure 4. Amplitude and phase profiles of the semidiurnal tide averaged seasonally and over a complete year (1985). The phase hour is in local solar mean time.

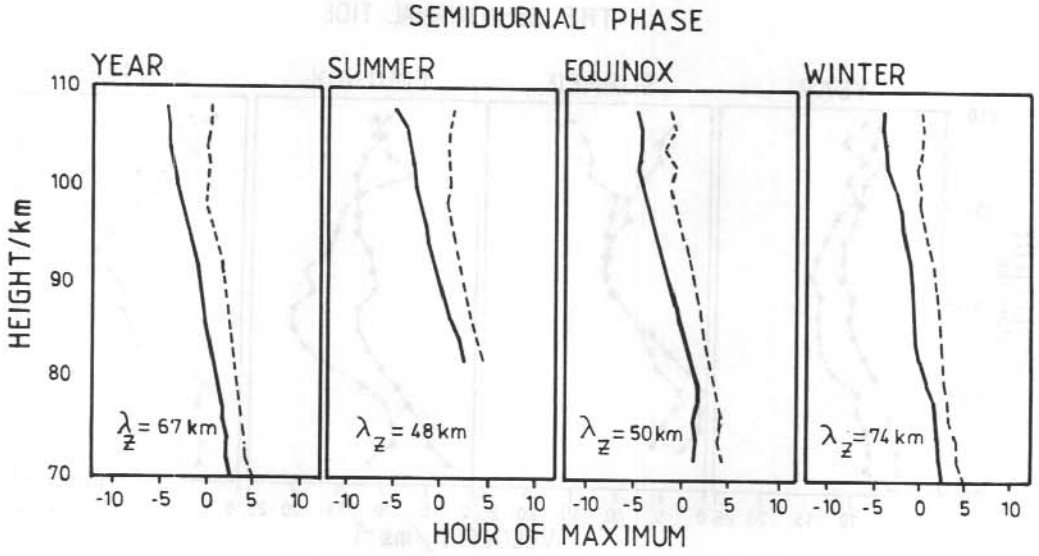

VERTICAL WAVELENGTHS

MODE		WAVELENGTH (Approx.)
S_2^2	—	200 km
S_3^2	—	75 km
S_4^2	—	48 km
S_6^2	—	31 km
S_7^2	—	25 km
S_{12}^2	—	14 km

ZONAL ————
MERIDIONAL --------

Figure 5. Phase profiles of the semidiurnal propagating tide at Mawson, Antarctica. The vertical wave length λ_z is shown averaged for each season and for the year. In the table below, theoretical wavelengths are tabulated for the various modes.

The semidiurnal phase profiles are quite different from the diurnal phase profiles, and are typical of a propagating tide; that is they show a steady phase shift with height, and a fixed phase relationship between the components, indicating an elliptically polarised wave. The phase separation is very close to three hours, which is ninty degrees of phase for a twelve hour tide.

The steepness of the phase slope can indicate which tidal mode is prevalent. From these phase diagrams, the vertical wavelength (the vertical distance for the phase to shift by one complete cycle) can be related back to the Laplace tidal equation, as the various modes of oscillation have different vertical wavelengths associated with them. Figure 5 shows that the vertical wavelength varies from approximately 45 to 75 km. During summer and equinox, the vertical wavelength is 48-50 km which strongly suggests the S_4^2 mode is dominant. Also, at equinox, the global heating function is roughly symmetric between hemispheres and the generation of mainly symmetric modes would be expected. The longer vertical wavelength in winter may be due to a non-symmetric mode, and is likely to be from (in part at least) the S_3^2 mode.

8.4 COMPARISON WITH OTHER DATA

Generally the Mawson data are consistent with expected results from a high latitude station. The MST radar at Poker Flat, Alaska (65°N, 147°W) has a very similar latitude to Mawson (67°S, 65°E) and is conveniently located for comparisons between hemispheres.

In Figure 6 the diurnal amplitudes and phases for Poker Flat (Tetenbaum and Avery 1986) are shown over three-month intervals; results from Mawson are also shown. Error bars are not shown with the Mawson data (for clarity), but generally the error in amplitude is less than 2 ms^{-1} and the error in phase is less than one hour.

Between Mawson and Poker Flat, there is good agreement with the zonal phase and the meridional phase is similar but shifted twelve hours. This type of phase relationship indicates that hemispherically symmetric modes are dominant.

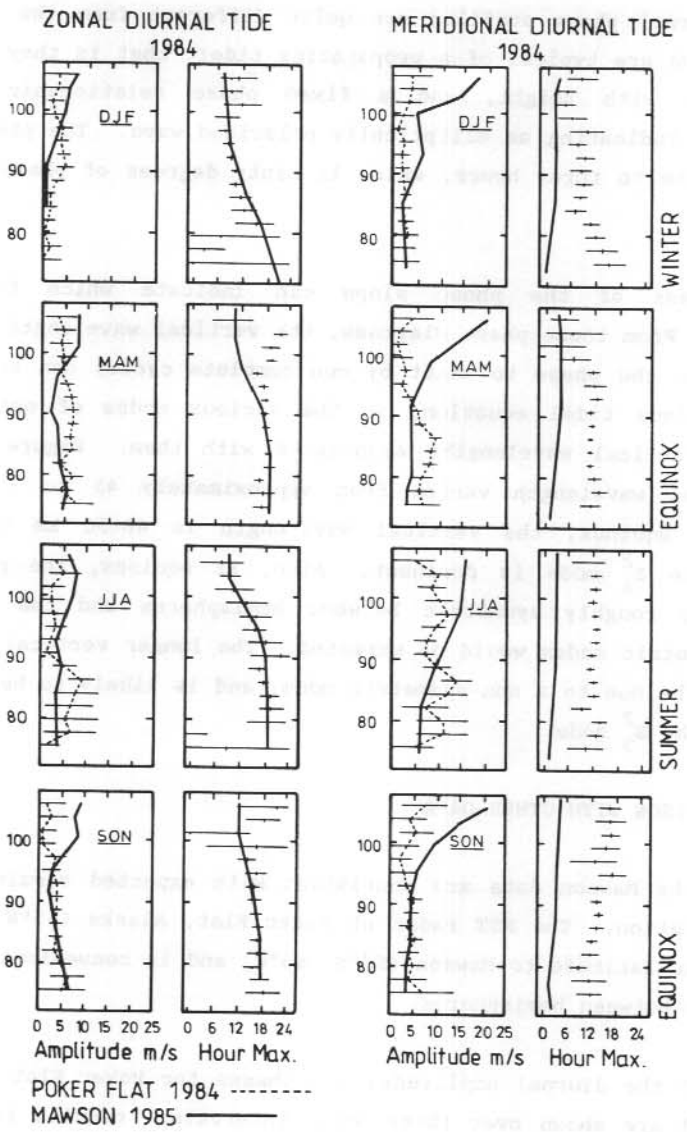

Figure 6. Diurnal amplitude and phase profiles from Poker Flat, Alaska (1984), are compared with data from Mawson, Antarctica, (1985). Poker Flat data have been averaged into four seasons shown by the months DJF (winter), MAM (spring), JJA (summer) and SON (autumn). For a seasonal comparison, the Mawson data have been shifted in time by six months; heights are in kilometres. Error bars have been omitted from the Mawson data for clarity, but generally errors are < 5 ms^{-1} for the amplitude, and < 1 hour for the phase.

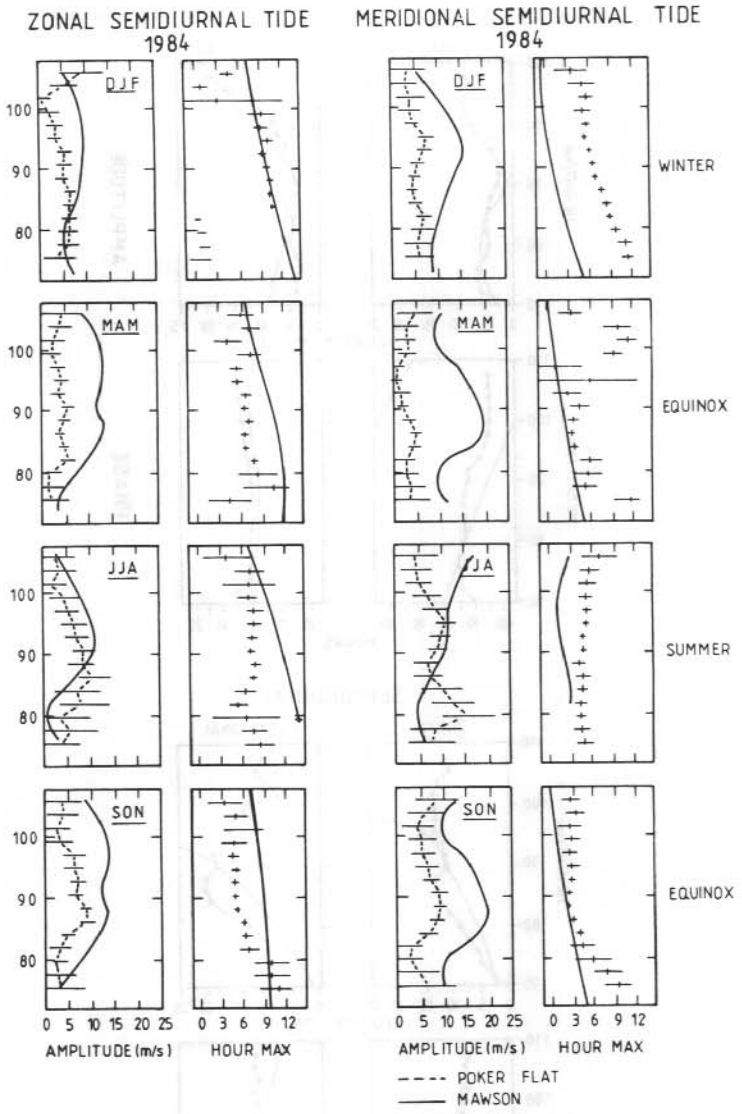

Figure 7. As for Figure 6, except for the semidiurnal tide.

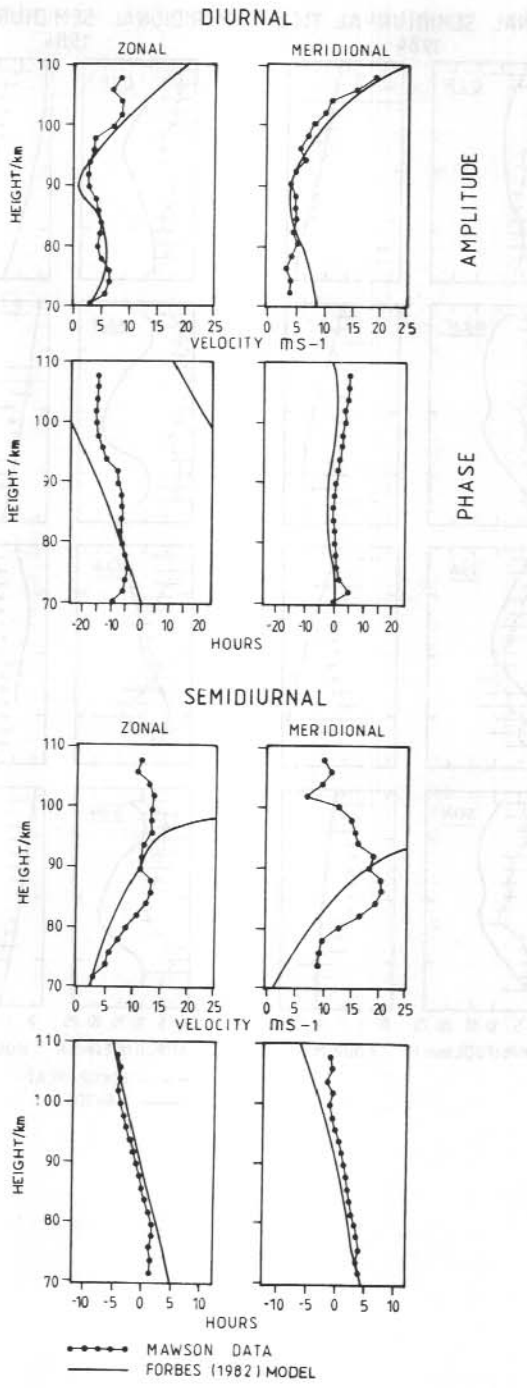

Figure 8. Comparisons with Forbes (1982a,b) model for the diurnal and semidiurnal tide.

Summertime meridional amplitudes are larger than in other seasons at both locations - typically 10-15 ms^{-1} at Poker Flat and 10-20 ms^{-1} at Mawson. Diurnal amplitudes are in general agreement below 90 km, but in all seasons the Mawson velocities are significantly larger, and sometimes very much larger near 110 km.

The semidiurnal tides (Figure 7) show general similarity, but the southern semidiurnal amplitudes tend to be larger and often much larger than in the Northern Hemisphere. Both sites show higher amplitudes during the summer, but results from the two stations only agree below 90 km for the meridional amplitude and above 90 km for the zonal amplitude. Although the southern equinoctial amplitudes are generally twice the size of those from Poker Flat, both places show a broad maximum between 85-95 km. The semidiurnal phases at Poker Flat do not show the distinct linear phase profiles observed in the Mawson data. During the winter, the zonal phases are comparable but the meridional components are in antiphase. As with the diurnal tides, this indicates that a symmetric mode is dominant, though at other times of the year, the picture is not so clear.

The data have also been compared with predictions from Forbes' (1982a) global tidal model. The predicted winds in Figure 8 from Forbes (1982a) are for the equinoctial winds. The model assumes that at this time only symmetric modes are present. Generally the agreement is very good for the diurnal meridional amplitude and phase, but not so good for the zonal phase and amplitude, especially at the higher levels. The predicted semidiurnal amplitudes are too big above about 90 km, but phase agrees quite well.

8.5 CONCLUSIONS

The Mawson mesospheric wind data contain the tidal components one would expect for a high latitude station. In comparison with current data from the Northern Hemisphere the amplitudes of the southern tides are generally larger, especially for the semidiurnal tide. The Forbes (1982a) model predictions require modification at high (southern) latitudes.

ACKNOWLEDGMENTS

The observations discussed here were carried out at the Australian National Antarctic Research Expedition's station at Mawson, Antarctica. The authors thank the Director, Antarctic Division, Department of Science for logistic support. This work was supported by the Australian Research Grants Scheme.

8.6 REFERENCES

Elford, W.A. (1974). A 6-year synoptic study of winds between 80 and 100 km, from meteor trail drifts. Proceedings of the international conference on structure and general circulation of the upper and lower atmospheres and possible anthropagenic perturbations 2:624-641.

Forbes, J.M. (1982a). Atmospheric tides 1. Model description and results for the solar diurnal component. Journal of Geophysical Research 87: 5222-5340.

Forbes, J.M. (1982b) Atmospheric tides 2. The solar and lunar semidiurnal components. Journal of Geophysical Research 87:5241-5252.

Forbes, J.M. and Hagan, M.E. (1986). Diurnal propagating tide in the presence of mean winds and dissipation. Journal of Geophysical Research (In press).

Tetenbaum D. and Avery S.K. (1986). Observations of mean winds and tides in the upper mesosphere during 1980-1984, using the Poker Flat, Alaska, MST Radar as a meteor radar. Journal of Geophysical Research (in press).

Vial, F. (1986). Numerical simulations of atmospheric tides for solstice conditions. Journal of Geophysical Research 91:8955-8969.

9. WINDS IN THE MIDDLE ATMOSPHERE AT MAWSON, ANTARCTICA: III. GEOMAGNETIC AND "METEOROLOGICAL" EFFECTS

A. Phillips and F. Jacka
Mawson Institute for Antarctic Research
University of Adelaide
Adelaide, S.A., Australia, 5000.

ABSTRACT

Winds in the region 70-110 km have been recorded continuously using the 'partial reflection drift' method at Mawson station (67°S,63°E) since July 1984. An investigation has been made to relate the short term fluctuations with the geomagnetic Kp index and with tropospheric data. Some positive correlations are found; possible causes are discussed.

9.1 GEOMAGNETIC EFFECTS

In the upper thermosphere at high latitudes winds are strongly affected by electric fields which are generated by the interaction of the solar wind with the geomagnetic field and mapped down the field lines to the ionosphere; this effect is generally thought to diminish rapidly in the lower thermosphere. The electric field also drives the ionospheric currents, especially the auroral electrojet and the polar cap current system.

In this study, the daily geomagnetic index Ap and the three hourly index Kp have been used as measures of the strength (or more precisely, the variability) of the currents. Johnson and Luhmann (1985a,b), and others have looked for a relationship between wind in the mesosphere and geomagnetic activity, but their results, as well as the results of others show no conclusive correlation. It is therefore expected that the geomagnetic effect is small, if it exists at all. The Mawson radar has been operating continuously since July 1984. It records three to four data points per hour, at 2 km intervals between 70-100 km. This is perhaps the most extensive data set for these heights at high southern latitudes currently available; it lends itself well to searching for small effects.

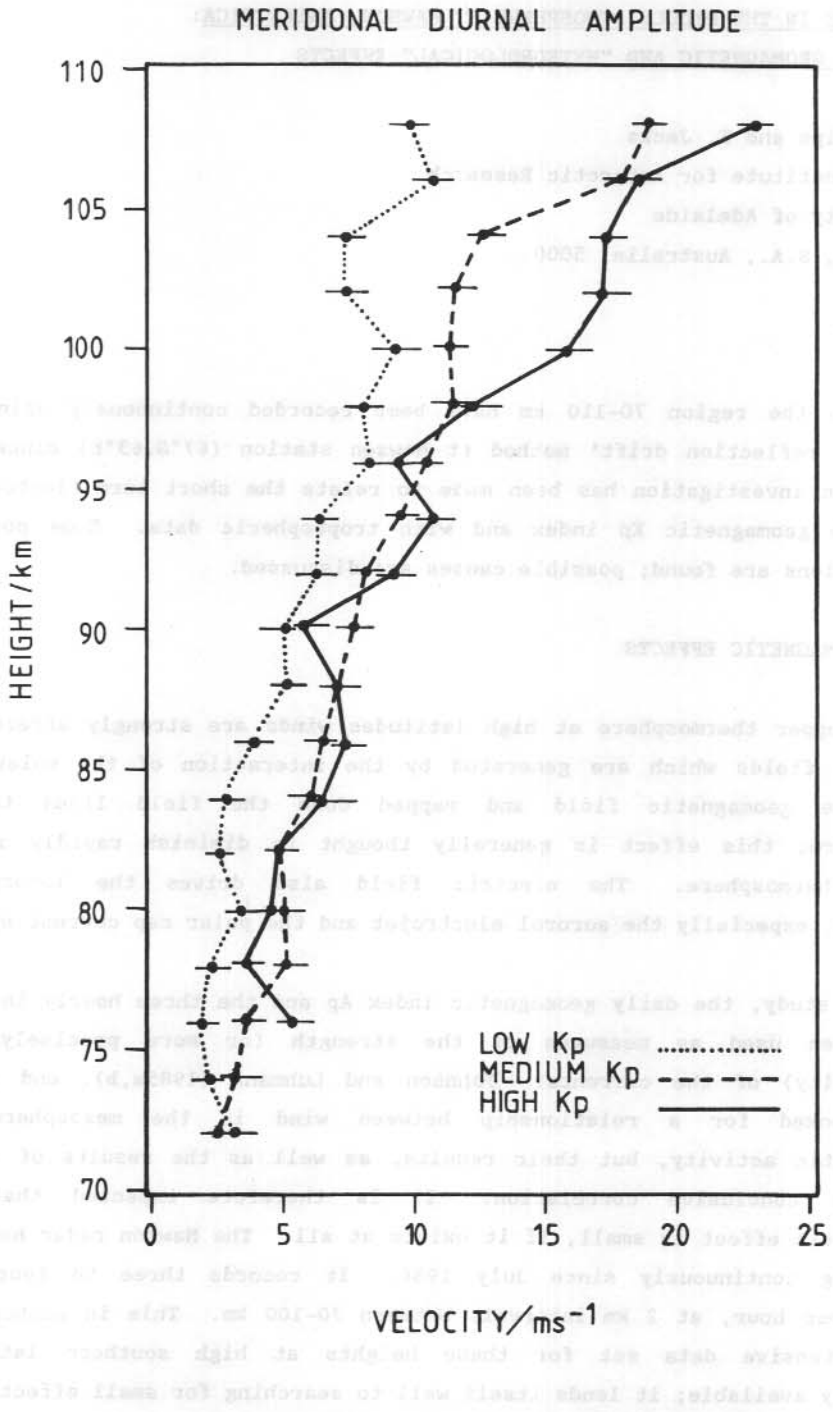

Figure 1. Variation of the magnitude of the meridional component of the diurnal wind as a function of geomagnetic Kp index.

In these studies Kp $\leq$ 2 is taken to indicate geomagnetic quiet and Kp $\geq$ 4 to indicate disturbed conditions. These disturbed periods are typically associated with intense auroral displays caused by higher than normal particle precipitation, when electrons penetrating downwards produce more ionisation in the D-region; this sometimes improves the PRD data acquisition at lower altitudes.

Taking the entire 1985 data set, the data were sorted into high, medium and low Kp bins, and a harmonic analysis was conducted by combining the data into an 'equivalent day'. (An equivalent day is generated by averaging the data according to time of day.) A least squares fit was made to the diurnal and semidiurnal components.

This analysis shows that the amplitude of the meridional component of the diurnal variation has a distinct connection with Kp; the diurnal amplitude increases with increasing Kp as shown by Figure 1. Between about 75 and 95 km the difference in amplitude between high and low Kp categories is 2-4 ms^{-1}. The northward component maximises near dawn. The semidiurnal component of the wind variation is small at all levels.

The planetary Ap index is used to characterise the level of geomagnetic disturbance on a daily basis. If the data are sorted according to high, medium or low Ap the results show nothing of significance. The authors' tentative conclusion is that whatever mechanism is relating the two phenomena it is shortlived and lasts in the order of hours.

The Kp effect seems to be present only in the meridional component of the diurnal variation. At first glance this would suggest that a disturbance to the north or south of Mawson is propagating along the geographic meridian. If for instance the disturbance were caused by sudden heating from the auroral electrojet it might be expected to propagate in a geomagnetic north-south direction. Working on this hypothesis the coordinate axes were rotated to the invariant magnetic L-coordinate system but the magnetic meridional component was no stronger than the geographic meridional component.

Forbes' (1986) tidal model predicts significant increases in the winds in the lower thermosphere between 100 and 110 km at times of high UV/EUV

heating. This has not been observed in the data. However, the sun is currently in the quiet phase of its eleven year cycle and is not producing the intense prolonged activity required for large UV/EUV heating. Since the geomagnetic effect is observed when sorted according to three hour Kp, yet not observed when sorting according to daily Ap, this suggests a rather rapid response to the forcing process.

An alternative hypothesis to explain the significant increase in the meridional component of the diurnal variation with increases in Kp invokes ion drag in the direction of the electric field E. At the height of the observations, the gyro-frequency is much less than the collision frequency so the component of motion in the $\underline{E} \times \underline{B}$ direction will be small. In the upper thermosphere this is dominant (cf. Wardill et al. 1987). In the lower thermosphere the wind direction lies between that of E and $\underline{E} \times \underline{B}$ (cf. Jones and Jacka 1987). An idealised representation of the equipotentials of the electric field is shown in Figure 2. While the earth rotates under this pattern, Mawson station moves around a circular path at 70° geomagnetic invariant latitude. The ion drag would be expected to be largely meridional and diurnal with the maximum northward component near dawn and enhanced at times of high Kp. This is what is observed and illustrated in Figures 1 and 2.

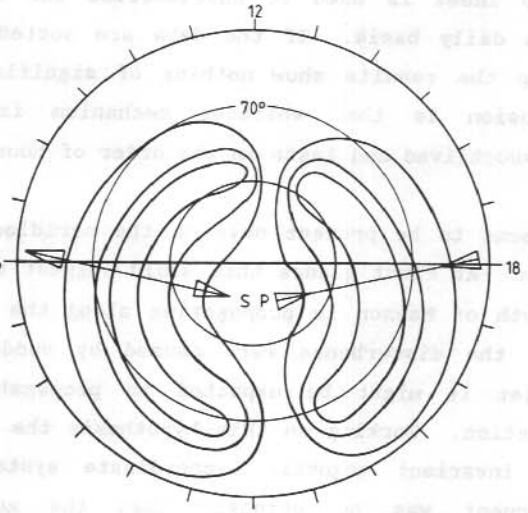

Figure 2. Equipotentials of the high latitude ionospheric electric field. The arrows indicate the approximate direction of the electric field across the dawn-dusk meridian. Coordinates are invariant latitude and magnetic local time. Adapted from Heelis et al. (1982).

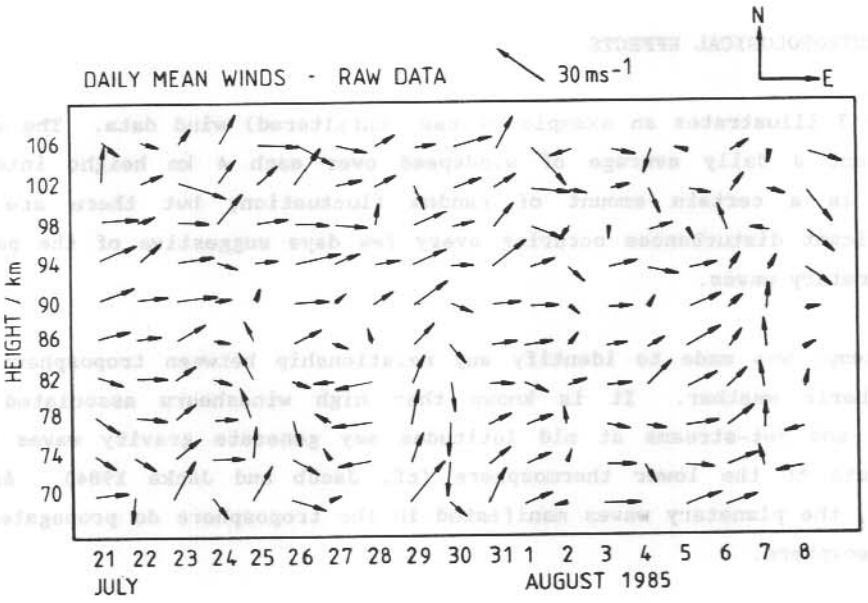

Figure 3. Average daily wind velocity vectors during July and August 1985. Each vector represents the average of 4 km of wind data centred on the height indicated.

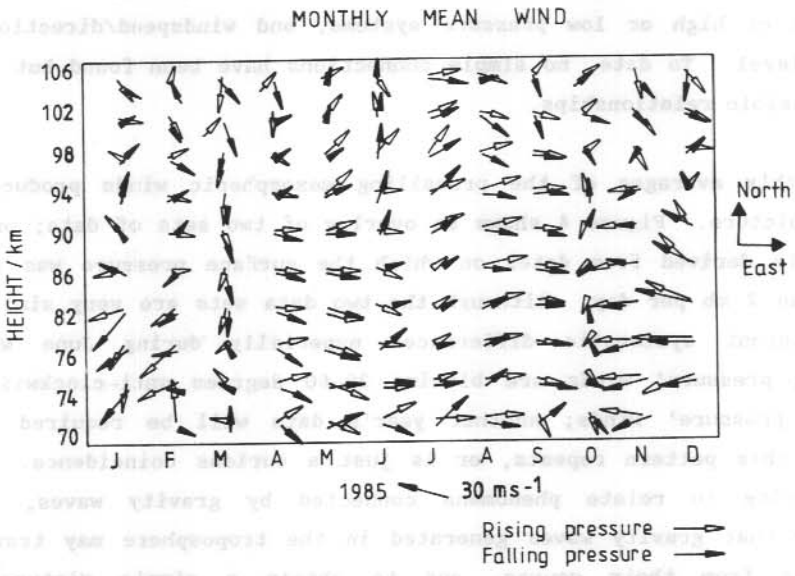

Figure 4. An overlay of two sets of data. The shaded arrows are derived from dates on which the surface pressure was falling by more than 2 mb per day and the unshaded arrows are from days when the pressure was rising by more than 2 mb per day.

9.2 METEOROLOGICAL EFFECTS

Figure 3 illustrates an example of raw (unfiltered) wind data. The arrows represent a daily average of windspeed over each 4 km height interval. There is a certain amount of random fluctuation, but there are also significant disturbances occuring every few days suggestive of the passage of planetary waves.

An attempt was made to identify any relationship between tropospheric and mesospheric weather. It is known that high windshears associated with fronts and jet-streams at mid latitudes may generate gravity waves which propagate to the lower thermosphere (cf. Jacob and Jacka 1984). And of course, the planetary waves manifested in the troposphere do propagate into the mesosphere.

Using charts published by the European Centre for Medium Range Forecast (consisting of a sea level pressure and 500 mb geopotential height chart) a comparison was made with the mesospheric disturbances. Comparisons were made with large changes of surface pressure, the passage of fronts, the presence of high or low pressure systems, and windspeed/direction at the 500 mb level. To date, no simple connections have been found but there are some possible relationships.

The monthly averages of the prevailing mesospheric winds produce a very smooth picture. Figure 4 shows an overlay of two sets of data; one set of arrows is derived from dates on which the surface pressure was rising by more than 2 mb per day. Although the two data sets are very similar there are apparent systematic differences especially during June where the 'falling pressure' winds are blowing 30-60 degrees anti-clockwise to the 'rising pressure' winds; another year's data will be required to check whether this pattern repeats, or is just a curious coincidence. However, when trying to relate phenomena connected by gravity waves, one must remember that gravity waves generated in the troposphere may travel great distances from their source, and to obtain a simple picture may be impossible.

ACKNOWLEDGMENTS

The observations discussed here were carried out at the Australian National Antarctic Research Expedition's station at Mawson, Antarctica. The authors thank the Director, Antarctic Division, Department of Science for logistic support. This work was supported by the Australian Research Grants Scheme.

9.3 REFERENCES

Forbes, J.M. (1986). Private communication.

Heelis, R.A., Lowell, J.K. and Spiro, R.W. (1982). A model of the high latitude ionospheric convection pattern. Journal of Geophysical Research 87:6339-6345.

Jacob, P.G. and Jacka, F. (1985). Internal gravity waves at the 95 km level. Middle Atmosphere Program Handbook 18:248-252.

Johnson, R.M. and Luhman, J.G. (1985a). Neutral wind spectra of the auroral zone mesopause: geomagnetic effect? Journal of Geophysical Research 90:1735-1743.

Johnson, R.M. and Luhmann, J.G. (1985b). High latitude mesopause neutral winds and geomagnetic activity: A cross-correlation analysis. Journal of Geophysical Research 90:8501-8506

Jones, N.D. and Jacka, F. (1987). Dynamics of the thermosphere over Mawson, Antarctica. IV The lower thermosphere. ANARE Research Notes. (Chapter 13 this volume).

Wardill, P., Jones, N.D. and Jacka, F. (1987). Dynamics of the thermosphere over Mawson, Antarctica. I. Diurnal variation and geomagnetic dependence. ANARE Research Notes (Chapter 10 this volume).

10. DYNAMICS OF THE THERMOSPHERE OVER MAWSON, ANTARCTICA: I. DIURNAL VARIATION AND GEOMAGNETIC DEPENDENCE

P. Wardill, N. Jones and F. Jacka
Mawson Institute for Antarctic Research
University of Adelaide
Adelaide, S.A., Australia, 5000.

ABSTRACT

A scanning Fabry-Perot spectrometer at Mawson, Antarctica (67.6°S, 62.9°E, invariant latitude 70°S) was used to measure Doppler shift and broadening of the OI λ630 nm emission in the night airglow and aurora. Analysis of these measurements has yielded estimates of neutral thermospheric temperatures and wind velocities in the 200-300 km region. Viewed in geomagnetic coordinates the averaged wind velocities were south-westward (sunward) during the afternoon and evening hours and equatorward (antisunward) around magnetic midnight. Wind speeds ranged from ~100 ms^{-1} during quiet and moderate geomagnetic conditions up to ~200 ms^{-1} during disturbed conditions. The results confirm that the principal momentum source in the high latitude thermosphere is ion drag, resulting from the motion of ions in response to the polar electric field pattern.

10.1 INTRODUCTION

The importance of ion drag forcing in the dynamics of the high latitude thermosphere has been recognised for over a decade (Cole 1971, Rees 1971, Meriwether et al. 1973). Ions within this region move in response to electric fields of magnetospheric origin which are mapped onto the polar ionosphere via the geomagnetic field lines. An idealised version of the resulting system of equipotentials is shown in Figure 1, adapted from Heelis et al. (1982).

At F-region heights the ion and electron gyro-frequencies exceed the collision frequencies and the ionospheric plasma moves in the direction of $\underline{E} \times \underline{B}$. The motion is therefore parallel to the equipotentials in the direction indicated by the arrows. The plasma convection pattern consists of two oppositely directed circulation cells with antisunward flow across

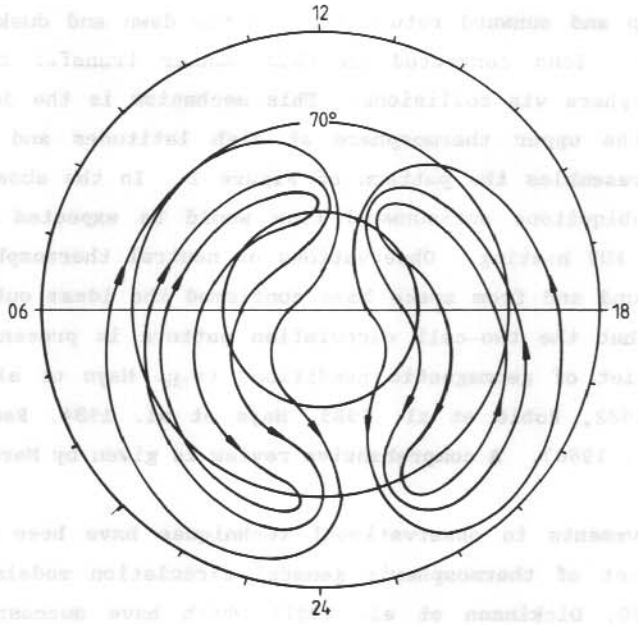

Figure 1. Idealised representation of the high-latitude ion convection pattern viewed from above the southern polar cap. The thick curves represent equipotentials; plasma is convected roughly parallel to these, in the direction indicated by the arrows. Coordinates are invariant latitude and magnetic local time. Adapted from Heelis et al. (1982).

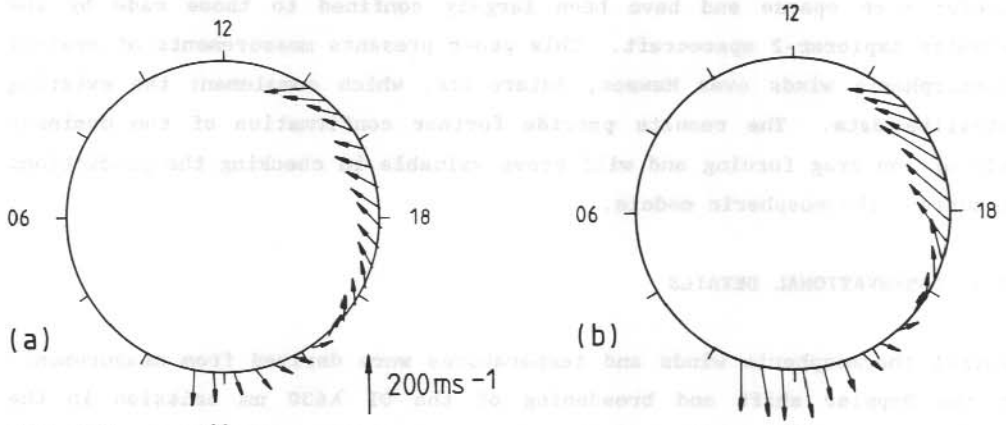

Figure 2.

(a) Averaged thermospheric wind vectors, observed at Mawson, for geomagnetically quiet and moderate conditions (A_p<25), plotted around the 70° invariant latitude circle as a function of magnetic local time.

(b) As above, but for disturbed conditions ($A_p \geq 25$).

the polar cap and sunward return flow in the dawn and dusk sectors of the auroral oval. Ions convected in this manner transfer momentum to the neutral atmosphere via collisions. This mechanism is the dominant momentum source for the upper thermosphere at high latitudes and so the neutral circulation resembles the pattern of Figure 1. In the absence of ion drag forcing, a ubiquitous antisunward flow would be expected as a result of solar UV and EUV heating. Observations of neutral thermospheric winds both from the ground and from space have confirmed the ideas outlined above and have shown that the two-cell circulation pattern is present under all but the most quiet of geomagnetic conditions (e.g. Hays et al. 1979, Heppner and Miller 1982, Roble et al. 1983, Hays et al. 1984. Rees et al. 1985, Killeen et al. 1986). A comprehensive review is given by Meriwether (1983).

Recent improvements in observational techniques have been complemented by the development of thermospheric general circulation models (Fuller-Rowell and Rees 1980, Dickinson et al. 1981) which have successfully predicted aspects both of the steady-state thermosphere and of the perturbations arising from geomagnetic energy and momentum sources (Fuller-Rowell and Rees 1981, Roble et al. 1982, Rees et al. 1983). The continued development of these models requires global-scale observations to permit detailed comparison with model predictions and hence to evaluate precisely the nature of the various model inputs. Observations from high southern latitudes have however been sparse and have been largely confined to those made by the Dynamics Explorer-2 spacecraft. This paper presents measurements of neutral thermospheric winds over Mawson, Antarctica, which complement the existing satellite data. The results provide further confirmation of the dominant role of ion drag forcing and will prove valuable in checking the predictions of current thermospheric models.

10.2 OBSERVATIONAL DETAILS

Neutral thermospheric winds and temperatures were derived from measurements of the Doppler shift and broadening of the OI λ630 nm emission in the airglow and aurora. This emission occurs over the height range ~200-300 km within which the vertical gradients of wind and temperature are usually small. The measurements were made using a 150 mm aperture, separation-scanned Fabry-Perot spectrometer. Further details of this instrument are given by Jacka (1984) and by Wardill and Jacka (1986).

The normal observing cycle consists of observations in the zenith and in the geographic cardinal directions at a zenith angle of 60 degrees, alternating with wavelength calibrations obtained from a neon source. The time required for accumulation of a single 630 nm line profile varies from five to twenty minutes. After correcting the observations for instrument wavelength drift, a zero velocity reference is obtained from the average of all zenith observations made during the observing period. The horizontal wind velocities are calculated from the off-zenith observations and these records are interpolated to give half-hourly samples. The meridional and zonal components of the wind velocity are then calculated by averaging the north and south and the east and west samples respectively. This procedure yields half-hourly estimates of the overhead wind vector which may then be averaged according to geomagnetic activity or other criteria.

10.3 RESULTS

Wind observations from fifty nights during the equinoxes and winter of 1983 were considered. In order to assess the dependence upon geomagnetic activity these data were divided night by night into two categories according to the A_p index. The first category ($A_p<25$) corresponded to quiet to moderate conditions and contained forty-one nights of observations. The second category, ($A_p \geq 25$), corresponding to disturbed conditions, contained nine nights.

Figure 2 shows the averages over these categories of the half-hourly wind vectors, transformed to geomagnetic coordinates. The general form of the circulation was similar in the two cases with south-westward (sunward) flow in the afternoon and evening hours changing to equatorward (antisunward) flow around magnetic midnight. Wind speeds were typically ~ 100 ms^{-1} during quiet/moderate conditions and increased to ~ 200 ms^{-1} during disturbed conditions. A pronounced reduction in wind speed was observed to coincide with the maximum rate of change of wind direction around 2000-2200 magnetic local time (MLT).

10.4 DISCUSSION AND CONCLUSIONS

The observed winds follow the pattern of ion convection described earlier and illustrated in Figure 1. The afternoon and evening measurements are

made within the sunward-flowing region of the dusk convection cell. Equatorward winds observed near magnetic midnight occur as Mawson enters the region of antisunward convection across the polar cap. Reduced wind speeds are observed around 2000-2200 MLT as the station passes close to the stagnant centre of the dusk cell.

During disturbed conditions, the polar electric field strength and the ionospheric conductivity are enhanced. Both of these effects lead to increased ion-neutral momentum transfer and hence to increased neutral velocities as observed.

These results therefore confirm that ion-drag forcing is the principal momentum source for the high-latitude thermosphere, in agreement with similar studies in the northern hemisphere and with the predictions of thermospheric general circulation models. Liaison with the modelling community is currently underway with the aim of making more detailed comparisons between observations and model predictions. It is hoped that these efforts will lead to better estimates of model parameters, particularly with regard to hemispheric asymmetries.

ACKNOWLEDGMENTS

The observations discussed here were carried out at the Australian National Antarctic Research Expedition's station at Mawson, Antarctica. The authors thank the Director, Antarctic Division, Department of Science for logistic support. This work was supported by the Australian Research Grants Scheme.

10.5 REFERENCES

Cole, K.D. (1971). Electrodynamic heating and movement of the thermosphere. Planetary and Space Science 19:59-75.

Dickinson, R.E., Ridley, E.C. and Roble, R.G. (1981). A three-dimensional general circulation model of the thermosphere. Journal of Geophysical Research 86:1499-1512.

Fuller-Rowell, T.J. and Rees, D. (1980). A three-dimensional time-dependent global model of the thermosphere. Journal of Atmospheric Science 37: 2545-2567.

Fuller-Rowell, T.J. and Rees, D. (1981). A three-dimensional time-dependent simulation of the global dynamical response of the thermosphere to a geomagnetic substorm. Journal of Atmospheric and Terrestrial Physics 43:701-721.

Hays, P.B., Meriwether, J.W. and Roble, R.G. (1979). Nighttime thermospheric winds at high latitudes. Journal of Geophysical Research 84:1905-1913.

Hays, P.B., Killeen, T.L., Spencer, N.W., Wharton, L.E., Roble, R.G., Emery, B.A., Fuller-Rowell, T.J., Rees, D., Frank, L.A. and Craven, J.D. (1984). Observations of the dynamics of the polar thermosphere. Journal of Geophysical Research 89:5597-5612.

Heelis, R.A., Lowell, J.K. and Spiro, R.W. (1982). A model of the high-latitude ionospheric convection pattern. Journal of Geophysical Research 87:6339-6345.

Heppner, J.P. and Miller, M.L. (1982). Thermospheric winds at high latitudes from chemical release observations. Journal of Geophysical Research 87:1633-1647.

Jacka, F. (1984). Application of Fabry-Perot spectrometers for measurement of upper atmosphere temperatures and winds. In: Vincent, R.A. (Ed.). Handbook for MAP 13:19-40.

Killeen, T.L., Roble, R.G., Smith, R.W., Spencer, N.W., Meriwether, J.W., Rees, D., Hernandez, G., Hays, P.B., Cogger, L.L., Sipler, D.P., Biondi, M.A. and Tepley, C.A. (1986). Mean neutral circulation in the winter polar F-region. Journal of Geophysical Research 91:1633-1650.

Meriwether, J.W. (1983). Observations of thermospheric dynamics at high latitudes from ground and space. Radio Science 18:1035-1052.

Meriwether, J.W., Heppner, J.P., Stolarik, J.D. and Westcott, E.M. (1973). Neutral winds above 200 km at high latitudes. Journal of Geophysical Research 78:6643-6661.

Rees, D. (1971). Ionospheric winds in the auroral zone. Journal of the British Interplanetary Society 24:233-246.

Rees, D., Fuller-Rowell, T.J., Gordon, R., Killeen, T.L., Hays, P.B., Wharton, L. and Spencer, N.W. (1983). A comparison of wind observations of the upper thermosphere from the Dynamics Explorer satellite with the predictions of a global time-dependent model. Planetary and Space Science 31:1299-1314.

Rees, D., Gordon, R., Fuller-Rowell, T.J., Smith, M., Carignan, G.R., Killeen, T.L., Hays, P.B. and Spencer, N.W. (1985). The composition, structure, temperature and dynamics of the upper thermosphere in the polar regions during October to December 1981. Planetary and Space Science 33:617-666.

Roble, R.G., Dickinson, R.E. and Ridley, E.C. (1982). Global circulation and temperature structure of the thermosphere with high-latitude plasma convection. Journal of Geophysical Research 87:1599-1614.

Roble, R.G., Dickinson, R.E., Ridley, E.C., Emery, B.A., Hays, P.B., Killeen, T.L. and Spencer, N.W. (1983). The high-latitude circulation and temperature structure of the thermosphere near solstice. Planetary and Space Science 31:1479-1499.

Wardill, P. and Jacka, F. (1986). Vertical motions in the thermosphere over Mawson, Antarctica. Journal of Atmospheric and Terrestrial Physics 48: 289-292.

11. DYNAMICS OF THE THERMOSPHERE OVER MAWSON, ANTARCTICA:
II. DEPENDENCE ON THE Y COMPONENT OF THE INTERPLANETARY MAGNETIC FIELD

N. Jones, P. Wardill and F. Jacka
Mawson Institute for Antarctic Research
University of Adelaide
Adelaide, S.A., Australia, 5000.

ABSTRACT

Ion drag, resulting from collisions between neutral particles and ions driven by the high-latitude electric field, constitutes the dominant momentum source for the neutral thermosphere at high latitudes. It is well known that the strength and geographic extent of the electric field increase with geomagnetic activity. More recently it has been learned that the characteristic geometry of the electric field shows a clear dependence on the sense of the Y (azimuthal) component of the interplanetary magnetic field (IMF-BY).

The thermospheric wind signatures that would be expected at a southern auroral zone location for each of the characteristic field geometries are considered, and thermospheric wind data obtained from the Mawson Institute's Fabry-Perot spectrometer (FPS) at Mawson, Antarctica (67.6°S, 62.9°E, invariant latitude 70°S) during 1981, 1982 and 1983 are examined for evidence of them.

Some features of the expected signatures are observed in the night-time wind data from 1981 and 1983. More convincing evidence is found in two separate twenty-four hour long continuous wind observations made using the daylight observing capability of the Mawson FPS.

NOTE ADDED IN PROOF:
The authors have recently learned that magnetic field measurements made by the ISEE-3 spacecraft during 1983 were not always representative of interplanetary conditions. The conclusions drawn from the 1983 data should therefore be regarded as provisional.

FIG. 1a

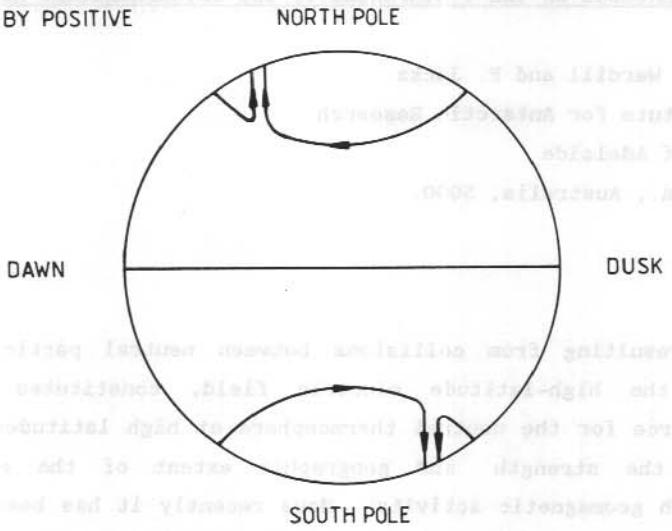

FIG. 1b

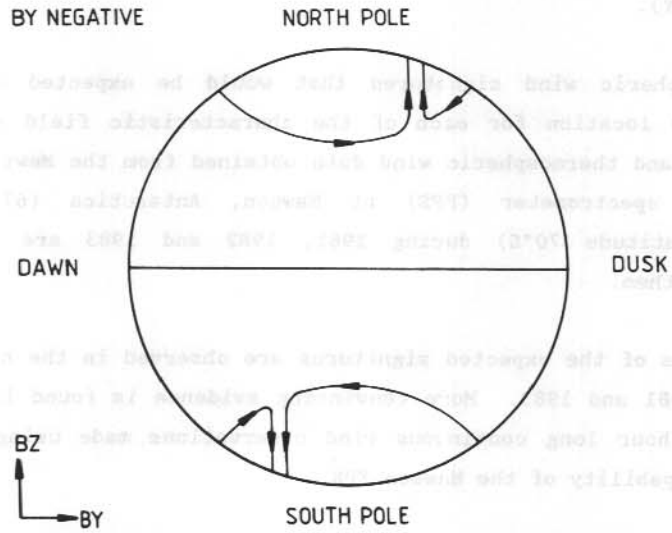

Figure 1. A schematic view of the earth from the sun, indicating the high-latitude ion convection patterns that prevail for;

(a) IMF-BY positive; the Northern Hemisphere dusk cell and the Southern Hemisphere dawn cell are enlarged.

(b) IMF-BY negative; the Northern Hemisphere dawn and Southern Hemisphere dusk cell are enlarged.

The coordinate system for the IMF is also indicated.

11.1 INTRODUCTION

The interaction of the solar wind and the geomagnetic field results in the generation of large scale electric fields which map down into the polar upper atmosphere because of high conductivity along the geomagnetic field lines. These electric fields cause the ionospheric plasma to flow in a characteristic double vortex pattern. Ions driven in this manner undergo collisions with, and thereby transfer momentum to, the neutral atmosphere. This ion drag process constitutes the dominant momentum source for the upper thermosphere at high latitudes and hence it also exhibits the double vortex circulation pattern.

As Wardill et al. (1987) have shown, many of the features of the night-time dynamical behaviour of the auroral zone thermosphere can be explained in terms of ion-drag control of the flow, assuming a roughly symmetric, sun-aligned model of the high-latitude electric field, such as the one due to Heelis et al. (1982). Since that model was published, a great deal of new data on the high-latitude electric field, from all local time zones, has been obtained from the Vector Electric Field Instrument on the Dynamics Explorer-2 spacecraft. During the same period, many properties of the interplanetary medium, in particular the interplanetary magnetic field (IMF), have been monitored by instruments on the International Sun-Earth Explorer-3 (ISEE-3) spacecraft. Analysis of this new data has confirmed earlier suggestions that the characteristic geometry of the high-latitude electric field shows a clear dependence on the sign of the Y (azimuthal) component of the IMF.

Recently, electric field models which show this dependence have been completed by Heppner and Maynard (1986). The most important feature of these new models is that they show a marked asymmetry in the relative sizes of the dawn and dusk circulation cells. The direction of this asymmetry is opposite in opposite hemispheres for a given direction of the IMF-BY (Figure 1). The coordinate system for the IMF is indicated on Figure 1; BZ is positive in the direction of the northward pointing normal to the ecliptic plane; BY is positive in the azimuthal direction opposite to the direction of the earth's orbital motion. Figure 1a shows a view of the earth from the sun for conditions of BY greater than zero. The Northern Hemisphere dusk cell and the Southern Hemisphere dawn cell are enhanced.

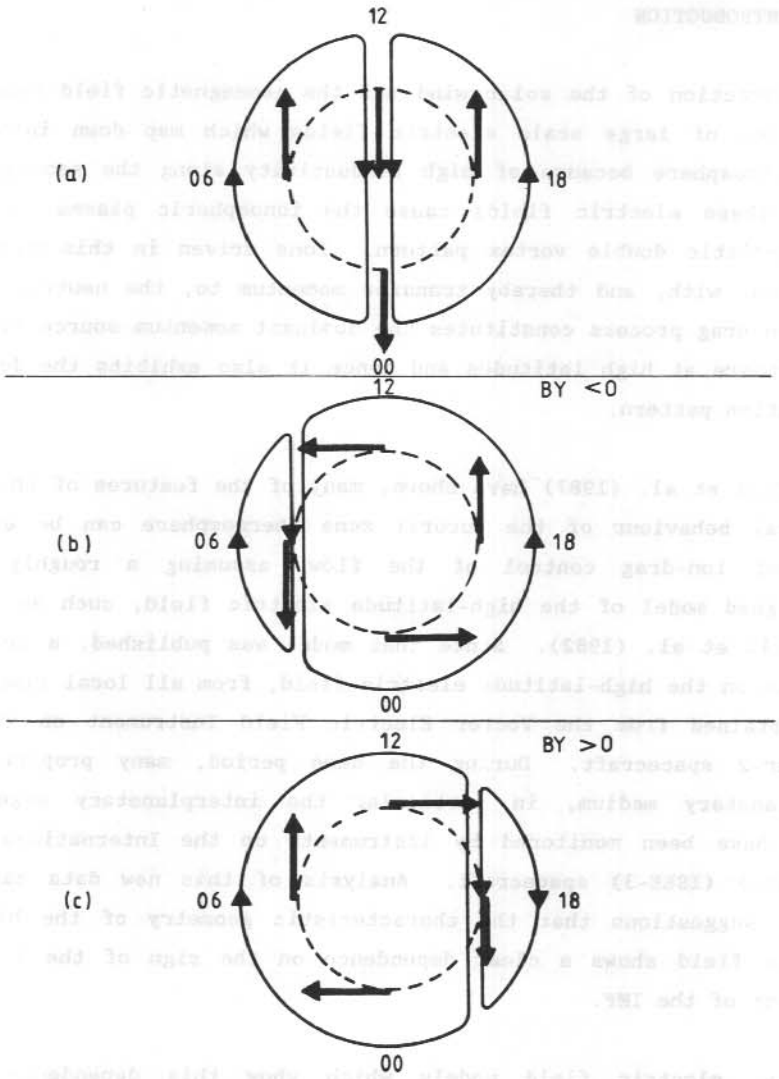

Figure 2. A schematic diagram indicating the characteristic thermospheric wind pattern that would be expected at a Southern Hemisphere auroral zone location for;

(a) A symmetric, sun aligned electric field distribution; the wind is westward (sunward) at dusk, equatorward (antisunward) at midnight, eastward (sunward) at dawn and poleward (antisunward) at midday.

(b) An enhanced dusk cell, as would be associated with a negative IMF-BY; the wind is to the magnetic west at all times.

(c) An enhanced dawn cell, as would be associated with a positive IMF-BY; the wind is always to the magnetic east.

Figure 1b shows the same view for BY less than zero. Here the Northern Hemisphere dawn and Southern Hemisphere dusk cells are enlarged.

Consider now, in a very elementary way, the characteristic wind fields that the different electric field geometries would generate at a southern auroral zone location.

Figure 2a shows a sun aligned electric field distribution; the winds expected to result are poleward at midday, westward (sunward) at dusk, equatorward at midnight and eastward (sunward) at dawn. Figure 2b shows the situation that prevails for negative BY; the dusk cell is enlarged, and the wind is always toward the magnetic west. Figure 2c shows the BY positive situation; the enlarged dawn cell results in the circulation being always to the magnetic east.

Thermospheric wind data from the Fabry-Perot spectrometer at Mawson obtained during 1981, 1982 and 1983 have been examined for evidence of any such characteristic behaviour associated with a particular sense of the IMF-BY.

11.2 RESULTS

Details of the Mawson Fabry-Perot spectrometer (FPS) and its application to the study of wind and temperature in the thermosphere are given in Wardill et al. (1987) (and references therein). IMF data from the ISEE-3 spacecraft were obtained and the night-time thermospheric wind data from the Mawson FPS were grouped according to whether the Y component of the IMF was positive, negative, or indeterminate. Data from periods when the IMF Z component was clearly positive (Northward) were rejected, since Heppner and Maynard (1986) have shown that under those conditions, the high latitude electric field may depart significantly from their models. This left roughly ten nights in each of the BY bins for each of the years 1981 and 1983 (no FPS data were obtained during the 1982 winter). The averages of the wind vectors for the BY positive and BY negative bins for each year are shown in Figure 3.

Identification of a particular wind pattern would be facilitated if wind data were available for the full diurnal cycle. In addition to the 150 mm diameter high resolution etalon, the Mawson FPS incorporates a second, low resolution etalon which may be brought into use to provide the extra

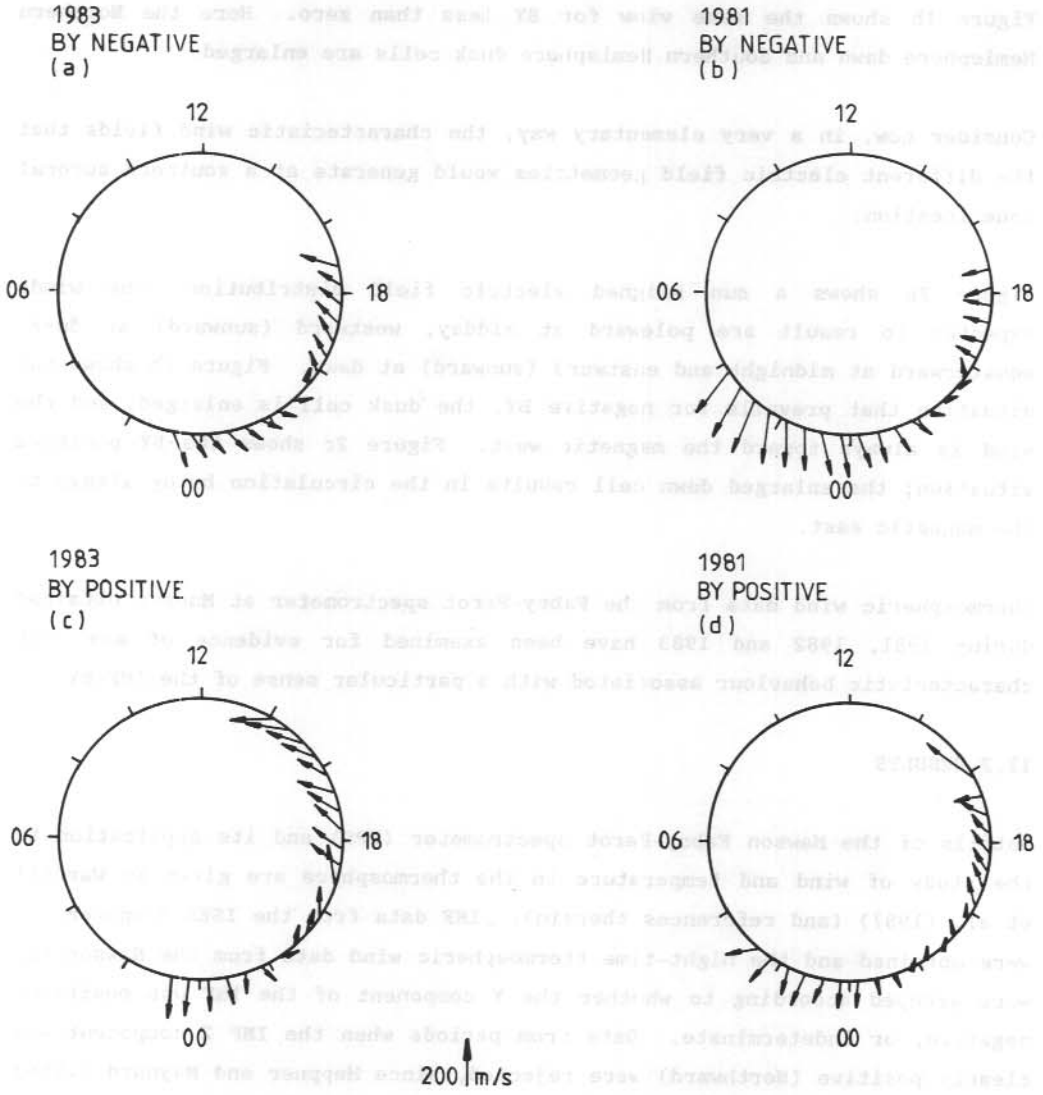

Figure 3. Nighttime thermospheric wind vectors measured with the Mawson FPS. The vectors are plotted in geomagnetic coordinates as a function of local magnetic time. The coordinate system rotates so that magnetic southward is everywhere toward the centre of the dial, and magnetic westward is anticlockwise.

(a) Average wind vectors for 1983 for IMF-BY negative

(b) Average wind vectors for 1981 for IMF-BY negative

(c) Average wind vectors for 1983 for IMF-BY positive

(d) Average wind vectors for 1981 for IMF-BY positive

filtering necessary to measure the Doppler width and shift of the oxygen red line during daylight hours, using the method described by Cocks et al. (1980) and Cocks (1983). This gives us the ability to monitor thermospheric neutral wind and temperature on a continuous basis (given clear skies).

Figure 4 shows the wind results from two separate daylight observing runs, the first in 1981 and the second in 1983. BY was negative for the duration of the 1983 data. Whilst the IMF record for the time of 1981 data was marred by two data gaps, and a period of a few hours near magnetic midday where the Y component made several brief positive excursions, BY was predominantly negative then also.

11.3 DISCUSSION AND CONCLUSION

11.3.1 Nighttime results

Recall that for BY negative, our simple model gave winds that were always toward the magnetic west, and that for BY positive, the winds were always toward the magnetic east. Clearly the results do not show such a dramatic difference between the two cases, but we should note the following;

1. The zonal flow around magnetic midnight was, although small, westward for the BY negative case in both years, and eastward for the BY positive case in both years, consistent with our expectations.
2. In the 1981 BY negative data, the maximum antisunward wind velocity occurred well after magnetic midnight, consistent with the expected enhanced dusk cell.
3. The eastward wind at dusk, predicted for the BY positive case, due to a dominant cyclonic dawn cell, was not observed, but this may be explained as follows. Using their thermospheric general circulation model, Fuller-Rowell and Rees (1984) have demonstrated that the anti-cyclonic neutral wind cell is more effectively excited by ion convection than is the cyclonic cell, since the geographic scale and typical velocities are such that the Coriolis force acts in such a way as to assist the anti-cyclonic vortex to develop. This can easily be seen to be the case if one recalls that a parcel of air in the Southern Hemisphere is deflected to the left of its path by the Coriolis force. Clearly the motion in the anti-cyclonic dusk cell is much more like the natural motion than is the motion in the cyclonic dawn cell.

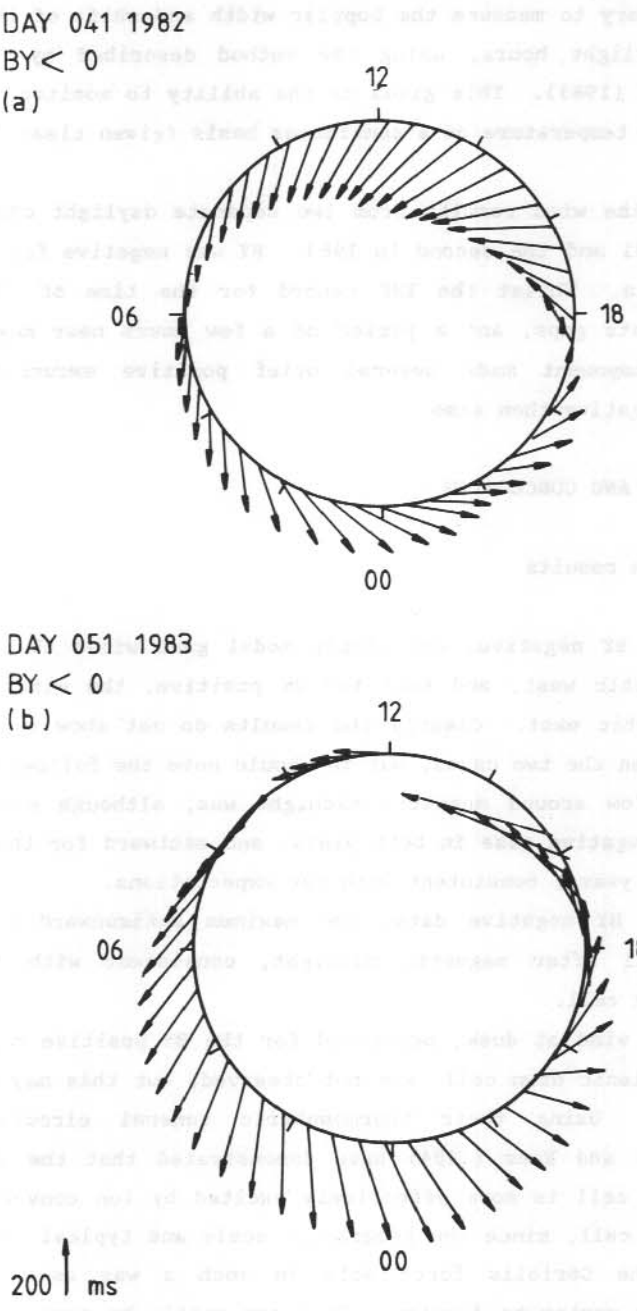

Figure 4. Half-hourly thermospheric wind vectors obtained during daylight using the dual etalon mode of the Mawson FPS;

(a) on day 41 of 1982

(b) on day 51 of 1983

11.3.2 Daytime results

Both wind records show a striking westward vorticity, which is as we would predict, given the negative IMF-BY. The wind patterns both show significant meridional flow in addition to the westward zonal flow. This meridional flow is mainly poleward (antisunward) during the day, and equatorward (also antisunward) at night. This antisunward flow is consistent with the flow expected to result from heating of the atmosphere by absorption of solar UV radiation.

11.3.3 Conclusion

This preliminary examination of the Mawson thermospheric wind data supports the thesis that the high-latitude thermospheric wind field is influenced by the sign of the Y component of the IMF. This argument will be more critically examined when Mawson FPS data from 1984 and 1986 are analysed.

ACKNOWLEDGMENTS

The IMF data from the ISEE-3 spacecraft were supplied by the World Data Center A for Rockets and Satellites, at the Goddard Space Flight Center, Maryland. The observations presented here were carried out at the Australian National Antarctic Research Expedition's station at Mawson, Antarctica. The authors thank the Director, Antarctic Division, Department of Science for logistic support. This work was supported by the Australian Research Grants Scheme.

11.4 REFERENCES

Cocks, T.D. (1983). Dual Fabry-Perot spectrometer measurements of daytime thermospheric temperature and wind velocity: Data analysis procedures. Applied Optics 2:726-732.

Cocks, T.D., Creighton, D.F. and Jacka, F. (1980). Application of a dual Fabry-Perot spectrometer for daytime airglow studies. Journal of Atmospheric and Terrestrial Physics 42:499-511.

Fuller-Rowell, T.J. and Rees, D. (1984). Interpretation of an anticipated long-lived vortex in the lower thermosphere following simulation of an isolated substorm. Planetary and Space Science 32:69-86.

Heelis, R.A., Lowell, J.K. and Spiro, R.W. (1982). A model of the high-latitude ionospheric convection pattern. Journal of Geophysical Research 87:6339-6345.

Heppner, J.P. and Maynard, N.C. (1976). Empirical high latitude electric field models. Journal of Geophysical Research (in press).

Wardill, P., Jones, N. and Jacka, F. (1987). Dynamics of the thermosphere over Mawson, Antarctica. I. Diurnal variation and geomagnetic dependence. ANARE Research Notes (Chapter 10 this volume).

12. DYNAMICS OF THE THERMOSPHERE OVER MAWSON, ANTARCTICA: III. HORIZONTAL DIVERGENCE OF THE WIND FIELD

P. Wardill and F. Jacka
Mawson Institute for Antarctic Research
University of Adelaide
Adelaide, S.A., Australia, 5000.

ABSTRACT

Measurements of the thermospheric neutral wind velocity at Mawson, Antarctica (67.6°S, 62.9°E, invariant latitude 70°S), frequently reveal large horizontal divergence. The observed wind field at any given time may be decomposed into contributions from a uniform background wind and from a divergent line source oriented along the geomagnetic east-west direction. The calculated motion of the hypothetical line source is in qualitative agreement with that of the auroral electrojet. It is proposed that the electrojet drives a divergent flow via momentum deposition resulting from the dissipation of gravity waves above ~200 km.

12.1 INTRODUCTION

It is well established that the auroral zones are important sources of thermospheric gravity waves resulting from Joule and particle heating in the lower thermosphere. The propagation of these waves at middle and low latitudes has been studied extensively and is reviewed by Francis (1975). Recent observations, made within the auroral zones, have revealed vertical motions in excess of 100 ms^{-1} and have demonstrated considerable wave activity even during relatively quiet geomagnetic conditions (Spencer et al. 1976, 1982; Rees et al. 1984; Wardill and Jacka 1986).

This paper presents observations of horizontal and vertical thermospheric winds over Mawson, Antarctica. The horizontal winds show large divergences which persist for many hours. It is proposed that the divergent flow is driven by momentum deposition from dissipating gravity waves generated within the auroral electrojet.

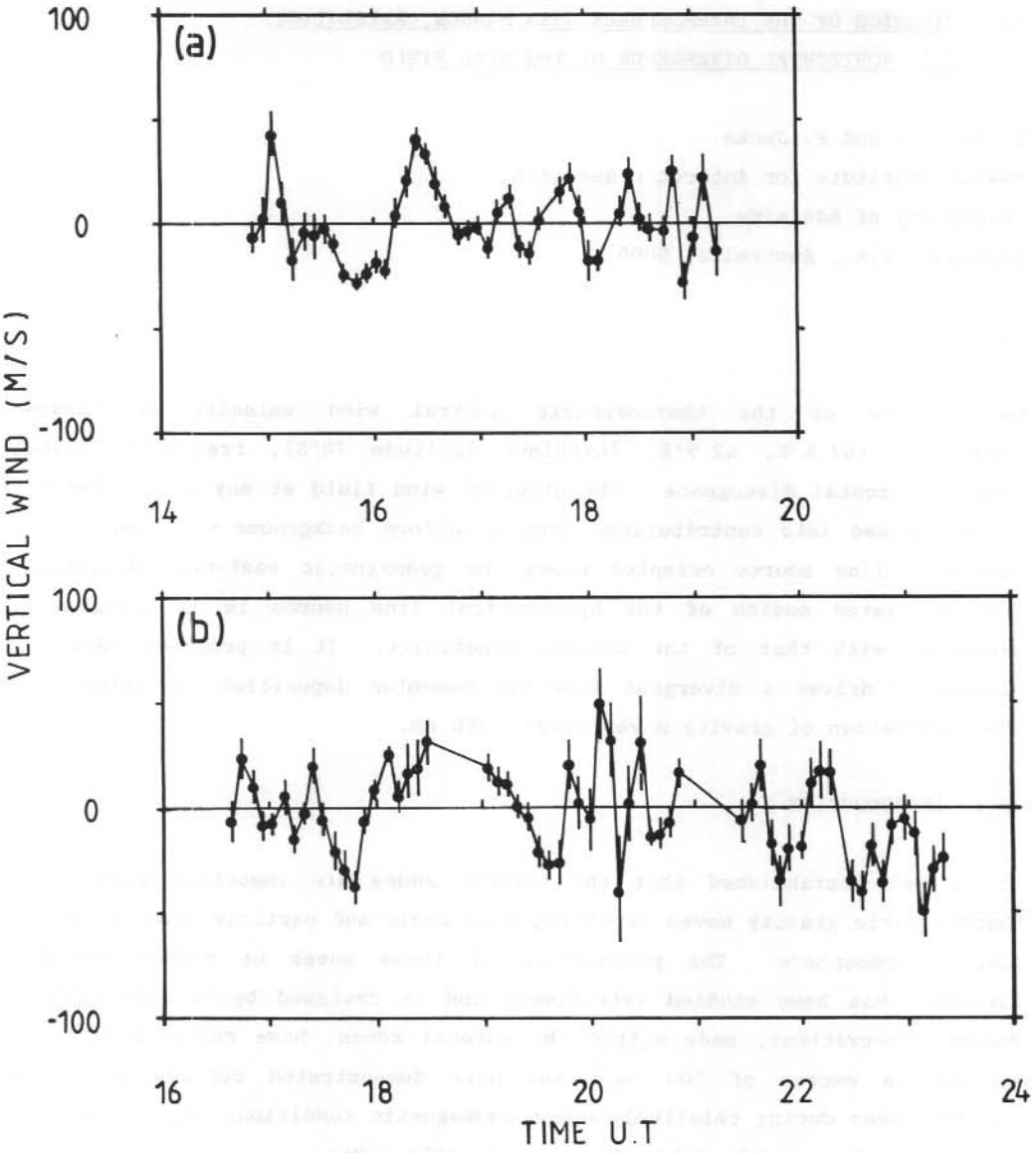

Figure 1. Vertical thermospheric wind (positive upward) measurements from:
(a) 14 April 1983 (A_p=45)
(b) 20 September 1983 (A_p=22)
Thermospheric gravity waves with periods in the range thirty to sixty minutes were observed on these and on five other nights during which similar measurements were made.

12.2 RESULTS

The wind velocities were derived from measurements of Doppler shift of the OI λ630 nm emission, produced at heights of ~200-300 km in the airglow and aurora. Measurements were made with a scanning Fabry-Perot spectrometer described by Jacka (1984). Details of the observing procedure are given by Wardill et al. (1987).

High time-resolution (~5 minutes) measurements of the vertical wind were made on seven nights during 1983 (Figure 1). Evidence of thermospheric gravity waves was found on each of these nights. Wave amplitudes of ~25 ms^{-1} and periods of ~30-60 minutes were typical of quiet to moderate geomagnetic conditions while vertical velocities of up to 100 ms^{-1} were associated with the expansion phases of auroral substorms (Wardill and Jacka 1986).

Figure 2 shows the averaged half-hourly samples of the geographic zonal and meridional wind components over forty-one nights during 1983. The A_p indices for these observing periods were less than twenty-five, corresponding to quiet to moderate conditions. Measurements of the zonal component made to the east and to the west were horizontally separated by ~800 km, as were meridional measurements to the north and south. Strong horizontal gradients, persisting for many hours, were observed in both components, indicating a highly divergent flow.

The observed wind field could be reproduced, within experimental error, by adding a divergent line source of velocity to a uniform background flow. The line source was taken to be oriented along the geomagnetic east-west direction (roughly parallel to the auroral electrojet) and its strength and location, together with the background wind, were varied to achieve the closest agreement with the observed winds. The calculated motion of the line source was similar to that of the auroral electrojet, moving geomagnetic northward during the night and passing over Mawson at ~2200 UT. The calculated background wind was consistent with that due to ion drag forcing.

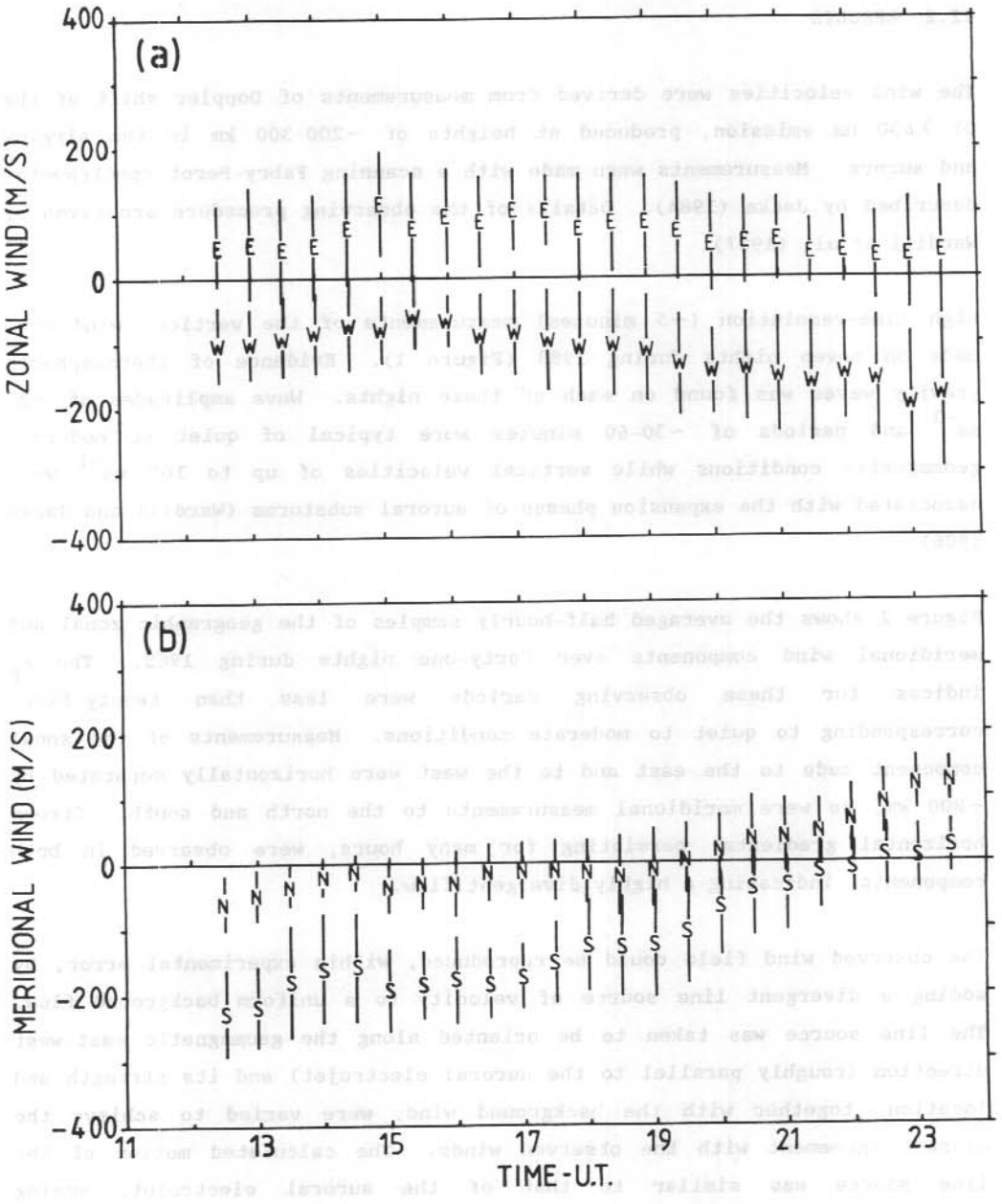

Figure 2.

(a) Half-hourly samples of the zonal component (positive eastward) of the neutral thermospheric wind, measured to the east (E) and west (W) and averaged over forty-one nights during which $A_p<25$.

(b) As above, but for the meridional component (positive northward) measured to the north (N) and south (S).

12.3 DISCUSSION

The above results suggest that large-amplitude gravity waves and large horizontal divergences are common features of the thermosphere over Mawson. The authors propose that the divergent flow is driven by momentum deposition from dissipating gravity waves generated in the vicinity of the auroral electrojet.

The acceleration of the background flow resulting from wave dissipation may be estimated from the measured wave parameters. It is noted that propagating gravity waves transport horizontal momentum, the vertical flux of which, denoted F_{xz}, is given by (Hines 1960, 1972):

$$F_{xz} = \rho w_0^2 \tau / \tau_g \qquad (1)$$

where ρ is the atmospheric density, w_0 the amplitude of the vertical velocity oscillation, τ the wave period and τ_g the Väisälä-Brunt period. In the absence of dissipation, F_{xz} is independent of height and the exponential decrease of ρ with height is compensated by an increase in w_0. This process is however limited by the high kinematic viscosity of the upper thermosphere; dissipation results and the wave energy and momentum are transferred to the background atmosphere. Midlatitude studies have found wave amplitudes to be independent of height above ~250 km (Testud 1970). Under such conditions the acceleration of the background flow is given by:

$$dU/dt = w_0^2 \tau / 2\tau_g H \qquad (2)$$

where H is the atmospheric scale height.

In the 200-300 km region we may take τ_g ~15 minutes and H~50 km. The vertical wind measurements suggest that w_0~25 ms^{-1} and τ~45 minutes are typical values of the wave parameters. Inserting these figures into the above equation yields a horizontal acceleration of 0.02 ms^{-2}. This is comparable to typical Coriolis accelerations and perhaps a factor of two lower than ion drag accelerations in this region of the atmosphere.

12.4 CONCLUSIONS

Measurements of horizontal divergence in the upper thermosphere are qualitatively consistent with the results expected from a line source of velocity oriented along the geomagnetic east-west direction. This source is identified with momentum deposition resulting from dissipating gravity waves which are generated within the auroral electrojet. The acceleration due to this source is estimated to be comparable to that due to Coriolis and ion-drag forces.

ACKNOWLEDGMENTS

The observations discussed here were carried out at the Australian National Antarctic Research Expedition's station at Mawson. The authors thank the Director, Antarctic Division, Department of Science for logistic support. This work was supported by the Australian Research Grants Scheme.

12.5 REFERENCES

Francis, S.H. (1975). Global propagation of atmospheric gravity waves: A review. Journal of Atmospheric and Terrestrial Physics 37:1011-1054.

Hines, C.O. (1960). Internal atmospheric gravity waves at ionospheric heights. Canadian Journal of Physics 38:1441-1481.

Hines, C.O. (1972). Momentum deposition by atmospheric waves, and its effect on thermospheric circulation. Space Research 12:1157-1161.

Jacka, F. (1984). Application of Fabry-Perot spectrometers for measurement of upper atmosphere temperatures and winds. In: Vincent, R.A. (Ed.). Handbook for MAP 13:19-40.

Rees, D., Smith, R.W., Charleton, P.J., McCormac, F.G., Lloyd, N. and Steen, . (1984). The generation of vertical thermospheric winds and gravity waves at auroral latitudes - I. Observations of vertical winds. Planetary and Space Science 32:667-684.

Spencer, N.W., Theis, R.F., Wharton, L.E. and Carignan, G.R. (1976). Local vertical motions and kinetic temperature from AE-C as evidence for aurora-induced gravity waves. Geophysical Research Letters 3:313-316.

Spencer, N.W., Wharton, L.E., Carignan, G.R. and Maurer, J.C. (1982). Thermosphere zonal winds, vertical motions and temperature as measured from Dynamics Explorer. Geophysical Research Letters 9:953-956.

Testud, J. (1970). Gravity waves generated during magnetic substorms. Journal of Atmospheric and Terrestrial Physics 32:1793-1805.

Wardill, P. and Jacka, F. (1986). Vertical motions in the thermosphere over Mawson, Antarctica. Journal of Atmospheric and Terrestrial Physics 48: 289-292.

Wardill, P., Jones, N., and Jacka, F. (1987). Dynamics of the thermosphere over Mawson, Antarctica: I. Diurnal variation and geomagnetic dependence. ANARE Research Notes (Chapter 10 this volume).

13. DYNAMICS OF THE THERMOSPHERE OVER MAWSON, ANTARCTICA: IV. THE LOWER THERMOSPHERE

N. Jones and F. Jacka
Mawson Institute for Antarctic Research
University of Adelaide
Adelaide, S.A., Australia, 5000.

ABSTRACT

During the austral spring of 1981, the Mawson Institute's Fabry-Perot spectrometer at Mawson, Antarctica (67.6°S, 62.9°E, invariant latitude 70°S) was used to make measurements of the spectrum of the nighttime λ558 nm emission from atomic oxygen in the lower thermosphere. The spectra have been analysed to yield wind and temperature information.

The inferred temperature was highly variable, and this is ascribed to variations in the emission altitude in response to changes in the energy spectrum of the precipitating electrons, rather than to actual variations in atmospheric temperature. An argument for assigning the emission to the 100-130 km altitude region is presented.

The wind, when viewed in the geomagnetic-coordinates/magnetic-local-time frame, was poleward and westward around dusk, equatorward and westward around midnight. This behaviour cannot be explained on the basis of solar UV heating of the atmosphere being the only important forcing process, but is consistent with what one would expect if ion drag due to collisions with ions driven by the high-latitude electric field was the dominant force on the neutral atmosphere at the emission altitude. The fact that observed winds increase in magnitude with increased geomagnetic activity supports this conclusion.

The observed winds show excellent qualitative agreement with the predictions of a three-dimensional, time-dependent, global thermospheric numerical model due to Fuller-Rowell and Rees (1980, 1984), which includes the effect of ion drag and a specification of the high-latitude electric field.

13.1 INTRODUCTION

The dynamics of the earth's polar upper thermosphere (200-300 km altitude) has been extensively probed by a variety of techniques including high-resolution studies of the OI λ630 nm emission from the ground and from space (e.g. Wardill et al. 1987) and by chemical releases from rockets (e.g. Heppner and Miller 1982). Similarly, the region in the vicinity of the mesopause (80-100 km) has been studied by meteor radars (e.g. Ogawa et al. 1986) and partial reflection radars (e.g. Macleod and Vincent 1985). To date, measurements of winds in the lower thermosphere (100-150 km) have been relatively rare, being mainly derived from chemical releases from rockets (e.g. Heppner and Miller 1982).

This paper presents the results of observations of the green OI λ558 nm emission line with the Mawson Institute's Fabry-Perot spectrometer (FPS) at Mawson, Antarctica (67.6°S, 62.9°E, invariant latitude 70°S) on ten nights in the austral spring of 1981. These spectra have been analysed to yield wind and temperature data using the technique described in Wardill et al. 1987.

13.2 TEMPERATURE RESULTS AND EMISSION ALTITUDE

The green emission results from the transition $O(^1S)$ to $O(^1D)$; the $O(^1S)$ upper state is metastable with a radiative lifetime of about 0.8 s.

Some of the reactions which contribute to the production of $O(^1S)$ in the atmosphere (dissociative recombination of O_2^+, for example) can produce the $O(^1S)$ with superthermal energy. If one is to be able to deduce the kinetic temperature of the emitting volume from the Doppler broadening of an emission line, one must be sure that the emitting species is in thermodynamic equilibrium with its environment. The collision frequency monotonically decreases with altitude, and has a value of 5 s^{-1} at about 200 km (U.S. Standard Atmosphere, 1976). We conclude that $O(^1S)$ atoms will be well thermalised below this altitude.

If we are to know what altitude to assign to the wind measurements, we must know the altitude distribution of the emission. It is well known that at midlatitudes the bulk of the λ558 nm airglow emission comes from a thin

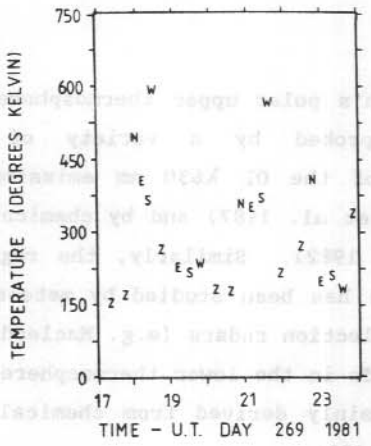

Figure 1. Temperatures in the lower thermosphere derived from one night's observation of atomic oxygen green line with the Mawson FPS. The large variability is attributed to variations in the emission height in response to changes in the energy spectrum of the precipitating electrons, and not actual changes in atmospheric temperature.

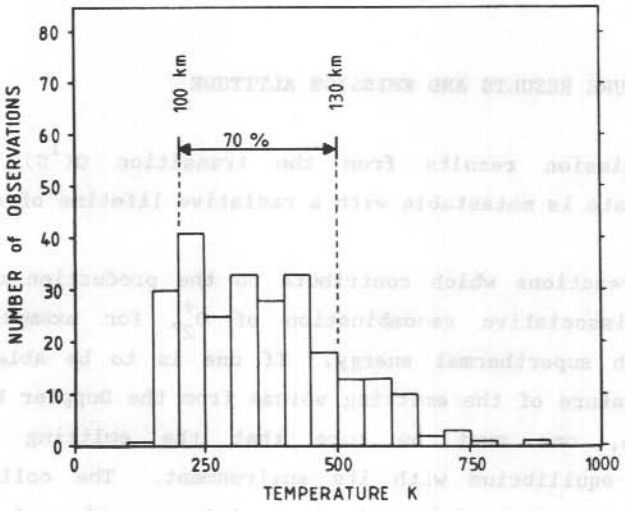

Figure 2. A histogram of all 252 temperature measurements in the present data set. Seventy per cent of the temperatures lie in the range 200-500 K. By assuming that the actual atmospheric temperature-height profile is well represented by the U.S. Standard Atmosphere (1976), we re-interpret the temperature distribution as an altitude distribution, i.e. we assume that the wind measurements are representative of the 100-130 km altitude region.

layer at around 97 km, with a secondary emission layer in the F-region contributing about 10% to the total intensity of a few hundred Rayleighs. The situation in the aurora is quite different. The λ558 nm line is the dominant feature in the visible aurora, and whilst the mechanism for the excitation of $O(^1S)$ in the aurora remains a topic of some controversy, there is little doubt that the altitude of peak emission intensity is variable and depends on the energy spectrum of the precipitating electrons. Measurements made by Parkinson and Zipf (1971), by flying a zenith-pointing rocket-borne photometer into a steady aurora, yielded an altitude of maximum emission rate at about 120 km. Similar measurements by Sharp et al. (1979) give an altitude of peak intensity just above 100 km.

This variability of the emission height needs to be taken into account when interpreting the present data. Examination of a standard atmospheric temperature-height profile (such as the US Standard Atmosphere, 1976) reveals that the region where the peak auroral green line intensities occur corresponds to the region of large vertical temperature gradient in the lower thermosphere. Hence one would expect the deduced temperatures to vary as the peak emission intensity altitude varied in response to changes in the electron energy spectrum. This effect is indeed observed. Figure 1 shows the temperature results from observation of the green line on one night; the great variability of the temperatures is clearly evident. This feature of the data implies that these observations are probably of limited value for determining anything about temporal changes in the temperature of the atmosphere, since without independent data on the altitude of the emission, one cannot distinguish between actual changes in atmospheric temperature, and changes in the emission height.

Figure 2 shows a histogram of all 252 temperature measurements in the present data set. Most (about 70%) of the temperatures lie in the range 200-500 K with about 15% being hotter, and 15% being cooler. If we assume the actual temperature profile is well represented by the U.S. Standard curve, then we can interpret the temperature distribution as an altitude distribution. This tells us that 70% of the measurements relate to altitudes between 100 and 130 km, and it is to that region that we will assign the wind results.

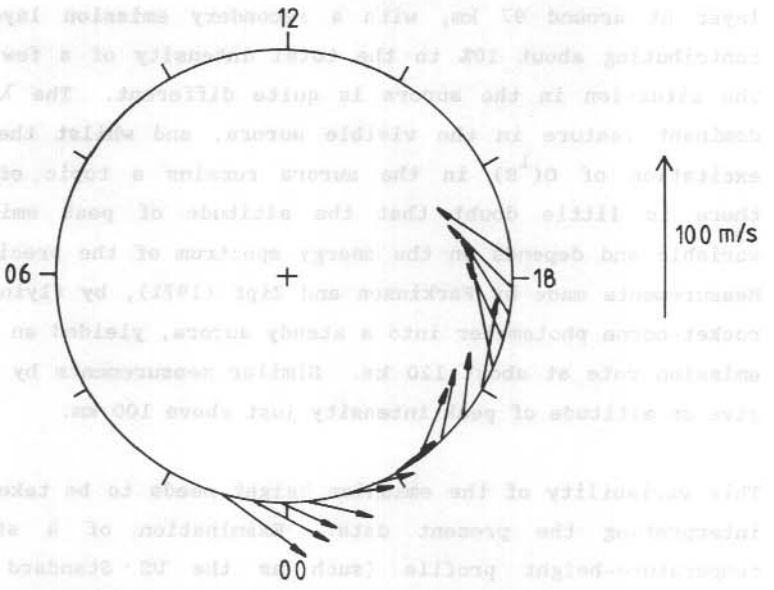

Figure 3. Average half-hourly wind vectors derived from ten night's observation of the oxygen green line with the Mawson FPS during the austral spring of 1981. The vectors are plotted in geomagnetic coordinates as a function of magnetic local time.

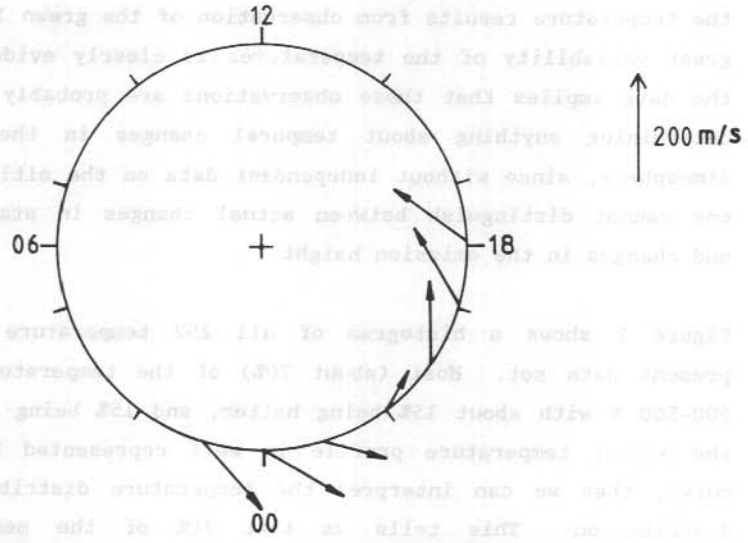

Figure 4. Winds predicted at the 120 km level by the thermospheric general circulation model of Fuller-Rowell and Rees (1984). The model run included a specification of the high latitude electric field. The predicted winds show excellent qualitative agreement with the present observations.

13.3 WIND RESULTS AND DISCUSSION

Figure 3 shows the half-hourly wind vectors, averaged over all the data, plotted in geomagnetic coordinates as a function of local magnetic time. Velocities are of the order of 60 ms^{-1}; the zonal flow is always toward the magnetic west; the meridional flow is equatorward around midnight and poleward around dusk.

This decade has seen the growth of three-dimensional, global, time-dependent numerical models of thermospheric dynamics, the so called 'thermospheric general circulation models'. These models have been used to simulate the response of the thermosphere to a variety of geophysical processes. An early application of these models was to calculate the global wind and temperature distribution that would be expected if heating by absorption of solar UV and EUV radiation were the only driving mechanism. Not surprisingly, these model runs predicted a thermospheric wind field that was approximately everywhere away from a pressure maximum at about 14:00 local time (e.g. Dickinson et al. 1981), i.e. a ubiquitous roughly antisunward flow. Clearly the measured winds do not agree with such model predictions; the winds observed around dusk are roughly sunward.

Sunward winds are frequently observed in the upper thermosphere evening auroral oval. The interaction of the solar wind and the geomagnetic field generates large scale electric fields which map down the geomagnetic field lines into the earth's polar upper atmosphere. A simple and widely used model of the high latitude electric field is the sun-aligned model 'A' due to Heppner (1977). The electric field in the polar cap is directed from dawn to dusk, while in the auroral belts, the field is from dusk to dawn. The magnetic field is directed upward in the Southern Hemisphere, and downward in the Northern Hemisphere. This means that the $\underline{E}$ X $\underline{B}$ drift of the ions is directed westward (sunward) in the evening auroral belts and equatorward (antisunward) in the polar caps. Ion-neutral collisions result in the transfer of momentum between the ions and the neutrals. It is this ion drag which is responsible for the observed sunward winds in the upper thermosphere. As one moves down in altitude, the increasing collision frequency results in a rotation of the ion drift direction away from $\underline{E}$ X $\underline{B}$ and toward $\underline{E}$. The observed flow is westward of the $\underline{E}$ X $\underline{B}$ direction around

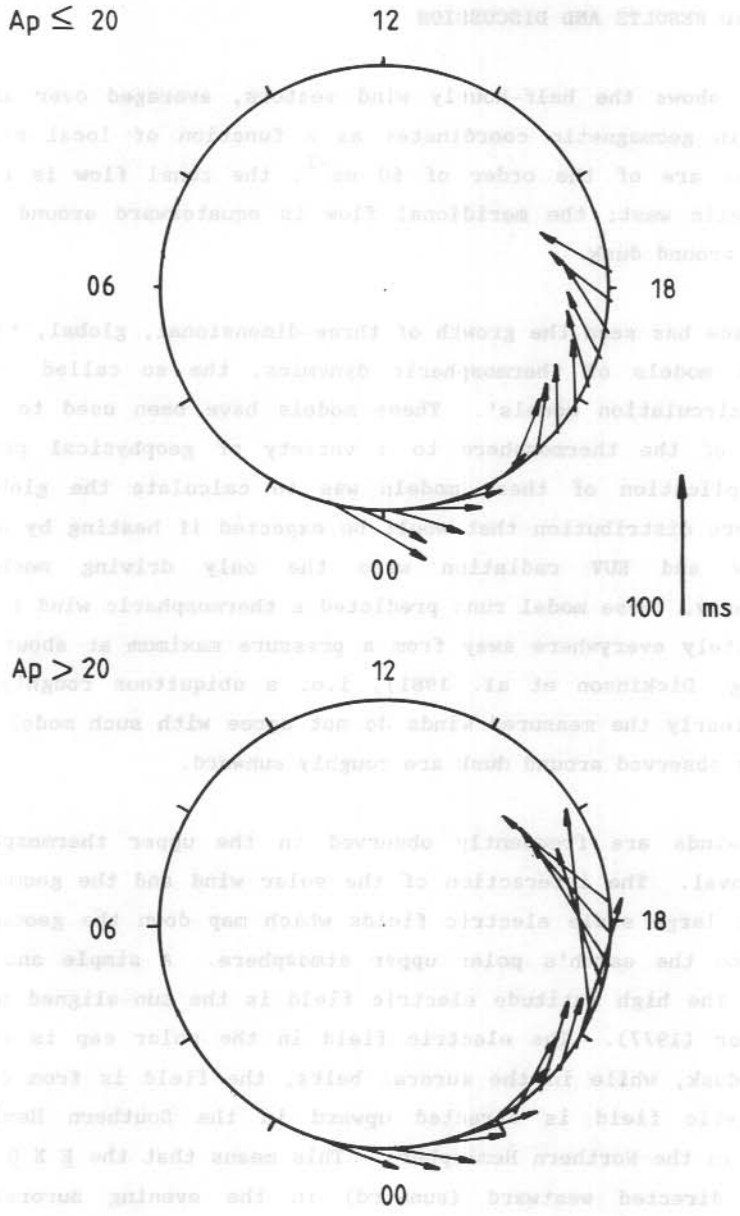

Figure 5. Average half-hourly observed wind vectors for:
(a) Quiet and moderate conditions (Ap≤20)
(b) Disturbed conditions (Ap>20)
It is clear that higher wind speeds are observed during disturbed conditions, as expected if the neutral winds are driven by the high-latitude electric field via ion drag.

midnight, and poleward of it around dusk. Both of these differences are consistent with the expected rotation of the ion flow direction at lower altitudes.

Figure 4 shows the winds predicted for 120 km altitude by a thermospheric general circulation model developed at University College London, by Fuller-Rowell and Rees (1980, 1984). The model includes a specification of the high-latitude electric field. Here the model is being used to simulate the response of the thermosphere to a geomagnetic substorm, the substorm being characterised by a linear increase in the strength of the electric field from an initial strength of half Heppner's 1977 'A' model, to twice Heppner's model over a thirty minute period. The results shown here are for one hour after the commencement of the storm. This model run was carried out with coincident geomagnetic and geographic poles. Because of the dominant effect on the winds of ion drag in this model, its predictions are most appropriately compared with the measured winds displayed in geomagnetic coordinates. Comparison of Figures 3 and 4 reveals that the direction of the predicted winds at the latitude of Mawson is in almost exact agreement with the observed winds; i.e. equatorward and westward around midnight, poleward and westward around dusk. The predicted magnitude of the winds (around 200 ms^{-1}) is larger than that observed. This is not surprising since the observed winds are representative of moderately disturbed conditions. (Ap around 18, Kp around 3), whilst the model electric field used is twice the strength appropriate to these conditions.

Figure 5 shows (in geomagnetic coordinates) the average winds grouped into low ($Ap \leq 20$) and high ($Ap > 20$) geomagnetic activity. It is clear that higher wind speeds are associated with more disturbed conditions, particularly in the dusk auroral oval. This is exactly as one would expect if the neutral winds are driven by the high-latitude electric field via ion drag.

13.4 CONCLUSIONS

1. Whilst high resolution spectroscopy of the oxygen green line is a viable method of studying the winds in the auroral zone lower thermosphere, it is of limited value for temperature studies.

2. It is clear that night-time winds in that region cannot be accounted for by solar ultraviolet heating alone, the effects of the high latitude electric field must be taken into account.
3. The observed winds are well described by numerical models provided the electric field is taken into account.

ACKNOWLEDGMENTS

The observations presented here were carried out at the Australian National Antarctic Research Expedition's station at Mawson, Antarctica. The authors thank the Director, Antarctic Division, Department of Science for logistic support. This work was supported by the Australian Research Grants Scheme.

13.5 REFERENCES

Dickinson, R.E., Ridley, E.C. and Roble, R.G. (1981). A three-dimensional general circulation model of the thermosphere. Journal of Geophysical Research 86:1499-1512.

Fuller-Rowell, T.J. and Rees, D. (1980). A three-dimensional time-dependent global model of the thermosphere. Journal of the Atmospheric Sciences 37:2545-2567.

Fuller-Rowell, T.J. and Rees, D. (1984). Interpretation of a long-lived vortex in the lower thermosphere following simulation of an isolated substorm. Planetary and Space Science 32:69-85.

Heppner, J.P. (1977). Empirical models of high-latitude electric fields. Journal of Geophysical Research 82:1115-1125.

Heppner, J.P. and Miller, M.L. (1982). Thermospheric winds at high latitudes from chemical release observations. Journal of Geophysical Research 87: 1633-1647.

Macleod, R. and Vincent, R.A. (1985). Observations of winds in the Antarctic summer mesosphere using the spaced antenna technique. Journal of Atmospheric and Terrestrial Physics 47:567-574.

Ogawa, T., Igarashi, K., Kuratani, Y., Fujii, R. and Hirasawa, T. (1986). Some initial results of 50MHz meteor radar observation at Syowa station. Memoirs of the National Institute of Polar Research (in press).

Parkinson, T.D. and Zipf, E.C. (1971). The auroral intensity ratio of OI(6300) and OI(5577). Planetary and Space Science 19: 267-270.

Sharp, W.E., Rees, M.H. and Stewart, A.I. (1979). Coordinated rocket and satellite measurements of an auroral event. 2: The rocket observations and analysis. Journal of Geophysical Research 84:1977-1985.

U.S. Standard Atmosphere, (1976). U.S. Government Printer. Washington.

Wardill, P., Jones, N. and Jacka, F. (1987). Dynamics of the thermosphere over Mawson, Antarctica. I. Diurnal variations and geomagnetic dependence. ANARE Research Notes (Chapter 10 this volume).

14. WINDS AND TEMPERATURES IN THE MESOSPHERE AND LOWER THERMOSPHERE AT MAWSON, ANTARCTICA

G. Price (1, 3), R.A. Vincent (2) and F. Jacka (3).

(1) Antarctic Division
Department of Science
Kingston, Tas., Australia, 7150.

(2) Department of Physics
University of Adelaide
Adelaide, S.A., Australia, 5000.

(3) Mawson Institute for Antarctic Research
University of Adelaide
Adelaide, S.A., Australia, 5000.

ABSTRACT

Records of temperature, and horizontal and vertical wind components in the mesosphere/lower thermosphere, were obtained at Mawson station (67.6°S, 62.9°E, invariant latitude 70.1°S), during September and October, 1985. A scanning Fabry-Perot spectrometer was used to obtain vertical wind and temperature measurements in the lower thermosphere. A 2 MHz partial reflection radar using the spaced antenna method, gave horizontal wind data over the height range 70 to 110 km. A preliminary examination of the results is presented.

14.1 INTRODUCTION

The wind and temperature structure in the mesosphere and lower thermosphere is determined by the joint actions of thermal forcing and the dissipation of propagating planetary and gravity waves (Garcia and Solomon 1985). At high latitudes, the auroral zone provides a major source of thermospheric gravity waves (Cole and Hickey 1981). Understanding the wind and temperature structure observed in the high latitude mesosphere and lower thermosphere, therefore requires consideration of gravity wave motions.

Wind and temperature measurements were made at Mawson, Antarctica during 1985. A scanning Fabry-Perot spectrometer (FPS) was used to observe the atomic oxygen 558 nm emission in the night sky, giving vertical wind and

temperature measurements. Horizontal winds over the height range 70 to 110 km, were measured at 2 km height intervals, by means of the Partial Reflection Drift (PRD) technique.

Data from the FPS were obtained on thirteen clear nights during the Austral Spring. Observations were limited to periods of darkness, which were typically of eight hours duration. The PRD was run almost continuously throughout the year. The data collected on the days when both experiments were operative are to be collated, and the sources and characteristics of gravity waves determined.

14.2 THE FABRY-PEROT SPECTROMETER

The FPS employs separation scanning to measure the peak position and Doppler broadening of the emission line in order to determine the temperature and line-of-sight velocity of the emitting species. The (λ558 nm) green emission results from the transition $O(^1S)$ to $O(^1D)$. At altitudes below 200 km the $O(^1S)$ atoms are well thermalised (Jones and Jacka 1987), which implies that the measured temperature represents that of the bulk neutral atmosphere.

An estimate of the emission height is inferred by a comparison of the observed temperature with measurements from rocket flights (Philbrick et al. 1985). Observed temperatures lie between 200 K and 600 K suggesting that the emission occurs at lower thermospheric heights, between 110 and 140 km, and is primarily an auroral emission. The hardness of the incoming particle spectrum determines the penetration of the particles and thus the emission height and temperature.

The instrument drift is monitored through regular observations of a laboratory source. Difficulties arise when instabilities within the instrument produce an instrument drift which represents a velocity that is large in comparison with the winds being measured. Vertical winds are relatively small so good instrument stability is required for variations in the vertical winds to be adequately mapped. Half the data were rejected because instrument drifts were too large. On some other nights irregular drift patterns made interpretation of the data difficult.

Vertical wind perturbations of up to 50 ms^{-1} about the nightly mean are typical of the data set. A sample of vertical wind measurements is shown in Figure 1, where the mean vertical wind over the observing period is assumed to be zero. Over the night presented, the instrument drift was less than the equivalent of 100 ms^{-1} variation in the wind velocity and does not influence the interpretation of the data. Auroral activity was moderate to high which enhanced the emission, and allowed an acquisition time of six minutes. An oscillation of period ninety minutes, and amplitude approximately 25 ms^{-1} is clearly seen in the wind data.

14.2.1 Gravity wave interpretation of results

A number of vertical wind measurements have been made in the upper thermosphere. Comparatively few have been made in the lower thermosphere. A degree of consistency is seen between the lower and upper thermospheric data which are summarised in Table 1. The reported vertical winds suggest that latitude, and in particular the presence or absence of auroral activity, is the most important factor contributing to the value of the vertical winds.

Vertical winds exceeding 100-150 ms^{-1} in the F-region, are frequently associated with the expansion phase of an auroral substorm (Herrero et al. 1984, Rees et al. 1984a, Wardill and Jacka 1986). During this phase, very rapid upward motions result from intense local heating of the neutral atmosphere down to 100 km. This initial vertical lifting of the atmosphere produces the largest vertical wind perturbations. Numerical models have confirmed this response and estimate that the local vertical wind can absorb at least 30% of the total substorm energy input (Rees et al. 1984a). Vertical oscillations of large amplitude and period accompany the disturbance and thermospheric gravity waves are generated which redistribute geomagnetic energy globally (Rees et al. 1984b, Testud 1970, Wardill and Jacka 1986).

It is suggested that the vertical wind parameters may be manifestations of internal, propagating gravity waves. An estimate of the wave energy per unit mass of atmosphere can be calculated using the expression below, from the parameters given in Table 1.

$$J/m \sim (\tau.w'/\tau_B)^2, \qquad (1)$$

where τ_B is the Väisälä-Brunt frequency, w' the vertical perturbation velocity and τ the intrinsic wave period. Here the effect of the background wind has been ignored and the intrinsic period replaced by the observed period.

In the absence of dissipation or reflection, a gravity wave grows exponentially with height, in order to maintain a constant energy density flux. Eventually, instabilities arising from large amplitude motions, cause the wave to lose energy through the production of turbulence. (Fritts 1984). Once in the thermosphere, dissipative processes become significant and act independently of the wave amplitude to further offset wave growth. As a result, gravity waves tend to show little change in amplitude with height above the mesosphere. The energy density per unit mass which is equal to the square of the gravity wave amplitude, is seen in Figure 2, to follow this trend.

Table 1. Summary of observations of vertical winds in the thermosphere.
*Dynamics Explorer-2 Wind and Temperature Spectrometer.

AUTHOR	LATITUDE	ALTITUDE	TECHNIQUE	VERT. VEL. (Peak)	PERIODS (Mins)	AURORAL ACTIVITY
Price	High	E region (110-140 km)	FPS (green)	25 ms^{-1}	90	auroral substorm
Peteherych	High	E region (110-140 km)	FPS (green)	15 ms^{-1}	60	auroral substorm
Herero	High	F region (250-300 km)	FPS (red)	95 ms^{-1}	90	auroral substorm
Hernandez	Mid	F region (200-300 km)	FPS (red)	25 ms^{-1}	40	
Wardill	High	F region (200-300 km)	FPS (red)	100 ms^{-1}	30	auroral substorm
Rees	High	F region (200-300 km)	FPS (red)	200 ms^{-1}	30	auroral substorm
Spencer	High	F region (300-340 km)	*DE-2 WATS	120 ms^{-1}	?	?
Testud	Mid	F region (240-380 km)	Incoherent Scatter Radar	30 ms^{-1}	120	

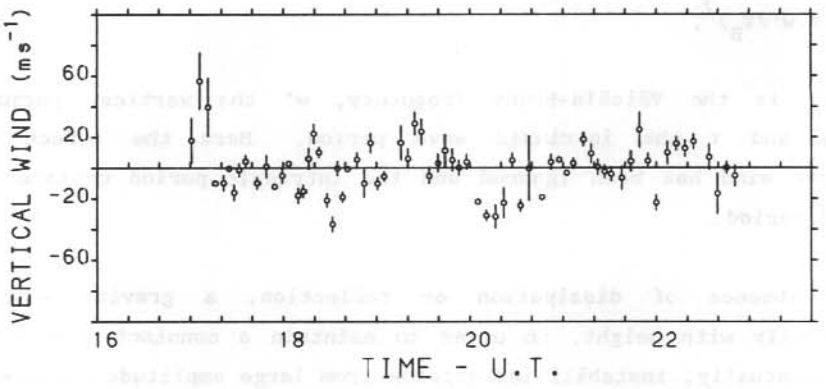

Figure 1. Lower thermospheric vertical velocity for 13 October 1985.

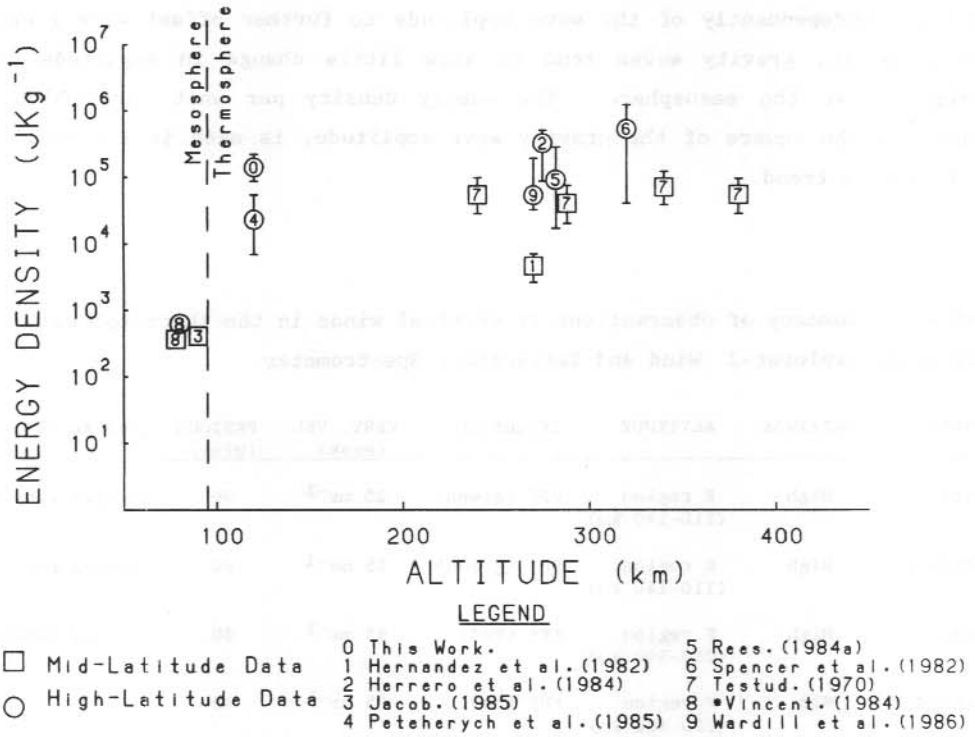

Figure 2. Energy density per unit mass of atmosphere versus altitude calculated from the observations reported in Table 1. Errors are calculated from the uncertainty in the observed vertical velocity and period. Where the period is unknown (Spencer et al. 1982) it was assumed to lie between 30 and 120 minutes.

***High latitude data reported by Vincent is an interpretation of data published by Carter and Balsley (1982).**

The largest values of energy density are observed at high latitude sites during auroral substorms and are attributable to processes occurring in the auroral electrojet. The oxygen green emission observed at Mawson occurs at the height of the auroral electrojet suggesting the wave energy per unit mass calculated from these observations is associated with thermospheric gravity waves in the source region.

14.2.2 The partial reflection drift technique

The PRD radar operates at 2 MHz and records signals partially reflected from ionized irregularities in the mesosphere. Recording the signal at three spaced receiving antennas allows the horizontal wind to be computed. Each 2 km height interval is sampled four times an hour with most data being obtained between 80 and 100 km. Outside this range, data collection is more dependent upon atmospheric conditions.

Averaging the PRD data in two week blocks gives the mean wind at each 2 km height interval. The transition from the pattern of winter eastward winds to summer westward winds is seen in Figure 3, which shows the September and October mean values. There is a particularly large swing of 18 ms^{-1} in the mean wind at 90 km between the first and last two weeks of October.

The semidiurnal and diurnal tides are calculated by using a harmonic analysis technique which is applied to each height giving the amplitude and phase of the tides at that height. The term tides is used here to refer to variations of period twelve or twenty-four hours, assumed to be forced primarily by solar heating. In order to reduce the effects of irregular wind fluctuations, and to give the mean daily tides, data from several days are folded with a period of one day using bins of length one hour. A vector field plot of the tides averaged over fourteen days is shown in Figure 4. The wind direction changes smoothly with height over the range 76 to 100 km, but less so outside of this range where the data are more sparse.

Short term variations in the tidal parameters can be seen by applying the harmonic analysis to four day running means of the data. An eight day period in early October analysed in this way, shows that the phase, of both the zonal and meridional components of the semidiurnal tide, increases by

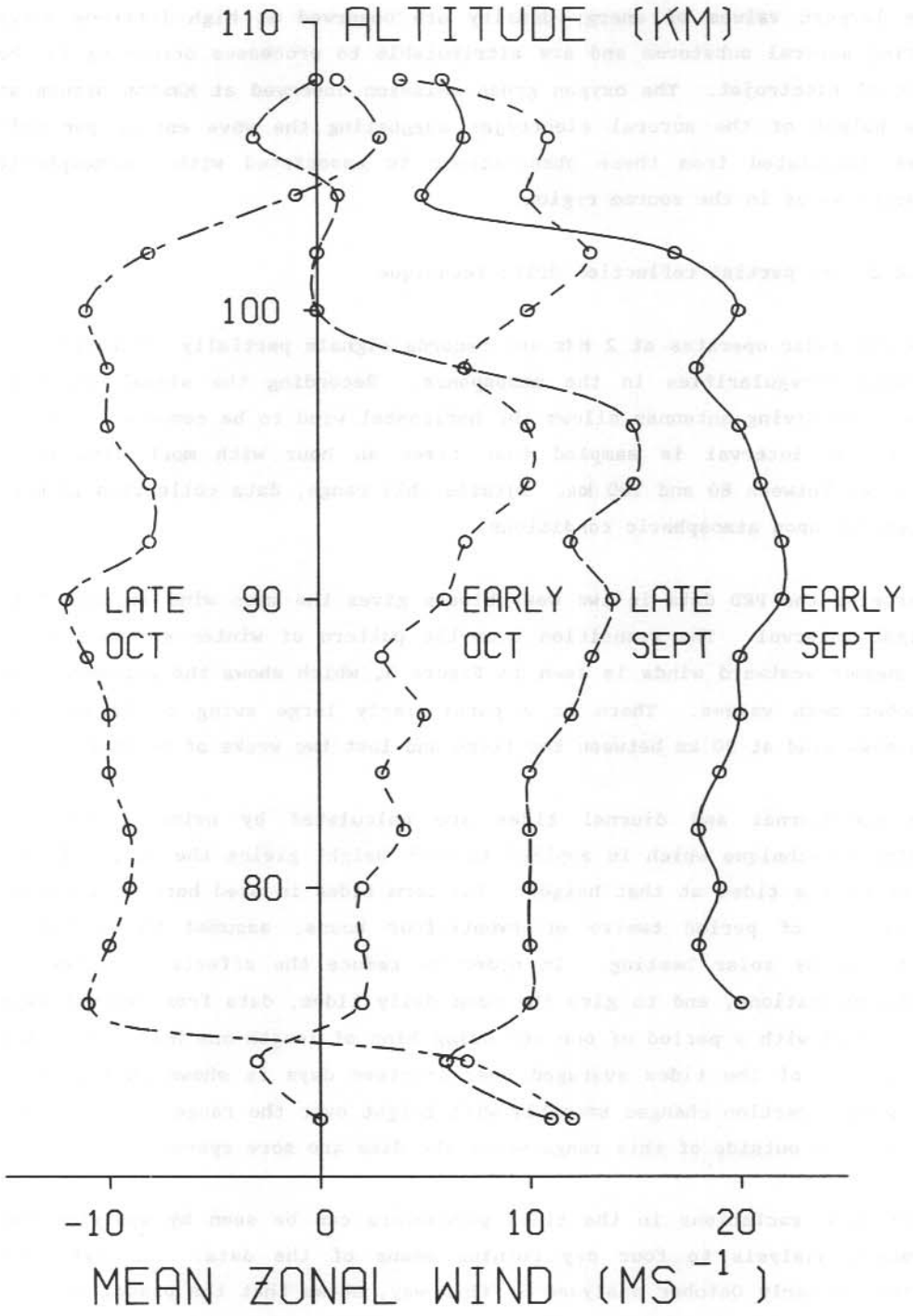

Figure 3. Mesospheric mean zonal winds for September and October 1985.

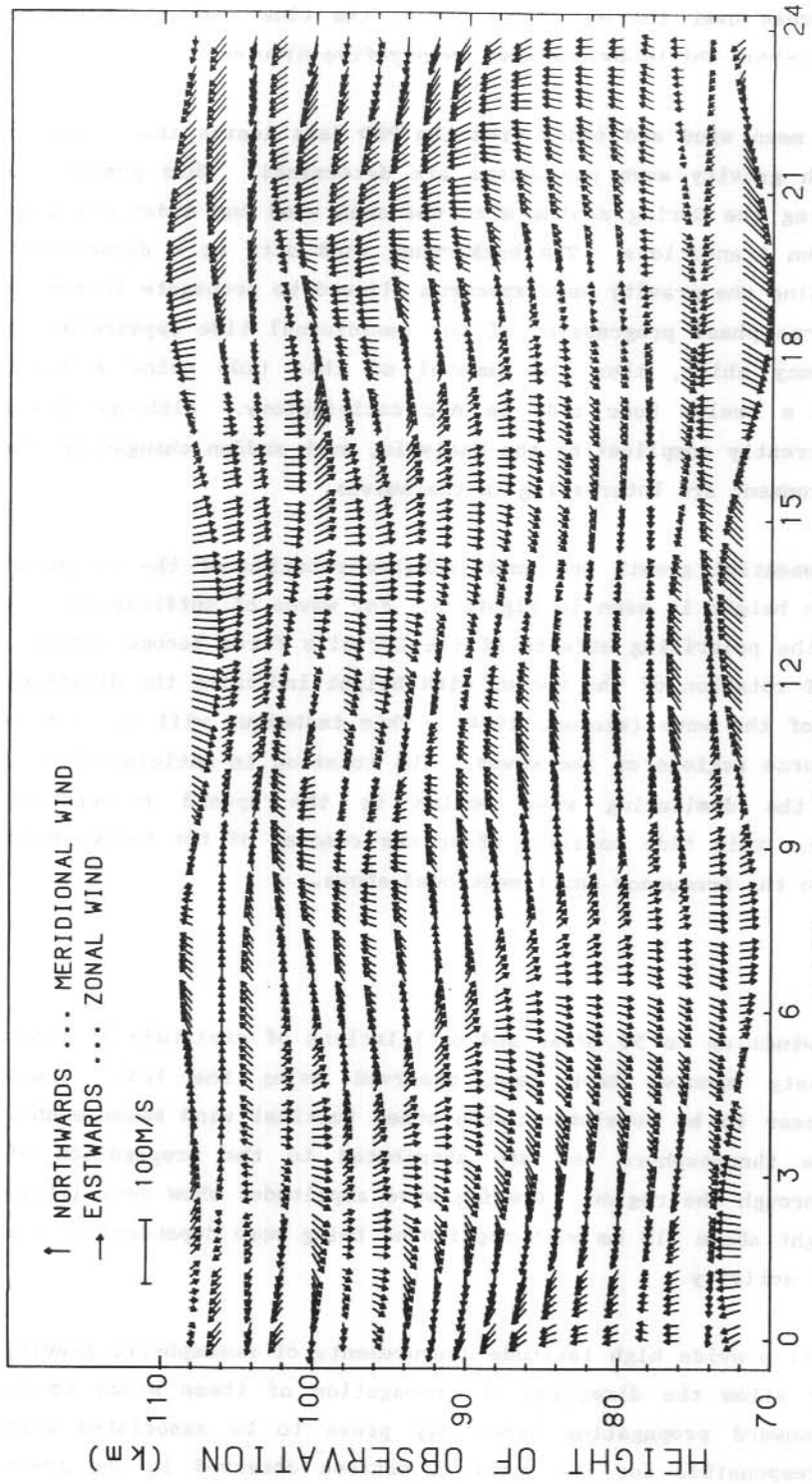

Figure 4. Vector field plot of the diurnal and semidiurnal tide, averaged over two weeks in early October 1985.

about fifty degrees over the eight days (i.e. the time that the eastward wind reaches a maximum shifts by one hour twenty-five minutes).

Subtracting the mean wind and tides from the PRD data leaves the irregular winds from which gravity wave parameters are determined. This process is complicated during the Spring months when the mean wind and tides are seen to undergo sudden transitions. The background wind acts as a directional filter, determining the gravity wave spectrum allowed to propagate through a region. The large phase progression of the semidiurnal tide appears as an apparent frequency shift, thus the removal of this tide using a least squares fit to a twelve hour tide is not satisfactory. Although these problems are currently complicating the analysis, such sudden changes in the background environment are interesting in themselves.

Approximate exponential growth and anticlockwise rotation of the irregular wind vector with height is seen in Figure 5. For waves of sufficiently low frequency that the polarizing effects of the Coriolis force become evident, the direction of rotation of the vector with height indicates the direction of propagation of the wave (Vincent 1984). This technique will be used to identify the source regions of the waves. The rotation is anticlockwise in Figure 5, as the dominating wave motion is the upward propagating semidiurnal tide. This tide persists after the removal of the twelve hour component, due to the frequency shift mentioned above.

14.3 DISCUSSION

Large vertical winds up to 50 m/sec and oscillations of amplitude 25 m/sec and period ninety minutes have been observed using the FPS. These measurements appear to be consistent with other vertical wind measurements reported in the thermosphere and are attributed to the propagation of gravity waves through the region. Gravity wave amplitudes show very little growth with height above 110 km with amplitudes being more dependent on the level of auroral activity.

The PRD data will provide high latitude measurements of mesospheric gravity waves which may allow the direction of propagation of these waves to be determined. Downward propagating waves may prove to be associated with gravity waves responsible for the vertical motions observed in the lower

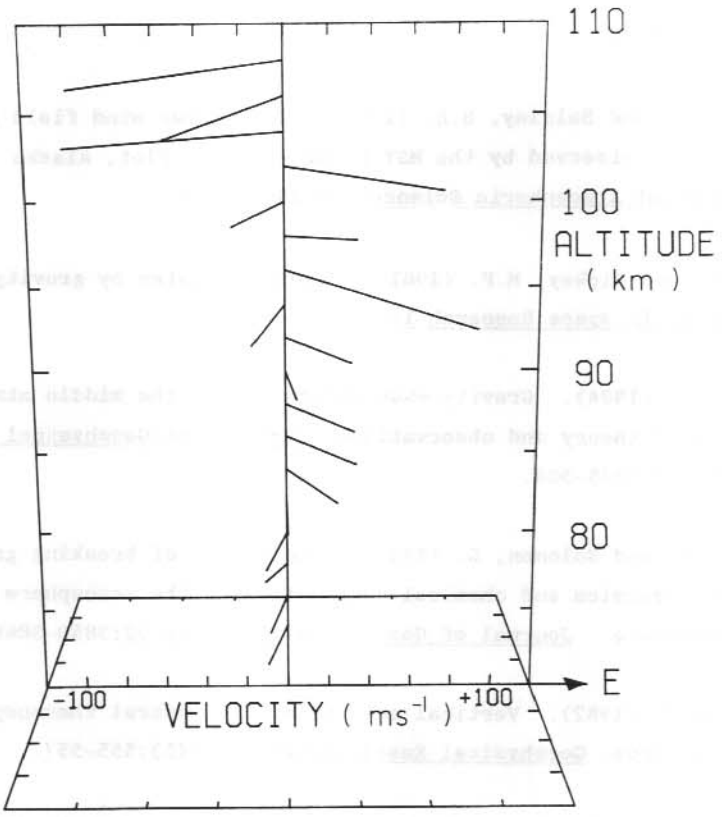

Figure 5. The hourly average, irregular wind vector plotted against height for 0800 to 0900Z on 14 October 1985.

thermosphere. Long period variations in the magnetic field are also to be analysed. It is interesting that the vertical component of the magnetic field, as observed with a fluxgate magnetometer, shows an oscillation of period ninety minutes during the hours prior to the observed vertical motions.

ACKNOWLEDGMENTS

The observations discussed here were carried out at the Australian National Antarctic Research Expedition's station at Mawson. The authors thank the Director, Antarctic Division, Department of Science for logistic support. This work was supported by the Australian Research Grants Scheme.

14.4 REFERENCES

Carter, D.A. and Balsley, B.B. (1982). The summer wind field between 80 and 93 km observed by the MST radar at Poker Flat, Alaska (65°N). Journal of Atmospheric Sciences 39:2905-2915.

Cole, K.D. and Hickey, M.P. (1981). Energy transfer by gravity waves. Advances in Space Research 1:65-75.

Fritts, D.C. (1984). Gravity wave saturation in the middle atmosphere: A review of theory and observations. Reviews of Geophysical and Space Physics 43:275-308.

Garcia, R.R. and Solomon, S. (1985). The effect of breaking gravity waves on the dynamics and chemical composition of the mesosphere and lower thermosphere. Journal of Geophysical Research 90:3850-3868.

Hernandez, G. (1982). Vertical motions of the neutral thermosphere at mid-latitude. Geophysical Research Letters 9(5):555-557.

Herrero, F.A., Mayr, H.G., Harris, I., Varosi, F. and Meriwether, J.W. (1984). Thermospheric gravity waves near the source: Comparison of variations in neutral temperature and vertical velocity at Sondre Stromfjord. Geophysical Research Letters 1(9):939-942.

Hines, C.D. (1974). The upper atmosphere in motion. A selection of papers with annotation. American Geophysical Union, Washington, D.C.

Jacob, P.G. (1985). Manifestations of atmospheric gravity waves in the airglow at 95 km. Ph.D. Thesis, Mawson Institute for Antarctic Research.

Jones, N. and Jacka, F. (1986). Dynamics of the thermosphere over Mawson, Antarctica: IV The lower thermosphere. ANARE Research Notes (Chapter 13, this volume).

Peteherych, S., Shepherd, G.G. and Walker, J.K. (1985). Observation of vertical E-region neutral winds in two intense auroral arcs. Planetary and Space Science 33(8):869-873.

Philbrick, C.R., Schmidlin, F.J., Grossman, K.U., Lange, G., Offermann, D., Baker, K.D., Krankowsky, D. and von Zahn, U. (1985). Density and temperature structure over Northern Europe. Journal of Atmospheric and Terrestrial Physics 47:159-171.

Rees, D., Smith, R.W., Charleton, P.J., McCormac, F.G., Lloyd N. and kesteen. (1984a). The generation of vertical thermospheric winds and gravity waves at auroral latitudes - I. Observations of vertical winds. Planetary and Space Science 32(6):667-684.

Rees D., Smith, M.F. and Gordon, R. (1984b). The generation of vertical thermospheric winds and gravity waves at auroral latitudes - II. Theory and numerical modelling of vertical winds. Planetary and Space Science 32(6):685-705.

Spencer, N.W., Theis, R.F., Wharton, L.E. and Carignan, G.R. (1976). Local vertical motions and kinetic temperature from AE-C as evidence for aurora-induced gravity waves. Geophysical Research Letters 3(6): 313-316.

Spencer, N.W., Wharton, L.E., Carignan, G.R. and Maurer J.C. (1982). Thermospheric zonal winds, vertical motions and temperature as measured from Dynamic Explorer. Geophysical Research Letters 9(a): 953-956.

Testud, J. (1970). Gravity waves generated during magnetic substorms. Journal of Atmospheric and Terrestial Physics 32:1793-1805.

Vincent, R.A. (1984). Gravity-wave motions in the mesosphere. Journal of Atmospheric and Terrestial Physics 46(2):119-128.

Wardill, P. and Jacka, F. (1986). Vertical motions in the thermosphere over Mawson, Antarctica. Journal of Atmospheric and Terrestrial Physics 48(3):289-292.

15. INITIATION, MAINTENANCE AND DECAY OF THE THERMOSPHERIC MOVEMENT DUE TO ELECTROSTATIC FIELDS

D.Y. Zhang and K.D. Cole
Physics Department
LaTrobe University
Bundoora, Vic., Australia, 3083.

ABSTRACT

The earlier work of Cole (1971) and Wu and Cole (1976) on the initiation and maintenance of thermospheric movement is extended here. The decay of the movement is also investigated.

15.1 INTRODUCTION

When an electric field E, orthogonal to the geomagnetic field B, is applied in the ionosphere the thermosphere is accelerated. The time constant required to reach a steady state in the absence of viscosity is given by $\rho/(\sigma_1 B^2)$ where σ_1 is the Pedersen conductivity and ρ the thermospheric density (see Cole 1971). Special cases for analysis occur when the characteristic time for existence of the electric field $t_E \gg \rho\ (\sigma_1 B^2)$. These occur often in the auroral zone and on the polar cap where electric fields can last sufficiently long to accelerate the thermosphere above altitudes of about 160 km. Above this altitude Pedersen currents dominate over Hall currents which may be neglected in approximate solution of the problems. Consideration of the effects of electric fields below this altitude must take into account Hall currents.

The maintenance of thermospheric movement associated with the auroral electrojet was discussed by Cole (1971). The initiation of thermosphere movements by the auroral electrojet was discussed by Wu and Cole (1976). The initiation, maintenance and decay of some other possible cases in the polar region are investigated here.

15.2 INITIATION AND MAINTENANCE

Because of the electric equipotential property of the geomagnetic field lines in the upper ionosphere, various electric fields in the magnetosphere could be mapped into the ionosphere by them. Let us suppose an electric field has the configuration as shown in Figure 1. The electric field has cylindrical symmetry with respect to the geomagnetic field line and is dependent on the radius in the cylinder only. The thermospheric motion is along the Θ-direction. Pedersen current flows in the r direction, and Hall current flows in Θ-direction but this is assumed negligible for the altitudes concerned which are above 160 km. The equation governing this motion can then be written as follows

$$\rho \frac{\partial u}{\partial t} - \mu\left(\frac{\partial^2 u}{\partial r^2} + \frac{1}{r}\frac{\partial u}{\partial r} - \frac{u}{r^2}\right) + J_r B = 0 \tag{1}$$

where u is the thermospheric flow velocity along the Θ-direction, ρ is the mass density, μ is the molecular viscosity, B is the geomagnetic field and J_r represents the Pedersen currents which can be given as

$$J_r = \sigma_1 (E+uB) \tag{2}$$

with σ_1 being the Pedersen conductivity. We assume σ_1 to be a function of altitude only. The independent variables are r and t. By substituting (2) into (1), we obtain

$$\frac{\partial u}{\partial t} - \frac{\mu}{\rho}\left(\frac{\partial^2 u}{\partial r^2} + \frac{1}{r}\frac{\partial u}{\partial r} - \frac{u}{r^2}\right) + \frac{\sigma_1 B^2}{\rho} u = -\frac{\sigma_1 EB}{\rho} \tag{3}$$

The term with factor μ is for viscosity, the term $\sigma_1 B^2/\rho$ relates to dynamo action and the term on the right hand side of (3) results from the electrostatic field. The initial conditions are specified as

$$u(r,0) = 0 \tag{4}$$

Equation (3) together with the initial condition of equation (4) form a complete mathematical problem which can be solved by Fourier-Bessel transforms, its solution being

$$u(r,t) = \frac{B\sigma_1}{2\mu}\int_0^t \frac{e^{-\alpha\tau - \frac{r^2\rho}{4\mu\tau}}}{\tau}d\tau \int_0^\infty xE(x)e^{-\frac{x^2\rho}{4\mu\tau}} I_1\left(\frac{\rho rx}{2\mu\tau}\right) dx \tag{5}$$

where $\alpha = \sigma_1 B^2/\rho$.

The steady state solution is immediately obtained by setting $t\to\infty$, thus (Gradshteyn and Ryzhik 1980)

$$u(r,\infty) = \frac{K_1(r\sqrt{\alpha\rho/\mu})\sigma_1 B}{\mu}\int_0^r xI_1(x\sqrt{\alpha\rho/\mu})E(x)dx$$

$$+ \frac{I_1(r\sqrt{\alpha\rho/\mu})\sigma_1 B}{\mu}\int_r^\infty xK_1(x\sqrt{\alpha\rho/\mu})E(x)dx \tag{6}$$

where E(r) is the distribution of electrostatic field along the r direction and I_1, K_1 are first order modified Bessel functions of the first and second kind respectively. We notice that the equilibrium characteristic time $t_c = \rho/\sigma_1 B^2$ is identical with that obtained by Cole (1971). Having found the velocity solution, the joule heating and viscous heating can be computed as follows

$$Q_j = \sigma_1(E + uB)^2 \tag{7}$$

$$Q_u = u(\mu\frac{\partial^2 u}{\partial x^2}) \tag{8}$$

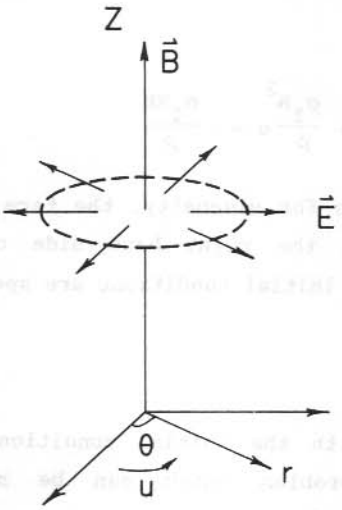

Figure 1. Geometry of the problem.

As an example the authors calculated the formulae (5) and (6). The results are presented in Figure 2 and Figure 3 respectively. The electric field is specified as follows:

$$E(r) = 0.01\ re^{-0.2r}\ \text{Volt m}^{-1}$$

The electric field is plotted in Figure 4. The maximum velocity does not occur where the electric field is maximum.

15.3 DECAY OF THERMOSPHERIC MOVEMENT FOR SOME CASES

15.3.1 Case one

Let us suppose for this case that the flow is laminar and the profile is initially $v(x,o) = f(x)$ for all altitudes z as shown schematically in Figure 5. The motion is along the y-direction only. Then for $t > 0$, the motion is governed by the equation

$$\rho\frac{\partial v}{\partial t} - \mu\frac{\partial^2 v}{\partial x^2} + \sigma_1 B^2 v = 0 \qquad (9)$$

Its solution is

$$v(x,t) = \frac{e^{-\alpha t}}{2\sqrt{(\mu\pi t/\rho)}}\int_{-\infty}^{\infty} f(\xi)e^{-\frac{(x-\xi)^2}{4t\mu/\rho}}\,d\xi \qquad (10)$$

For example, if initially the velocity profile is

$$v(x,0) = ae^{-bx^2} \qquad (11)$$

then the decay of this velocity is

$$v(x,t) = \frac{ae^{(-\alpha t - \frac{bx^2}{1+4bt\mu/\rho})}}{\sqrt{(1+4bt\mu/\rho)}} \qquad (12)$$

where $\alpha = \sigma_1 B^2/\rho$.

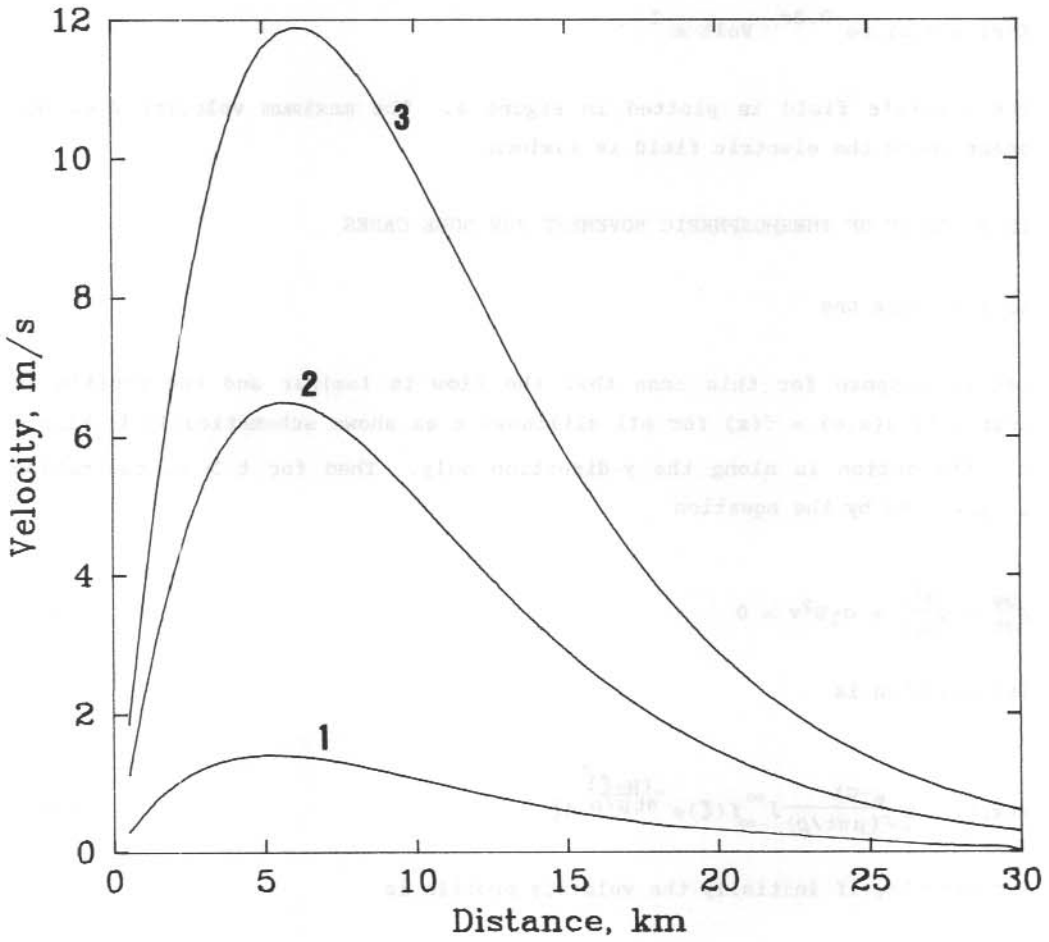

Figure 2. The time evolution of the velocity profile. Line 1 is for t = 10 s. Line 2 is for t = 50 s. Line 3 is for t = 100 s. The parameters are assumed as follows: B = 0.5 Gauss, $\mu = 3.2 \times 10^{-5}$ kg s m^{-1}, $\sigma = 10^{-4}$ mho m^{-1}, $\rho = 6.38 \times 10^{-10}$ kg m^{-3}. This represents the 170 km altitude thermosphere.

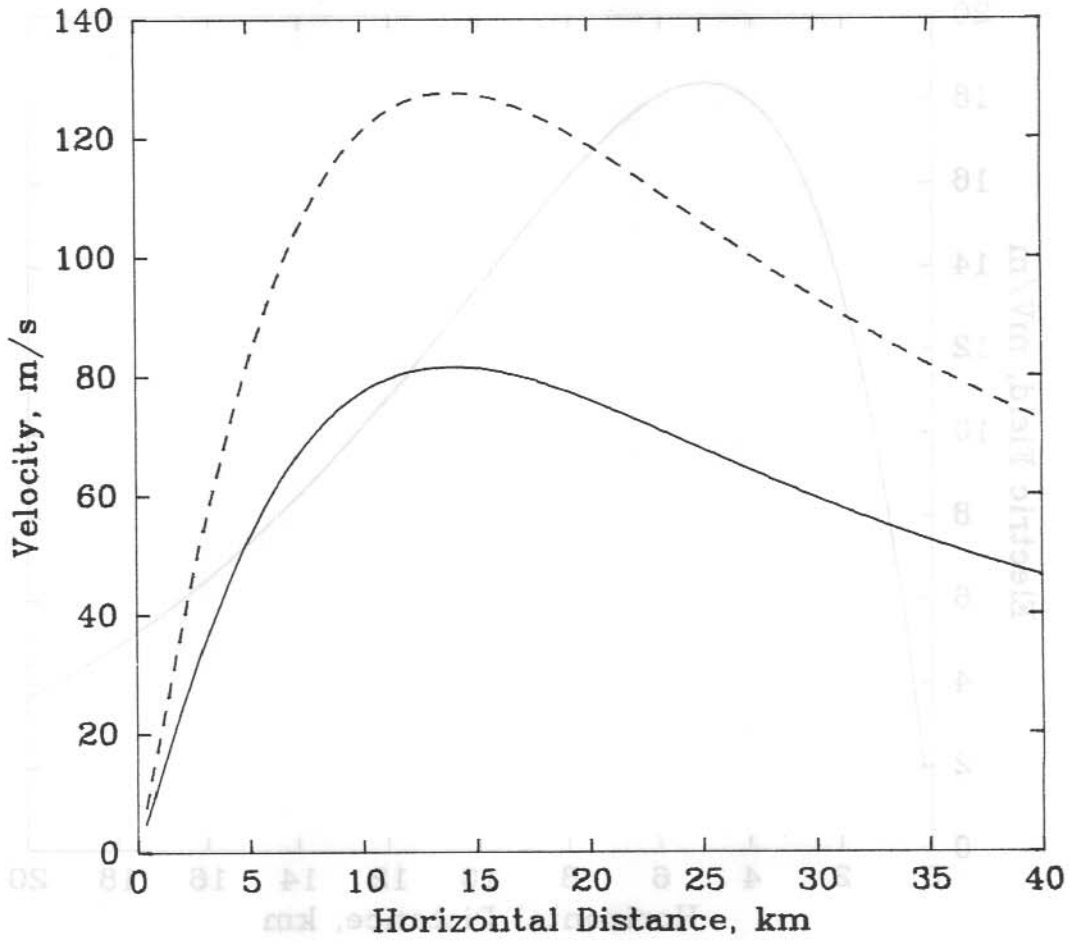

Figure 3. The steady state velocity profile. The dashed line is for the 170 km altitude thermosphere. The solid line is for the 200 km altitude thermosphere. The parameters for 200 km are chosen as follows: $\mu = 3.5 \times 10^{-5}$ kg s m^{-1}, $\sigma = 7.0 \times 10^{-5}$ mho m^{-1}, $\rho = 1.92 \times 10^{-10}$ kg m^{-3}.

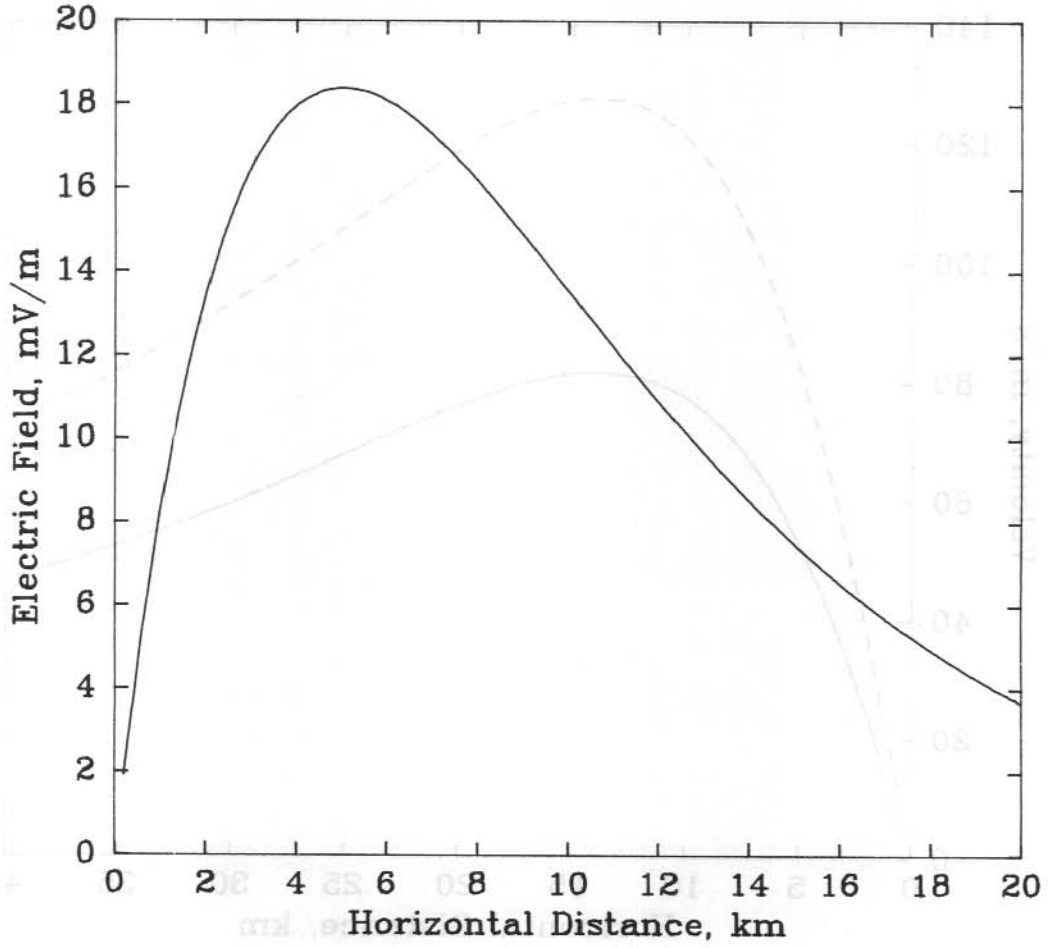

Figure 4. The specified electric field.

For the same situation but with two dimensions in space, it can be shown that the solution with initial velocity profile

$$v(r,0) = ae^{-br^2}$$

is given by

$$v(r,t) = \frac{ae^{(-\alpha t - \frac{br^2}{1+4bt\mu/\rho})}}{(1+4bt\mu/\rho)} \qquad (13)$$

It is worth noting that the decay is due to two mechanisms, one is the dynamo action, the other is viscosity. The characteristic time for the thermosphere to recover the still state is given by $t_c = \rho/\sigma_1 B^2$ which is the same as it takes the thermosphere to recover to steady state in the presence of an electrostatic field. The decay due to viscosity is dependent on the initial velocity profile shape and therefore dependent on the actual cases. As an example, a numerical calculation is presented in Figure 6.

15.3.2 Case two

For the situation described in 15.2, the equation governing the decay of the movement is written as

$$\frac{\partial u}{\partial t} - \frac{\mu}{\rho}\left(\frac{\partial^2 u}{\partial r^2} + \frac{1}{r}\frac{\partial u}{\partial r} - \frac{u}{r^2}\right) + \alpha u = 0 \qquad (15)$$

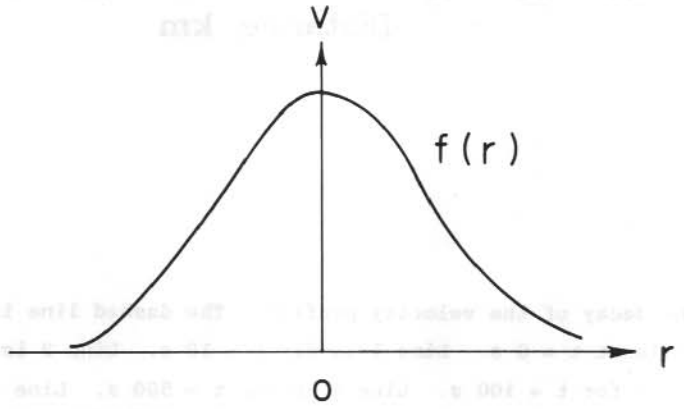

Figure 5. Geometry of the problem.

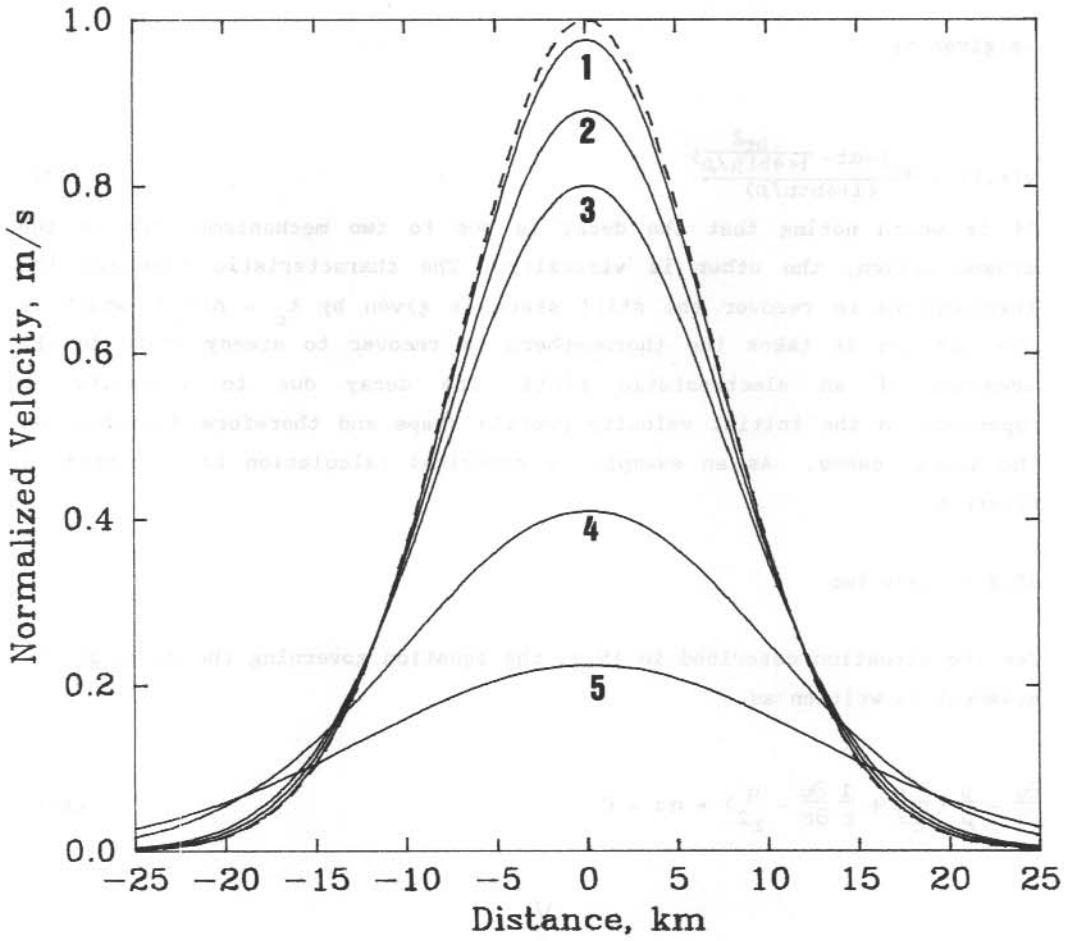

Figure 6. The decay of the velocity profile. The dashed line is the velocity profile at t = 0 s. Line 1 is for t = 10 s. Line 2 is for t = 50 s. Line 3 is for t = 100 s. Line 4 is for t = 500 s. Line 5 is for t = 1000 s. The graph represents the 170 km altitude thermosphere.

Its solution with initial velocity profile f(r) is

$$u(r,t) = e^{-\alpha t} \int_0^\infty \xi J_1(\xi r) F(\xi) e^{-t\xi^2 \mu/\rho} \, d\xi \tag{16}$$

where

$$F(\xi) = \int_0^\infty \eta f(\eta) J_1(\xi\eta) d\eta \tag{17}$$

$$\text{If } f(r) = are^{-br^2} \tag{18}$$

the decay of the velocity is

$$v(r,t) = \frac{are^{\left(-\alpha t - \frac{br^2}{1+4bt\mu/\rho}\right)}}{(1+4bt\mu/\rho)^2} \tag{19}$$

where $\alpha = \sigma_1 B^2/\rho$.

For the initial velocity profile shape cited in this section, the characteristic time of decay due to the viscosity is proportional to $\rho/\mu b$, where b is the velocity profile parameter.

15.4 REFERENCES

Cole, K.D. (1971). Electrodynamic heating and movement of the thermosphere. Planetary Space Science 19:59-75.

Gradshteyn, I.S. and Ryzhik, I.M. (1980). Table of integrals, series and products. Academic Press, New York.

Wu, S.T. and K.D. Cole (1976). Transient thermospheric heating and movement caused by an auroral electric field. Planetary Space Science 24:727-730.

16. THE DISTRIBUTION OF ELECTRIC FIELD AND CURRENT AROUND A COLUMN OF ELECTRIC CURRENT FROM THE MAGNETOSPHERE

D.Y. Zhang and K.D. Cole
Physics Department
LaTrobe University
Bundoora, Vic., Australia, 3083.

ABSTRACT

Various observations indicate the existence of columns of very strong field-aligned electric currents in the auroral ionosphere. The distributions of electrostatic field and joule heating in this localised phenomenon are determined.

16.1 INTRODUCTION

The magnetosphere has a great influence in the ionosphere. In the upper ionosphere and magnetosphere of the auroral region, because of the almost collisionless plasma, or the great conductivity along the geomagnetic field lines, electric fields of various scales in the magnetosphere can penetrate into the ionosphere and thermosphere. This penetration depends on the conditions of the ionosphere and thermosphere. Chiu (1974) studied the self consistent mapping of electric field for a planar electric current configuration. He found that the penetration is dependent very much on the scale of the electric field and that the perpendicular and parallel components of the electric field are interrelated. This paper confirms these conclusions. The purpose of this paper is to examine the penetration of a column of electric current from the magnetosphere into the ionosphere and its horizontal spreading.

16.2 FORMULATION

The basic starting point of this electric field mapping is that the electric current $\underline{J}$ is continuous everywhere in the ionosphere, i.e.

$$\nabla.\underline{J} = 0 \qquad (1)$$

The current is driven by an electro-static or quasi-electrostatic field $\underline{E}$ which must satisfy the Maxwell equation:

$$\nabla \times \underline{E} = 0 \tag{2}$$

Now

$$\underline{J} = \underline{P}\underline{E}_{\perp} + C\underline{b}\times\underline{E} + D(\underline{b}.\underline{E})\underline{b} \tag{3}$$

where $E_{\perp}$ is the component of $\underline{E}$ perpendicular to the magnetic field whose direction is $\underline{b}$. P, C and D are the Pedersen conductivity, cross field conductivity and the direct conductivity respectively.

Equation (2) is satisfied by a potential field such that

$$\underline{E} = -\nabla\Phi \tag{4}$$

Let a cylindrical coordinate system be set up with the z axis directed upwards along the geomagnetic field lines which are assumed vertical. Then equations (1), (3) and (4) combine to give the following second order partial differential equation:

$$\frac{\partial^2\Phi}{\partial r^2} + \frac{1}{r}\frac{\partial\Phi}{\partial r} + \frac{1}{r^2}\frac{\partial^2\Phi}{\partial\theta^2} + \frac{1}{P}\frac{\partial}{\partial z}\left(P\frac{\partial\Phi}{\partial z}\right) = 0 \tag{5}$$

It is noticed that the potential is independent of the cross field conductivity, C. It is a linear second-order partial differential equation. Employing a Fourier-Bessel transform, the general solution can be written as follows:

$$\Phi(r,\theta,z) = \sum_{m=-\infty}^{\infty} \int_0^{\infty} \alpha J_{|m|}(\alpha r) e^{im\theta} \psi_{\alpha}(z)\, d\alpha \tag{6}$$

where J_m are Bessel functions of the first kind and $\psi_{\alpha}(z)$ satisfies the following second order ordinary differential equation:

$$\frac{\partial}{\partial z}\left(D\frac{\partial\psi_{\alpha}}{\partial z}\right) - \alpha^2 P\psi_{\alpha} = 0 \tag{7}$$

The solutions of this equation depend on the conductivity profile function P and D.

16.3 MODELS OF THE ATMOSPHERE AND IONOSPHERE

The models of the atmosphere and ionosphere adopted here are due to Chiu who approximated the US Standard atmosphere and Chiu's phenomenological ionospheric models by piecewise polynomials as follows:

$$P \simeq \frac{Ne^2}{m_i} \frac{\nu}{\nu^2 + \Omega^2}, \quad C \simeq \frac{P\nu}{\Omega}, \quad D \simeq \frac{Ne^2}{m_i} \frac{1}{\xi + \eta} \tag{8}$$

where

$$\nu \simeq \nu_{in}, \quad \xi \simeq m_e \nu_{ei}/m_i, \quad \eta \simeq m_e \nu_{en}/m_i$$

and Ω is the gyrofrequency. The collision frequencies ν_{in}, ν_{ei} and ν_{en} are written above 100 km as follows:

$$\nu_{in} \simeq N_n K_{in}, \quad \nu_{ei} \simeq NK_{ei}, \quad \nu_{en} \simeq N_n K_{en} \tag{9}$$

where K_{in} K_{ei} and K_{en} are assumed to be constant. Then the dimensionless profile functions p(z) and q(z) are introduced for the ion and neutral densities N and N_n respectively; thus:

$$N(z) \simeq N(z_0)p(z), \quad N_n(z) \simeq N_n(z_0)q(z) \tag{10}$$

where z_0 is any altitude in general. Then for the average condition, the profile functions p and q are approximated by piecewise polynomials. Thus, the whole thermosphere is divided into six layers, a, b, c, d, e, f, with the interfacial altitudes of the layers being z_F, z_0, z_E, z_B, z_M. The top side boundary is at 400 km altitude and the bottom side boundary is at ground level. Then the solution of equation (7) in each layer is expressed as follows:

For Regions i = a and b, the solution for (7) is:

$$\psi_i = [A_i M(\frac{k_i-\lambda_i}{2k_i},1,2k_i\rho) + B_i U(\frac{k_i-\lambda_i}{2k_i},1,2k_i\rho)]\, e^{-(k_i-\lambda_i)\rho} \qquad (11)$$

where

$$\rho \simeq e^{(z-z_0)/h_\alpha}, \quad \lambda_i \simeq h_\alpha/2h_i, \quad k_i^2 \simeq \lambda_i^2 + h_\alpha^2\alpha^2 ,$$

A_i and B_i are constants determined by the appropriate boundary conditions and M and U are confluent hypergeometric functions of the first and second kind respectively.

For regions i = c,d,

$$\psi_i = R_i e^{\xi_{+i}(z-z_i)} + S_i e^{\xi_{-i}(z-z_i)} \qquad (12)$$

where R_i and S_i are constants to be determined by boundary conditions and z_i refers to the appropriate interface z_0 or z_E.

The constants $\xi_{\pm i}$ are determined by:

$$\xi_{\pm i} = [-1 \pm (1 + 4h_i^2\alpha^2)^{1/2}]/(2h_i)$$

For region e, where $z_B \geq z \geq z_M$,

$$\psi_e = [A_e I_\gamma(\beta s) + B_e K_\gamma(\beta s)]s^\gamma \qquad (13)$$

where I_γ and K_γ are Bessel functions and A_e and B_e are constants to be determined by boundary and interfacial conditions. The parameters γ, β, and s are defined in terms of the conductivity parameters as follows:

$$\gamma = \frac{h_p}{h_p - h_D}, \qquad \beta = 2\gamma h_D K , \quad s = e^{(\frac{z_B - z}{2h_D\gamma})}$$

For region f, where $z_M \geq z \geq 0$,

$$\psi_f = R_f e^{\zeta_{+f}(z-z_M)} + S_f e^{\zeta_{-f}(z-z_M)} \qquad (14)$$

where R_f and S_f are constants to be determined by boundary conditions. The constants $\zeta_{\pm f}$ are determined by:

$$\zeta_{\pm f} = (-1 \pm (1 + 4h_T k^2)^{1/2}]/(2h_T)$$

16.4 SOLUTIONS

At the top and bottomside boundaries, the following are assumed,

$$\left.\frac{\partial\phi}{\partial z}\right|_{z=400} = -(j_0/D)e^{-ar^2} \qquad 0 < r < \infty$$
$$\left.\frac{\partial\phi}{\partial z}\right|_{z=0} = 0 \qquad 0 < r < \infty \tag{15}$$

where j_0 is the parallel electric current on the top side boundary. Note that the problem now is cylindrically symmetric. Hence the solution is as follows:

$$\phi(r,z) = \int_0^\infty \alpha J_0(\alpha r)\psi_\alpha(z)\, d\alpha \tag{16}$$

At interfaces $z_M < z_B < z_E < z_0 < z_F$, the potential values and the normal components of electric field should be continuous, i.e.

$$\phi_a(r,z_F) = \phi_b(r,z_F), \quad \left.\frac{\partial\phi_a}{\partial z}\right|_{z=z_F} = \left.\frac{\partial\phi_b}{\partial z}\right|_{z=z_F}$$
$$\phi_b(r,z_0) = \phi_c(r,z_0), \quad \left.\frac{\partial\phi_b}{\partial z}\right|_{z=z_0} = \left.\frac{\partial\phi_c}{\partial z}\right|_{z=z_0}$$
$$\phi_c(r,z_E) = \phi_d(r,z_E), \quad \left.\frac{\partial\phi_c}{\partial z}\right|_{z=z_E} = \left.\frac{\partial\phi_d}{\partial z}\right|_{z=z_E} \tag{17}$$
$$\phi_d(r,z_B) = \phi_e(r,z_B), \quad \left.\frac{\partial\phi_d}{\partial z}\right|_{z=z_B} = \left.\frac{\partial\phi_e}{\partial z}\right|_{z=z_B}$$
$$\phi_e(r,z_M) = \phi_f(r,z_M), \quad \left.\frac{\partial\phi_e}{\partial z}\right|_{z=z_M} = \left.\frac{\partial\phi_f}{\partial z}\right|_{z=z_M}$$

There is no need to impose continuous constraints on the horizontal components of the electric field because at every point in space, the horizontal component is related to the vertical component of electric field by equations (6) and (7).

Substituting (11)-(14) and (16) into (15) and (17), all the unknown coefficients can be determined. The solution to the electric potential is therefore obtained. The electric currents and joule heating can consequently be obtained. The numerical results are proceeding.

16.5 REFERENCES

Abramowitz, M. and Stegun, L.A. (1964). Handbook of Mathematical functions. U.S. Government Printing Office, Washington, D.C.

Chiu, Y.T. (1974). Self-consistent electrostatic field mapping in the high-latitude ionosphere. Journal of Geophysical Research 79:2790-2802.

17. OH NIGHTGLOW OBSERVATIONS AND TEMPERATURE DETERMINATIONS AT DAVIS, ANTARCTICA

P.F.B. Williams
Antarctic Division
Department of Science
Kingston, Tas., Australia, 7150.

ABSTRACT

Observations of OH(8-3) nightglow at Davis, Antarctica, in 1984 were used to estimate rotational temperatures for the emitting region. Possible causes for the apparent non-Boltzmann like distribution of the rotational populations were investigated. A periodic intensity variation on 12 June was also recorded.

17.1 INTRODUCTION

During the Austral winter of 1984 a six position (seven channels, one position being used as a dark current channel as well as a filter channel) zenith photometer was deployed at the Australian Antarctic station, Davis (68.58°S, 77.96°E geographic). Relative intensities of three lines in the Meinel (8-3) vibrational-rotational band of the hydroxyl nightglow were measured for the purpose of determining the nighttime rotational temperature with a time resolution of approximately seven minutes. Both long term trends (nocturnal and seasonal) and shorter period irregularities were sought in the temperatures. The possibility of deposition of auroral energy producing thermal variations at the emitting altitudes (85 to 95 km) was investigated. Short term variations in the airglow intensity were also studied.

17.2 INSTRUMENTATION

The photometer, previously used at Mawson by Stubbs et al. (1983), was operated under the control of an LSI/11-02 minicomputer, data being stored on hard magnetic disk. Channels were allocated as in Table 1. The 'open' channel (G) was employed for testing and calibration, as well as monitoring general photometric conditions.

Table 1. Deployment of channels.

POSITION	CHANNEL	OBSERVATION	FILTER		
			Peak Freq nm	Peak Trns %	FWHM nm
1	A	Dark (shutter closed)	-	-	-
	B	Background (open)	734.89	50.0	.41
2	C	OH(8-3) P1(2), 731.64nm	731.59	57.3	.48
3	D	OH(8-3) P1(4), 736.96nm	736.94	36.4	.49
4	E	OH(8-3) P1(5), 740.18nm	740.18	48.7	.50
5	F	Aurora/a'glow, 630.0nm	629.85	60.1	1.14
6	G	Open (no filter)	-	-	-

Table 2. Data selection.

Day	Date	Segment	From UT	To UT	Day	Date	Segment	From UT	To UT
175	23/6	Z	1500	2000	212	30/7	Z	2140	2330
176	24/6	Z	1430	1750	213	31/7	Z	1640	2120
183	1/7	Z	1110	1320	227	14/8	Z	1300	1400
184	2/7	Y	1155	1330	231	18/8	Z	1510	1815
		Z	1600	1740	233	20/8	Y	1650	1750
204	22/7	W	1210	1340			Z	2200	0030
		X	1650	1920	238	25/8	Z	1630	2240
		Y	1940	2150	240	27/8	Y	1720	1850
		Z	2220	0040			Z	1950	2210
205	23/7	Y	1620	1850	258	14/9	Z	1650	1800
		Z	1940	2110	264	20/9	Z	1740	2130
206	24/7	Z	1400	1700	265	21/9	Z	1740	2120
208	26/7	Z	2140	0030					

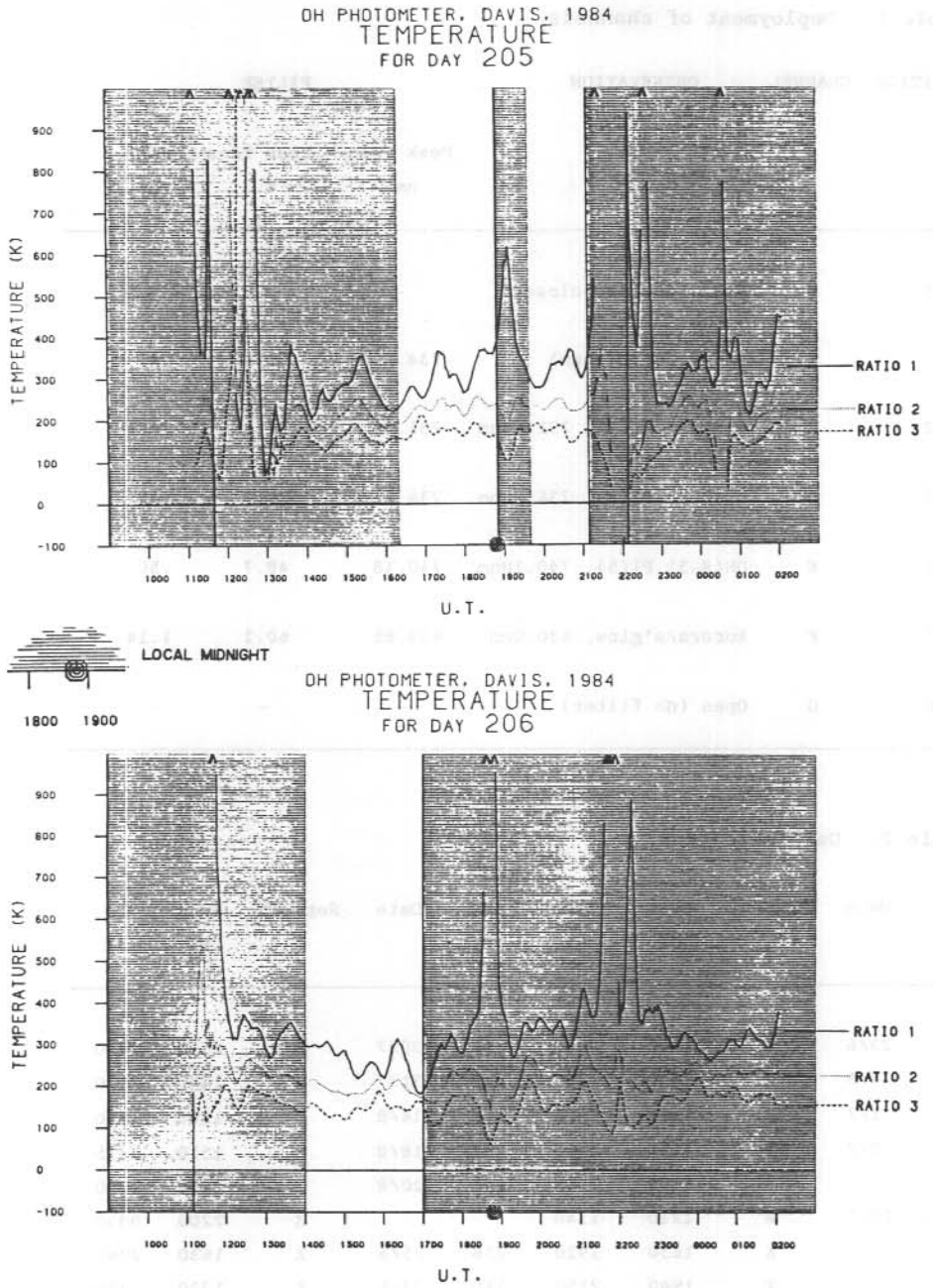

Figure 1. Derived rotational temperatures from OH intensities at Davis on 23 July (day 205) and 24 July (day 206) 1984. Raw data were subjected to 1-4-6-4-1 running mean. Shaded areas indicate data rejected according to criteria described in text.

A wide-angle twin channel photometer, observing 557.7 nm and 427.8 nm emissions was operated simultaneously, providing an indication of the level of auroral activity.

17.3 DATA SELECTION AND TEMPERATURE ANALYSIS

Data were recorded on 118 nights from 29 May to 20 October. Of these, the major portion was discarded due to weather conditions, instrumental problems and lunar contamination. From the remainder, only segments of half an hour or greater duration, for which no auroral activity was indicated, were accepted for analysis. Sixty-five hours of data were thus recovered from eighteen separate nights (Table 2).

Rotational temperatures were derived from the three possible ratios of intensities of the hydroxyl lines, according to the equation:

$$T_{n,m} = \frac{E_{v'}(J'_m) - E_{v'}(J'_n)}{k \ln \left\{ \frac{I_n}{I_m} \cdot \frac{A(J''_{m+i}, v'' \leftarrow J'_m, v')}{A(J''_{n+i}, v'' \leftarrow J'_n, v')} \cdot \frac{2J'_m+1}{2J'_n+1} \right\}} \qquad (1)$$

where $T_{n,m}$ is the rotational temperature estimated from intensities, I, of two lines from rotational levels J'_n, J'_m in the upper vibrational level v', and J''_{m+i} in the lower vibrational level v"; $E_v(J)$ is the energy of level J, v; and A(J",v"←J',v') is the einstein coefficient for transition from J',v' to J",v". For the P branch of OH(8-3), v"=8, v'=3 and i=+1.
(The above equation was adapted from that of Mies 1974.)

It is assumed that, within a given vibrational state, the rotational level populations attain a Boltzmann distribution. The einstein coefficients were based on the transition probabilities of Mies.

Figure 1 shows a selection of the temperatures derived, after filtering the raw data with a 1-4-6-4-1 running mean. Ratios 1, 2 and 3 correspond to the intensity ratios $P_1(2)/P_1(4)$, $P_1(2)/P_1(5)$ and $P_1(4)/P_1(5)$ respectively.

Table 3. Averaged temperatures.

RATIO:	$P_1(2)/P_1(4)$		$P_1(2)/P_1(5)$		$P_1(4)/P_1(5)$	
SEGMENT	AVE.TEMP ^{o}K	NO.POINTS	AVE.TEMP ^{o}K	NO.POINTS	AVE.TEMP ^{o}K	NO.POINTS
175Z	189.	141	154.	129	123.	129
176Z	221.	87	182.	74	150.	74
183Z	815.	54	339.	54	217.	54
184Y	229.	33	231.	27	171.	27
184Z	529.	39	341.	39	241.	39
204W	426.	33	246.	33	166.	33
204X	373.	63	234.	63	167.	63
204Y	361.	57	249.	57	188.	57
204Z	352.	60	246.	60	183.	60
205Y	328.	63	239.	63	179.	63
205Z	335.	36	235.	36	173.	36
206Z	272.	81	201.	81	154.	81
208Z	408.	75	266.	75	210.	75
212Z	1197.	45	287.	45	184.	45
213Z	187.	129	159.	120	147.	120
227Z	327.	21	238.	21	175.	21
231Z	297.	78	223.	78	176.	78
233Y	241.	21	184.	21	160.	21
233Z	314.	66	227.	66	172.	66
238Z	478.	174	304.	174	255.	174
240Y	294.	36	232.	36	193.	36
240Z	392.	60	287.	60	238.	60
258Z	379.	24	268.	24	221.	24
264Z	413.	99	234.	99	153.	99
265Z	360.	81	236.	81	167.	81
Grand Average	370.	1656	237.	1616	182.	1616

Characteristic of the temperatures thus calculated was a marked difference between the three estimates. Namely, ratio 1 led to higher, more variable estimates than ratio 2, while ratio 3 produced generally lower and less variable results. Table 3 shows clearly a similar difference in the temperature estimates (°K) averaged over all segments of data analysed (with no filtering applied). This discrepancy suggests either that the populations of the rotational states were not distributed Boltzmann-wise (a distinct possibility at the eighth vibrational level, due to the cascading effect - see Suzuki and Tohmatsu 1976), or that the apparent intensities measured were not truly representative of the transition rates in the OH emission region (implying contamination of, or interference to the observed line intensities, in a fairly systematic fashion).

Assuming the latter cause, and further that the interference be predominantly in just one line, then a study of the functional relationship between the individual line intensities and the resulting temperature estimates (for "true" temperatures around 200°K) reveals two possible causes for the observed tends. Firstly, the $P_1(2)$ intensity may have been underestimated, implying strong absorption of this line at altitudes below the emitting region. It is considered more likely that this line would have been overestimated due to contamination from the auroral OII emission at 731.86 nm (see Figure 2a). Secondly, the $P_1(4)$ line may have been overestimated. Diagram 2b shows a published spectrum in which the $N_2(5-3)$ band, headed at 738.72 nm, is distinct, while the OII emission is not so apparent. This nitrogen band overlies the $P_1(4)$ line of OH, and the question must be addressed as to whether it may have contributed significantly to the measured intensity through channel 3, even during apparently aurorally quiet times.

Assuming ratio 2, involving no $P_1(4)$, to be the most reliable estimator, further studies were undertaken to investigate nocturnal and seasonal trends, as well as attempting to correlate the temperatures with magnetic and auroral activity. However, the limited amount of acceptable data, and the high statistical errors involved, yielded no valid conclusions.

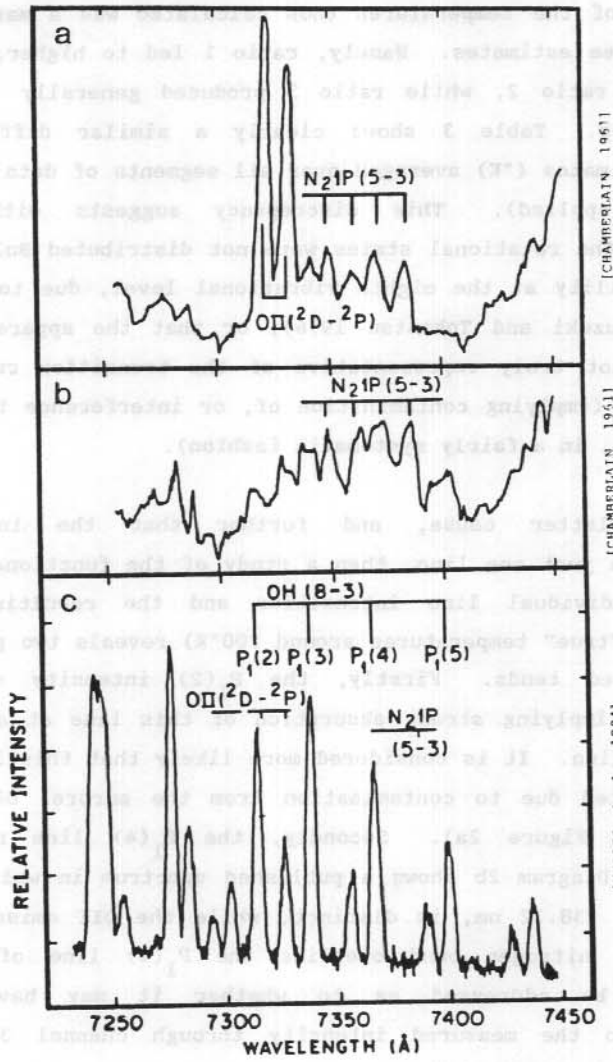

Figure 2.

(a) Portion of an auroral spectrum, showing strong OII (^2D-^2P), and weaker $N_2P(5-3)$ bands masking the OH(8-3) P_1 and P_2 branches. (From Chamberlain 1961).

(b) Portion of an auroral spectrum, in which the $N_2(5-3)$ band dominates, with little OII emission. OH(8-3) P_1 and P_2 are again masked. (From Chamberlain 1961).

(c) Example of an OH(8-3) band spectrum, without auroral contamination. (From Myrabo et al. 1984)

17.4 INTENSITY VARIATIONS

As with the temperatures, nocturnal trends in intensity of the OH airglow were not readily suited to study, due to poor scatter of acceptable data. Seasonal variations, or nocturnal variations based on data from different nights could not be investigated since the photometer response was not calibrated to a standard radiant source.

On day 164 (12 June) a noteworthy intensity variation occurred. As shown in Figure 3a, all three hydroxyl lines exhibited a periodic fluctuation between about 1710 and 2150 UT, and possibly also prior to 1610 UT. (An instrument failure occurred between 1610 and 1710 UT). The period diminished from about thirty-five to twenty-five minutes, and the amplitude also decreased. Figure 3b shows similar variations to have occurred in the 630.0 nm emissions (channel F) and background continuum at 735.0 nm (channel B). All these variations exhibited similar characteristics and were in phase to within the seven minute time resolution.

That the sources of the variations were not instrumental is evidenced by their failure to show in either the dark count or the 'open' channel count (channel G). The latter also eliminates weather or artificial contamination as causes.

Temperatures were not estimated for the duration of this event because of lunar contamination. Magnetic conditions, monitored by a three component fluxgate magnetometer and two horizontal component micropulsation coils, were exceptionally quiet, as was cosmic noise reception via a standard riometer. The only auroral activity, indicated by both twin channel photometer and all-sky-camera records, was minor, occurring at the times indicated in Figure 3.

No explanation for this observation is offered here, but if gravity waves at mesopause altitudes are to be shown responsible, then it must also be explained why the 630.0 nm emissions exhibited similar characteristics with no appreciable phase difference.

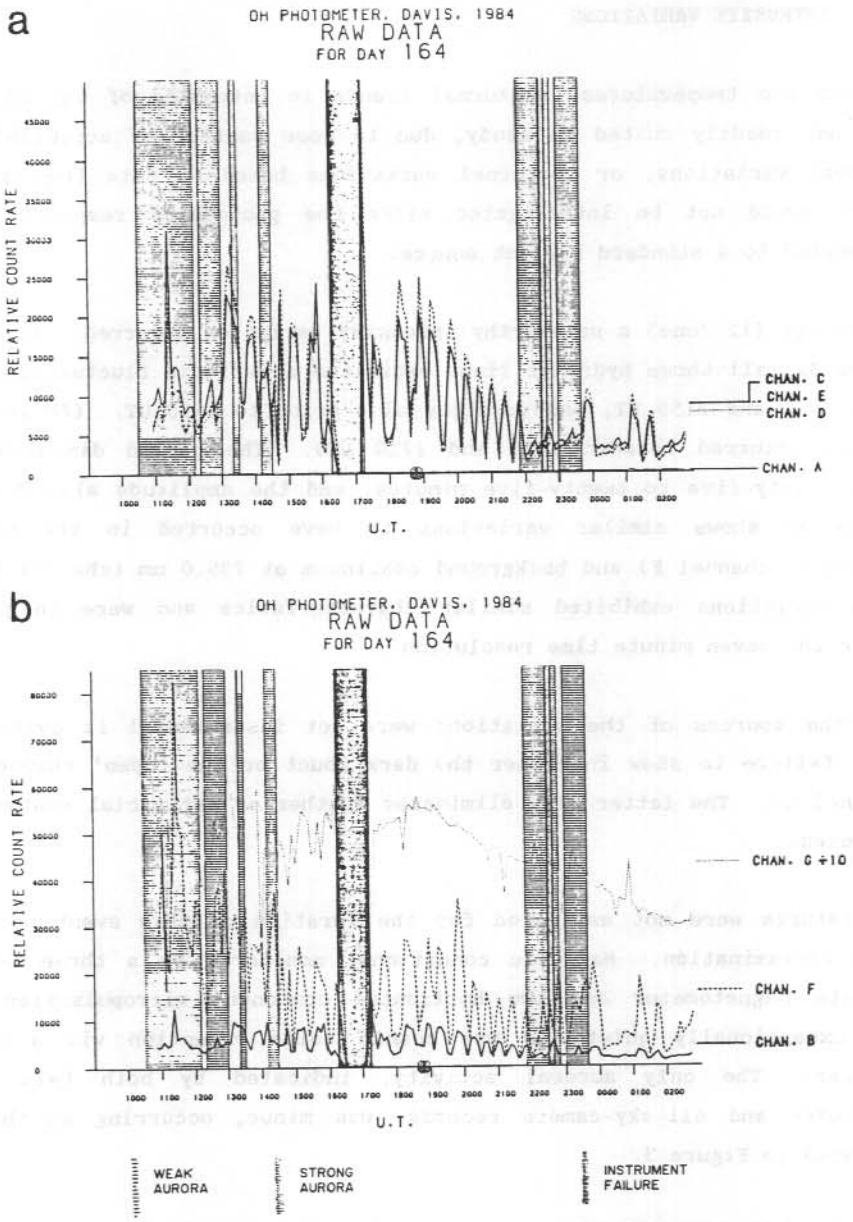

Figure 3. Intensities measured by 6-channel photometer on 12 June 1984 showing wavelike form from:

(a) channels observing OH lines $P_1(2)$, $P_1(4)$ and $P_1(5)$, (C,D and E respectively) and dark current (A), and

(b) channels observing 630.0 nm (F), 'background' at 735.0 nm (B) and unfiltered spectrum (G).

It may be that emissions from the N_2 1P (10-7) or (11-8) bands, headed at around 632.29 nm and 625.30 nm respectively, were also detected through the 630.0 nm filter (with full width at half maximum transmission of about 1.1 nm). This band is normally associated with the type B red aurorae, which are excited at a much lower altitude than the 630.0 nm type A aurorae (Chamberlain 1961), and would account for the phase relationship with OH (8-3). Further, the background filter, at 734.89 nm, was tuned very closely to one line of the N_2 1P (5-3) band, thought to be contaminating the OH (8-3) $P_1(4)$ line observations.

17.5 CONCLUSIONS

To successfully measure mesopause temperatures at high southern latitudes via OH intensities it is essential to learn more of the general spectrum in the region of the lines used. In particular, the presence of contaminating emissions and the form of the background continuum must be investigated. To this end, a scanning spectrometer is to be deployed along with the 6-channel photometer at Davis for 1987. This should, at minimum expectations, reveal the state of thermalization of the eighth vibrational level of hydroxyl.

Periodic intensity variations, with a period close to that expected for gravity waves near the mesopause, have been observed in the OH(8-3) nightglow, and were intimately associated with variations in the background continuum in this spectral region, along with emissions around 630.0 nm.

17.6 REFERENCES

Chamberlain, J.W. (1961). Physics of the Aurora and Airglow. Academic Press, New York and London.

Mies, F.H. (1974). Calculated vibrational transition probabilities of $OH(X^2\Pi)$. Journal of Molecular Spectroscopy 53:150-188.

Myrabo, H.K. Romick, G.J., Sivjce, G.G. and Deehr C.S. (1984). Night airglow OH (8-3) band rotational temperatures at Poker Flat, Alaska. Journal of Geophysical Research 89(10):9153-9156.

Stubbs, L.C., Boyd, J.S. and Bond, F.R. (1983). Measurement of the O-H rotational temperature at Mawson, East Antarctica. Planetary and Space Science 31(8):923-932.

Suzuki, K. and Tohmatsu, T. (1976). An interpretation of the rotational temperature of the airglow hydroxyl emissions. Planetary and Space Science 24:665-671.

18. A SIMULTANEOUS OBSERVATION OF LARGE-SCALE PERIODIC TIDS IN BOTH HEMISPHERES FOLLOWING AN ONSET OF AURORAL DISTURBANCES

L.A. Hajkowicz (1) and R.D. Hunsucker (2)

(1) Department of Physics
University of Queensland
St. Lucia, Qld., Australia, 4067.

(2) Geophysical Institute
University of Alaska
Fairbanks, Alaska 99 775-0800, U.S.A.

ABSTRACT

An onset of an auroral substorm at the equatorward edges of the southern and northern auroral zones preceded the occurrence of the periodic variations in the virtual height (h'F) of the F-region in the Southern and Northern Hemispheres. The variations in h'F had characteristics typical of large scale TIDs (LS TIDs) propagating equatorwards with a velocity of about 800 ms^{-1}, and with a constant period of 135 minutes in both hemispheres. The horizontal wavefront of LS TIDs was observed in mid-latitudes to be in excess of 7000 km. The LS TIDs were found to be in phase at the stations which are equidistant from the auroral sources. From this it was concluded that the periodic LS TIDs were likely to produce a constructive interference effect at the points of their encounter, near the equator.

It was concluded that the sources of LS TIDs in both hemispheres were elongated along the L-shell with L-value between 4 and 5, and had a large longitudinal extent, exceeding 60°. The source locations were consistent with the positions of the belts of energetic particle precipitations as inferred from the standard riometer and magnetometer data. The large quasi-linear extent of the source is consistent with the wide horizontal wavefronts of LS TIDs.

18.1 INTRODUCTION

Recently it has been pointed out that standard riometer data, obtained in the auroral region, can provide accurate high-latitude reference points for

Table 1. Geomagnetic coordinates and principle instrumentation of some of the stations used in the analysis.

Station	Geomagnetic Coordinates Latitude	Longitude	L-value	Instrument	D* KM
Macquarie Island (M)	61.0°S	243.6°E	5.3	Riometer Magnetometer	0
Campbell Island (CI)	57.2°S	253.7°E	4.0	Riometer	
Hobart (H)	51.6°S	224.9°E	2.9	Ionosonde	1280
Canberra (Ca)	43.9°S	224.8°E	2.0	Ionosonde	2100
Brisbane (B)	35.7°S	227.4°E	1.5	Ionosonde	2940
Norfolk Island (N)	34.7°S	243.7°E	1.5	Ionosonde	
Townsville (T)	28.4°S	219.3°E	1.3	Ionosonde	3840
Vanimo (V)	12.5°S	211.6°E	1.0	Ionosonde	5640
Fort Yukon (F)	66.7°N	257.3°E	6.5	Riometer Magnetometer	
Tixie Bay (TB)	60.5°N	191 7°E	5.6	Magnetometer	0
College (C)	64.8°N	257.0°E	5.4	Riometer Magnetometer	
Sheep Mountain (S)	62.0°N	260.3°E	4.4	Riometer	
Anchorage (A)	61.0°N	258.6°E	4.1	Riometer	
Wakkanai (W)	35.3°N	206.5°E	1.6	Ionosonde	2970
Akita (Ak)	29.5°N	205.9°E	1.4	Ionosonde	3580
Kokobunji (K)	25.5°N	205.8°E	1.2	Ionosonde	4060
Maui (MA)	21.0°N	268.6°E	1.1	Ionosonde	
Yamagawa (Y)	20.4°N	198.3°E	1.1	Ionosonde	4520
Okinawa (O)	15.3°N	196.0°E	1.0	Ionosonde	5020

* Great circle distances from the auroral source locations.

tracing large-scale ionospheric disturbances (LS TIDs) over a wide range of southern and northern latitudes (Hajkowicz 1983a,b, Hajkowicz and Hunsucker 1985).

The previous studies have been mainly concerned with an impulse-like propagation of LS TIDs (Davis 1971, Hajkowicz 1983b). There has been no evidence on a periodic wave propagation of LS TIDs launched simultaneously from the southern and northern auroral ovals at the onset of a geomagnetic disturbance. The present results, which concern such a case, were selected from a large amount of data derived from the analysis of mid-latitude ionograms (the detailed analysis, based on thirty-two events, was given by Hajkowicz and Hunsucker 1985).

18.2 METHODS AND RESULTS

The presence of periodic LS TIDs, following an onset of a geomagnetic substorm on 9 November 1979, was detected from the analysis of the virtual height (h'F) rises obtained at fifteen minute intervals at the Japanese and Australian stations. The onset of auroral disturbances was deduced from the vertical-incidence riometer data obtained in the conjugate auroral locations. The geomagnetic locations of the stations, principle instrumentation used and other relevant data are given in Table 1.

The substorm activity commenced first at lower latitude auroral stations, with absorption increases reaching maxima at 1420 UT (0424 LT) at Anchorage (northern auroral zone) and at 1420 UT (0120 LT) at Campbell Island (the conjugate location in the southern auroral zone). It can be seen (Figure 1) that the absorption level at the time of the substorm commencement decreased rapidly at the stations polewards of Anchorage and Campbell Island. In the north, absorption levels decreased from 3.0 dB at Anchorage (L-value = 4.1) to a trace of absorption at Fort Yukon (L-value = 6.5). A similar trend in the absorption decrease was present in the south where a large absorption peak at Campbell Island (L-value = 4.0) at 3.6 dB decreased to a small absorption peak at Macquarie Island (L-value = 5.3). It should be noted that larger absorption activity developed later at higher latitude stations, indicating the polewards shift of auroral particle precipitation regions during a later stage of the substorm.

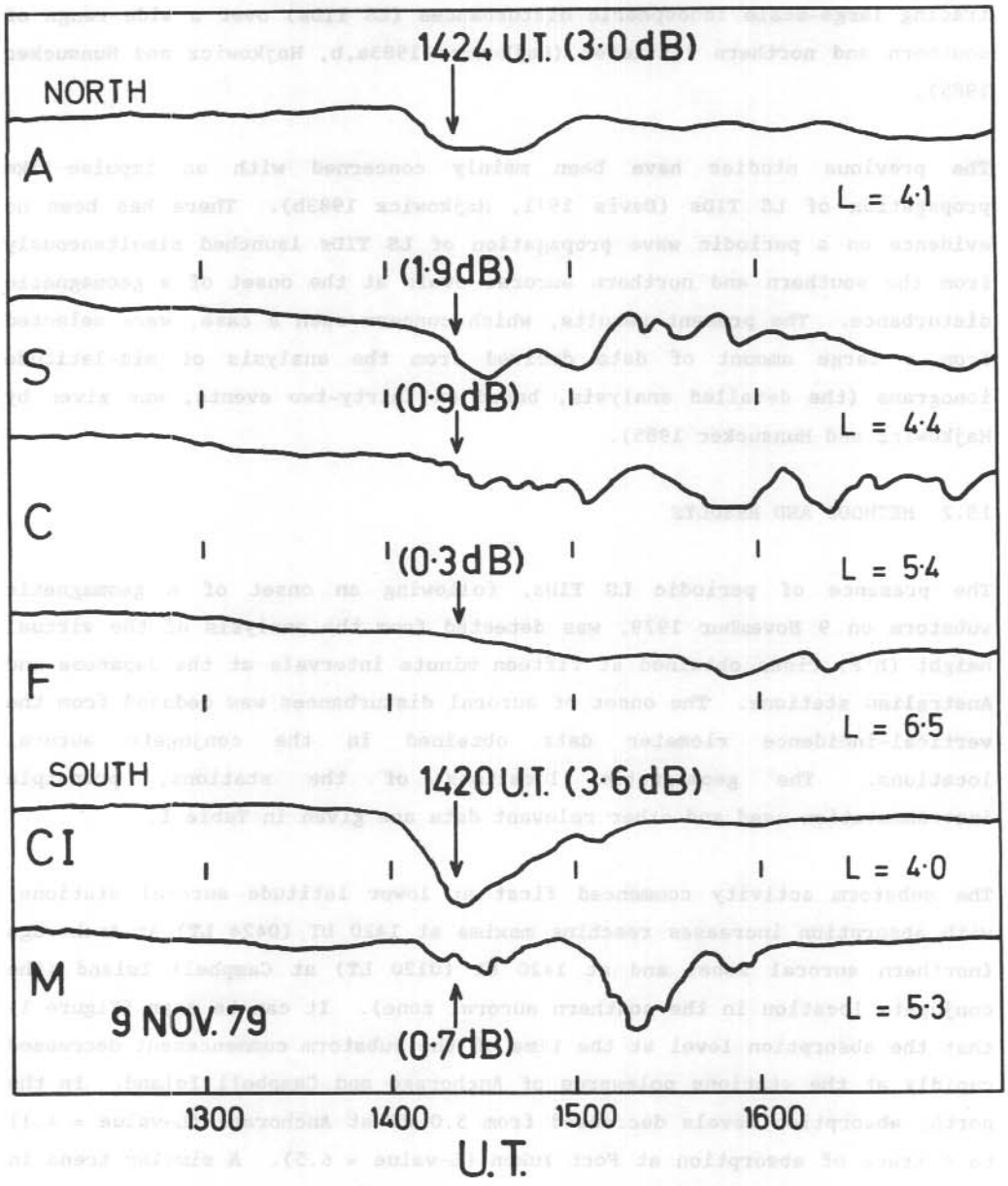

Figure 1. The onsets of auroral absorptions in the northern and southern auroral zones, preceding the occurrence of LS TIDs (station's symbol explained in Table 1).

The onset of geomagnetic activity during the substorm had a wide longitudinal extent, as inferred from the H-component magnetograms and magnetic K-indices for northern auroral stations. Thus, in the three hour interval (09-12 UT) before the onset of the substorm the K-index was 2 at College (257.0°E geom.) and 1 at Tixie Bay (191.7°E geom.), increasing to 6 and 8 respectively at these stations in the following time interval (12-15 UT). Figure 2 shows the H-component magnetograms obtained on 9 November 1979 at a number of Alaskan stations (S-Sachs Harbor, CP-Cape Perry, I-Inuvik, AV-Arctic Village, F-Fort Yukon, C-College and TL-Talkeetna), in the Siberian sector (TB-Tixie Bay) and in the southern auroral zone (M-Macquarie Island). It is evident that the period before the onset of a geomagnetic substorm was quiet; the rapid onset of a negative magnetic bay started at lower latitude stations (TL, C and F) and moved polewards, decreasing rapidly between the invariant latitudes 71.0°-74.4°N. The negative swing in the H-component exceeded 500 nT for most of the stations, reaching 1400 nT at Fort Yukon. There was a sharp onset of a negative bay at Tixie Bay, reaching 500 nT at 1416 UT; it is evident that almost a simultaneous auroral electrojet was established in the northern auroral zone, exceeding 60° in geomagnetic latitude. In the Southern Hemisphere (Macquarie Island) a sharp onset of geomagnetic disturbance resulted in a negative magnetic bay reaching its maximum deviation of 400 nT at 1420 UT (K-index for this station changed from 2 at 09-12 UT to 6 at 12-15 UT) It is evident that the geomagnetic storm onset had a large geographical extent and was almost simultaneous at the northern and southern stations. Both riometer and magnetometer records indicate that the substorm commenced at lower auroral latitudes and subsequently shifted polewards.

The onset of the geomagnetic substorm preceded the occurrences of sequentially shifted periodic waves in the ionosphere, inferred from the variations in h'F at the northern (Japanese) and southern (Australian) stations, during night-time (at about 00-05 LT). Figure 3 shows that the wave-like formations simultaneously developed in the Southern and Northern Hemispheres, propagating towards the equator. The periodic structure is not so well defined for higher latitude stations in the south (Hobart and Canberra) but becomes pronounced for mid-latitude stations, between about 25° to 35° geomagnetic latitude (north and south). The second peak in the wave was of a smaller amplitude than the first one and decreased rapidly as the disturbance propagated equatorwards, totally disappearing in Okinawa,

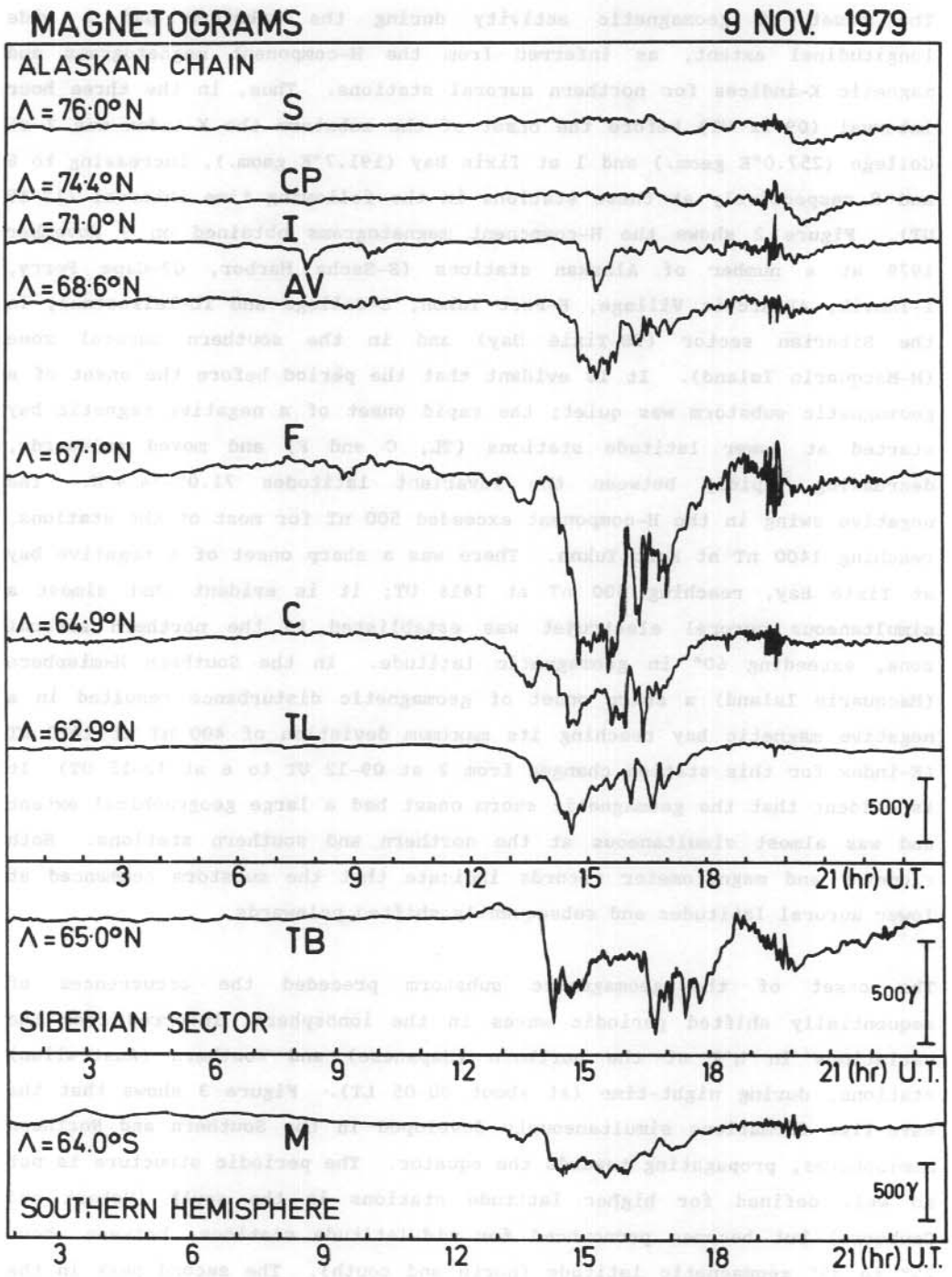

Figure 2. H-component magnetograms obtained on 9 November 1979.

and to a lesser extent in Vanimo. The waves appear to be of a non-dispersive type, with a constant period of one hundred and thirty-five minutes in both hemispheres. The period is within the range of periods (thirty minutes to three hours) characteristic of LS TIDs (Hunsucker 1982).

The waves appear to have fronts with large horizontal extents as can be inferred from the variations of h'F at two more stations: Maui (MA; = 20.5°, Hawaii Islands) and Norfolk Island (N; = 35.0°N, Southern Pacific). It can be seen that a close similarity exists between the waves for the pairs of stations: Brisbane-Norfolk Island and Yamagawa-Maui, each pair having almost the same invariant latitude. It follows, from the longitudinal separation of the stations in each pair (Table 1), that the wavefronts were aligned along constant invariant latitudes, extending in the east-west direction at least 1600 km in the Southern Hemisphere and 7000 km in the Northern Hemisphere. These wide longitudinal extents are consistent with the extent of the auroral electrojet, recorded after the onset of the substorm (Figures 1 and 2).

The horizontal velocity of the waves was obtained from the linear extrapolation of the time delay (Δt) between the position of the first peak h'F (indicated by the arrow) for the polewards most stations (i.e. Hobart and Wakkanai) and the corresponding positions for the subsequent stations (Figure 4). Linear regression analysis (with the correlation coefficients r = 1.00 - south, and r = 0.98 - north - yielded velocities of 810 ms^{-1} and 790 ms^{-1} in the Southern and Northern Hemispheres respectively. The analysis also indicates that the points of the origin of LS TIDs (i.e. the geographic latitudes for which Δt = 0) were located at the shells with L-value 4.4 and 4.6 in the southern and northern auroral zones. This is in agreement with the positions of the particle precipitation belts which were located equatorwards of both auroral zones, at the shells with L-value between 4 and 5 (Figure 1).

There appears to be a close relation between the occurrence of the first absorption peak at Campbell Island at 1420 UT and the subsequent occurrence of the peak of LS TID at 1445 UT at Hobart (Figures 1 and 3). During that time, the peak of LS TID would have travelled a distance of 1215 km (with a velocity of 810 ms^{-1}). It follows that the source location, at which LS TID was generated, was slightly equatorwards of Macquarie Island (as the

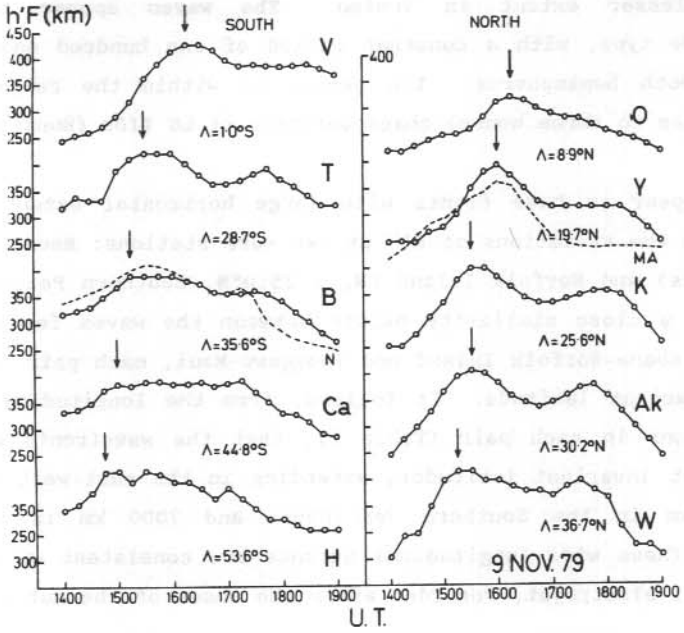

Figure 3. The periodic variations in the virtual height (h'F) of the F-region, following the onsets of the substorm in the Southern and Northern Hemispheres. Dotted lines refer to the variations in h'F at Maui (MA) and Norfolk Island (N).

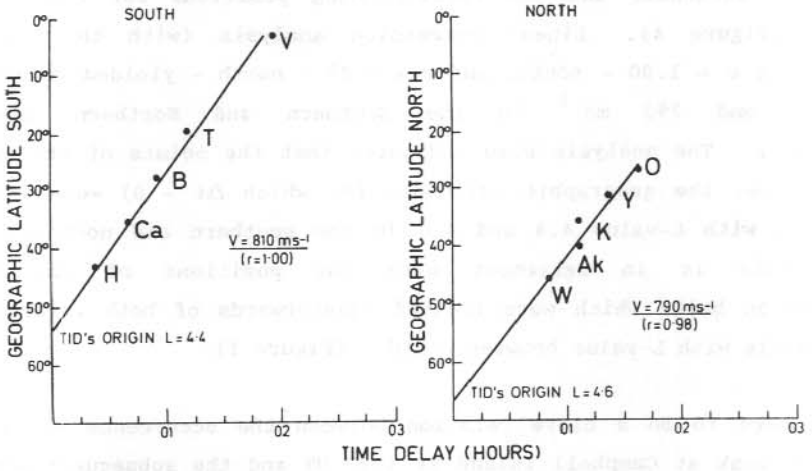

Figure 4. The velocities and the latitudinal positions of the auroral sources of LS TIDs, derived from the linear regression analysis (station's symbols explained in Table 1). The assumed commencements of LS TIDs were at 1420 UT and 1416 UT in the southern and northern auroral zones respectively.

distance: Macquarie Island - Hobart is 1280 km, Table 1). A similar computation for the northern hemisphere would indicate that the source location is 2417 km polewards of Wakkanai, assuming that the time of generation of LS TID coincided with the occurence of an absorption peak at 1424 UT at Anchorage. This would give the location of the source well equatorwards of the northern auroral zone. The earlier occurences of the peak in the negative bay H-component magnetogram at Tixie Bay at 1416 UT gives a location of the source which is more consistent with the source position in the southern auroral zone, since the source would be then located 2840 km polewards of Wakkanai and slightly equatorwards of Tixie Bay. The second time of commencement of LS TID is also more appropriate because Tixie Bay is located in the same longitudinal sector as the Japanese sounding stations.

It follows that the LS TIDs source locations are between L-values of 4 and 5 in both hemispheres as found from three independent observations:

1. linear extrapolations of the source positions (Figure 4),
2. the position of auroral particle precipitation and the location of auroral electrojet, and
3. the onset times of the first maximum in auroral disturbances followed by subsequent enhancements in h'F for the polewards most stations.

It is of a considerable interest that both Townsville and Kokubunji, which are located at similar distances from the auroral sources (Table 1), have also approximately the same extrapolated time delay ($\Delta t \sim 70$ minutes), as measured from the above defined times of auroral disturbances. In addition, the waves recorded at these stations are very similar (Figure 3). This would indicate that the disturbances would travel with the same horizontal velocity and are likely to reinforce the amplitude of LS TIDs at the point of their encounter, near the equator. A constructive interference can then produce a substantial height rise in the low latitude virtual height (h'F), exceeding that of the mid-latitude stations.

18.3 CONCLUSIONS

The present results indicate that rapid onsets in the auroral particle precipitation, at the time of commencements of the intense geomagnetic substorms in the northern and southern auroral zones can be associated with

a simultaneous launching of periodic LS TIDs, propagating equatorwards in both hemispheres. The wavefronts of LS TIDs had large longitudinal extents along constant invariant latitudes, exceeding 1600 km and 7000 km in the Southern and Northern Hemispheres respectively. The horizontal velocity of the wave peak was about 800 ms^{-1}, and the period was constant at 135 minutes. Since the waves propagated with almost the same velocity in both hemispheres, LS TIDs were found to be in phase at the stations, Townsville and Kokubunji, which are equidistant from the southern and northern auroral sources. The implication of this is that the waves can produce a constructive interference at the points of encounter, near the equator. This could lead to a substantial virtual height (h'F) rise in the equatorial region, exceeding that at higher latitudes.

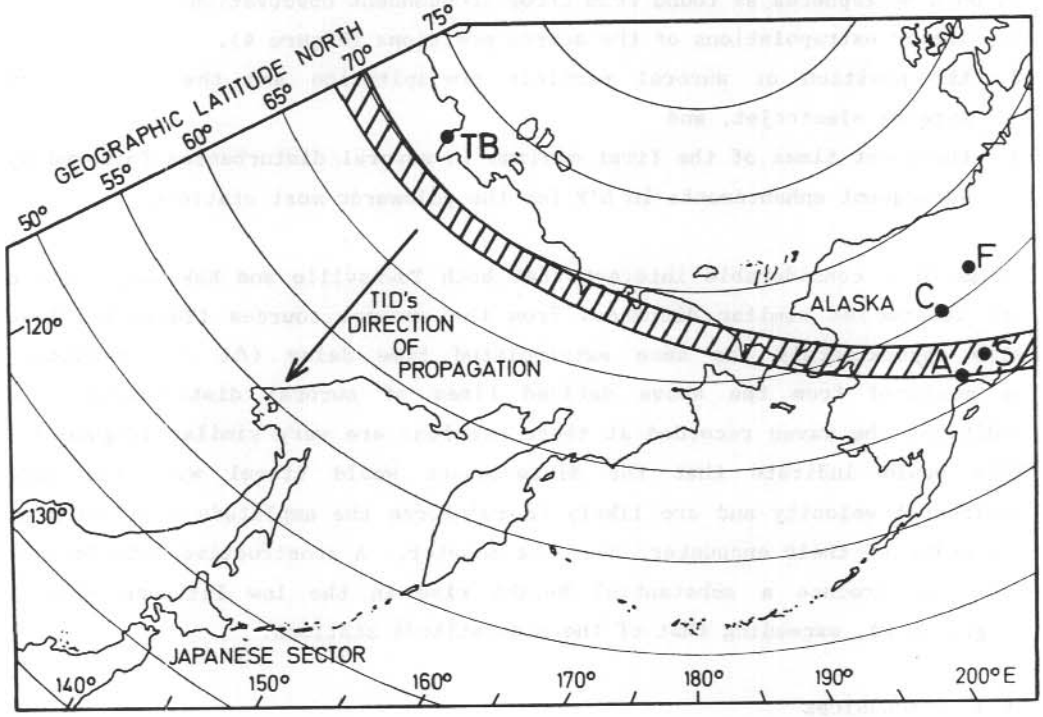

Figure 5. The auroral source location (shaded area) of LS TID, in the Northern Hemisphere, inferred from the geomagnetic and ionospheric data of the substorm on 9 November 1979.

ACKNOWLEDGMENTS

The ionosonde data were supplied by the Ionospheric Prediction Service (IPS), Sydney, Australia and by the Radio Research Laboratories, Ministry of Posts and Telecommunications, Tokyo, Japan. The riometer data were made available by the Antarctic Division of the Department of Science, Australia, The World Data Center A, Boulder, Colorado, U.S.A., and by the Department of Scientific and Industrial Research, New Zealand. The magnetometer data were supplied by the Bureau of Mineral Resources, Geology and Geophysics, Canberra, Australia and by the Geophysical Institute, University of Alaska, U.S.A. The authors are grateful to Mrs D.J. Dearden for her assistance with the data analysis. This material is based upon work supported by the Aeronomy Program of the Division of Atmospheric Sciences of the National Science Foundation under Grant ATM-8316713.

18.4 REFERENCES

Davis, M.J. (1971). On polar substorms as the source of large-scale travelling ionospheric disturbances. Journal of Geophysical Research 76:4525-4533.

Hajkowicz, L.A. (1983a). Auroral riometer absorptions and the F-region disturbances observed over a wide range of latitudes. Journal of Atmospheric and Terrestrial Physics 45:175-179.

Hajkowicz, L.A. (1983b). Conjugate effects in the generation of travelling ionospheric disturbances (TIDs) in the F-region. Planetary and Space Science 31:1409-1413.

Hajkowicz, L.A. and Hunsucker, R.D. (1985). The conjugate source location of large-scale TIDs. Ionospheric Research Section Report Number 12. Department of Physics, University of Queensland, Australia.

Hunsucker, R.D. (1982). Atmospheric gravity waves generated in the high-latitude ionosphere: A review. Reviews of Geophysics and Space Physics 20:293-313.

19. STUDIES OF IONOSPHERIC IRREGULARITIES AROUND L=4 IN THE SOUTHERN HEMISPHERE USING SATELLITE BEACONS

M. Lambert (1) and E.A. Essex (2)

(1) Antarctic Division
Department of Science
Kingston, Tas., Australia, 7150.

(2) Department of Physics
La Trobe University
Bundoora, Vic., Australia, 3083.

ABSTRACT

From 28 December 1983 to 10 March 1985 total electron content (TEC) data were gathered from Macquarie Island (54.5°S, 158.9°E geographic) in the southern auroral zone using the Faraday rotation technique. The beacons on the geostationary satellites ATS-1 and ETS-2 transmitting on 137.35 MHz and 136.112 MHz were used. Preliminary analysis of the data indicates that large scale fluctuations in the TEC occur which are associated with auroral activity. Some of these disturbances propagate towards the mid latitudes with speeds of from 200 to 1000 ms^{-1}. Large scale rapid decreases in TEC were observed during the evening hours on about one third of the September equinox days studied. These decreases occurred at a geomagnetic latitude assumed 60°S and could be associated with the main ionospheric trough travelling through the ray path from the satellite to the receiving station.

19.1 INTRODUCTION

Total electron content (TEC) studies of the auroral ionosphere using geostationary satellites have been limited by either the low elevation angle to the satellite or the lack of a land-based station, particularly in the Southern Hemisphere. Macquarie Island is the most favourable location in the Southern Hemisphere for TEC studies as it has geomagnetic and geographic latitudes of 65°S and 54.5°S respectively (see Figure 1).

From 28 December 1983 to 10 March 1985 TEC data were gathered from Macquarie Island (54.5°S, 158.9°E geographic) using the Faraday rotation technique.

TEC data were also available for Beveridge (37.3°S, 144.6°E geographic) for this period. Some preliminary results and conclusions are presented below.

19.2 EXPERIMENTAL DETAILS AND RESULTS

The 136.112 MHz beacon signal for the geostationary satellite ETS-2 located at 130°E was used in this study. During equinoxes when the ETS-2 was switched off, the beacon signal on 137.35 MHz from the geostationary satellite ATS-1 located at 166°E was used. Although ATS-1 had a higher elevation of 28° average from Macquarie Island when compared to the 20° for ETS-2, ATS-1 had a large inclination of 11°. In the preliminary analysis presented here, the correction for this large inclination has not been made. The correction, ranging from 0 to approximately ± 10% over a day, does not affect the interpretation of the gross features in the TEC variation.

The TEC baseline is obtained from the f_oF_2 data for the Macquarie Island and Hobart ionosondes (see Figure 1) (Smith 1971). A preliminary analysis indicates that, for fifty autumn equinox days, the average nighttime minima is of the order of 25×10^{15} em^{-2}.

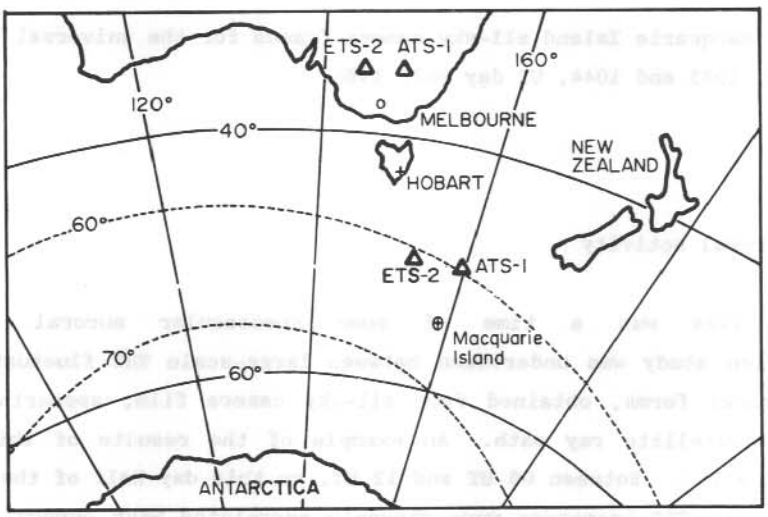

Figure 1. Location map showing Faraday rotation monitoring station (0), ionosondes (+), average satellite/station sub-ionospheric points (Δ) and geomagnetic latitudes (dashed lines).

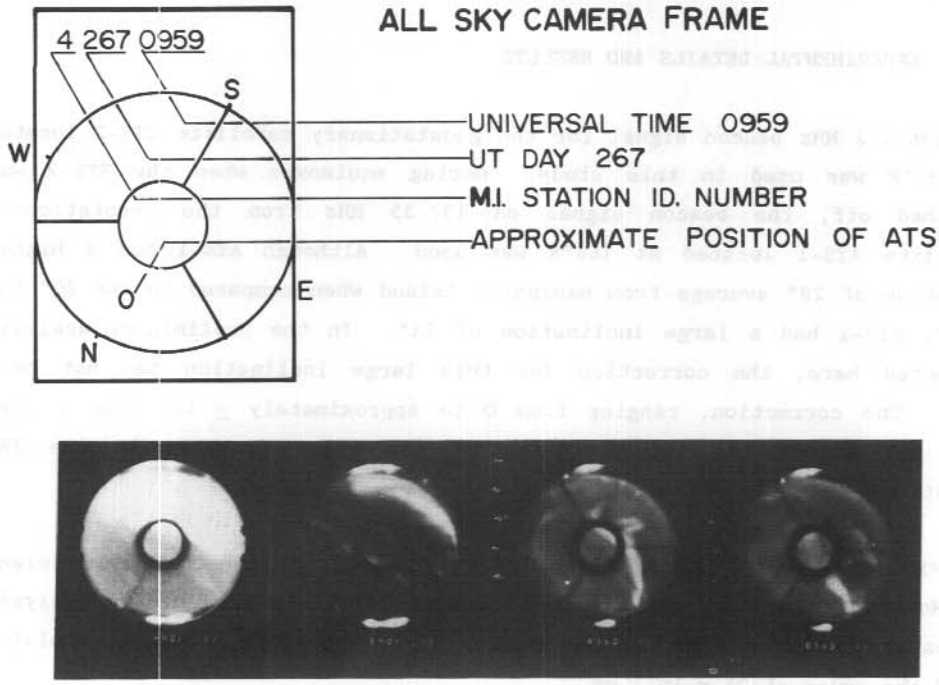

Figure 2. Macquarie Island all-sky camera frames for the universal times; 0958, 0959, 1043 and 1044, UT day 267, 1984.

19.2.1 Auroral activity

September 1984 was a time of some spectacular auroral displays. A correlation study was undertaken between large-scale TEC fluctuations and bright auroral forms, obtained from all-sky camera film, appearing in the station to satellite ray path. An example of the results of this day is that for day 267. Between 08 UT and 12 UT, on this day half of the fourteen observed rapid TEC increases were strongly correlated with auroral activity (Figures 2 and 3). Increases in the nighttime TEC of up to 60% in the space of a few minutes have been observed. Nights of continuing auroral activity show elevated nighttime TEC for several hours (Figure 4).

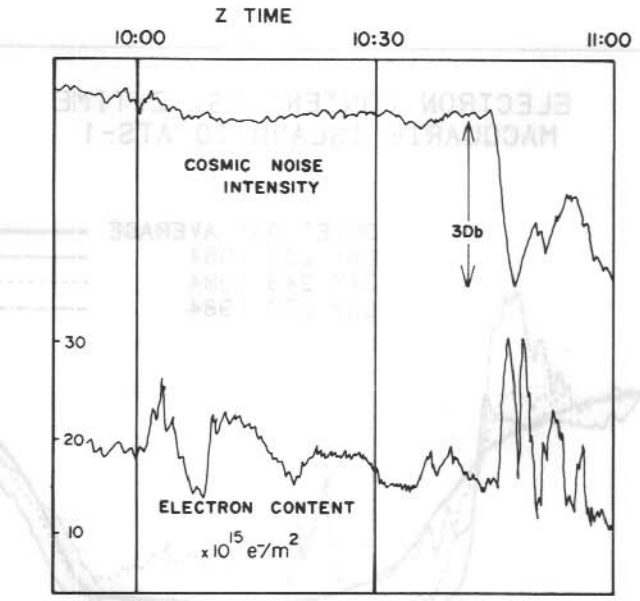

Figure 3. Cosmic noise intensity from a standard riometer at Macquarie Island and the TEC fluctuations from Macquarie Island to ATS-1 for the UT day 267, 1984. TEC fluctuations around 1000 UT correspond to northward travelling auroral forms. The cosmic noise absorption event and TEC fluctuations around 1045 UT correspond to the sudden appearance of a bright auroral form in the northern sky.

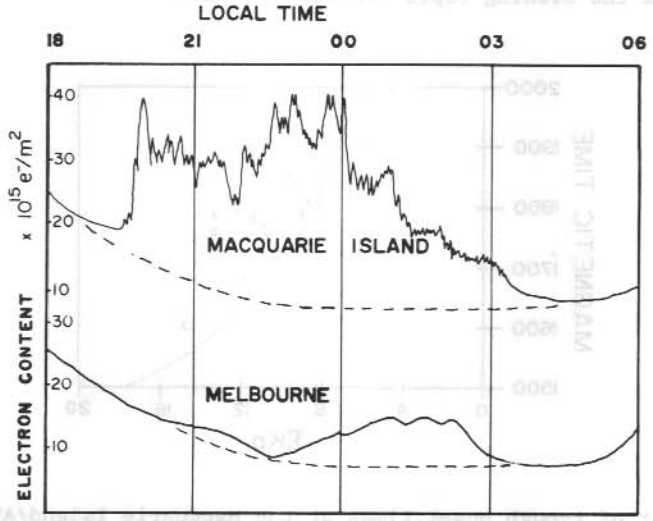

Figure 4. Large-scale ionospheric TEC fluctuations as seen from Macquarie Island and Beveridge to ATS-1 during the days 263, and 264, 1984.

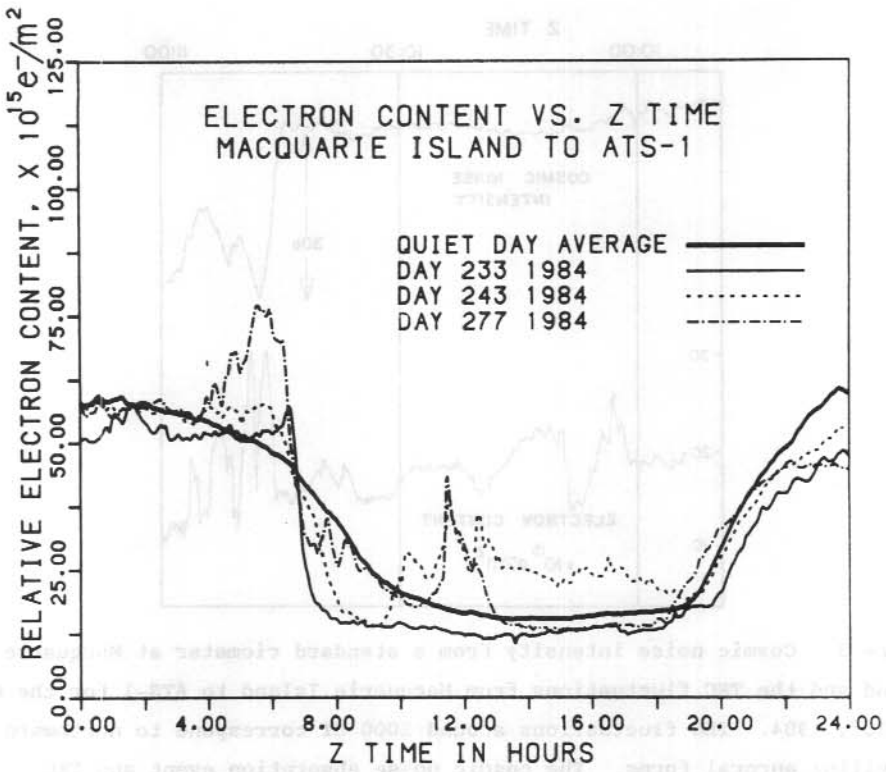

Figure 5. Daily TEC plots showing an average of eight quiet days plus three days which show the evening rapid decrease in TEC.

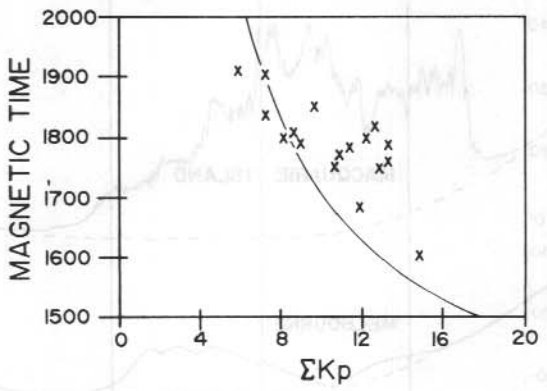

Figure 6. Plot of trough onset times at the Macquarie Island/ATS-1 ionospheric point against the sum of three Kp indices. Also shown is the curve fitted by Bowman (1969) to similar data from Ellsworth.

19.2.2 TID's

A study was made of the large scale nighttime TEC fluctuations observed from Macquarie Island for sixty days around the 1984 spring equinox to determine if these disturbances propagated through the Beveridge ionospheric points, 2000 km to the NW. Large nighttime TEC increases were observed from Macquarie Island on more than half of the nights studied but only ten cases of reasonable correlation with Beveridge TEC were observed (Figure 4). The speeds of the disturbances were from 200 to 1000 ms^{-1}. With a two-station monitoring system it is not possible to determine whether this spread in velocities is due to differences in the TID angle of propagation or due to a true reflection of the TID velocity distribution. The speeds and origins of these disturbances are consistent with those of the disturbances studied by Thome (1968). The small number of correlated events reported in our study may be evidence of a strong damping mechanism in the ionosphere or that the TID's tend to travel in directions other than NW.

19.2.3 Trough features

Sharp depletions in TEC during the evening have been observed and are thought to be evidence of the equatorial edge of the main ionospheric trough which can occur between the geomagnetic latitudes of 55°S and 70°S (Bowman) (Figure 5). These decreases occurred on about one third of the fifty-five spring equinox days studied and are often preceded by a ridge or a relative increase in the TEC. The magnitude of these rapid decreases in TEC can be as high as 1.3×10^{15} em^{-2} min^{-1} compared with the normal evening decays of 0.14×10^{15} em^{-2} min^{-1}. During the 'quiet' days shown in Figure 5, it is possible that either the trough is not as pronounced or does not travel through the ionospheric point being monitored. The trough onset time was found to be best correlated with the sum of the three Kp indices during the local daytime immediately before the trough was detected. A similar relationship was found by Bowman (1969) for Ellsworth (62.6°S, geomagnetic) (Figure 6).

19.3 DISCUSSION

Initial analysis of the TEC data gathered from Macquarie Island has shown some interesting effects due to auroras, TID's and the main ionospheric

trough. It is suggested that in future studies, a narrow angle photometer and directional riometer, both directed at the satellite being monitored, be deployed at Macquarie Island. These would provide more information on the electron-ion production and recombination rates and mechanisms. Also, a two station network around the auroral zone should be deployed to determine whether the large-scale TEC enhancements travel westward, as indicated by the observations of Weber et al. (1985) in the northern auroral zone. It would appear from the observations presented here, that large-scale TEC disturbances in the southern auroral region do not always produce TID's which travel large distances toward the equator.

Further work to be undertaken on the TEC data base for Macquarie Island include the study of medium scale TID's and their cut-off period from which the scale height may be calculated (Titheridge 1971), comparison of the seasonal and solar cycle variation with the ionospheric model for the region, and a comparison with Northern Hemisphere data from around L=4.

ACKNOWLEDGMENTS

Most of the experimental work towards this paper was done at the Australian National Antarctic Research Expedition's station on Macquarie Island. The research was supported by the Antarctic Division of the Department of Science and the Division of Theoretical and Space Physics at LaTrobe University. The authors would like to thank Gary Burns and David Rasch for their technical support, and the Ionospheric Prediction Service for the use of their ionosonde data.

19.4 REFERENCES

Bowman, G.G. (1969). Ionisation troughs below the F2-layer maximum. Planetary and Space Science 17:777-796.

Smith, D.H. (1971). Removal of the nπ ambiguity in observations of total electron content. Journal of Atmospheric and Terrestrial Physics 33: 1161-1168.

Thome, G. (1968). Long-period waves generated in the polar ionosphere during the onset of magnetic storms. Journal of Geophysical Research 73:6319-6336.

Titheridge, J.E. (1971). The spectrum of electron content fluctuations in the ionosphere. Planetary and Space Science 19:1593-1608.

Weber, E.J., Tsunoda, R.T., Buchau, J., Sheehan, R.E., Strickland, D.J., Whiting, W. and Moore, J.G. (1985). Coordinated measurements of auroral zone plasma enhancements. Journal of Geophysical Research 90:6497-6513.

20. THE ROLE OF THE ANTARCTIC IN INTERNATIONAL UPPER ATMOSPHERE PROGRAMS

K.D. Cole*
Department of Physics
La Trobe University
Bundoora, Vic., Australia, 3083.

ABSTRACT

A brief outline of the importance of upper atmosphere physics research in Antarctica is given. This is followed by short descriptions of the programs of the Scientific Committee on Solar-Terrestrial Physics and the opportunities for Australian Antarctic input. Spin-offs from the research are highlighted.

20.1 INTRODUCTION

There are several general considerations which provide the basis for doing research in upper atmosphere physics in Antarctica.

Firstly, it is possible to run the globe of the earth so that virtually all that is seen is Antarctica, Australia, New Zealand, Oceania and oceans. This means that in any truly global geophysical program, the Antarctic must play a prominent role.

Secondly, the geomagnetic pole which is offset from the rotation pole is tilted greatly towards Australia. This has two important consequences:

1. that phenomena in the upper atmosphere associated with the aurora frequently affect upper atmosphere phenomena over Australia. This applies particularly to ionospheric and magnetospheric ones.
2. that the separation of effects in the upper atmosphere related to solar zenith angle and those associated with magnetic latitude and longitude can be more clearly determined in Antarctica than in the Arctic.

* Immediate past-President of the Scientific Committee on Solar-Terrestrial Physics.

Thirdly, the clear asymmetries of the upper atmosphere and magnetic fields between the Northern and Southern Hemisphere make the appearance of many phenomena significantly different in the two hemispheres.

Fourthly, the potential for international cooperation is enhanced locally in Antarctica because of the multinational interest in the region. Japan has probably the best developed upper atmosphere physics program in Antarctica, while USSR does much such research in the Australian sector and USA and UK have very strong Antarctic upper atmosphere programs.

20.2 INTERNATIONAL PROGRAMS

Though the Scientific Committee on Antarctic Research (SCAR) coordinated some aspects of Antarctic upper atmosphere research, there are now and will be in the future, international interdisciplinary research programs conducted by the Scientific Committee on Solar-Terrestrial Physics (SCOSTEP) which upper atmosphere physics programs in Antarctica could not only contribute to, but also derive much benefit from. SCAR is represented in SCOSTEP. Both are scientific committees of the International Council of Scientific Unions (ICSU).

Two SCOSTEP programs are currently in place:

20.2.1 Middle Atmosphere Cooperation (MAC)

MAC is a follow-on to the previous Middle Atmosphere Program (MAP) - a study of the earth's atmosphere from 10 - 110 km altitude. This region is of fundamental importance in atmospheric physics

1. because it contains the ozone layer,
2. it controls the circulation of numerous minor but important atmospheric constituents (This is now important in understanding dispersal of volcanic effusions and radio-active pollutants released or injected into the stratosphere.) and
3. it is the region of transmissal of energy between the troposphere (where the weather is) and the thermosphere (which contains the ionosphere), see Figure 1.

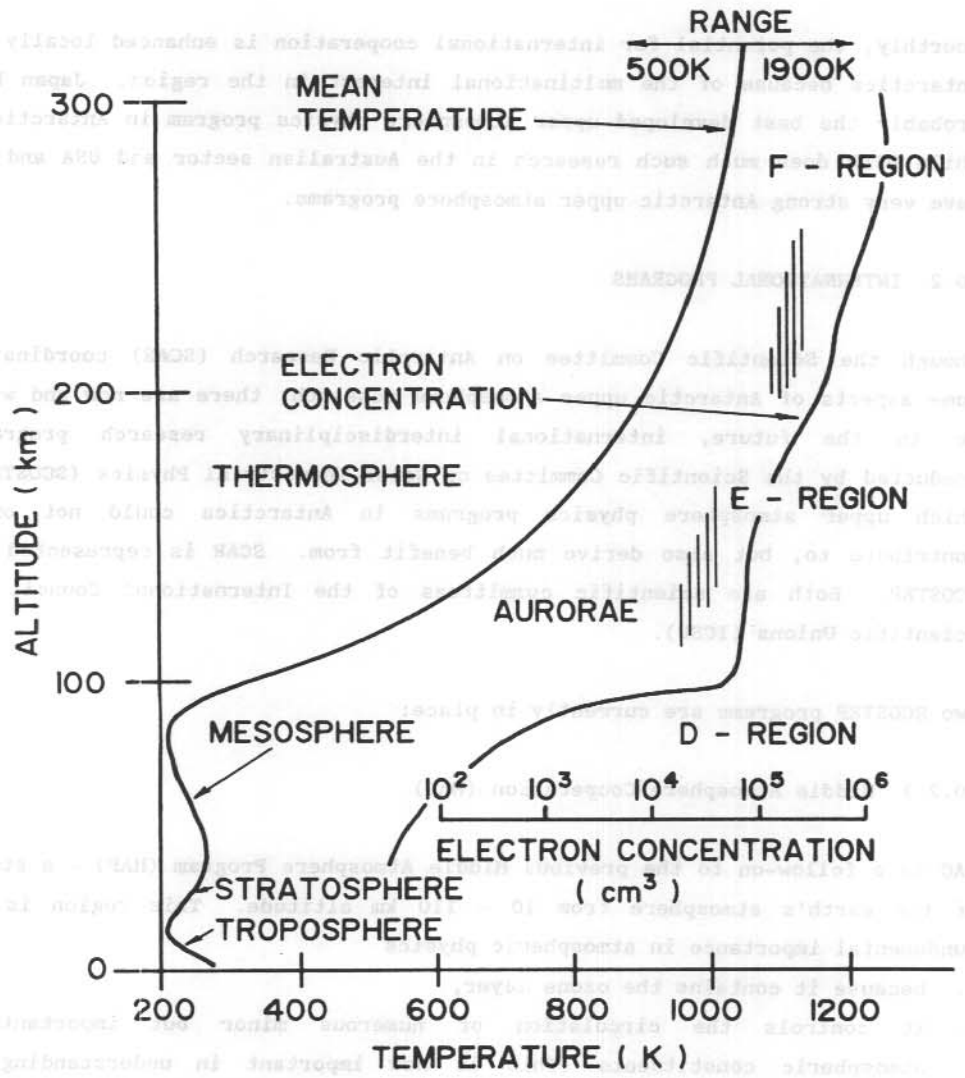

Figure 1. Regions of the earth's atmosphere.

Four important problems of middle atmosphere physics are the general circulation there, the irregular dynamical structure of it, its minor chemical and dust constituents and its ionised gas component. The Antarctic is of special importance because of the general factors mentioned in the introduction. [The role of the Antarctic middle and upper atmosphere in the general scheme of the earth's middle and upper atmosphere is something unique to which Australian scientists can contribute understanding, given the opportunity.]

20.2.2 Polar Auroral Dynamics (PAD)

This is a three year study of the aurora employing satellites, rockets, balloons and ground-based techniques. At work above the aurora is an acceleration process which causes energetic electrons to bombard the atmosphere to produce the phenomenon. Satellite instruments can now measure many details of the parameters of this accelerator but need support of ground-based observations of the aurora for their full interpretation.

Opportunities exist in Antarctica either to make simultaneous ground-based measurements of the aurora when satellites are passing overhead or when they are passing over the conjugate point in the Northern Hemisphere. The conjugate point is the location at the opposite hemisphere of the magnetic field line which goes through the observer.

Conveniently the conjugate point of Mawson is in Scandinavia where numerous upper atmospheric facilities exist.

The physics of the aurora involves fundamental plasma physics and nature has created conditions in space for the production of many plasma phenomena which simply cannot be produced on earth. Nature compensates for our lack of control over these plasma phenomena by its ability to faithfully reproduce them time and time again. Thus 'space' plasma physics is now making most significant and fundamental contributions to this subject.

[Plasma physics is a basic subject in the understanding of approaches to the control of thermo-nuclear fusion. It is of interest to note that the

energy sources in the aurora are of power about equal to all that used on earth by man.]

Two new programs of SCOSTEP have been introduced and will commence in July 1987. These are now described.

20.2.3 World Ionosphere/Thermosphere Study (WITS)

This is a three year study of the ionised component of the upper atmosphere and its relation to solar interplanetary magnetospheric and atmospheric processes. The ionosphere of course is the layer of ionised gas in the upper atmosphere responsible for the reflection of short radio waves. Communication via the ionosphere is now big business, important not only in commerce but also in defence (e.g. as in the Jindalee 'over-the-horizon' radar system).

Never before has there been such a study on a global basis and it will involve over thirty-five nations and several thousand scientists and technologists.

There are two major areas of research in the WITS program:

1. Global Ionosphere/Thermosphere Dynamics

Under this heading come many inter-related studies including inputs of energy from the sun (via EUV radiation), from the solar wind (via polar electrodynamic processes), from the magnetosphere generally (by energetic particles), from the lower atmosphere (via tides, planetary scale and acoustic gravity waves), and from meteorites. Also included are the dynamic and aeronomical interactions between ionized and neutral species in the region. These studies should incorporate the asymmetries of the geomagnetic field vis a vis the asymmetries of the thermosphere and atmosphere generally.

2. Ionospheric Irregularities

Ionospheric inhomogeneities are created in a wide range of temporal and spatial scales. These include field-aligned irregularities in equatorial

and polar regions, irregularities caused by acoustic gravity waves (e.g. TIDs), hydromagnetic waves and a variety of plasma instabilities. The source of energy and the conditions and mechanisms of formation and their differing manifestations in different parts of the globe need further elucidation.

It is important to note that WITS provides opportunities for participation at different technological levels for all countries of the world. Many WITS projects can be accomplished only with performance of experiments in developing countries. This applies particularly to equatorial and Southern Hemisphere regions.

Clearly the Antarctic should play an important role in WITS again because of the general reasons given in the introduction which highlight the great difference between the Arctic and the Antarctic. Having a fullsome WITS program at Australian Antarctic stations would be important for understanding ionospheric and upper atmospheric behaviour over Australia. Ionospheric and thermospheric variations over Australia are caused not only by localised processes but also by disturbances coming from the Antarctic auroral zone. These include winds, waves, and electric fields and currents. Some of these effects also occur in the space into which the Jindalee 'over-the-horizon' radar 'looks'.

Spin-offs from the WITS program will be new developments, amongst other things, in (i) global communications systems, (ii) understanding of the couplings of the ionosphere to the atmosphere and the space above (known as the magnetosphere), (iii) mineral exploration, some aspects of which rely upon the understanding of ionospheric and magnetospheric electric currents, (iv) navigation, (v) transmission of time and frequency standards, (vi) prediction and forecasting of optimal communication frequencies, (vii) HF remote sensing, (viii) VHF and S band remote sensing, (ix) radio astronomy, (x) plasma physics.

The WITS program will draw upon observations of approximately ten satellites and will employ a range of ground-based systems using about a dozen different techniques.

The organisers of the WITS program identify Antarctica as one of the important regions in which special effort is required. The returns to Australian science from a soundly based Australian Antarctic WITS program combined with a campaign also in Australia would be quite significant.

20.2.4 Solar-Interplanetary Variability (SIV)

This program, to commence 1 July 1987, is proposed to last three years and to study the sun in its transition phase from between the minimum and the maximum phase of activity.

Though principally based upon solar and interplanetary observations, this program will have important consequences and opportunities for improving understanding of upper atmosphere processes in Antarctica and their relation to solar and interplanetary phenomena.

20.2.5 Solar-Terrestrial Energy Program (STEP)

It is intended that all of SCOSTEP's programs should lead up to a six year long program 1991-1996 (inclusive) called STEP to study the chain of processes linking solar phenomena with their results in the atmosphere of the earth. This program will concentrate on the electromagnetic, mechanical, plasma, and 'atomic-process' linkages between the various parts of the solar-terrestrial system. The outcomes of the PAD, MAC, WITS and SIV programs will be crucial in setting up STEP.

SCOSTEP is the international body within ICSU charged with conducting international, interdisciplinary programs in solar-terrestrial physics. Its bureau has representatives from the International Union of Radio Science, the International Union of Pure and Applied Physics, the International Association of Geomagnetism and Aeronomy, the International Association of Meteorology and Atmospheric Physics, and the Committee on Space Research.

Scientists interested in any of the above programs should contact the chairmen, listed below, of the various programs.

Middle Atmosphere Cooperation (MAC)

Prof. S.A. Bowhill
Department of Electrical
Engineering
University of Lowell
One University Avenue
LOWELL MA 01854 USA

Polar Auroral Dynamics (PAD)

Prof. H. Oya
Tohoku University
Sendai
JAPAN

World Ionosphere/Thermosphere Study (WITS)

Prof. K.D. Cole (Co-Chairman)
La Trobe University
BUNDOORA AUSTRALIA 3083

or

Prof. C.H. Liu (Co-Chairman)
Department of Electrical
Engineering
University of Illinois
1406 West Green Street
URBANA IL 61801 USA

Solar Interplanetary Variability (SIV)

Dr E.J. Smith
Jet Propulsion Laboratory
4800 Oak Grove Drive
PASADENA CA 91103 USA

Solar-Terrestrial Energy Programs (STEP)

Dr S. Shawhan (Co-Chairman)
NASA Headquarters, EE8
600 Independence Avenue, SW
WASHINGTON DC 20546 USA

or

Prof. V.A. Troitskaya (Co-Chairman)
Soviet Geophysical Committee
Molodezhnaya 3
MOSCOW B-296 USSR

21. DYNAMICS AND ENERGETICS OF THE UPPER ATMOSPHERE AT MAWSON - RECOMMENDATIONS FOR FUTURE WORK

F. Jacka (1) and R.A. Vincent (2)

(1) Mawson Institute for Antarctic Research

(2) Physics Department
University of Adelaide
Adelaide, S.A., Australia, 5000.

ABSTRACT

A brief summary of ideas about the dynamics of the upper atmosphere in high latitudes is presented along with references to the results of work at Mawson. Recommendations are made for continuation of work with the 'partial reflection drift' (PRD) radar and the Fabry-Perot spectrometer (FPS) at Mawson. For the longer term it is recommended that consideration be given to the construction and installation of an imaging FPS for use at Mawson, and transfer of the present FPS to Casey. Finally, if the opportunity arises with international collaboration, the installation of an incoherent scatter radar at Mawson should be given serious consideration.

21.1 INTRODUCTION

In the polar regions the dynamics of the thermosphere is dominated by the electric field which is generated by the interaction of the solar wind with the outer fringes of the earth's magnetic field, and which is mapped down along the magnetic field lines. This interaction is also responsible for the precipitation of energetic particles into the atmosphere, exciting the aurora and causing enhanced ionization and electric currents in the thermosphere, especially along the 'auroral oval'. The energetic particles and associated electric currents are important energy sources in the polar upper atmosphere.

Figure 1 illustrates the mean location of the auroral oval in geomagnetic invariant latitude - time coordinates. The pattern of particle precipitation and electric currents within the auroral oval varies hour by hour and the boundaries of the oval vary day by day. The broad features of the oval remain roughly constant as viewed from the sun, while the earth

rotates underneath it. The position of Mawson is shown in Figure 1 at 06, 12, 18 and 24 hours local magnetic time; it is almost ideally located to study the phenomena of the auroral oval.

Tracing the magnetic field lines outwards from the auroral oval brings one to the equatorial plane about 6-9 earth radii out - to the region of geostationary satellite orbits. It is suggested that any opportunities to study this region directly, especially to measure energetic particle fluxes, should be taken up. However, in the long term the conditions 6-9 earth radii out might more effectively be studied by ground based recording of particle fluxes precipitated into the atmosphere and through observations of the effects on the upper atmosphere of those particle fluxes and associated electric fields. Within a few decades accurate knowledge of the 'climate' to which satellites are exposed and even forecasts of the 'weather' there might well be of great practical and economic importance. Apart from its great intrinsic scientific interest the research advocated in this paper is directly relevant to this problem.

Because of the very different distributions of land in the Northern and Southern Hemispheres, and because of the different asymmetries of the magnetic field in the two hemispheres, the upper atmosphere in the Arctic and Antarctic behaves differently. The study of the differences is necessary for a full understanding of the dynamics and energetics of the whole system.

21.2 WHAT DRIVES THE WIND?

Throughout the atmosphere, pressure gradients are established through differential solar heating and radiative cooling. In the troposphere these pressure gradients, combined with the Coriolis force and viscous drag, are the dominant forces which drive the wind. Planetary waves and gravity waves are generated in the troposphere and, propagating upwards, they deposit momentum at higher levels. In the middle atmosphere this is a major contributor to the general circulation, (Phillips and Vincent - Chapters 7 and 8 of this volume) and even in the 200 - 300 km region there is evidence of significant effects of gravity waves (Wardill and Jacka 1986 and Chapter 12 of this volume).

In the thermosphere, especially at high latitudes, additional forces operate. The thermosphere is pervaded by the electric field which is generated by the interaction of the solar wind with the earth's magnetic field. This electric field, at thermospheric heights, drives the ionization which is produced by the action of short wave solar radiation; through collisions between the ions and neutral molecules, momentum is thus transferred to the wind. In the 200 - 300 km height region, where the dynamic viscosity is high and the collision frequency low, this driving force is in the direction perpendicular to the electric field (in the direction of E x B) (Wardill, Jones and Jacka - Chapter 10 of this volume and Jones, Wardill and Jacka - Chapter 11 of this volume). At 120 km, where the collision frequency is much higher, the direction of the driving force is intermediate between that of E x B and E. (Jones and Jacka - Chapter 13 of this volume). At lower levels, around 90-110 km, the effect of the electric field is certainly much weaker, but there is still some evidence of its influence (Phillips and Jacka - Chapter 9 of this volume).

21.3 RECOMMENDED FUTURE WORK

As a result of the work described in this volume and cited above, the dynamics of the upper atmosphere at Mawson is understood at least in broad and somewhat uncertain outline. However, much remains to be done to fill out the detail, to verify a number of tentative hypotheses and to integrate the Mawson results more adequately with the global picture. The achievement of these objectives necessitates further observations, more intensive study of the results and collaboration with colleagues internationally to relate our results to global circulation models, e.g. those from University College, London (Fuller-Rowell and Rees 1980) and from N.C.A.R., Boulder (Dickinson et al. 1981).

It is recommended that during the next five years, work should continue at Mawson with the PRD radar to study winds in the 60-110 km region and with the Fabry-Perot spectrometer to study winds and temperatures in the thermosphere - in the 85, 95 and 250 km regions.

Australia was a pioneer in these studies in Antarctica but others are now following. A PRD radar is operating at Scott Base and similar equipment is planned by Chile and by the United Kingdom at Halley. A Fabry-Perot

spectrometer is also installed at Halley. This wider coverage will assist greatly in the evolution of an understanding of the upper atmosphere.

In the longer term, to permit major advances in the study of thermospheric dynamics three new developments should be considered. The first is the construction and installation at Mawson of an imaging Fabry-Perot spectrometer (one possible design is described by Jacka 1984). This would permit much more detailed and rapid acquisition of data and, for the first time, make it possible to study the dynamics of the thermosphere in detail through the course of auroral sub-storms which are the dominant feature of that region. Detailed design and construction of the equipment should commence as soon as feasible and the work should be sub-contracted to local industry.

It is recommended that, when the present Fabry-Perot spectrometer is withdrawn from Mawson, it should be installed at Casey, along with a digital ionosonde (Dyson - Chapter 26 of this volume). At that site it can be used to measure neutral atmosphere winds and temperatures and in addition, the ion drift velocity - by observing the O^+ emission at a wavelength of 732 nm.

The third and major new development suggested for serious consideration is the installation, with international collaboration, of an incoherent scatter radar (IS radar) at Mawson. The possibility that such a radar might be located in the Antarctic has been discussed for a number of years but recently, V.B. Wickwar of the Radio Physics Laboratory of SRI International, U.S.A., acting on behalf of his colleagues in the radar community has stressed the need for at least one such facility in this region. A typical IS radar might operate near 500 MHz and transmit pulses with peak powers of several MW. With such powers it is possible to detect scatter from the ionosphere under favourable conditions from 60-600 km. Measurements can be made with height resolutions ranging from a few hundred metres up to tens of kilometres and with time resolutions of seconds or minutes. By steering the radar beam it is possible to view a large area. Amongst the quantities which can be measured are electron densities, electron and ion temperatures, ion composition, ion-neutral collision frequencies, plasma drift velocities, conductivities and ionization rates.

IS radars are not confined to ionospheric measurements as it has been shown that they can detect scatter from irregularities in the neutral atmosphere from near ground level up to heights of about 30 km, depending on frequency and power. Consequently, these radars are now also powerful tools for studies of the dynamics of the troposphere and lower stratosphere.

All existing IS radars are located in the Northern Hemisphere, except for one at Jicamarca (12°S) on the geomagnetic equator. A radar located in the Antarctic would enable simultaneous observations in different hemispheres and hence different seasons. The amount of scientific information which can be obtained would be maximized by locating the radar at a site magnetically conjugate to a Northern Hemisphere radar. Two sites stand out; they are the South Pole station which is approximately conjugate to the Sondrestrom radar in Greenland, and Mawson which is approximately conjugate to the European EISCAT radar in northern Scandinavia. The approximate field of view of an IS radar and of the Fabry-Perot spectrometer viewing the thermosphere and located at Mawson, is shown in relation to the auroral oval in Figure 1.

No other ground-based technique can compete with an IS radar for the breadth of scientific problems which can be tackled. A radar located at Mawson would have a major impact on magnetospheric and ionospheric as well as middle atmospheric research being carried out in Australia while providing a focus for upper atmosphere science on a global scale. The high costs involved in establishing and running such a radar would require international collaboration and funding but because of the benefits to Australian science it is suggested that any approach for the location of an incoherent scatter radar at Mawson should be encouraged.

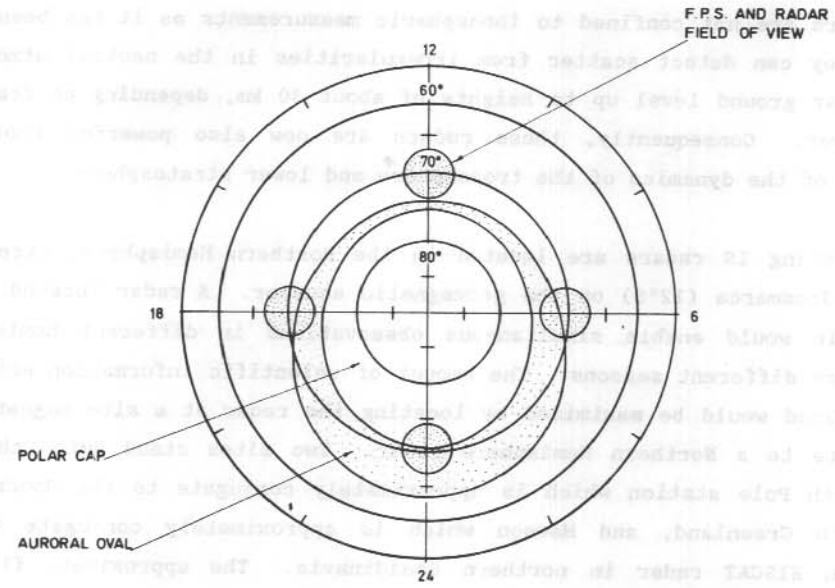

Figure 1. The mean location of the auroral oval in geomagnetic invariant latitude-time coordinates; Mawson is at 70°S. The approximate field of view of the Fabry-Perot spectrometer and of an incoherent scatter radar at Mawson is shown at 06, 12, 18 and 24 hours local magnetic time.

21.4 REFERENCES

Dickinson, R.E., Redley, E.C. and Roble, R.G. (1981). A three-dimensional general circulation model of the thermosphere. Journal of Geophysical Research 86:1499-1512.

Fuller-Rowell, T.J. and Rees, D. (1980). A three-dimensional time-dependant global model of the thermosphere. Journal of Atmospheric Science 37: 2545-2567.

Jacka, F. (1984). Application of Fabry-Perot spectrometers for measurement of upper atmosphere temperatures and winds. Middle Atmosphere Program - Handbook 13:19-40.

Wardill, P. and Jacka, F. (1986). Vertical motions in the thermosphere over Mawson, Antarctica. Journal of Atmospheric and Terrestrial Physics 48: 289-292.

22. A PROPOSAL FOR STUDY OF THE DYNAMICS, ENERGETICS AND CHEMISTRY OF THE STRATOSPHERE OVER MAWSON, ANTARCTICA

F. Jacka
Mawson Institute for Antarctic Research
University of Adelaide
Adelaide, S.A., Australia, 5000.

ABSTRACT

It is proposed that studies on the dynamics, energetics and chemistry of the stratosphere be initiated at Mawson using a lidar to measure density, temperature and wind velocity, and high resolution spectroscopic or lidar techniques to measure some of the chemically active minor constituents, especially ozone.

It is suggested that this work should be developed also as a contribution to the world-wide monitoring of long-term stratospheric changes, and to the study of sun-weather relationships.

22.1 INTRODUCTION

In broad terms this proposal is directed towards a better understanding of the physics of the middle atmosphere over Antarctica. More specifically it is proposed that work should begin as soon as feasible at Mawson to study:

1. The spatial structure and time variations of density, temperature and wind velocity in the atmosphere up to a height of 70 km, with particular reference to the perturbations caused by turbulence, gravity waves, planetary waves and tides in the stratosphere; for this purpose a lidar is proposed, the performance capabilities of which are discussed by Jacka and Argall - Chapter 23 of this volume.
2. The height and time variations in some of the more important chemically active minor constituents, including especially ozone, in the same height region.

22.2 DISCUSSION

The Middle Atmosphere Program (MAP) of the ICSU Scientific Committee on Solar Terrestrial Physics (SCOSTEP) has highlighted the importance, as judged by the international scientific community, of a better understanding of the atmosphere in the 10-100 km height range. Although considerable progress has been made in understanding the region below 30 km and above 60 km, the 30-60 km region has remained largely inaccessible to ground based observation.

Whilst satellite borne radiometers yielding temperature-height profiles give global coverage of the stratosphere they do not achieve particularly good temporal or height resolution. Routine meteorological balloon flights are limited to about 30 km and do not provide good temporal resolution. Radar techniques are limited to the regions below 30 km and above 60 km.

The lidar technique, based on the detection of incoherently back-scattered light pulses from a laser, holds great potential for detailed study of the dynamics of the atmosphere in the 30 km to 60 km height interval (cf. Chanin and Hauchecorne 1981).

Recent observations have demonstrated that there is considerable coupling between the various levels of the atmosphere. Gravity waves generated in the troposphere propagate through the stratosphere into the mesosphere where they dissipate and deposit energy and momentum, significantly modifying the mean circulation (cf. Holton 1983). Filtering of the waves also occurs, due for example to critical level interaction; a significant amount of the filtering occurs in the stratosphere - hence the importance of studying this region for a better understanding of the higher levels.

The mean circulation and the eddy motions in the middle atmosphere, derived mainly from the dissipation of planetary waves and gravity waves, are important in redistributing the chemically active minor constituents including ozone. Variations in ozone distribution modify absorption and heating and so affect the radiative forcing at other levels.

A better understanding of the dynamics and energetics of the middle atmosphere requires detailed data on the sources of gravity waves, the

spectra of their periods, horizontal and vertical wavelengths and phase speeds, and the energy and momentum fluxes transported by them.

While the H.F. 'partial reflection drift' radar at Mawson is excellent for studying the 70 - 110 km region, (see Phillips et al. - Chapters 7, 8, 9 of this volume) a lidar is certainly the most suitable equipment for studying the dynamics of the region below this; indeed it is uniquely suited for high resolution study of density perturbations and for investigating the characteristics of gravity waves, gravity wave-mean flow interactions and gravity wave-planetary wave interactions in the stratosphere. The possibility also exists to apply the lidar to the direct measurement of the vertical flux of horizontal momentum deposited by gravity waves and to the direct measurement of vorticity in the stratosphere. Data on aerosol content can also be obtained.

It is of interest to compare the tidal components of wind with current theory as developed for example by Forbes (1982). Although this treatment is broadly successful, the stratospheric data available for comparison with prediction are sparse; the lidar can provide the data required.

If combined with studies in the field of chemical aeronomy, this technique promises important contributions to the understanding of the spatial and temporal variations in the chemically active minor constituents. Conversely, study of the variations in these minor constituents will help in understanding the energetics and dynamics of the middle atmosphere.

The ozone content of the atmosphere controls the penetration of solar UV radiation to the Earth's surface while the vertical distribution of ozone controls the temperature structure in the stratosphere and may significantly influence climate. The temperature determines various chemical reaction rates, these in turn affecting the rates of production and destruction of ozone.

Other species involved in stratospheric ozone chemistry are chlorine and the chlorine oxide radical, water vapour and nitrogen oxides. The chlorine species have been predicted to increase steadily through the breakdown of chlorofluorocarbons of anthropogenic origin.

Aerosols, especially after major volcanic eruptions, may also be important in affecting some chemical reaction rates and through their influence on radiation transfer.

Of topical interest is the steady year by year decrease in stratospheric ozone content in the Spring amounting to about 30% in the past five years over central Antarctica but extending progressively towards mid latitudes. Whether the cause of this is essentially a dynamical process or a chemical process arising from anthropogenic disturbances or natural disturbances such as volcanic activity, cannot be assessed on present evidence. If it is basically anthropogenic it is potentially of enormous importance especially in relation to agricultural production in Australia and other southern continents.

It is recommended that investigations in the field of chemical aeronomy be initiated at Mawson, based on the application of higher resolution optical spectroscopic or lidar techniques for ground based remote sensing. Initially the principal constituent of interest would be ozone but others including chlorine and nitrogen compounds should be considered.

It is further suggested that this work should be developed not only to study the basic physics of the stratosphere, but also as a contribution to the world wide monitoring of long term changes in the stratosphere - see "Network for the Detection of Stratospheric Change", Report of the Workshop, Boulder, Colorado, March 5-7, 1986 (NASA Headquarters, Washington, D.C.).

Finally, as a further long term aim, the author proposes that attention should be directed towards the search for and explanation of the so-called sun-weather relationships. This might be linked with the study of atmospheric electric fields being developed by Prof. K.D. Cole of La Trobe University.

Speculation on mechanisms of sun-weather relationships include

1. chemical and subsequent energetic modifications of the stratosphere, for example through destruction of stratospheric ozone by nitric oxide which is produced indirectly by the action of energetic particles on molecular nitrogen, and
2. modification of the global electrical circuit (cf. Taylor 1986).

Both of these mechanisms involve modulation of energetic particle fluxes injected into the middle atmosphere as 'auroral' particles, solar protons or galactic cosmic rays; these particle fluxes are already recorded at Mawson. Taylor (1986) concludes that 'There can be no question that if it could be isolated and explained, evidence for external forcing of short-term variations in the dynamics of the lower atmosphere would represent a major scientific accomplishment' and 'it seems compelling to me that the question continue to be examined.'

22.3 REFERENCES

Chanin, M.-L. and Hauchecorne, A. (1981). Lidar observation of gravity and tidal waves in the stratosphere and mesosphere. Journal of Geophysical Research 86(C10):9715-9721.

Forbes, J.M. (1982). Atmospheric tides, 1, Model description and results for the solar diurnal component. Journal of Geophysical Research 87: 5222-5240.

Forbes, J.M. (1982). Atmospheric tides, 2, the solar and lunar semidiurnal components. Journal of Geophysical Research 87: 5241-5252.

Holton, J.R. (1983). The influence of gravity wave breaking on the general circulation of the middle atmosphere. Journal of Atmospheric Sciences 40:2497-2507.

Taylor, H.A. (1986). Selective factors in sun-weather research. Reviews of Geophysics 24:329-348.

23. A LIDAR SYSTEM FOR STRATOSPHERE STUDIES - PERFORMANCE SIMULATION

F. Jacka and P.S. Argall
Mawson Institute for Antarctic Research
University of Adelaide
Adelaide, S.A., Australia, 5000.

ABSTRACT

A brief description is presented of a lidar system which is currently under construction. This lidar will be used to study the structure and dynamics of the atmosphere in the height range 5 to 70 km; it's expected performance is discussed.

A copper vapour laser (λ=510.6 nm) with a time averaged power output of 8 watts and a pulse repetition rate of 2 kHz is used. A high speed rotating shutter permits the use of the same telescope with an objective diameter of 1 m, for both transmission and reception.

Initially back-scattered intensity as a function of height and azimuth (with a fixed zenith angle) will be recorded. At a later stage a dual, scanning Fabry-Perot spectrometer will be incorporated to record the spectral line profile of the back-scattered light.

The simulations presented here relate to determinations of density, temperature and wind from the back-scattered intensity; and wind and temperature from the line profile of the back-scattered light.

Attention is drawn to the importance of the lidar technique for application in the Antarctic, along with existing facilities, especially if it is combined with measurements on the active minor constituents of the stratosphere.

23.1 INTRODUCTION

This paper relates to a lidar system that is currently under construction and was designed to study the structure and dynamics of the atmosphere in the height range 5 - 70 km.

It is proposed to use the lidar in two different modes. The first involves the recording of back-scattered light intensity as a function of height and azimuth angle. This will allow the calculation of density and drift velocity - height profiles.

The second mode of operation will make use of a dual, scanning Fabry-Perot spectrometer to allow the measurement of the doppler shift and broadening of the back-scattered laser line profile. From these measurements wind velocity and perhaps temperature and aerosol concentration may be inferred.

An analysis of the performance of the lidar system has been carried out for each of these modes of operation. The results of these analyses will be presented.

23.2 DESCRIPTION OF THE SYSTEM

The construction of the lidar system is illustrated in Figure 1. A copper vapour laser was chosen because of its relatively high power/cost ratio and high pulse repetition frequency. The copper vapour laser, supplied by Quentron Optics Pty Ltd., emits two spectral lines - one in the green at 510 nm with time averaged power of about 8 watts, and one in the yellow at 578 nm of about 2 watts; the latter is not used. The pulse repetition frequency is 2 kHz; this limits the maximum sounding range of the lidar to 75 km. A lower pulse repetition frequency with the same time averaged power would increase the intensity of individual back-scattered pulses, causing increased difficulties in detecting the low intensity signal from the higher levels soon after the much more intense return from the low levels.

The light from the laser is reflected via a prism to a dichroic beam splitter which reflects only the 510 nm emission. The laser pulse is reflected from the mirrored face of the shutter. From there it passes to a pair of prisms which allow the telescope to be tilted and rotated about the axes shown.

The telescope may be tilted to a maximum zenith angle of 45° and may rotate continuously at speeds up to three revolutions per minute. The telescope is of Cassegrain design with a 1 m diameter primary. Both the primary and the

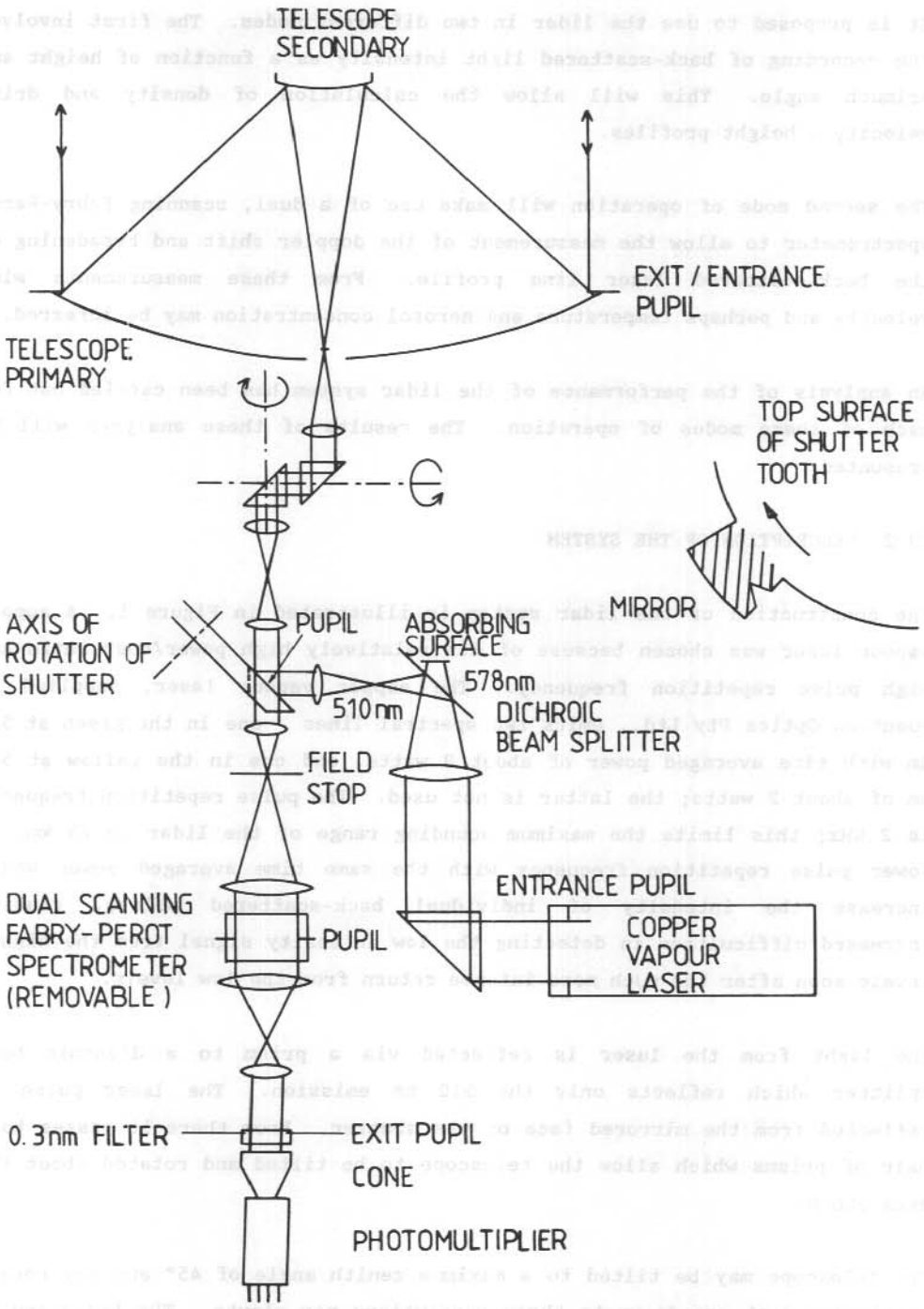

Figure 1. Schematic diagram of lidar.

secondary are made of aluminium. They were machined to the required shape before polishing.

Back-scattered light is collected with the same telescope. By the time a pulse has been scattered from a height of 5 km and returned to the instrument, the shutter will have begun to open and the light will pass into the detection optics. Below the shutter a dual scanning Fabry-Perot spectrometer (FPS) may be swung into the beam for operation when required. Below this a 0.3 nm bandpass filter selects the spectral region of interest. The light then passes to a photomultiplier tube; fast pulse counting circuitry will be used to record the output.

The shutter, illustrated in Figure 1 (insert), consists of a wheel 200 mm in diameter with six mirrored teeth and rotates at 20 000 revolutions per minute so that 2000 teeth per second pass any particular point. This is the same as the laser pulse repetition frequency which is synchronised to fire so that the light is reflected from a tooth. The trailing edge of the tooth form is shaped to serve as an attenuator. It cuts off all of the light back-scattered from below 5 km. Between 5 and 18 km it cuts off part of the light, the attenuation decreasing with time so that the amount of light reaching the photomultiplier remains fairly constant. Above 18 km the signal needs no attenuation. The shutter/attenuator will of course be calibrated.

23.3 SYSTEM PERFORMANCE

Initially it is proposed to use the lidar system without the FPS. This will be limited to night time when the 0.3 nm filter is sufficient to keep the background light at an acceptable level. Later, when the FPS is added it will be used as a very narrow bandwidth filter and will provide adequate rejection of scattered solar photons so that daytime observations will be possible.

The data recorded will consist of back-scattered intensity as a function of scattering height. It is not possible directly to calculate absolute densities from such intensity profiles because of uncertainties in equipment parameters, atmospheric transmittance and aerosol concentrations. However, by fitting the data to an assumed value at any level or to radiosonde data

Table 1. Estimates of precision of measurements of atmospheric density and wind velocity

Ht resolution	100 m		100 m		2 km		
Time resolution	1 hr		100 s		1 hr		
	$\frac{\sigma(\rho)}{\rho}$ x 100%		$\frac{\sigma(\rho)}{\rho}$ x 100%		$\frac{\sigma(V)}{V}$ x 100%		ms^{-1}
Height (km)	Night	Noon	Night	Noon	Night	Noon	Doppler
10	0.005	0.005	0.03	0.03	0.75	0.91	0.3
20	0.02	0.02	0.12	0.14	3.1	7.0	0.35
30	0.07	0.12	0.41	0.73	10.4		1.1
40	0.19	0.84	1.2	5.1	29.0		3.2
50	0.48	5.0	2.8				8.0
60	1.0		6.3				
70	2.4						

in say the 30 km region it will then be possible to derive the atmospheric density-height profile. Assuming the perfect gas equation and hydrostatic equilibrium one may then derive the temperature height profile.

It is also proposed to measure the wind velocity by using a method of moving pattern analysis similar to that of Meek and Manson (1983) which is a development from the work of Briggs (1968). This basically involves the 'tracking' of density perturbations caused by turbulence which is assumed to be carried with the wind. This mode of operation involves tilting the telescope and rotating it about a vertical axis so that the laser spot sweeps out a circle at each level of the atmosphere. Back-scattered photons will be collected for each of a number of height intervals and probably sixteen azimuth intervals. For each height interval the intensity of the back-scattered light as a function of time for each of sixteen azimuth

intervals will be recorded. Analysis of these sixteen time series will provide a set of transit velocities which will in turn be used to calculate the drift velocity of the moving pattern - that is the wind velocity.

If the 'high' frequency components of the time series are filtered out the 'drift' velocity so determined will be the phase velocity of gravity waves traversing the region.

By using a statistical analysis based on that of Freund and Jacka (1979) estimates have been made of the precision with which the density and wind velocity may be inferred. These estimates are presented in Table 1 and are calculated using the equations below and by making the conservative assumption of peak to peak density fluctuations of 0.2% due to turbulence.

$$\frac{\sigma(\rho)}{\rho} = \frac{\sqrt{L + S}}{L} \quad , \quad \frac{\sigma(V)}{V} = \frac{\sqrt{8\ (L + S)}}{\pi\ \beta\ L} \qquad (1)$$

L = no. of collected back-scattered laser photons

S = no. of collected photons not from the laser

$\beta = \frac{\Delta\rho}{\rho}$ (Taken as 0.002)

The second proposed mode of operation of the lidar involves using the FPS with a bandwith of about 2 pm and in a scanning mode. This will allow the recording of the spectral line profile of the back-scattered light (as has been done by Fiocco 1971) using the techniques described by Jacka (1984). From this profile the line of sight wind velocity and perhaps temperature and some information on aerosol density may be inferred. Numerical simulations of the lidar operating in this mode have been carried out yielding estimates of the precision with which wind velocities may be made.

Let us consider the profiles that may be recorded and the way in which the required information may be extracted from them as they are illustrated in Figure 2.

Firstly one may record the spectral line profile of the back-scattered light. This profile is the convolution of:

1. the laser emission line profile, this has a width of ~ 6 pm at the base cf. Tenenbaum et al. (1980)

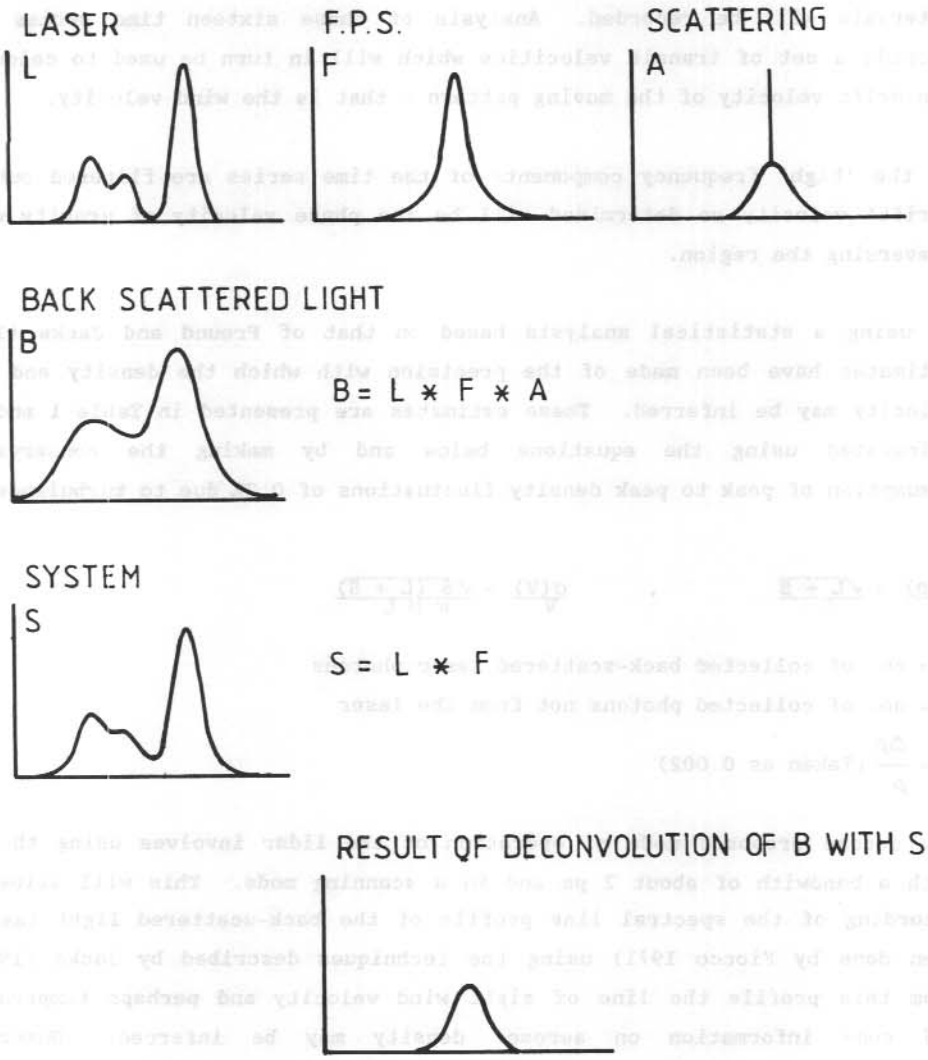

Figure 2. The two spectral line profiles that will be recorded by the lidar: B- the back scattered light and S- the system profile. The latter will be recorded by injecting some laser light directly into the detection optics just below the shutter. The deconvolution of B with S does not faithfully reproduce the scattering profile but it does permit the determination of line of sight velocity of the scattering volume.

2. the scattering profile, the broad base is the gaussian distribution due to Rayleigh scattering and the sharp spike is due to scattering from much heavier aerosols, and
3. the FPS profile, this is the convolution of the Airy function, the plate defect function and the aperture function.

Now by admitting some of the laser light directly into the top of the detection optics of the lidar one may record a profile which is the convolution of the laser profile and the FPS profile. This will be called the system profile. So by deconvolving the recorded profile with the system profile one is left with the scattering profile. From the scattering profile one may calculate the wind velocity from the position of the peak.

Ideally one might also expect to calculate the temperature from the width of the gaussian base and the aerosol density from the height of the aerosol spike. However, due to the effects of noise and the extremely narrow width of the aerosol spike compared to the other profiles, the scattering profile is not faithfully reproduced. It has been found through simulations that what is actually derived is a single, approximately gaussian shaped profile. There is no evidence of the aerosol spike, but it has the effect of narrowing the base gaussian curve, thus giving a temperature lower than it should. The effects on the velocity measurements are very small.

Numerical computer analyses based on the method described above have been carried out and they give estimates for the precision in velocity measurements shown for comparison with the previous estimates obtained using the moving pattern analysis method (see Table 1).

Three other applications of the data are being considered. Firstly, below about 30 km the computed density-height curve is expected sometimes to show positive excursions over limited height intervals due to scattering by aerosols. The amplitude of these excursions will give a measure of the aerosol content. Secondly, using the equipment in the second mode of operation and adapting the method of Vincent and Reid (1983), it may be possible to measure directly the vertical flux of horizontal momentum deposited by gravity waves. Finally, Professor H.S. Green, a collaborator in this project, is examining the possibility of directly determining the

vorticity from the data obtained while using the equipment in the first mode of operation.

23.4 CONCLUSIONS

The lidar will initially be operated at Buckland Park, along side the University of Adelaide Physics Department's facilities for measuring winds in the troposphere and mesosphere - see Briggs et al. (1969) and Vincent et al. (1982). Later it is proposed that a similar system should be installed at Mawson, Antarctica, along with existing facilities for measurements on winds and temperatures in the mesosphere and thermosphere.

The results of the numerical simulations of performance of the proposed lidar system demonstrate its considerable potential for detailed studies of the dynamics of the stratosphere. Used in conjunction with the techniques for wind measurements at higher levels the system will also greatly assist in the evaluation of data from those levels. If combined with other techniques for measurement of content and distribution of chemically active minor constituents of the stratosphere, especially ozone, it should greatly assist in understanding the photochemistry of the region, especially in the Antarctic.

ACKNOWLEDGMENTS

This work is supported by the Australian Research Grants Scheme.

23.5 REFERENCES

Briggs, B.H. (1968). On the analysis of moving patterns in geophysics - I. Correlation analysis. Journal of Atmospheric and Terrestrial Physics 30:1777-1788.

Briggs, B.H., Elford, W.G., Felgate, D.G., Golley, M.G., Rossiter, D.E. and Smith, J.W. (1969). Buckland Park aerial array. Nature 223: 1321-1325.

Fiocco, G., Benedotti - Michelangeli, G., Maischberger, K. and Madonna, E. (1971). Measurement of temperature and aerosol to molecule ratio in the troposphere by optical radar. Nature 229:78-79.

Freund, J.T. and Jacka, F. (1979). Structure in the λ577.7 nm [01] airglow. Journal of Atmospheric and Terrestrial Physics 41:25-31.

Jacka, F. (1984). Application of Fabry-Perot spectrometers for measurement of upper atmosphere temperatures and winds. Middle Atmosphere Program - Handbook 13:19-40.

Meek, C.E. and Manson, A.H. (1983). Measurement of the structure and drift velocities of airglow (λ=557.7 nm) irregularities: Saskatoon (52°N, 107°W), Canada. Journal of Atmospheric and Terrestrial Physics 45: 203-212.

Tenenbaum, J., Smilanski, I., Gabay, S., Levin, L.A., Erez, G. and Lavi, S. (1980). Structure of the 510.6 and 578.2 nm copper laser lines. Optics Communications 32:473-477.

Vincent, R.A., Elford, W.G. and Briggs, B.H. (1982). V.H.F. radar for middle atmospheric studies. The Australian Physicist 19:70.

Vincent, R.A. and Reid T.M. (1983). H.F. doppler measurements of mesospheric gravity wave momentum fluxes. Journal of the Atmospheric Sciences 40: 1321-1333.

24. AUSTRALIA'S MAGNETOSPHERIC RESEARCH IN ANTARCTICA

B.J. Fraser (1) and R.J. Morris (2)

(1) Physics Department
University of Newcastle
Newcastle, N.S.W., Australia, 2308.

(2) Antarctic Division
Department of Science
Kingston, Tas., Australia, 7150.

ABSTRACT

Antarctica is a very important continent for the study of magnetospheric physics since the polar cap and cusp region provide the most direct connections we have between ground recording stations and the outer boundaries of the earth's magnetosphere. It is these boundaries that couple energy from the solar wind into the inner magnetosphere and the high latitude ionosphere. The auroral zone, situated at slightly lower latitudes than the cusp, is a region of great energy deposition where the effects of electric fields, currents, energetic particles and plasma waves are seen on the ground. The Australian Antarctic stations are favourably situated to study the physics of these regions. A five year program using five Antarctic stations to study the transport of energy through the auroral and cusp regions by ultra low frequency plasma waves is proposed and involves the Antarctic Division, two universities and international collaboration.

24.1 INTRODUCTION

The exploration of the space environment near the earth has revealed a dynamic and complex system of plasmas interacting with magnetic fields and electrical currents surrounding our planet. Solar influence shapes and links the three major regions encompassing the domain of the earth's magnetic field: the magnetosphere, the ionosphere and the earth's neutral atmosphere.

The solar wind compresses the dayside magnetosphere and stretches the nightside into a long comet-like tail (Figure 1). Some solar wind plasma penetrates this magnetic shield and mixes turbulently with local plasma.

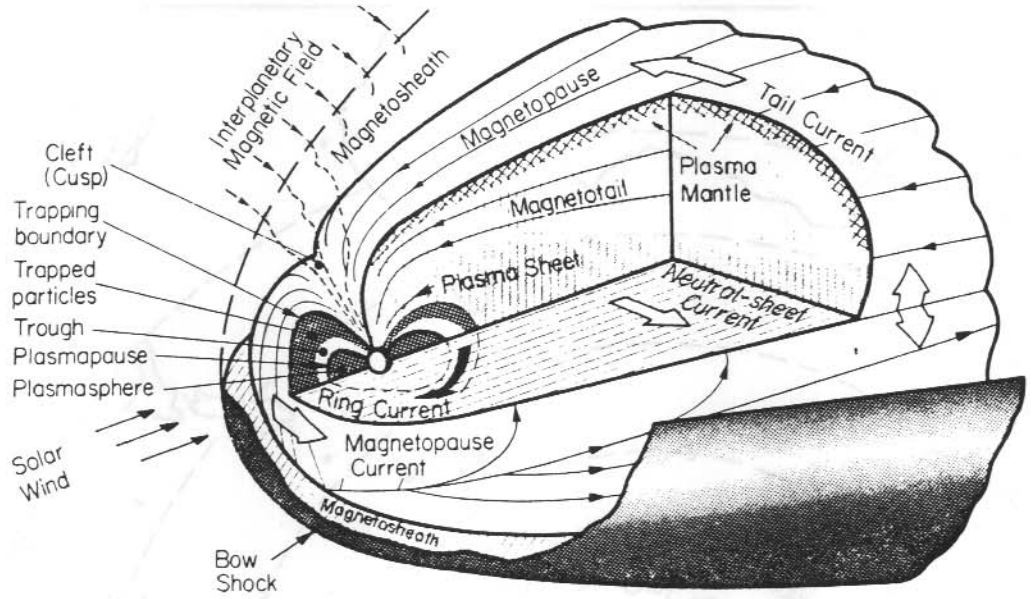

Figure 1. The earth's magnetosphere (after Heikkila 1973).

Antarctica is a very important continent for the study of magnetospheric physics since the polar cap and cusp region provide the most direct connections we have between earth recording stations and the outer boundaries of the earth's magnetosphere. The dayside cusp is the boundary between the closed field line region and the open field line polar cap region thereby providing a path for the direct entry of solar wind plasma. On the nightside, turbulent plasma gives rise to magnetic storms, when charged particles stored in the tail are accelerated along magnetic field lines towards the earth, releasing their energy as aurorae at low altitudes. This takes place in the auroral zone, which is situated at slightly lower latitudes than the cusp region.

Magnetospheric signatures observed in the auroral zone, the cusp region and the polar cap are characterised by the transport of energy, momentum and plasma in and out of these regions, and the associated perturbation of magnetic and electric fields and the flow of electric currents. These phenomena are observed directly in space by high and low altitude polar orbiting and synchronous spacecraft and indirectly on the ground by

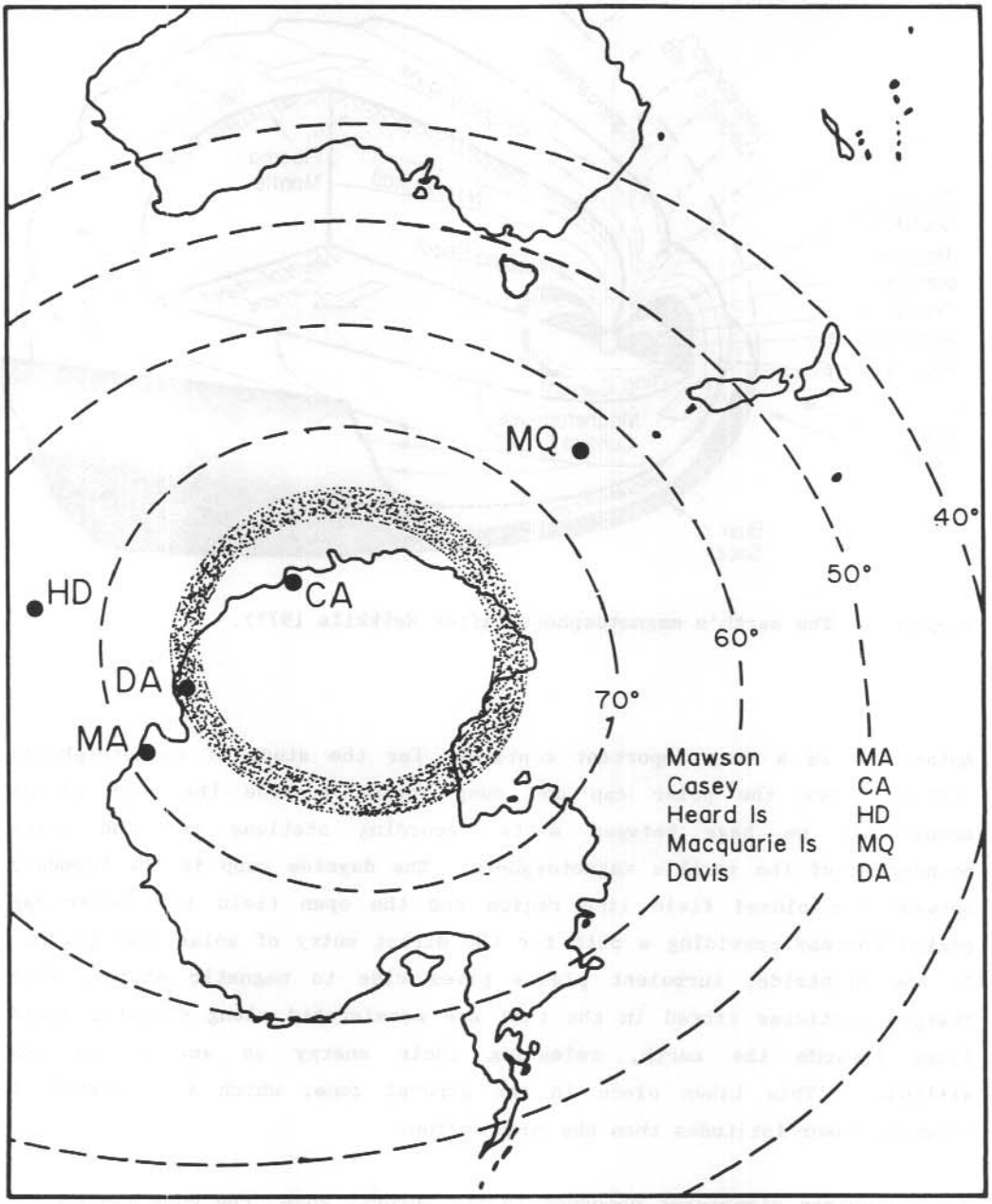

Figure 2. Pc1-2 pulsation stations.

ionospheric and atmospheric observations using magnetometers, photometers, radars, riometers and all-sky cameras. The Australian Antarctic stations are favourably situated to study the physics of these regions, with Davis and Casey near the cusp region, Mawson at auroral latitudes and Macquarie Island at sub-auroral latitudes, near the plasmapause (Figure 2).

24.2 FIVE YEAR COLLABORATIVE RESEARCH PROPOSAL

There are obviously many aspects of high latitude magnetospheric physics that can be studied at the Australian Antarctic stations. Realising the limited resources available both within the Antarctic Division of the Department of Science and the universities, a relatively inexpensive five year program to study the transport of energy through this region by observing ultra low frequency (ULF) plasma waves has been jointly planned between the following scientists and institutions:

1. Associate Professor, B.J. Fraser, Dr F.W. Menk
   University of Newcastle, Department of Physics, Newcastle, N.S.W.
2. Dr G.B. Burns, Mr R.J. Morris
   Antarctic Division, Department of Science, Hobart.
3. Prof. K.D. Cole
   La Trobe University, Division of Theoretical Physics and Space Physics, Melbourne.
4. Prof. V.A. Troitskaya
   Institute of the Physics of the Earth, Moscow, U.S.S.R.

The main thrust of the research will be the joint responsibility of these four institutions, while other Australian Government agencies will provide supplementary data.

Since magnetospheric physics is global in extent collaborative programs with researchers in other countries are necessary to study large scale effects. This may be arranged informally or by participation in dedicated international programs. The Australian contribution is vital since we occupy a large portion of the Antarctic continent. Formal co-operative research between La Trobe University, the University of Newcastle and the Institute of the Physics of the Earth Moscow began under the Australia-USSR Scientific and Technology Agreement in 1977. Research co-operation has

continued on an informal basis since 1980, and will continue. This is an important part of the research proposed here.

24.3 ULTRA LOW FREQUENCY PLASMA WAVES

The ULF plasma waves to be studied fall into two characteristic frequency bands; ion cyclotron waves and hydromagnetic waves. Ion cyclotron waves are observed on the ground as Pc1-2 geomagnetic pulsations in the 0.1-5 Hz frequency band. They are predominantly generated within the magnetosphere by instabilities associated with substorm processes, although some waves seen in the high latitude cusp region may be the result of external processes with subsequent propagation into the magnetosphere. On the other hand, the source of hydromagnetic waves which are observed on the ground and in the cusp region as Pc3-4 (5-100 mHz) geomagnetic pulsations is external and located in the near-earth upstream region controlled by the solar wind and the interplanetary magnetic field.

In order to study these waves from their initial generation, internal or external to the magnetosphere, through to the surface of the earth using spacecraft and ground stations the following topics are important:

1. The physics of the wave excitation regions.
2. The propagation mechanism through the magnetosphere to the region of the earth.
3. The coupling of the signals into the ionosphere.
4. The ionospheric transmission of wave energy across wide areas of the earth from the coupling region.

24.3.1 Pc1-2 pulsations in the polar cap

Pc1-2 signals propagate as ion cyclotron wave packets along high latitude field lines and transmit energy into an ionospheric duct centred on the F2 region, which distributes this energy to higher and lower latitudes. The proposed study concentrates on topics 1, 2 and 4 using the Antarctic network of five stations shown in Figure 2. In addition to the well-known regular structured Pc1-2 pulsations there is a group of newly discovered and distinctive emissions which are localised in the daytime cusp region. This five year collaborative program will in particular investigate the following unique high latitude phenomena:

1. Pc1-2 continuous regular pulsations which propagate to the polar cap from lower latitude internal magnetospheric sources. Their frequency range is 0.1 - 5 Hz, with a duration from ten minutes to several hours.
2. Pc1-2 continuous unstructured pulsations, unique to the polar cusp and cap regions. Frequencies are lower, at 0.1 - 0.3 Hz, with durations from a few tens of minutes to several hours.
3. Pc1-2 discrete regular emissions, recently discovered daytime cusp region pulsations, with intervals of rising, constant, alternating and falling frequencies in the range 0.1 - 1 Hz and a duration of three to seven minutes.
4. The serpentine emission showing a distinct and often continuous frequency band at frequencies 0.1 - 1 Hz. Durations range from minutes to days.

Although the spectral properties of the emissions in 2 and 3 above are reasonably well documented and generation mechanisms associated with the equatorial boundary layer have been suggested, we really know very little about their origin. The proposed experimental studies involve the recording of Pc1-2 pulsations at Macquarie Island, Heard Island, Davis, Casey and Mawson using induction coil magnetometers (Figure 2). The data will be digitised at the Antarctic Division and the University of Newcastle.

Subsequent digital analysis of the multistation data will be undertaken in order to determine the following:

1. Morphological properties in order to characterise the phenomena, viz. diurnal and seasonal occurrence, frequency range, amplitude distribution, power spectra, dynamic spectra and wave polarization.
2. Interstation coherency and phase, and group velocity. These will lead to an understanding of wave propagation mechanisms in the cusp region and to what extent the ionospheric duct is involved.
3. Interstation comparison of wave polarization characteristics. This will help the identification of wave types propagating directly from the magnetosphere to the earth's surface.
4. Distribution of wave amplitudes with latitude and longitude, in order to recognise localised sources.
5. A comparison of daytime cusp associated pulsations observed at Mawson, Heard Island, Davis and Casey with those at the lower latitude plasmapause station, Macquarie Island.

6. The effects of magnetic activity and movement of the cusp on the spatial and temporal properties of the pulsations.
7. Correlation studies with global indices such as Kp and AE, with other ground based experiments such as riometers, fluxgate magnetometers, electric fields, photometers, ionosondes and all-sky cameras. Data from in situ satellite measurements of electric and magnetic fields, cold, warm and energetic particles in the magnetosphere, and solar wind and interplanetary magnetic field parameters in the region upstream from the bow shock, will be obtained from individual experimeters and data banks at the US National Satellite Situation and Data Centre and the World Data Centres in Boulder, Colorado and Kyoto, Japan.

24.3.2 Pc3-4 pulsations in the polar cusp region

The source of Pc3-4 pulsation (5-100 mHz) energy is generally considered to be waves generated externally to the magnetosphere, upstream of the bow shock, in the solar wind. There are two possible paths for the entry of upstream waves into the magnetosphere, one directly through the subsolar region of the magnetosheath, and the other along high latitude field lines into the cusp region. The importance of these two propagation paths for the transmission of wave energy into the magnetosphere and their relative contribution to high latitude Pc3-4 pulsations must be established. In the present study the authors are primarily interested in topics 2 and 4 of section 24.3. Extensive high latitude observations in the cusp region are necessary to check theoretical predictions and the following specific questions must be answered.

1. Does the upstream wave energy propagate directly into the cusp region and through the ionosphere to the ground, or does it just modulate the magnetopause and/or the last closed field line boundary?
2. Is the frequency spectrum of waves seen on the ground below the cusp broadband or monochromatic, and how does it compare with the spectrum of upstream waves?
3. Does the ground signature of the waves show the amplitude and phase variations of a field line resonance?
4. To what extent are harmonics seen in the wave signature?
5. Do the high latitude signals exhibit wave packet structure and phase jumps?

6. What are the similarities and differences between waves seen at low and high latitudes?

It is hoped to answer many of these questions in the proposed five year study. Particular Pc3-4 studies to be undertaken using the network include the following:

1. Morphological studies to characterise the phenomena, viz. diurnal and seasonal occurrence, frequency range and signal amplitude distribution.
2. The study of longitudinal coherency and phase variations in relation to azimuthal wave numbers, harmonic structure and phase jumps.
3. The study of latitudinal coherency and phase and polarisation variation in order to identify the role played by field line resonances.
4. A comparison of wave properties seen at Antarctic stations with simultaneous observations at low latitude stations in Eastern Australia operated by Newcastle University.

24.4 GEOMAGNETIC PULSATION DATA ACQUISITION AND ANALYSIS

The experimental network will comprise the four permanent induction coil magnetometers currently located at Mawson, Davis, Casey and Macquarie Island. Heard Island will be operated over the summer months only. Pc1-2 pulsations will be continuously recorded on both FM slow speed magnetic tape and paper chart. Subject to the availability of DEC-LSI-11 computer support (currently at Davis and Macquarie Island, and at Casey from 1988) data may be recorded on RL02 disks for limited world data event intervals and other strategic periods. Pc3-4 pulsations will be simultaneously recorded by the induction magnetometers on paper chart recorders. During the course of the project microcomputers recording Pc3-4 data on floppy disk will be added at all stations.

With such a large quantity of data to be analysed, rapid initial analysis techniques must be available for specific event identification. For this purpose systems will be available at the Antarctic Division and Newcastle University to display continuous frequency-time grey-scale dynamic spectra on 35 mm film. More detailed event analysis will involve the use of digital pure state vector analysis techniques on multi-channel time series using IBM-AT compatible microcomputers and VAX 11/780 or similar main frame machines.

Background monitoring of the general state of the high latitude magnetosphere and the auroral ionosphere at the time of geomagnetic pulsation events will be provided by observatory data gathered from fluxgate magnetometer, riometer, all-sky camera and ionosonde networks operated by the Antarctic Division in association with the Geomagnetism Section of the Bureau of Mineral Resources, Geology and Geophysics (BMR) and the Ionospheric Prediction Service (IPS). Of particular importance is the magnetometer network of the BMR which will observe the gross magnetic field features and provide data in digital form.

24.5 DISCUSSION AND SUMMARY

It is imperative that the current experimental installations be up-graded and standardised as soon as possible. Funding is required to replace the old induction magnetometer at Macquarie Island and for the construction of a portable system for Heard Island. For standardisation, a number of preamplifiers based on an Antarctic Division prototype unit, and replacement detector coils constructed at Newcastle University are required. The Antarctic Division also requires funding for a new commercial dynamic frequency analyser system.

In order to pursue the science at the high level demanded, the research would benefit enormously by the employment of a full-time post-doctoral Research Associate, to be responsible for the preprocessing and contribute to the interpretation of both the Pc1-2 and Pc3-4 pulsation data. It is anticipated that implementation of the project, following the proposed budget suggestions would cost an average of $60 000 per year over the five years, with major equipment expenditures occurring in the first two years. Data collection, analysis and ultimately publication would be seriously hampered without this level of support.

The proposed research in Pc1-2 and Pc3-4 geomagnetic pulsations in Antarctica is necessary in order to establish the source regions of the various types of high latitude pulsations. This will contribute to the assessment of present wave generation mechanisms and wave propagation modes and hasten the formulation of new theories for the explanation of these interesting phenomena. Moreover, the morphological study of these pulsation

regimes will provide ground-based diagnostic tools for studying and monitoring high latitude ionospheric and magnetospheric parameters.

24.6 REFERENCE

Heikkila, W.J. (1973). EOS Transactions. American Geophysical Union 54:764.

25. AUSSAT BEACON PROPOSAL - RELEVANCE TO ANTARCTIC STATIONS

E.A. Essex
Department of Physics
La Trobe University
Bundoora, Vic., Australia, 3083.

ABSTRACT

The second generation AUSSAT (1992 et seq.) satellites provide the Australian upper atmosphere scientific community with the opportunity to re-enter the space age. To this end a proposal for a radio beacon experiment on AUSSAT has been prepared by the Ionospheric Prediction Service, Department of Science, in conjunction with the universities of La Trobe and Monash. The location of the spacecraft in geosynchronous orbit at 156° - 164° east longitude means that the subantarctic station of Macquarie Island is ideally suited as a ground station. Unless the longitude position is moved further west, the Australian Antarctic mainland stations are not suitably located for ionospheric studies using the AUSSAT beacons. This paper outlines possible ionospheric studies using the AUSSAT beacons.

25.1 INTRODUCTION

The second generation AUSSAT (1992 et seq.) satellites provide the Australian upper atmosphere scientific community with the opportunity to re-enter the space age. To this end a proposal for a radio beacon experiment on AUSSAT has been prepared by the Ionospheric Prediction Service, Department of Science, in conjunction with the Universities of La Trobe and Monash. The proposed beacon would transmit four phase coherent frequencies (nominally 136 MHz, 400 MHz, 1.2 GHz and 25 GHz) with modulation to permit Faraday, differential Doppler and group path measurements to be made at ground stations within sight of the satellite. The location of the spacecraft in geosynchronous orbit at 156° - 164° east longitude means that the subantarctic station of Macquarie Island is ideally suited as a ground station. Unless the longitude position is moved further west, the Australian Antarctic mainland bases are not suitably located for ionospheric

studies using the AUSSAT beacons. The following sections outline the various techniques using AUSSAT beacons which may be used to study the ionosphere.

25.2 THEORY AND EXPERIMENTAL DESIGN

Phase path length variation and the derived Doppler shifts are two ionospheric effects which can be monitored using a radio beacon to obtain information on ionospheric parameters. Depending on the type of modulation used, it is also possible to measure the group path delay due to the presence of the ionosphere. These techniques are outlined below as well as their application to the AUSSAT beacon.

25.2.1 Phase path length and doppler shift

Following the method of Garriott et al. (1970) and Tucker and Fannin (1968), the phase path length P under ray theory of a wave propagating between a satellite transmitter T_x and a receiver R_x on the ground is given by:

$$P = \int_{T_x}^{R_x} \mu_p \cos\alpha \, ds \qquad (1)$$

where μ_p is the phase refractive index in the wave normal direction and α is the angle between the ray and the wave normal. Under free space conditions, the value of P is R, along the straight line path.

So the phase path reduction ΔP is given by:

$$\Delta P = R - P \qquad (2)$$

Using the QL approximation, two modes exist at high frequencies. The differential phase shift between the two modes gives the angular motion Ω where:

$$\Omega = \frac{\pi}{\lambda} \{\Delta P_{ord} - \Delta P_{ext}\} \text{ radians} \qquad (3)$$

The Doppler shift at the receiver is given by:

$$f_D = -\frac{1}{\lambda}\frac{dR}{dt} + \frac{1}{\lambda}\frac{d\Delta P}{dt} \qquad (4)$$

corresponding to the free space and ionospheric Doppler shifts.

Neglecting absorption and assuming refraction effects are small, the phase path reduction and the differential phase shift may be written as, to a first approximation:

$$\Delta P \cong \Delta P_o = \frac{K_1}{2f^2} \int N ds \qquad (5)$$

$$\Omega \cong \Omega_o = \frac{K_1 \pi e \overline{B\cos\psi}}{mcf^2} \int N ds \qquad (6)$$

where f is the wave frequency, K_1 is a constant, the average bar denotes the weighted mean over the integration along the straight line path and the other symbols have their usual meaning. Assuming the ionosphere is spherically stratified, (5) and (6) may be written as:

$$\Delta P_o = \frac{K_1 I}{2f^2} \overline{\sec\theta} \qquad (7)$$

$$\Omega_o = \frac{K_2 \bar{M}}{f^2} I \qquad (8)$$

where θ is the vertical angle of the path, K_2 a constant,

$\bar{M} = \overline{B \cos\psi \sec\theta}$

and I is the electron content in electrons per square metre.

The ionospheric Doppler shift becomes:

$$\Delta f_{Do} = \frac{K_1}{2cf}\frac{d}{dt}(I \overline{\sec\theta}) \qquad (9)$$

It is noted that the first order expression for the phase path defect ΔP_o does not involve the magnetic field, whereas the expression for the Faraday rotation, Ω_o, is weighted by the magnetic field.

The higher order approximations for ΔP_o do however involve the magnetic field (see Garriott et al. 1970, Davies et al. 1975).

25.2.2 Group path delay

The group path delay ΔT, relative to free space, between a satellite transmitter T_x and a ground receiver R_x is given by:

$$\Delta T = \frac{1}{c}\int_{R_x}^{T_x} \mu_g \, dl - \frac{1}{c}\int_{R_x}^{T_x} dl \qquad (10)$$

where μ_g is the group refractive index at VHF and above. This expression may, to the first approximation, be written as:

$$\Delta T = \frac{K_3 I}{cf^2} \qquad (11)$$

where K_3 is a constant.

Hence the dispersive group path delay in the ionosphere, relative to the free space time of arrival, is proportional to the ionospheric electron content and independent of the magnetic field in the first approximation.

25.2.3 Experimental design

Depending on the type of modulation used on the AUSSAT beacon, equations (7), (8), (9) and (11) enable different methods and sensitivities to be used to study the variation in the ionospheric and protonospheric content.

Considering first the expression (8) for the Faraday rotation, for two closely spaced frequencies, such as 136 MHz and 1 MHz modulation, the differential Faraday rotation is given by:

$$d\Omega = \frac{-2 K_2 \bar{H} I \, \delta f}{f^3} \qquad (12)$$

with an error of:

$$\frac{d\Omega}{\Omega} = \frac{-2\ \delta f}{f} \qquad (13)$$

This enables the ionospheric electron content to be measured without an ambiguity in Ω, a problem in the past when only a single frequency has been available (see Lambert and Cohen 1986).

When three coherent frequencies are used such as 136 MHz, 400 MHz and 1.2 GHz, it is possible by the use of equation (9) to determine the differential Doppler variation between the pairs of frequencies and hence the ionospheric electron content free of any baseline uncertainty. The differential Doppler (or phase) carrier technique is more sensitive than the Faraday technique and is hence suitable for the study of finer scale irregularities, such as the interaction of micropulsations with the ionosphere, possibly one of the chief mechanisms for the transfer of energy to the ionosphere in the auroral regions (Crowley et al. 1985, Davies and Hartmann 1976).

It is also possible to obtain the total electron content by comparing the differential phase between a carrier and its sideband using three carrier frequencies. If the modulation used is in the form of a code, then it is possible to apply equation (11) directly to determine the group path delay between two frequencies (Grubb and Jones 1980).

25.3 SCIENTIFIC RELEVANCE

The techniques outlined above present exciting possibilities for the study of the ionosphere not only in the Australian Pacific and Asian regions, but also at the Australian Antarctic stations. From Macquarie Island a continuous monitoring of the whole ionosphere would be possible as well as the protonosphere (Kersley and Klobuchar 1978). In addition features associated with the aurora, the main trough, large scale disturbances and their propagation direction, and such fine scale effects as micropulsations on the ionosphere could be studied in detail. Macquarie Island is the most favourable location in the Southern Hemisphere for TEC studies of the aurora using a geostationary satellite as its low geographic latitude compared to its geomagnetic latitude means that a higher elevation angle to the satellite is possible (see Figure 1). The proposed AUSSAT beacon would make

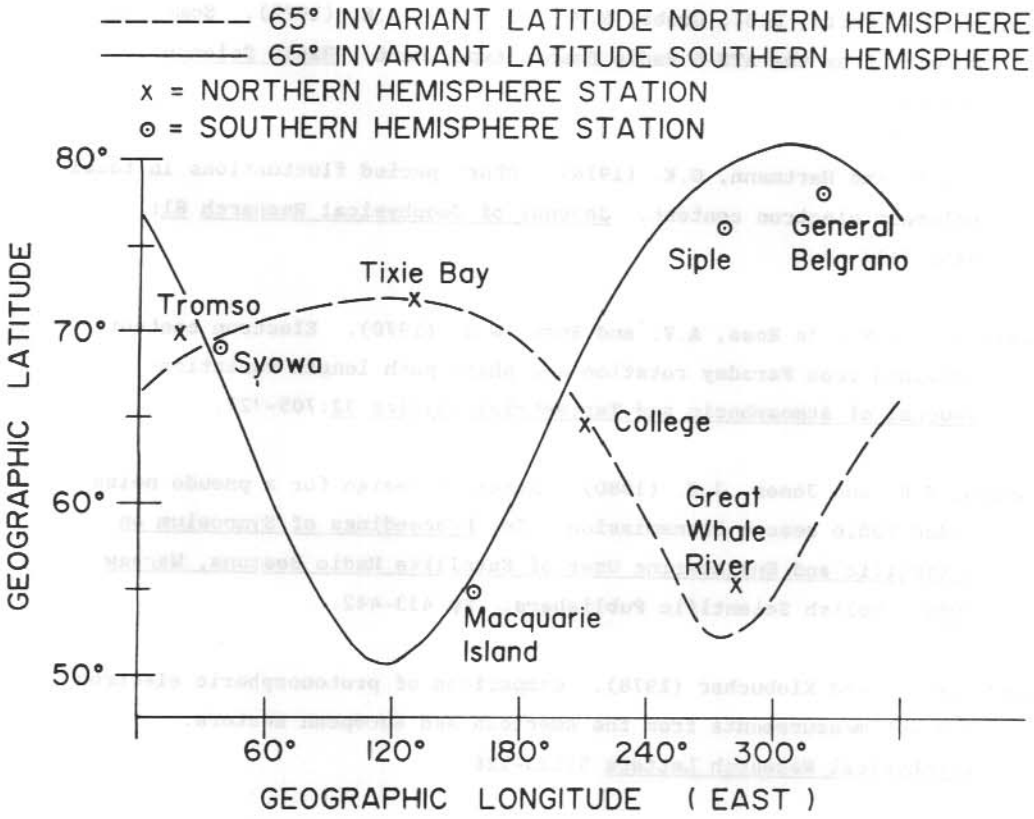

Figure 1. The location of Macquarie Island in geographic coordinates and the 65° invariant latitude north and south.

possible for the first time a detailed study of the whole of the ionosphere using several different techniques. If the AUSSAT geostationary orbit were located further to the west, it would be possible to study not only ionospheric disturbances associated with the auroral oval but also their propagation around the oval and into and out of the polar cap (Klobuchar et al. 1986).

25.4 REFERENCES

Crowley, G., Wade, N., Waldock, J.A., Robinson, T.R. and Jones, T.B. (1985). High time resolution observations of periodic frictional heating associated with a Pc5 micropulsation. Nature 316:528-530.

Davies, K., Fritz, R.B., Grubb, R.N. and Jones, J.E. (1975). Some early results from the ATS-6 Radio Beacon Experiment. Radio Science 10: 785-799.

Davies, K. and Hartmann, G.K. (1976). Short period fluctuations in total columnar electron content. Journal of Geophysical Research 81: 3431-3434.

Garriott, O.K., da Rosa, A.V. and Ross, W.J. (1970). Electron content obtained from Faraday rotation and phase path length variations. Journal of Atmospheric and Terrestrial Physics 32:705-727.

Grubb, R.N. and Jones, J.E. (1980). Receiver design for a pseudo noise coded radio beacon transmission. In: Proceedings of Symposium on Scientific and Engineering Uses of Satellite Radio Beacons, Warsaw 1980. Polish Scientific Publishers. Pp 433-442.

Kersley, L. and Klobuchar (1978). Comparison of protonospheric electron content measurements from the American and European sectors. Geophysical Research Letters 5:123-126.

Klobuchar, J.A., Bishop, G.J. and Doherty, P.H. (1986). Measurements of trans-ionospheric propagation parameters in the Polar Cap Ionosphere. In: Beacon Satellite Symposium, Oulu, Finland 1986, Abstracts. University of Oulu Printing Center. P. 54.

Lambert, M. and Cohen, E.A. (1986). Monitoring ionospheric irregularities in the southern auroral region by means of a satellite beacon. Radio Science 21:347-350.

Tucker, A.J. and Fannin, B.M. (1986). Analysis of ionospheric contributions to the Doppler shift of CW signals from artificial earth satellites. Journal of Geophysical Research, Space Physics 73:4325-4334.

26. THE POLAR CAP IONOSPHERE

P.L. Dyson
Physics Department
La Trobe University
Bundoora, Vic., Australia, 3083.

ABSTRACT

A proposal is presented for the establishment of a modern ionosonde at Casey station (66.2°S, 110.4°E), Antarctica.

26.1 INTRODUCTION

Over the last decade or more, the main thrust of high latitude upper atmosphere research has been to study the aurora and associated processes. In a recent review, Akasofu (1985) pointed out that this has led to an emphasis on auroral oval phenomena so that much less has been achieved in the study of polar cap phenomena. In the same article, Akasofu states that 'systematic observational programs specifically designed to study (polar cap) phenomena in the Antarctic region could make significant contributions to upper atmospheric physics and magnetospheric physics' and 'there is little doubt that the polar cap ionosphere has much to be explored further'.

The range of phenomena occurring in the polar cap include polar cap auroral arcs, solar energetic electrons, auroral precipitation, convection, and ionospheric currents. The ionosphere is affected by these processes and we do not yet understand the details of the ionospheric response nor the extent to which the observation of ionospheric phenomena can be used to infer properties of other phenomena. On this latter point, the evidence to date is encouraging. For example, Reinisch (1986) has shown that it is possible to monitor polar convection by measuring the drift of ionospheric irregularities with a digital ionosonde. A modern digital ionosonde would provide an excellent means of studying the ionosphere in the polar cap region. It would:

1. enable a systematic study of the polar cap ionosphere to be carried out,

2. provide essential information on the state of the ionosphere to aid the interpretation of optical and magnetic measurements,
3. provide a means of studying auroral phenomena during daylight hours.

26.2 SCIENTIFIC INVESTIGATIONS

It is envisaged that a digital ionosonde installed at Casey would be available as a long term facility which various researchers could propose to use. Consequently it is not possible to forsee all the scientific projects which will use the facility. Initially it is proposed that the major areas of research be the following.

26.2.1 Ionospheric structures

Irregular structures occur in the polar cap ionosphere due to such things as particle precipitation. There has been no systematic study of the types of irregularities produced and the extent to which they can be associated with specific polar cap phenomena. One reason for this is that the irregular structures produce severe spread F on ionograms and with conventional ionosondes it is difficult to do more than record that spread F is present. However modern digital ionosondes, which measure angle of arrival and doppler shift, enable the irregular structures to be located in space and their motion to be measured. Consequently, such an ionosonde can be used to study systematically the spatial and temporal behaviour of these phenomena and so more readily determine their origin and association with other phenomena. In particular it is planned to study the behaviour of the background polar cap ionosphere, the structures produced by the polar cusp, and the irregularities produced by particle precipitation. Such measurements will provide a data base to test theoretical models of the ionosphere.

26.2.2 Micropulsation effects

Accurate measurements of the height of ionospheric layers can reveal the effects of micropulsations on the ionosphere (e.g. Menk et al. 1983). Micropulsation measurements at a polar cusp station such as Casey show specific characteristics such as the occurrence of intervals of pulsations

with rising periods (Morris et al. 1982). The effects of such pulsations on the ionosphere is largely unexplored and will be studied in this project.

26.2.3 Polar cap convection

The results of Reinisch (1986) show that polar cap convection can be monitored by measuring the drift of ionospheric irregularities. It is proposed to use this method to systematically study the convection occurring at Casey. Such measurements will provide new information on the temporal variations of convection so that processes responsible for producing changes in convection can be identified. In particular the response of polar cap convection to changes in the interplanetary magnetic field can be studied in detail.

26.2.4 Coupling between the neutral atmosphere and ionosphere

Many polar cap processes will affect the neutral atmosphere producing optical auroral effects. Photometers and All-Sky-Cameras can map these features and the thermospheric wind can be measured using a Fabry-Perot spectrometer. Such studies combined with the digisonde measurements would provide an excellent means of studying polar cap dynamics.

26.2.5 Correlation with satellite measurements

The permanent installation of a digital ionosonde at Casey will provide an important opportunity for collaborative studies with satellite experimenters. The study of geophysical phenomena requires a global as well as a local approach so that ground based measurements provide an important complement to satellite observations and satellite researchers studying the polar cap region will want to co-operate in conducting joint campaigns of observations.

Of particular relevance is the possibility to study the details of ionospheric irregularities well beyond the region of Casey by utilising Doppler and Faraday rotation measurements of satellite signals.

26.3 EQUIPMENT

In recent years ionosondes have been extensively developed so that they now measure not only the virtual range (time delay), but also the amplitude, angle of arrival, phase, and doppler shift of the echoes. Furthermore, the computer control facilities enable specific modes of operation appropriate to phenomena being studied, to be programmed. Consequently, the modern digital ionosonde is a very powerful research tool.

At present the only commercially available digital ionosonde is the Digisonde 256 built by the University of Lowell Centre for Atmospheric Research. From the scientific point of view, this instrument would be ideal. Currently one is operated by La Trobe University at Beveridge near Melbourne. Having two similar systems has considerable advantages which include the possibility of developing new software routines and training people on the La Trobe instrument, before venturing to Casey.

The cost of the Lowell instrument depends on various options chosen etc., however, for a remote station like Casey, it will be important to have as flexible an instrument as possible and the cost may be as high as A$300 000. Considerable expertise in designing, manufacturing and marketing of various types of ionospheric sounders exists in Australia with the Ionospheric Prediction Service, KEL Aerospace, and Andrew Antennas having had various involvements. From a research point of view, no current Australian instrument has the full capabilities required, nevertheless it may be worthwhile to carry out a cost-benefit study to determine whether local development of a suitable instrument is a feasible alternative.

26.4 REFERENCES

Akasofu, S.-I. (1985). The Polar Caps. Memoirs of National Institute of Polar Research, Japan, Special Issue Number 38(1).

Menk, F.W., Cole, K.D. and Devlin, J.C. (1983). Associated geomagnetic and ionospheric variations. Planetary and Space Science 31:569-572.

Morris, R.J., Cole K.D., Matveeva, E.E. and Troitskaya, V.A. (1982). Hydromagnetic 'whistles' at the dayside cusps: IPRP events. Planetary and Space Science 30:113-128.

Reinisch, B.W. (1986). New techniques in ground based ionospheric sounding and studies. Radio Science 21:331-341.

27. THE SUNDIAL CAMPAIGNS

P.J. Wilkinson
IPS Radio and Space Services
Department of Science
P.O. Box 702
Darlinghurst, N.S.W., Australia, 2010.

ABSTRACT

An outline of a co-ordinated campaign to develop a real-time prediction capability for the ionosphere is presented. The contributions Antarctic stations can make to this program are noted.

27.1 INTRODUCTION

SUNDIAL is the name chosen for a series of campaigns which will improve our understanding of the solar terrestrial environment. The principal objective of SUNDIAL is quite ambitious, namely, by coupling global data collection and first principles modelling, a real-time predictive capability will be achieved for the ionosphere.

This objective recognises that the principal energy inputs causing changes in the ionosphere are a result of solar wind disturbances and that the coupling between the solar wind and the ionosphere is complex and probably occurs at high latitudes. In this region closed magnetospheric field lines map down into the ionosphere and non-radiative heating of the neutral thermosphere occurs.

Data collection programs, and the models used with SUNDIAL campaigns, are summarised in this note and where appropriate the importance of high latitude data will be emphasised.

27.2 DATA, MODELS AND METHODOLOGY

One of the strategic objectives of SUNDIAL is to encourage an interplay between data and models on a global scale. Data is used both to define the boundary conditions for the models and also to test the subsequent evolution

of events forecast by the models. Data analysis is therefore carried out on several complementary levels encompassing the solar terrestrial environment and large time and spatial scales.

The data and models planned for use in the SUNDIAL campaigns are summarised in Table 1.

Table 1. The models and data available for SUNDIAL campaigns. Those items flagged with an x were available during the first campaign. It is expected that data will be available from the CEDAR programmes (Coupling, Energetics and Dynamics of the Atmospheric Regions) for the thermospheric input data.

	MODEL	MEASUREMENT	
Solar wind	No model used	in situ (limited)	
Solar wind - magnetosphere	No model	inferences	
Magnetosphere	Rice	Ae, Dst, (possible) solar wind ram pressure particle distribution polar cap potential	x
Ionosphere	Utah State	Ionosondes	x
		Total electron content	x
		Incoherent scatter radar	x
Thermosphere	NCAR	CEDAR	
Test	IRI	Baseline predictions	x

Data only are collected for the solar surface, solar wind and magnetopause as there are no appropriate large scale models available for these regions. Models are available for the other three major regions; the magnetosphere, the ionosphere and the thermosphere. The last two models are coupled and it is expected that the magnetospheric model will also be coupled to both these by the conclusion of the campaigns.

Campaigns are scheduled for future dates, rather than retrospectively, partly to ensure maximum data collection and partly to avoid preconceptions about what is interesting. Campaigns last at least seven days and are already scheduled to cover all four seasons for two levels of solar activity. Subsequent to a campaign, scaled data is distributed among investigators and one or two days are selected for immediate study. All data are archived for general study at a later date. This type of analysis highlights the strong and weak aspects of the models and will eventually define the temporal and spatial scales of change within the ionosphere that can be realistically forecast using global first principles models.

To date, the majority of the global data collected comes from ionosondes and total electron content experiments. Incoherent scatter data and optical data will be added for future campaigns. All regions of the globe are well represented, although only a small amount of high latitude data were available from high latitude regions for the first campaign.

This is expected to improve in future SUNDIAL campaigns as data will be available from the incoherent scatter radars in North America and EISCAT, in Europe. In the Southern Hemisphere, data will be available from the British and Japanese bases as well as Australian stations.

As indicated in the introduction, most of the coupling between models will occur at high latitudes so data from this region could play a fundamental role in the SUNDIAL campaigns. This will be especially true of Antarctic data because the bulk of the high latitude data will be Northern Hemisphere incoherent scatter data.

27.3 PROGRESS TO DATE

Only one SUNDIAL campaign has been analysed to date. The first campaign coincided with the arrival at the earth of a high speed solar wind stream. Thus the first day of the period was quiet and successive days were more disturbed geomagnetically.

The main body of data available for this campaign were ground based ionosonde data, which were analysed for this period in two ways:

1. First, scaled parameters were distributed, allowing interesting periods to be selected for more detailed study.
2. Second, real height electron density profiles were calculated for the quiet day at the beginning of the analysis period for comparison against profiles predicted by the ionospheric model initialised to run for the same period.

This analysis is still continuing with only preliminary results being available at present. These results are summarised below:

1. Operation of the magnetospheric model has had limited success as there were no in situ data available for setting the boundary conditions. For this reason, an attempt will be made to initialise the model using ground based magnetometer data. If successful, ground based high latitude magnetometer data will be even more important in future campaigns.
2. Although the thermospheric and ionospheric models are coupled, the thermospheric wind model was based on average zonal winds. This will be improved in later campaigns, using CEDAR data.
3. Although little high latitude data were available for the first campaign, there was some evidence for coupling between low and high latitudes, quite similar behaviour in the two high latitude hemispheres, and the high and mid latitudes appeared de-coupled.
4. At mid-latitudes, the ionosphere showed some regions of storm conditions, but generally the disturbance was minor.
5. At low latitudes, the most interesting event was the occurrence of a marked equatorial spread F in the South American sector.
6. Finally, comparisons of the electron density height profiles obtained from ionograms were in good agreement with those predicted using the ionospheric model.

27.4 CONCLUSION

The main data and modelling problems facing the SUNDIAL campaigns arise at high latitudes. The theoretical and practical problems of coupling the models, although not small, are soluble. While the ionospheric and thermospheric models have been successfully coupled, the contribution from the magnetospheric model has still not been assessed. In future SUNDIAL campaigns, rather more emphasis will be placed on obtaining and using ground based high latitude data. While some incoherent scatter data will be available, these will be most useful when supplemented by other data from a variety of high latitude locations. Contributions from Antarctica will be particularly important.

While the SUNDIAL objective may be premature, physical modelling, refined by global measurements, should highlight those features of most interest for ionospheric forecasting, as well as place scale size limits on predictable phenomena. This could be significant for the continued monitoring of high latitude phenomena.